Available online at www.sciencedirect.com

ScienceDirect

Procedia Engineering00 (2015) 000–000

Procedia Engineering

www.elsevier.com/locate/procedia

6th BSME International Conference on Thermal Engineering (ICTE 2014)

Natural Convection Heat Transfer In An Arch Enclosure Filled With A Nanofluid

Manoj Kr. Triveni[a], Dipak Sen[b], RajSekhar Panua[a,b]*

National Institute of Technology, Agartala, Tripura-799046, India

Abstract

This paper provides a numerical analysis of laminar natural convection in an arch enclosure filled with Al_2O_3-water based nanofluid with different volume fractions. The heat transfer surfaces such as side walls of the enclosure are maintained at constant temperatures while the bottom and curve walls are kept adiabatic. Two-dimensional steady-state governing equations along with the Boussinesq approximation have been solved using the finite volume method (FVM). The problem is solved for volume faction (ϕ) = 0 – 9%, curvature ratio (CR) = 1 – 1.5 and Rayleigh number (Ra) = 1×10^4 to 1×10^6. From the analysis, it is found that the both fluid flow and heat transfer are affected by these pertinent parameters. The enhancement in heat transfer rate has been observed for a volume fraction up to 5% and beyond that it starts decreasing as the concentration constantly increasing compared to the base fluid of water. Also, the heat transfer rate increases with the increase of curvature ratio and Rayleigh number. A good agreement has been found between the present work and experimental & numerical results from the literature.

Peer-review under responsibility of organizing committee of the 6th BSMEInternational Conference on Thermal Engineering (ICTE 2014).

Keywords: Natural convection; arch enclosure; nanofluid; curvature ratio; Nusselt number

1. Introduction

Miniaturization of electronics equipment and increasing industrial needs require high performance fluids. An innovative technique, which uses a mixture of nanoparticles and the base fluid, was first introduced by Choi [1] in order to develop advance heat transfer fluids with substantially higher conductivities. Lai and Yang [2] used lattice Boltzman method for natural convection heat transfer in a square cavity filled with Al_2O_3-water based nanofluid.

* Corresponding author. Tel.: 09862225569; fax: +0-000-000-0000 .
*E-mail address:*triveni_mikky@yahoo.com

Peer-review under responsibility of organizing committee of the 6th BSME International Conference on Thermal Engineering (ICTE 2014).

Results indicated that the average Nusselt number increases with the increase of Rayleigh number and particle volume concentration. Wen and Ding [3] concerned about the formulation of aqueous based nanofluids and its application for natural convection heat transfer conditions. The preliminary results have shown a systematic decrease in the natural convective heat transfer coefficient with the increase of particle volume concentration. Khanafer *et al*. [5] have investigated heat transfer enhancement in a two-dimensional enclosure using nanofluids for various pertinent parameters. It was found that the suspended nanoparticles substantially increase the heat transfer rate at any given Grashof number. Abu-Nada *et al*. [6] worked for heat transfer enhancement in a differentially heated enclosure using variable thermal conductivity and variable viscosity of Al_2O_3–water and CuO–water nanofluids. It was observed that enclosures having high aspect ratios, experience more deterioration in the average Nusselt number compared to enclosures having low aspect ratios. Ho *et al*. [7] have done a numerical analysis to identify the effects due to uncertainties in effective dynamic viscosity and thermal conductivity of nanofluid on laminar natural convection in a square enclosure filled with alumina–water nanofluid. The investigation revealed that, as the Rayleigh number increases above 10^4, the average heat transfer coefficient is decreasing. Mansour *et al*. [8] has been performed a numerical simulation of mixed convection in a square lid-driven cavity partially heated from below and filled with water-based nanofluid. It has been concluded that increase in solid volume fraction leads to increase the average Nusselt number.

The above brief literature survey summarized that the closed space as square, rectangular, quadrantal and triangular enclosures filled with nanofluid have been studied extensively to obtain the heat transfer rate. However, no work has been done in arch cavity filled with water or nanofluid. Hence, the major interest in the present work to study the heat transfer characteristic in arch cavity. The present work may help the researchers and designers to enhance the heat transfer rate from the electronic goods and solar collectors.

Nomenclature

g	acceleration due to gravity, m s^{-2}
k_f	thermal conductivity of the fluid, W $m^{-1}K^{-1}$
H	height of the arch cavity, m
L	width of the arch cavity, m
p	pressure, Pa
P	dimensionless pressure
u, v	x and y component of dimensional velocity
U, V	x and y component of dimensionless velocity
T	temperature, K
T_h	temperature of the hot wall, K
T_c	temperature of the cold wall, K
Pr	Prandtl number
Ra	Rayleigh number
Nu_x	local nusselt number
Nu	average nusselt number
CR	curvature ratio
Greek symbols	
α	thermal diffusivity, m^2 s^{-1}
β	thermal expansion coefficient, K^{-1}
θ	dimensionless temperature
ρ	density, kg m^{-3}
μ	dynamic viscosity, kg m^{-1} s^{-1}
υ	kinematic viscosity, m^2 s^{-1}
ψ	stream function
Ψ	dimensionless stream function

2. Problem description and Mathematical Formulation

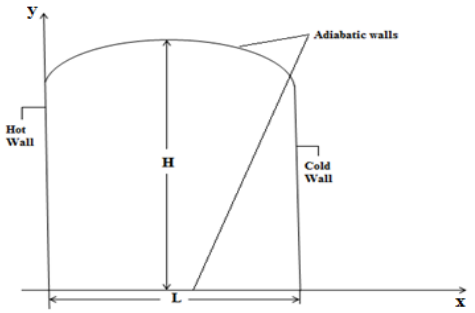

Fig.1. Schematic diagram of physical domain

The schematic diagram of an arch cavity is shown in figure 1. The width of the cavity is L and height H. The curvature ratio (CR = H/L) of the arch cavity is varying from 1 to 1.5. The left side wall is considered as hot (T_h) and right side as cold wall (T_c) while bottom and upper walls are kept adiabatic. Al_2O_3-Water based nanofluid is intended for heat transport which physical properties are shown in table 1. Plexiglas is used as an insulating material to prevent the heat leakage from thermally insulated walls.

Table 1: Properties of water and Al_2O_3 nanoparticle at 22^0C

Physical Properties	C_p (j/kg k)	ρ (kg/m^3)	k (w/mk)	β×10^{-5} (1/k)	d_p (mm)	$\mu_f \times 10^{-3}$ (Ns/m^2)
Water	4179	997.1	0.613	21	384	0.9576
Al_2O_3 Nanoparticles	765	3970	25	0.85	47	

Certain assumptions have been made for the present problem such as:

- All walls are impermeable.
- Radiation effect is negligible.
- Fluid is steady and laminar.
- Gravitational effect has considered in vertical direction.
- All properties of the fluid are constant except density which changes with temperature (Boussinesq approximation).

Based on these assumptions the dimensionless governing equations can be written, using the change of variables

$$X = \frac{x}{H}, Y = \frac{y}{H}, U = \frac{uH}{\alpha_f}, V = \frac{vH}{\alpha_f}, \theta = \frac{T - T_c}{T_h - T_c}, P = \frac{pH^2}{\rho_{nf}\alpha_f^2}, \Pr = \frac{\vartheta_f}{\alpha_f},$$

$$Ra = \frac{g\beta_f (T_h - T_c) H^3}{\alpha_f \vartheta_f} \quad (1)$$

as:

$$\frac{\partial U}{\partial X} + \frac{\partial V}{\partial Y} = 0 \quad (2)$$

$$U\frac{\partial U}{\partial X} + V\frac{\partial U}{\partial Y} = -\frac{\partial P}{\partial X} + \frac{\mu_{nf}}{\rho_{nf}\alpha_{nf}}\left(\frac{\partial^2 U}{\partial^2 X} + \frac{\partial^2 U}{\partial^2 Y}\right) \quad (3)$$

$$U\frac{\partial V}{\partial X} + V\frac{\partial V}{\partial Y} = -\frac{\partial P}{\partial Y} + \frac{\mu_{nf}}{\rho_{nf}\alpha_f}\left(\frac{\partial^2 V}{\partial^2 X} + \frac{\partial^2 V}{\partial^2 Y}\right) + \frac{(\rho\beta)_{nf}}{\rho_{nf}\beta_f} RaPr\theta \quad (4)$$

$$U\frac{\partial \theta}{\partial X} + V\frac{\partial \theta}{\partial Y} = \frac{\alpha_{nf}}{\alpha_f}\left(\frac{\partial^2 \theta}{\partial^2 X} + \frac{\partial^2 \theta}{\partial^2 Y}\right) \quad (5)$$

Boundary conditions

$$U(X,0) = U(X,1) = U(0,Y) = U(1,Y) = 0$$

$$V(X,0) = V(X,1) = V(0,Y) = V(1,Y) = 0 \quad (5)$$
$$\theta(0,0) = \theta(0,1) = 1, \theta(1,0) = \theta(1,1) = 0$$
$$\frac{\partial\theta}{\partial Y}(X,Y) = 0 \; between \; 0 < X < 1$$

3. Numerical methodology

The finite volume method has been used to solve the governing equations. It provides smooth solutions in the interior domain including the corners. The pressure based segregated SIMPLE algorithm is used because it is more appropriate for convergence than the other algorithms available in FLUENT [9]. Solutions are assumed to converge when the following convergence criterion is satisfied at every point in the solution domain:

$$\left|\frac{\phi_{new} - \phi_{old}}{\phi_{new}}\right| \leq 10^{-6} \quad (7)$$

where ϕ represent primary variables U, V, P, and θ [10].

The heat transfer coefficient in term of the local Nusselt number is expressed as:

$$Nu_x = \frac{hx}{k} = -\frac{k_{nf}}{k}\frac{\partial\theta}{\partial n} \quad (8)$$

where h is heat transfer coefficient, θ is dimensionless temperature and *n* denotes normal direction to the plane.

And the average Nusselt number as:

$$Nu = \frac{1}{H}\int_0^H Nu_x \, dY \quad (9)$$

4. Grid independency test and validation

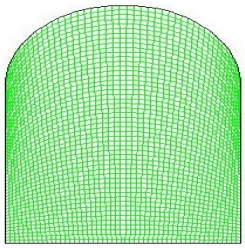

Fig 2: Grid structure for arch cavity

In this study, five different grid sizes (41×41, 51×51, 61×61, 71×71 and 81×81) are adopted to check the mesh independence. A uniform grid structure in arch cavity is shown in fig 2. A detailed grid independency test has been performed for average Nusselt number at Ra = 1×10^5 and φ = 0.05. The table 2 elucidate that the relative error value of the average Nusselt number is very less for grid size 51×51 and 61×61 compare to others. Since, at high grid size solution will take more time to converge the solution and the accuracy level is almost same. So 51×51 grid adopted for computational time limits.

Table 2: Relative error data at different grid size

Grid size	41×41	51×51	61×61	71×71	81×81
Nu	4.879	4.894	4.897	4.881	4.893
Relative Error	0.31%	0.061%	0.33%	0.25%	

The present work is validated with experimental result of Krane and Jesse [4] and numerical results of Khanefer [5] and Abu-Nada [6] at Ra = 1×10^5 and Pr = 0.7. The above dimensionless temperature and position graph shows the values of experimental and numerical results are varying within ± 12 %.

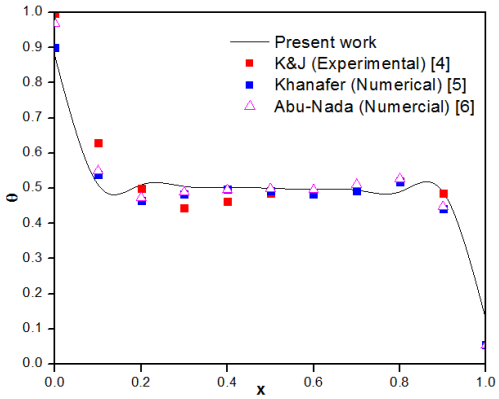

Fig. 3. Comparison between present work and other published data for temperature distribution along the width of the enclosure for nanofluid (Ra = 1×10^5 and Pr =0.7)

5. Results and discussions

Numerical analysis of free convection has been performed in an arch cavity. The Rayleigh number, curvature ratio and volume fraction are taken as governing parameters for heat transfer analysis. The effects of governing parameters on heat transfer are presented by average Nusselt number.

5.1. Effect of volume fractions

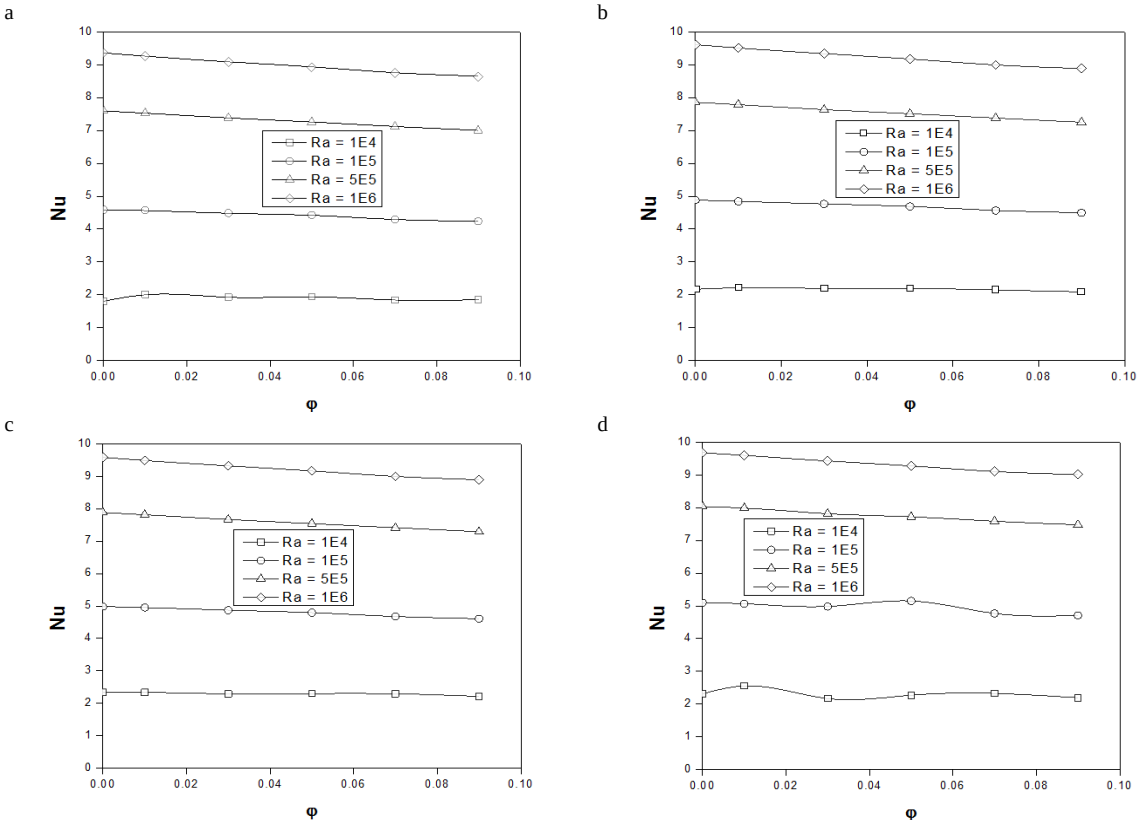

Fig 4: Average Nusselt number at different volume fractions for a) CR =1, b) CR = 1.16, c) CR = 1.33 and d) CR = 1.5

Fig. 4 (a) – (d) demonstrates the effect of solid volume concentration on heat transfer for different size of the enclosure. At φ = 1% and Ra = 10^4, variation in Nusselt number has been observed for CR = 1 and 1.5. But higher variation has been noticed in CR = 1.5 at φ = 5% and Ra = 10^5. From the above observation, it is clear that at low Ra and small volume fraction, heat transfer rate increases. Since, higher value of φ at low Ra renders the fluid more viscous which reduces the flow velocity. The reduction in velocity tends to reduce the convection current which leads to increase the thickness of the thermal boundary layer. These increment in boundary layer sluggish the heat transfer rate. Thus, the heat transfer rate decreases with the increase volume fraction. Meanwhile, at volume fraction 5% depicts the enhancement of average Nusselt number compare to other volume fractions which is shown in figure 4(d). The use of nanoparticles at low Ra number is more beneficial than at high Ra number. Water is more suitable for high Rayleigh number.

5.2. Effect of curvature ratio

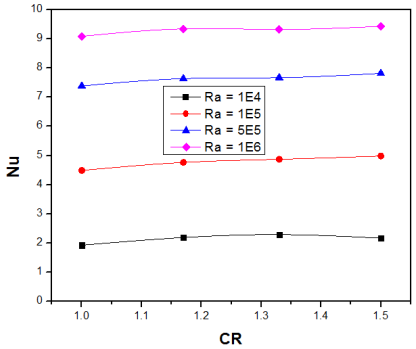

Fig. 8. Variation of average Nusselt number with curvature ratio for φ = 3%

Figure 5 portrays the variation in average Nussselt number with curvature ratio at φ = 3% for different Rayleigh number. Small enhancement in heat transfer rate is observed for low curvature ratio. But, with the increase of Rayleigh number, the heat transfer rate increases along with the increase of curvature ratio. Also, increment in nusselt number has been observed for low Ra at φ = 5% and higher value of Nu around 9.6 is reported at Ra = 10^6. Hence, arch cavity with CR= 1.5 is more useful than square and Low CR arch cavity.

5.3. Effect of Rayleigh number

a

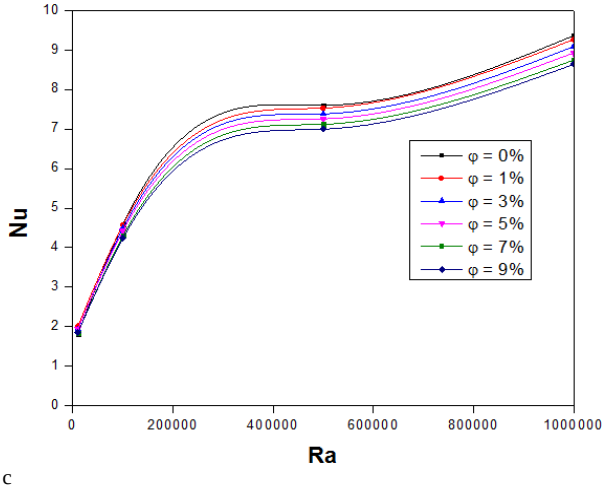

b

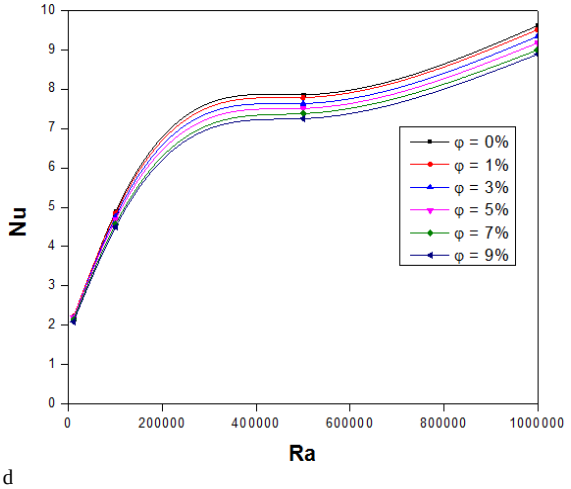

c d

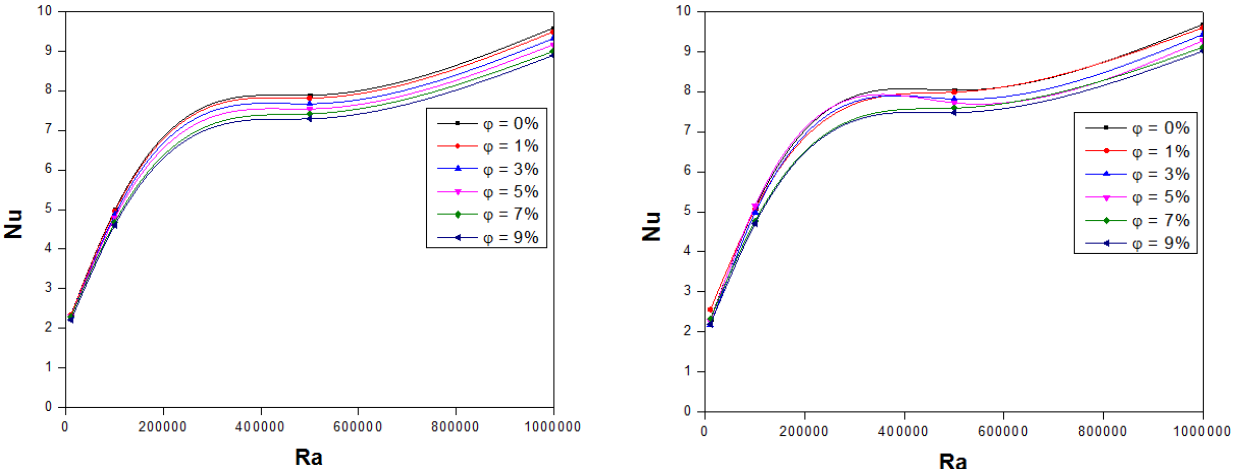

Fig 6: Variation of average Nusselt number with Rayleigh number for a) CR =1, b) CR = 1.16, c) CR = 1.33 and d) CR= 1.5

Figure 6 depicts the impacts of variation in Rayleigh number on heat transfer rate. The variation in Nu has been reported for various size of the arch cavity and for distinct volume fraction. The fluid velocity increases with the increase of Rayleigh number due to which convection current become dominant over conduction. This augmentation in convective heat transfer leads to enhance the nusselt number. The obtained results stated that the nusselt number is deteriorating with the higher value of φ and enhancing with the increase of curvature ratio.

6. Conclusion

The objective of the current numerical study was to investigate the effect of Rayleigh number, curvature ratio and volume fraction on the fluid flow and heat transfer in an arch cavity filled with Al_2O_3-water based nanofluid. It has been observed that the enclosure filled with Al_2O_3 based nanofluid shows a better heat transfer characteristics compared to enclosure filled with pure water at low Rayleigh number. Results revealed that the increasing Rayleigh number and curvature ratio enhances the convective heat transfer coefficient, while, increasing the nanofluid concentration increases the conductive heat transfer coefficient. From this investigation, the following conclusions have been drawn which are listed below:

- The enhancement in heat transfer by convection is more for water, while in case of nanofluid, enhancement in heat transfer is more due to conduction.
- The average Nusselt number diminishes with the increase of solid volume fraction (beyond 5%).
- The heat transfer rate increases with the increase in curvature ratio.
- At low Rayleigh number (Ra) = 1×10^5, high heat transfer is occurred at volume fraction (φ) = 0.05 and curvature ratio (CR) = 1.5.
- As expected, heat transfer rate increases with the increase in Rayleigh numbers.

References

[1] S. U. S. Choi, Enhancing Thermal Conductivity of Fluids with Nanoparticles, Development and Applications of Non-Newtonian Flows, FED-Vol. 231/MD-vol. 66, 1995, pp. 99-105.

[2] F. H. Lai et al., Lattice Boltzmann simulation of natural convection heat transfer of Al_2O_3/water nanofluids in a square enclosure, Int. J. Thermal science, 50 (2011) 1930-1941.
[3] D. Wen and Y. Ding, Formulation of nanofluids for natural convective heat transfer applications, Int. J.Heat and Fluid Flow, 26 (2005) 855-864.
[4] R.J. Krane and J. Jessee, Some Detailed Field Measurements for a Natural Convection Flow In A Vertical Square Enclosure, in: 1st ASME-JSME Thermal Engineering Joint Conference, vol. 1, 1983, pp. 323–329.
[5] K. Khanafer, Vafai, M. Lightstone, Buoyancy-driven heat transfer enhancement in a two-dimensional enclosure utilizing nanofluids. Int. J. Heat Mass Transfer, 46 (2003) 3639–3653.
[6] E. Abu-Nada et al., Effect of nanofluid variable properties on natural convection in enclosures, Int. J. Thermal Science, 49 (2010) 479-491.
[7] C. J. Ho et al., Numerical simulation of natural convection of nanofluid in a square enclosure: Effects due to uncertainties of viscosity and thermal conductivity, Int. J. Heat and Mass Transfer, 51 (2008) 4506-4516.
[8] M. A. Mansour et al., Numerical simulation of mixed convection flows in a square lid-driven cavity partially heated from below using nanofluid, Int. Communication in Heat and Mass Transfer, 37 (2010) 1504–1512.
[9]Fluent User's Guide, Release 6.3.26, Fluent Incorporated (2005-01-06).
[10]Patankar, Suhas V. (1980), "Numerical Heat Transfer and Fluid Flow" Taylor & Francis.

Available online at www.sciencedirect.com

ScienceDirect

Procedia Engineering 00 (2015) 000–000

Procedia Engineering

www.elsevier.com/locate/procedia

6th BSME International Conference on Thermal Engineering (ICTE 2014)

Stability of Al_2O_3-water Nanofluid for Electronics Cooling System

S.S. Khaleduzzaman[a], M.R. Sohel[a], R. Saidur[a,b*], J. Selvaraj[b]

[a]*Department of Mechanical Engineering, Faculty of Engineering, University of Malaya, 50603 Kuala Lumpur, Malaysia.*

[b]*UM Power Energy Dedicated Advanced Centre (UMPEDAC), Level 4, Wisma R & D, University of Malaya, 59990 Kuala Lumpur, Malaysia*

Abstract

For stability of nanofluid need to study, before going to passed it through the electronic device. Because need to more stability of nanofluid and avoid the sedimentation and clogging substance of nanofluid. Stability effect on rectangular shape minichannel heat sink is experimentally investigated for electronics cooling using nanofluids as coolants instead of water. Al_2O_3-water nanofluids with 0.10 to 0.25 vol. % of nanoparticle was used as coolants. From experiment result, final particle cluster size, microstructure, zeta potential, sedimentation, Transmission Electron microscope and photo capture method analyze for stability purpose. Shown the 0.10 vol. % was better performance on electronic cooling system respect of stability.

Peer-review under responsibility of organizing committee of the 6th BSME International Conference on Thermal Engineering (ICTE 2014).

Keywords: Stability; Minichannel; Nanofluid

1. Introduction

The stability of nanofluids is a critical factor in the evaluation of nanofluids. Stability of nanofluids must be taken into account in the investigation as this will affect the performance of any systems. Nanoparticles are able to coagulate easily with the period elapsed for its high surface energy. The aggregation of nanoparticles is a reason for sedimentation and decreases the thermal conductivity of nanofluids [1]. There are several ways which includes addition of surfactant, pH control and increase of ultrasonic time and vibration means to elevate the stability of

* Corresponding author.
E-mail address: saidur@um.edu.my; saidur912@yahoo.com (R. Saidur); phone: +603 7967 7611; fax: +603 7967 5317.

Peer-review under responsibility of organizing committee of the 6th BSME International Conference on Thermal Engineering (ICTE 2014).

nanofluids [2]. Ruan and M. Jacobi [3] reported that, ultrasonication is a common way to break up agglomerates and promote dispersion of nanoparticles into base fluids to get more stable nanofluid. Wen and Ding [4] studied on the stability of Al_2O_3-water nanofluid by using SDBS as dispersant followed by ultrasonication for 16-20 hours. Nanofluids only remained stable for a week. Ding, Alias [5] applied GA as dispersant, together with ultra-sonication, and high-shear mixing on CNT-water nanofluid and the stability was observed until two months.

After preparation, the sedimentation photograph of nanofluids can be captured by a camera after certain period of time. These photos can be observed and compared to evaluate the stability of nanofluids. Compared to other techniques, the drawback of this method is observation for long period of time is required [1]. On the other hand, sedimentation balance method can be used to measure the stability as well. The plate of sedimentation balance is immersed in the newly produced nanofluids. The weight of sediment nanoparticles during a particular time can be measured [2]. According to Stokes' law the sedimentation velocity (V) in a colloid can be expressed as follows Eq. (1).

$$V = \frac{2R^2}{9\mu}(\rho_p - \rho_l)g \tag{1}$$

The rate of sedimentation decreases with decreasing particle radius (R), density difference between the particle and the liquid ($P_\rho - P_l$), and increasing base liquid viscosity (μ). These are all important parameters for a kinetically stable nanofluid [6]. Each nanofluid was left to stand and the absorbency was measured by ultra violet visible spectrophotometer at regular intervals. The absorbency of the suspension is defined by Eq. (2).

$$A = \lg(I_i / I) = \varepsilon bc \tag{2}$$

Eq. (2) indicates that the absorbency is proportional to the mass fraction of the particles in suspension. Higher absorbency means higher mass fraction of nanoparticles in the solution, namely, the better dispersion of nanofluid [7].

It is observed that, stability of the nanofluids is still a big challenge before it can be successfully implemented in large scale applications. More research is required in terms of stability and simple and cost effective techniques in near future. For this circumstance, analyse the stability effect on minichannel heat sink using Al_2O_3-water nanofluid.

2. Methodology

For the examine purpose, prepare the Al_2O_3-water nanofluid where Al_2O_3 nanoparticle size was 13 nm received from manufactured by Sigma Aldrich, USA and waster as a base fluid. Follow the two steps method for prepare without add any surfactants by ultrasonic homogenizer machine.

From the literature have some instruments and methods that can rank the relative stability of nano suspension. The list includes UV–Vis spectrophotometer, zeta potential, sediment photograph capturing, TEM (Transmission Electron Microscopy) and SEM (Scanning Electron Microscopy), light scattering, three omega and sedimentation balance method. Therefore, the rate or percentage of sedimentation will be identified by analyzing gathered data [2]. In this research work used final particle cluster size, microstructure, zeta potential and sedimentation method for characterized nanofluid after preparation. The Zetasizer (Model 3000HS, Malvern, UK) was used to check the average particle cluster size and zeta potential after preparation of nanofluid. Transmission Electron microscope (TEM) (Model LIBRA 120, Zeiss, Germany) was used to capture the microstructures of nanofluid to analyze the nanoparticle distribution. After preparation, 10 ml of nanofluid was poured into small measuring cylinder. The

photos of the cylinders with nanofluids were captured after 30 days of preparation for stability inspection. Sedimentation of the nanofluids was observed referring to the photograph to examine the stability of the nanofluids.

3. Result & Discussion

Ultrasonication processes reduce the colloid size of particles and homogenize particles with fluid. The mean particle cluster size of nanoparticles using dynamic light scattering has shown in Fig. 1. Average cluster size was found to be 131.0 nm, It is proved that, the nanofluid passed through the minichannel without blocking the passages. Because, the width of the minichannel was 0.5 mm [8] that is enough larger compare to maximum cluster size that was approximated to be 220 nm from Fig. 1. Zeta potential analysis to quantify the stability of 0.10 vol. % of Al_2O_3-water nanofluid has been reported in Fig. 2. For this suspension the absolute Zeta potential value was found to be 53.6 mV as shown in Fig. 2. It is pronounced that the absolute Zeta potential value over 60 mV show excellent stability, above 30 mV are physically stable, below 20 mV has limited stability and lower than 5 mV are evident to agglomeration [9]. Therefore, the zeta potential value of this experiment is very near to excellent stability.

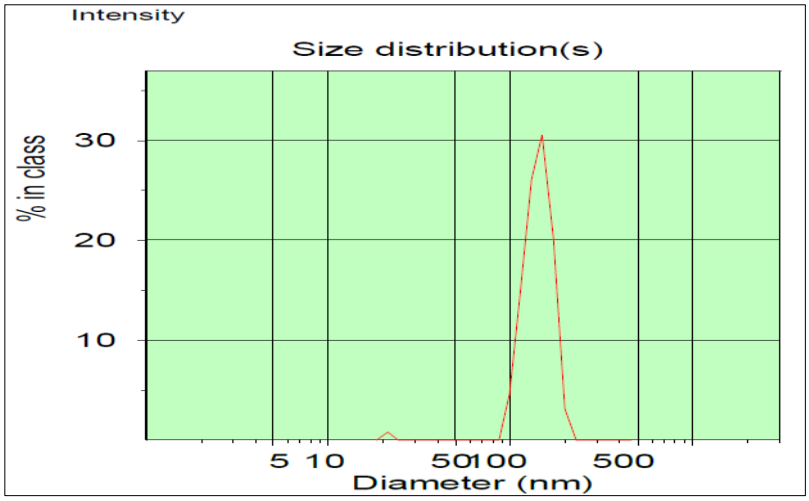

Fig. 1. Particle cluster size of 0.10 vol. % of Al_2O_3-water nanofluid.

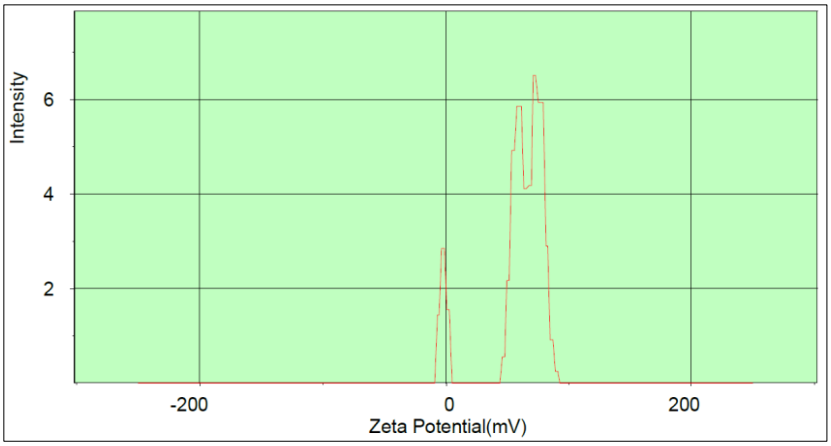

Fig. 2. Absolute Zeta potential of 0.10 vol. % of Al_2O_3-water nanofluid.

The microstructure and particle distribution have been captured using TEM. Fig. 3 shows the TEM image of 0.10 vol. % of Al_2O_3-water nanofluid after preparation. Good dispersion of particles has been observed in Fig. 3 within the range of 100 nm scales. Nevertheless, few overlapping of nanoparticles have also been observed.

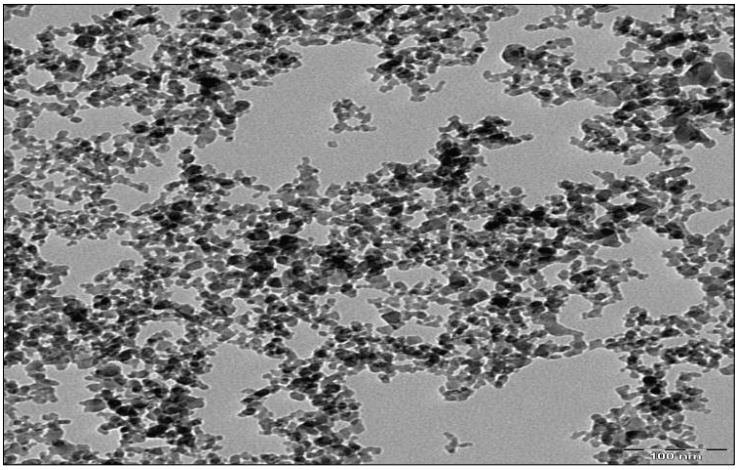

Fig. 3. The TEM microstructure of 0.10 vol. % Al_2O_3-water nanofluid.

The stability of the Al_2O_3-water nanofluid was examined by observing the photograph capturing method. The photos have been captured after 30 days of the nanofluids preparation and presented in Fig. 4.

It is clear from Fig. 4 that no sedimentation is formed at the bottom of the nanofluids. The supernatant levels are marked and found to be higher for lower concentration of nanofluid. At 0.10 vol. % there is no sedimentation and higher level of supernatant level have been observed. For 0.15 vol. % there is no sedimentation is obvious, but there have little amount of supernatant level. The supernatant level slowly decreases with the rise of nanoparticle volume fraction as they are observed in 0.20 vol. % to 0.25 vol. %. So it is conclude that, stability of nanofluid is good and it can avoid overcrowding problem in minichannel.

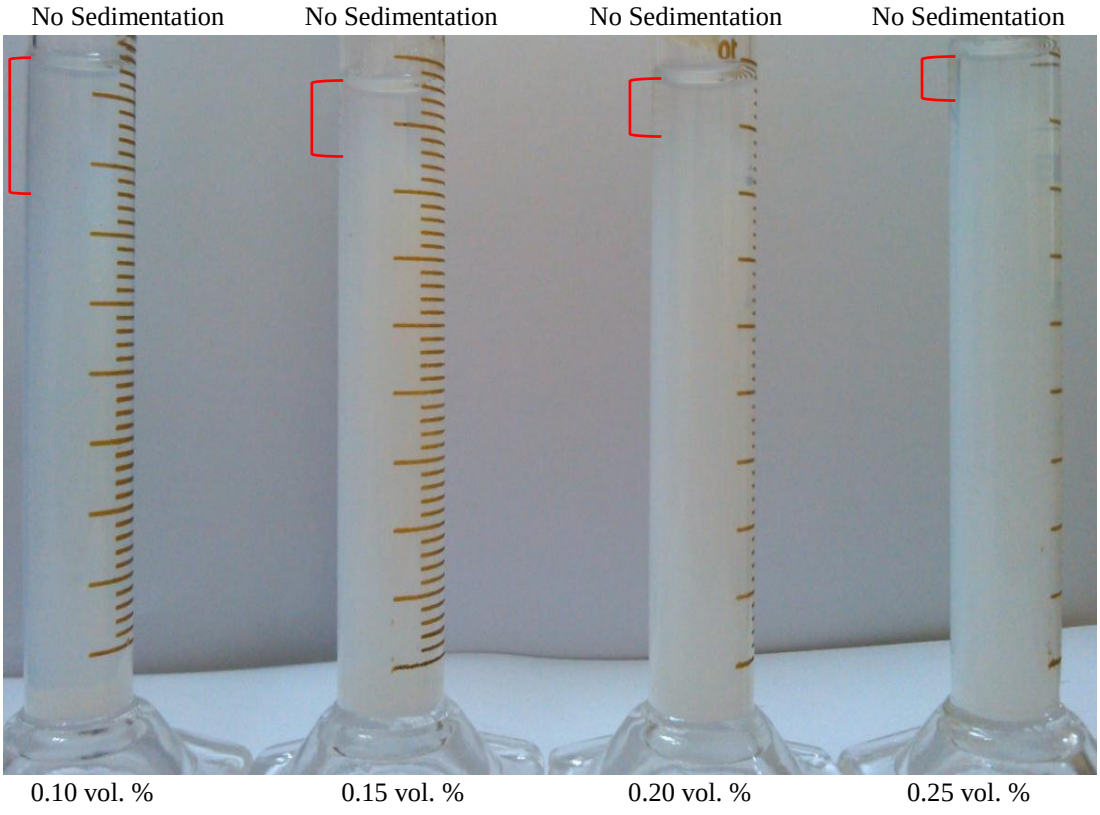

Fig. 4. The Al_2O_3-water nanofluids with various volume fractions after 30 days of preparation.

4. Conclusion

For characterization Zetasizer analyzer and TEM indicate that nanofluids are physically stable. The photo capture method refers to low rate of sedimentation at high volume fraction of nanofluids. The stability of nanofluid was excellent even at high volume fraction. Also nanoparticle size no matter for passed through the minichannel. Without sedimentation and clogging nanofluid passed in minichannel.

Acknowledgements

The authors would like to acknowledge the University of Malaya. This research is supported by High Impact Research MoE Grant UM.C/625/1/HIR/MoE/ENG/40 from the Ministry of Education Malaysia.

References

[1] Li, Y., et al., *A review on development of nanofluid preparation and characterization.* Powder Technology, 2009. **196**(2): p. 89-101.
[2] Ghadimi, A., R. Saidur, and H.S.C. Metselaar, *A review of nanofluid stability properties and characterization in stationary conditions.* International Journal of Heat and Mass Transfer, 2011. **54**(17–18): p. 4051-4068.
[3] Ruan, B. and A. M. Jacobi, *Ultrasonication effects on thermal and rheological properties of carbon nanotube suspensions.* Nanoscale Research Letters, 2012. **7**(1): p. 127-127.
[4] Wen, D. and Y. Ding, *Effective thermal conductivity of aqueous suspensions of carbon nanotubes (carbon nanotube nanofluids).* Journal of Thermophysics and Heat Transfer, 2004. **18**(4): p. 481-485.
[5] Ding, Y., et al., *Heat transfer of aqueous suspensions of carbon nanotubes (CNT nanofluids).* International Journal of Heat and Mass Transfer, 2006. **49**(1-2): p. 240-250.
[6] Witharana, S., et al., *Stability of glycol nanofluids — The theory and experiment.* Powder Technology, 2013. **239**(0): p. 72-77.
[7] Yang, L., et al., *Preparation and stability of Al2O3 nano-particle suspension of ammonia–water solution.* Applied Thermal Engineering, 2011. **31**(17–18): p. 3643-3647.
[8] Sohel, M.R., et al., *An experimental investigation of heat transfer enhancement of a minichannel heat sink using Al2O3–H2O nanofluid.* International Journal of Heat and Mass Transfer, 2014. **74**(0): p. 164-172.
[9] Müller, R.H., *Zetapotential and Partikelladung in der Laborpraxis*. First ed. 1996, Stuttgart: Wissenschaftliche Verlagsgesellschaft.

Available online at www.sciencedirect.com

ScienceDirect

Procedia Engineering 00 (2015) 000–000

Procedia Engineering

www.elsevier.com/locate/procedia

6th BSME International Conference on Thermal Engineering (ICTE 2014)

Convective performance of 0.1 % volume fraction of TiO_2/water nanofluid in an electronic heat sink

S.S. Khaleduzzaman[a], M.R. Sohel[a], R. Saidur[a,b*], J. Selvaraj[b]

[a]*Department of Mechanical Engineering, Faculty of Engineering, University of Malaya, 50603 Kuala Lumpur, Malaysia.*

[b]*UM Power Energy Dedicated Advanced Centre (UMPEDAC), Level 4, Wisma R & D, University of Malaya, 59990 Kuala Lumpur, Malaysia*

Abstract

Heat dissipation is critical issue in modern electronic component due to rise heat flux and decrease the feature size. This present work TiO_2/water nanofluids of only one volume fraction 0.1% are prepare by dispersing the nanoparticle in distil water. Fluid pass through a thin channelled copper water block of overall dimension (94×94×20) mm with flow rate of 1.0, 1.25, 1.50 l/min used for the analysis. The base temperature of water block was minimum for nanofluid compare with water. The heat transfer coefficient found maximum improved 18.91 % compare with water.

Peer-review under responsibility of organizing committee of the 6th BSME International Conference on Thermal Engineering (ICTE 2014).

Keywords: Nanofluid, water block, heat transfer coefficient

1. Introduction

The electronic chips integration and compaction rise at high level with technological advances recently. Due to electronics chip more component and offer more processing power than ever before. Increase the power dissipation

* Corresponding author.
E-mail address: saidur@um.edu.my; saidur912@yahoo.com (R. Saidur); phone: +603 7967 7611; fax: +603 7967 5317.

Peer-review under responsibility of organizing committee of the 6th BSME International Conference on Thermal Engineering (ICTE 2014).

electronics chip more component and offer more processing power than ever before. Increase the power dissipation per unit area from few past decades [1, 2].

Nomenclature

A	area (m^2)	h	Heat transfer coefficient ($W/m^2.K$)
H	Height of channel (m)	L	Channel length (m)
n	number of channels	Q	heat generation (W)
R	thermal resistance (K/W)	T	temperature (K)
W	Channel width (m)	ch	channel
b	base		

Huang, Weng [3] investigated the thermal performance of a thermoelectric water-cooling device for electronic equipment. They developed a novel analytical model of a thermal analogy network to predict the thermal capability of the thermoelectric device. Peng and Peterson [4] experimentally showed the single-phase forced convective heat transfer and flow characteristics of water in microchannel structures/plates with small rectangular channels. The results indicated that the geometric configuration had a significant effect on the single-phase convective heat transfer and flow characteristics for both laminar and turbulent flow. Heat transfer improvement can be made by increasing either heat transfer area or heat transfer co-efficient [5]. Selvakumar and Suresh [6]passed Cuo-water nanofluid through the water block; they found the maximum rise of heat transfer coefficient 29.63 % for 0.2 vol. % compare with water. Roberts and Walker [7]study on water block with alumina based nanofluid, they observer the enhancement of heat transfer up to 1.5 vol. % of nanofluid. Putra, Yanuar [8] investigate the heat pipe liquid block combined with the thermoelectric system has a significant effect on heat transfer from the CPU by using alumina and titania (TiO_2) nanoparticle with water as base fluid.

This study focuses on the effect of volume concentration of nanoparticles on flow rates, heat transfer coefficient, and thermal resistance for a water block heat sink.

2. Methodology

Pure 99.50% Titania (TiO_2) nanoparticles (21 nm) were received from manufactured by Sigma Aldrich, USA. Nanofluids of 0.10 vol. % with water as the base fluid of pure distilled. Used Sonic Dismembrator System (FB505, Fisher Scientific, USA) for cell disruption and homogenization applications. Ultrasonicated continued for 2 hours without adding any surfactant.

The schematic diagram of the experimental set up is depicted in Fig. 1, which is a closed loop for cooling of electronic system consisting of water block, cooling fluid loop and data acquisition system. The experimental apparatus is also shown in Fig. 2.

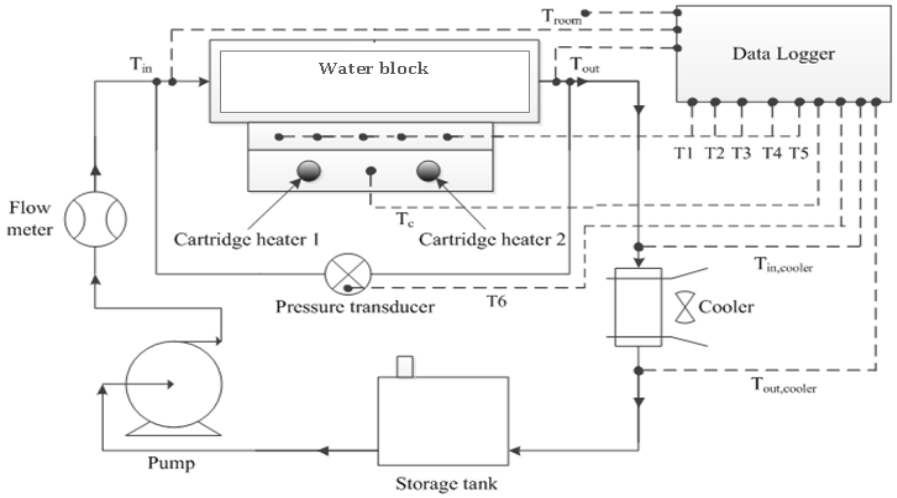

Fig. 1. Schematic diagram of experimental set up.

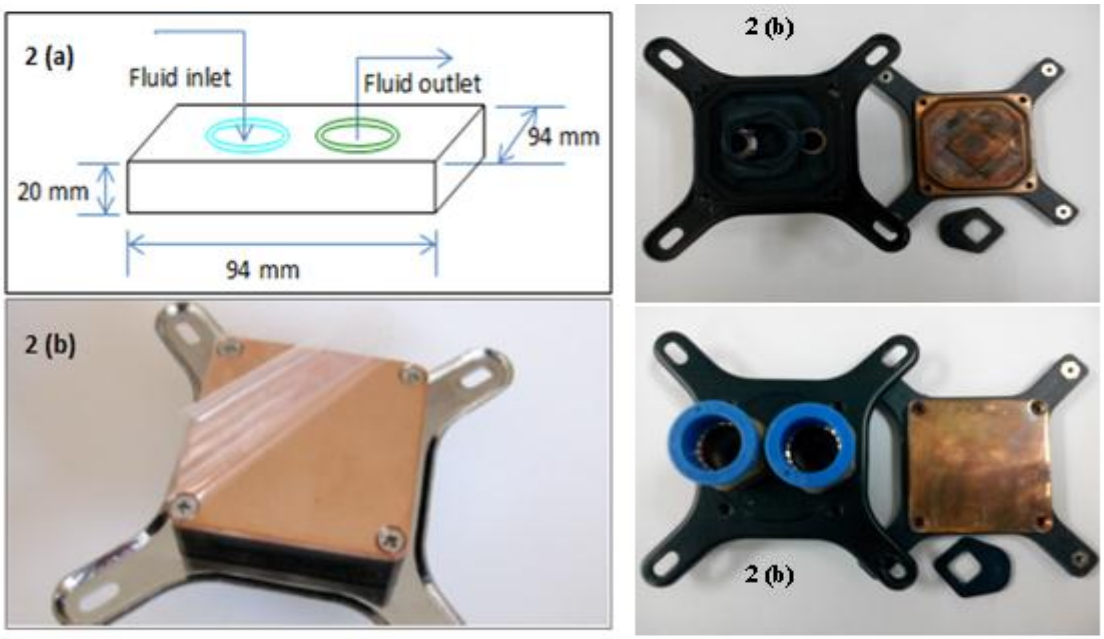

Fig. 2. (a) Schematic view of water block, and (b) Photograph of water block.

The connection within the piping system and the test section are designed such that parts can be changed or repaired easily. The closed loop consists of storage tank, pump, flow meter, and air cooled radiator. First, working fluid is chilled by the surrounding air. After the fluid is cooled to the desired level, a pump (model: XSPC X20 750) is used to pump it out of the storage tank, and then is passed through a flow meter, water block The coolant absorbs the heat from the heat sink and becomes hot. An air-cooled radiator type cooler (model: SSPC RS360) is used to cool down the coolant before entering the storage tank for recirculation. The flow rates of the coolant are controlled by adjusting the flow meter. A pressure transducer is also installed across the heat sink to measure the pressure drop.

The base temperature of the water block is calculated using Eq. (1) where the base height effect is considered.

$$T_b = T_{b,(av,tc)} - \left(\frac{QH_b}{k_{hs} A_b} \right) \tag{1}$$

Where, the area of base of water block is obtained by Eq. (2)

$$A_b = Ln(W_{ch} + W_{fin}) \tag{2}$$

The thermal resistance is defined by Eq. (3).

$$R_{th} = \frac{T_b - T_{nf,in}}{Q} \tag{3}$$

From the collected data of temperatures and mass flow rates, the convective heat transfer coefficient of the heat sink (h), can easily be determined based on the heat balance equation of the latter, which is written as follows Eq. (4):

$$h = \frac{Q}{A_{sf}(T_b - T_{m,nf})} \tag{4}$$

Where, mean temperature of nanofluid is determined using Eq. (5).

$$T_{m,nf} = \frac{(T_{nf,in} + T_{nf,out})}{2} \tag{5}$$

The surface area available for heat transfer is counted by Eq. (6).

$$A_{sf} = nW_{ch}L + 2n\eta H_{ch}L \tag{6}$$

Where, *n* is the number of cooling channels and fin efficiency is 100% due to high thermal conductivity of copper. Fin efficiency of water block was computed by Eq. (7) and (8). The fin efficiency (η_{fin}) is calculated by Eq. (7) and (8).

$$m \times H_{ch} = \sqrt{\frac{2h}{k_{hs}W_{fin}}} \times H_{ch} \tag{7}$$

Where, k_{hs} is thermal conductivity of the copper microchannel heat sink.

$$\eta_{fin} = \frac{\tanh(m \times H_{ch})}{m \times H_{ch}} \tag{8}$$

3. Result and discussion

The base temperature measured between the heated and water block is an indication of performance of the cooling system. The effect of TiO_2/water nanofluids of volume concentrations 0.1% on base temperature at different volume flow rate of water and nanofluids is shown in Fig. 3. It is clear from the figure that the interface temperature reduces with increasing volume flow rate of the water and TiO_2/water nanofluids. The volume flow rate of the water and nanofluids are varied from 1.0 LPM to 1.5 LPM. At the minimum volume flow rate of 1.0 LPM the temperature gain obtained for 0.1% volume concentration TiO_2/water nanofluids compared to water are 6.40 ºC. At a maximum volume flow rate of 1.5 LPM, the base temperature obtained for 0.1% volume concentration TiO_2/water nanofluid is 64.18 ºC which is 2.17 ºC lower than the temperature obtained for water. It can be understood from the values of base temperature that the nanofluids remove more heat from the heated block compared to water and keep the base temperature minimum.

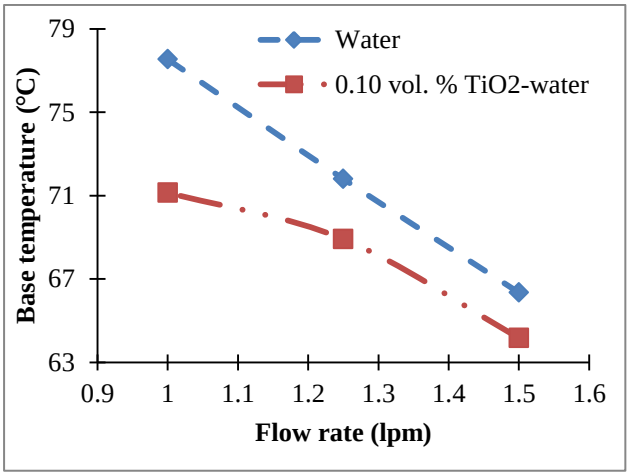

Fig. 3. Effect of volume flow rate on base temperature.

The thermal resistance decreases with the rise of flow rate and nanoparticle volume fraction compared with water as demonstrated in Fig. 4. The minimum thermal resistance was found at 1.50 l/min flow rate for 0.1 vol. %. The maximum reduction of thermal resistance (17.76 %) occurred at 1.5 l/min flow rate for 0.1 vol. % of TiO_2-water nanofluid. This significant reduction in thermal resistance, acts as a motivation to use nanofluid as an electronics coolant.

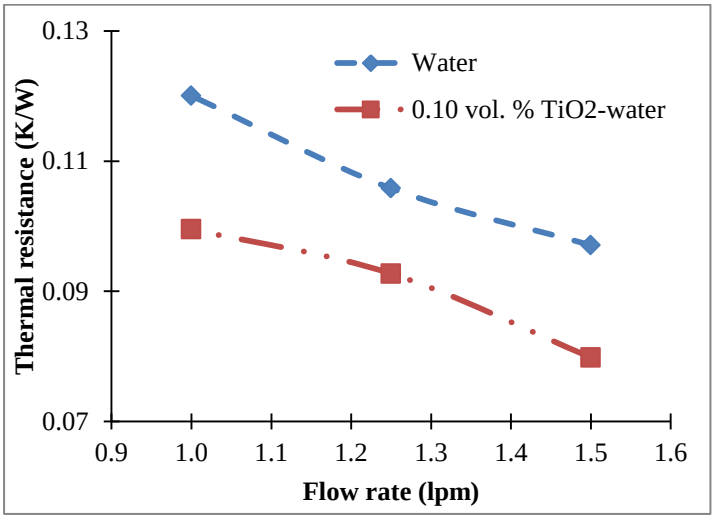

Fig. 4. Thermal resistance with flow rate.

The heat transfer coefficient augmented with the nanoparticle volume fraction compare with water. In fig. 5 it is shown that the maximum heat transfer coefficient enhancement was found to be 18.91% for 0.1 vol. % at 1.0 l/min flow rate compared with water as the base fluid. The results indicate that the tread are increasing with the rise of flow rate.

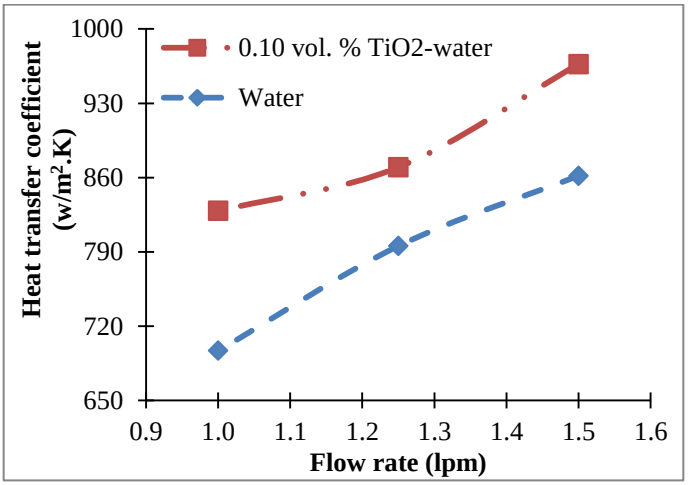

Fig. 5. Effect of flow rate with Heat transfer coefficient.

4. Conclusion

The effect of TiO_2/water nanofluid in water block with studied with different flow rate. As a result of base temperature of water block reduction by nanofluid rather than water. Also the heat transfer coefficient improves 18.91%. It indicates that nanofluid is good candidate of coolant for cooling of electronics devices.

Acknowledgements

The authors would like to acknowledge the University of Malaya. This research is supported by High Impact Research MoE Grant UM.C/625/1/HIR/MoE/ENG/40 from the Ministry of Education Malaysia.

References

[1] Bash, C.E., C.D. Patel, and R.K. Sharma, *Efficient Thermal Management of Data Centers—Immediate and Long Term Research Needs.* HVAC&R Research, 2003. **9**(2): p. 137-152.
[2] Shah, A.J., et al., *An Exergy-Based Figure-of-Merit for Electronic Packages.* Journal of Electronic Packaging, 2006. **128**(4): p. 360-369.
[3] Huang, H.-S., et al., *Thermoelectric water-cooling device applied to electronic equipment.* International Communications in Heat and Mass Transfer, 2010. **37**(2): p. 140-146.
[4] Peng, X.F. and G.P. Peterson, *Convective heat transfer and flow friction for water flow in microchannel structures.* International Journal of Heat and Mass Transfer, 1996. **39**(12): p. 2599-2608.
[5] Saidur, R., K.Y. Leong, and H.A. Mohammad, *A review on applications and challenges of nanofluids.* Renewable and Sustainable Energy Reviews, 2011. **15**(3): p. 1646-1668.
[6] Selvakumar, P. and S. Suresh, *Convective performance of CuO/water nanofluid in an electronic heat sink.* Experimental Thermal and Fluid Science, 2012. **40**: p. 57-63.
[7] Roberts, N.A. and D.G. Walker, *Convective Performance of Nanofluids in Commercial Electronics Cooling Systems.* Applied Thermal Engineering, 2010. **30**(16): p. 2499-2504.
[8] Putra, N., Yanuar, and F.N. Iskandar, *Application of nanofluids to a heat pipe liquid-block and the thermoelectric cooling of electronic equipment.* Experimental Thermal and Fluid Science, 2011. **35**(7): p. 1274-1281.

Available online at www.sciencedirect.com

ScienceDirect

Procedia Engineering 00 (2015) 000–000

Procedia Engineering

www.elsevier.com/locate/procedia

6th BSME International Conference on Thermal Engineering (ICTE 2014)

Natural Convection and Entropy Generation in a Nanofluid-Filled Semi-Circular Enclosure with Heat Flux Source

Ali Al-Zamily[a], M. Ruhul Amin[b]*

[1]*Department of Mechanical Engineering, Babylon University, Babylon, Iraq*
[b]*Deptarment of Mechanical & Industrial Engineering, Monatna State University, Bozeman, MT 59717, USA*

Abstract

The effect of present of nanoparticles on natural convection and entropy generation in a semi-circular enclosure with present heat flux is investigated numerically in the present work. The enclosure is filled with nanofluids (Cu-water). The heat flux is supplied partly in the center of the base wall, and the other parts of base wall of the enclosure are assumed adiabatic. The center of the circular arc ($-45°\leq\gamma\leq+45°$) is assumed at constant cold temperature and the other parts of the circular arc are adiabatic. Finite element method based on the variational formulation is employed to solve momentum and energy as well as post-processing streamfunctions. The results are based on visualization of isotherms, streamfunction and entropy generation. Comparison with previously published work is performed and the results are found to be in a good agreement. The influence of pertinent parameters such as Rayleigh number ($10^4\leq Ra\leq 10^7$) and solid volume fraction of nanoparticles ($0\leq\Phi\leq 0.15$ step 0.05) on the flow, temperature, and entropy generation are examined in the present paper. The results show that the heat transfer rate increases with an increase of the Rayleigh number and the nanoparticles volume fraction. The system irreversibility increases as nanoparticles fraction increase.

Peer-review under responsibility of organizing committee of the 6th BSME International Conference on Thermal Engineering (ICTE 2014).

Keywords: Nanofluid; Natural Convection; Entropy Generation.

1. Introduction

The problem of natural convection in enclosures has many engineering applications such as the cooling systems of electronic components, the building and thermal insulation systems, the built-in-storage solar collectors, the nuclear reactor systems, the food storage industry and the geophysical fluid mechanics [1]. Various techniques have been

* Corresponding author. Tel.: +1-406-994-6295; fax: +1-406-994-6295.
E-mail address: ramin@me.montana.edu

Peer-review under responsibility of organizing committee of the 6th BSME International Conference on Thermal Engineering (ICTE 2014).

proposed to enhance the convection heat transfer performance of fluids inside the enclosure. Convective heat transfer can be enhanced by changing flow geometry, boundary conditions and by enhancing thermal conductivity of the fluid.

The effect of flow geometry on the natural convection was investigated in many researches. Different cavities shape were studied: rectangular [2], triangular [3], trapezoidal [4], sinusoidal [5], octagonal [6], prismatic [7] and annulus area [8]. Different boundary conditions had been employed for the convection heat transfer inside cavity, like: constant wall temperature and constant heat flux. The present of heat flux inside enclosure which is filled with nanofluid had been studied in different works. Aminossadati and Ghasemi, [9], numerically analyzed natural convection inside a cavity embedded with heat source on the bottom wall and filled with nanofluids. Their results indicated that the adding of nanoparticles into pure water improves its cooling performance especially at low Rayleigh numbers. Mahmoudi et al [10], studied the entropy generation and heat transfer in natural convection flow inside enclosure which is filled by nanofluid (Cu-water). Their analysis has been done for a two dimensional trapezoidal enclosure with the left vertical wall and inclined walls kept in a constant cold temperature and a heat flux source embedded on the bottom wall. The results show that at $Ra=10^4$ and 10^5 the enhancement of the Nusselt number increases due to presence of nanoparticles.

The present study may be encountered in a number of electronic cooling devices equipped with nanofluids. Hence, the main purpose of present analysis is to be investigate numerically the effects of a present of nanoparticles on the natural convection and entropy generation inside semi-circular cavity. The study is performed for various values of Rayleigh number ($10^4 \leq Ra \leq 10^7$) and volume fraction of the nanoparticles ($0 \leq \Phi \leq 0.15$ step 0.05).

Nomenclature

q"	heat flux (W/m^2)
Pr	Prandtl number
T	temperature (K)
Be	Bejan number
Ra	Rayleigh number
Nu	Nusselt number on the heat source surface
U	dimensionless velocity component in x-direction
V	dimensionless velocity component in y-direction
X	dimensionless coordinate in horizontal direction
Y	dimensionless coordinate in vertical direction
α	thermal diffusivity (m^2/s)
ε	length of heat source at base wall (m)
ψ	dimensionless stream function
μ	dynamic viscosity (kg.s/m)
Φ	nanoparticle volume fraction
ζ	dimensionless length of base heat source (ε/Lc)

2. Problem description and assumptions

The physical model of the present study shows in Fig.1. It consists of a two dimensional semi-circular cavity of radius(r). A heat source with length (2ε) is embedded on the enclosure base wall. The remaining boundary parts of the base wall are thermally insulated. The center of the circular arc ($-45° \leq \gamma \leq +45°$) kept at constant cold temperature (T_c) and the other parts of the boundary circular arc are adiabatic. The fluid in the enclosure is a nanofluid (Cu-water).

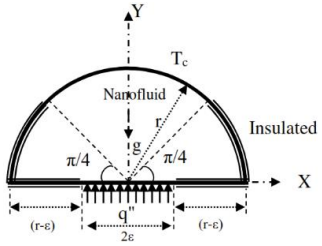

Fig. 1. Schematic of the case study.

The assumptions that used here as follows [1]: the nanofluid are assumed to be Newtonian and incompressible. The flow is assumed to be laminar. The base fluid and the nanoparticles are assumed to be in thermal equilibrium and no slip occurs between them. Thermophysical properties of the nanofluid are assumed to be constant except the density variations causing a body force term in the vertical component of momentum equation.

3. Mathematical formulation and simulation

The final governing equations (mass, momentum and energy) for steady state two-dimensional natural convection in the semi-circular cavity can be written with following dimensionless variables or numbers [9]:

$$X=\frac{x}{L_c}, Y=\frac{y}{L_c}, U=\frac{uL_c}{\alpha_f}, V=\frac{vL_c}{\alpha_f}, P=\frac{pL_c^2}{\rho_{nf}\alpha_f^2}, \theta=\frac{T-T_c}{\Delta T}, \Delta T=\frac{q^{''}L_c}{k_f}, Ra=\frac{g\beta_f L_c^2\Delta T}{\nu_f\alpha_f}, \qquad Pr=\frac{\nu_f}{\alpha_f}$$

$$\frac{\partial U}{\partial X}+\frac{\partial V}{\partial Y}=0 \tag{1}$$

$$U\frac{\partial U}{\partial X}+V\frac{\partial U}{\partial Y}=-\frac{\partial P}{\partial X}+\frac{\mu_{nf}}{\rho_{nf}\alpha_f}\left(\frac{\partial^2 U}{\partial X^2}+\frac{\partial^2 U}{\partial Y^2}\right) \tag{2}$$

$$U\frac{\partial V}{\partial X}+V\frac{\partial V}{\partial Y}=-\frac{\partial P}{\partial Y}+\frac{\mu_{nf}}{\rho_{nf}\alpha_f}\left(\frac{\partial^2 V}{\partial X^2}+\frac{\partial^2 V}{\partial Y^2}\right)-\frac{(\rho\beta)_{nf}}{\rho_{nf}\beta_f}Ra\,Pr\,\theta \tag{3}$$

$$U\frac{\partial \theta}{\partial X}+V\frac{\partial \theta}{\partial Y}=\frac{\alpha_{nf}}{\alpha_f}\left(\frac{\partial^2 \theta}{\partial X^2}+\frac{\partial^2 \theta}{\partial Y^2}\right) \tag{4}$$

Here, ρ_{nf} is the effective density of the nanofluid defined as: $\rho_{nf}=(1-\Phi)\rho_f+\Phi\rho_p$. According to Brinkman's formula [1], the effective dynamic viscosity of the nanofluid as: $\mu_{nf}=\frac{\mu_f}{(1-\Phi)^{2.5}}$. The thermal expansion coefficient of the nanofluid is given by: $(\rho\beta)_{nf}=(1-\Phi)(\rho\beta)_f+\Phi(\rho\beta)_p$. The thermal diffusivity of the nanofluid is given by: $\alpha_{nf}=\frac{k_{nf}}{(\rho C_p)_{nf}}$, where k_{nf} is the nanofluid thermal conductivity is given by:$k_{nf}=k_f\frac{(k_p+2k_f)-2\Phi(k_f-k_p)}{(k_p+2k_f)+\Phi(k_f-k_p)}$.The nanofluid heat capacitance is:$(\rho C_p)_{nf}=(1-\Phi)(\rho C_p)_f+\Phi(\rho C_p)_p$. The thermophysical properties of the base fluid and the nanoparticles in this study are given in Table 1 as reported in [9].

Table 1. Thermophysical properties of base fluid and nanoparticles [9].

Properties	Water	Cu
Cp (J/kg.K)	4179	385
K (W/m.K)	0.613	401
ρ (kg/m^3)	997.1	8933
β(1/K)×10^5	21	1.67

The fluid motion is described using the streamfunction that obtained from velocity components U and V. The relationships between streamfunction and velocity components for two dimensional flows are [1]:

$$U=\frac{\partial \psi}{\partial Y}, V=-\frac{\partial \psi}{\partial X} \qquad \frac{\partial^2 \psi}{\partial X^2}+\frac{\partial^2 \psi}{\partial Y^2}=\frac{\partial U}{\partial Y}-\frac{\partial V}{\partial X} \tag{5}$$

The no-slip condition is valid at all boundaries as there is no cross flow, hence ψ = 0 is used as residual equations at the nodes for the boundaries.

The boundary conditions that combined with the governing equations (Eqs. 1-5), as following:

At horizontal base wall

For $Y=0$, $-1\le X\le -\zeta$ and $\zeta\le X\le 1$ $\quad U(X,0)=V(X,0)=0,\ \frac{\partial\theta}{\partial Y}=0, \psi=0$

For $Y=0$ and $-\zeta\le X\le\zeta$ $\quad U(X,0)=V(X,0)=0,\ \frac{\partial\theta}{\partial Y}=-\frac{k_f}{k_{nf}}, \psi=0$

At circular arc

For $0 \le \gamma \le 45°$ and $135° \le \gamma \le 180°$, $X = \cos(\gamma)$, $Y = \sin(\gamma)$ $U(X,Y) = V(X,Y) = 0, \frac{\partial\theta}{\partial n} = 0, \psi = 0$
For $45° \le \gamma \le 135°$, $X = \cos(\gamma), Y = \sin(\gamma)$ $U(X,Y) = V(X,Y) = 0, \theta = 0, \psi = 0$

The local Nusselt number on the heat sources can be defined as follows: $Nu(x) = \frac{hL_c}{k_f}$ Where $h = \frac{q''}{T_s - T_c}$. Rearranging the local Nusselt number at the heat source by using the temperature dimensionless. The local Nusselt number at constant heat flux is obtained for the nanofluid case using the following relation: $Nu(X) = \frac{1}{\theta_s(X)}$, Where, θ_s is the dimensionless heat source temperature. The average Nusselt number is determined by integration local Nusselt number along the heat source.

$$\overline{Nu} = \frac{1}{2\zeta}\int_{-\zeta}^{\zeta} Nu_s(X)dX = \frac{1}{2\zeta}\int_{-\zeta}^{\zeta} \frac{dX}{\theta_s(X)} \tag{6}$$

The local entropy generation rate produced in cavity has two different sources; heat flow and viscous dissipation. The local entropy generation rate can be written as [10]:

$$S_{gen} = S_{gen,T} + S_{gen,\mu} = \frac{k_{nf}}{k_f}\left[\left(\frac{\partial\theta}{\partial X}\right)^2 + \left(\frac{\partial\theta}{\partial Y}\right)^2\right] + \chi\left[2\left(\frac{\partial U}{\partial X}\right)^2 + 2\left(\frac{\partial V}{\partial Y}\right)^2 + \left(\frac{\partial U}{\partial Y} + \frac{\partial V}{\partial X}\right)^2\right] \tag{7}$$

Where $\chi = \frac{T_o U_o^2}{\Delta T^2}\frac{\mu_{nf}}{k_f}$. The first and second terms on the right hand side of the Eq.8 represent the entropy generation produced by heat flow and viscous dissipation, respectively. To evaluate the total entropy generation rate it is necessary to integrate the local entropy generation rate over a unit area of the cavity. The Simpson numerical method is used for integration over a unit area. The non-dimensional total entropy generation is obtained through the integration of the local entropy generation in all computational domains, as indicated in equation, $\dot{S}_{gen} = \int S_{gen}\, dA$. An alternative parameter for irreversibility distribution is the Bejan number defined as:

$$B_e = \frac{\dot{S}_{gen,T}}{\dot{S}_{gen}} \tag{8}$$

4. Numerical Method and Validation

The main equations (Eqs. 1-5) were discretized using finite element method based on the variational formulation. A non-uniform triangular mesh arrangement is implemented especially near the walls to capture the rapid changes in the dependent variables. In the present analysis to predict the final steady state velocity, temperature and pressure, an improvement over Chorin's algorithm, given by Rannacher is used here [1]. Convergence criteria for streamfunction and temperature are: $\frac{\sum_{i=1}^{No.of\ nodes}|\eta_i^{m+1} - \eta_i^m|}{\sum_{i=1}^{No.of\ nodes}|\eta_i^{m+1}|} \le 10^{-7}$, where η represents ψ or θ.

Accuracy testing for the grid sensitivity is examined to ensure the grid-independence solutions. Series of trial calculation of different non-uniform grid systems for the case: nanofluid (Cu-water) with Φ=0.1, ε=r/2, L_c=r and $Ra=10^5$ were conducted as shown in table 2. From these comparisons, the difference between the results of the elements 5576 and that of the elements 6997 is very small. In order to optimize appropriate grid refinement with computational efficiency, it is suggested that 5576 non-uniform elements is sufficient to produce an accurate results.

Table 2. Accuracy testing results.

No. of element	$\lvert\psi_{max}\rvert$	θ_{max}	$\overline{Nu}$
2154	3.49759	0.350552	5.0854
3083	3.49456	0.350569	5.08402
4131	3.4955	0.350593	5.0827
5576	3.49132	0.350604	5.08111
6997	3.4914	0.350608	5.0810

The accuracy of the present numerical study was checked against a published numerical results of Aminossadati

and Ghasemi [9] for natural convection with present heat source embedded. The results for average Nusselt number, maximum temperature and streamfunction showed relative very low differences (Table 3.).

Table 3. The nanofluid (Cu- water) (Φ=0.1).

Ra	$\lvert\psi_{max}\rvert$		θ_{max}		$\overline{Nu}$	
	[9]	Present	[9]	Present	[9]	Present
10^3	0.023	0.022	0.205	0.21	5.45	5.56
10^4	0.251	0.248	0.205	0.202	5.47	5.57
10^5	2.988	2.96	0.172	0.171	7.12	7.19
10^6	11.593	11.5	0.107	0.107	13.8	13.42

5. Results and Discussion

The results of the present study are computed for different values of Rayleigh number ($10^4 \leq Ra \leq 10^7$) and nanoparticles volume fraction ($0 \leq \Phi \leq 0.15$ step 0.05). The base fluid is water with (Pr=6.2). The heat sources length (ζ=0.5) is considered for all cases. The characteristic length equal the radius of the enclosure (L_c=r). In all figures, the nanofluid represented by solid lines (——) and the pure water by dashed lines (- - - -).

5.1. Streamfunction

The strength of convection heat transfer is evaluate using streamfunction. The effect of nanoparticle volume fraction on the streamfunction is plotted in Fig.2 for different values of Rayleigh. For all cases, the buoyancy forces is generated due to the fluid temperature differences. The hot fluid over the heat source rises from the middle portion of the bottom wall to the upper cold wall. The rising hot fluid that gets blocked at the top adiabatic wall, which turns the flow and then descends downwards along the curved adiabatic wall and turns back to the central region after hitting the bottom wall. This processing creates two symmetrical cells with anticlockwise and clockwise rotations inside the enclosure. Because of the symmetrical boundary conditions about the vertical Y-axis, the streamfunction is symmetric about the vertical centerline of the enclosure. The flow inside the enclosure are controlled by these cells.

The maximum streamfunction increases as the Ra increases. This is due to increase the fluid motion and velocity and then increase streamfunction. While, the maximum streamfunction decreases as the nanoparticle volume fraction increases due to decrease the fluid movement and increase the fluid density. The core center of the streamfunction is moving toward the upper curved surface with increasing of the nanoparticle volume fraction. The table 4 shows the change of the maximum streamfunction with Rayleigh and nanoparticles volume fraction.

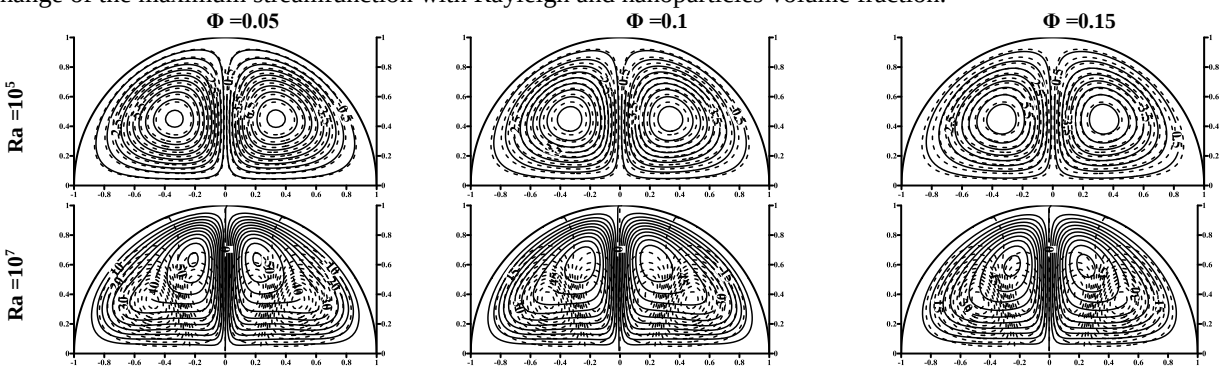

Fig. 2. Streamfunction.

Table 4. The maximum streamfunction.

Φ	$Ra=10^4$	$Ra=10^5$	$Ra=10^6$	$Ra=10^7$
0	2.96148	10.4573	26.5423	58.2011
0.05	2.43411	9.74823	26.616	55.8727
0.1	1.79271	8.9846	24.335	52.3449
0.15	1.10721	8.14714	22.869	51.4386

5.2. Isotherms

The effect of the nanoparticle volume fraction on the isotherms for different values Rayleigh plots in Fig.3. Because of the symmetrical boundary conditions about Y-axis, the isotherms is symmetrical about the vertical centerline of the enclosure. The maximum isotherms increases as the Rayleigh number decreases due to decrease the fluid movement and reduce the heat removed by the fluid. The maximum isotherms decreases as the nanoparticles volume fraction increases due to increase the conduction effect and then increase the heat removed. The effect of the nanoparticles volume fraction on the maximum isotherms increases at lower Rayleigh than for high Rayleigh due to increase the conduction effect. The slope of the isotherms contours with Y-axis reduces as nanoparticles volume fraction increases due to increase conduction in X-axis. The table 5 shows the change of the maximum isotherms with Ra and nanoparticles volume fraction.

Table 5. The percentage of the maximum isotherms.

Φ	$Ra=10^4$	$Ra=10^5$	$Ra=10^6$	$Ra=10^7$
0	0.47256	0.28695	0.18636	0.11032
0.05	0.46068	0.26857	0.1756	0.10459
0.1	0.4485	0.25319	0.16801	0.09932
0.15	0.41892	0.24078	0.15792	0.08778

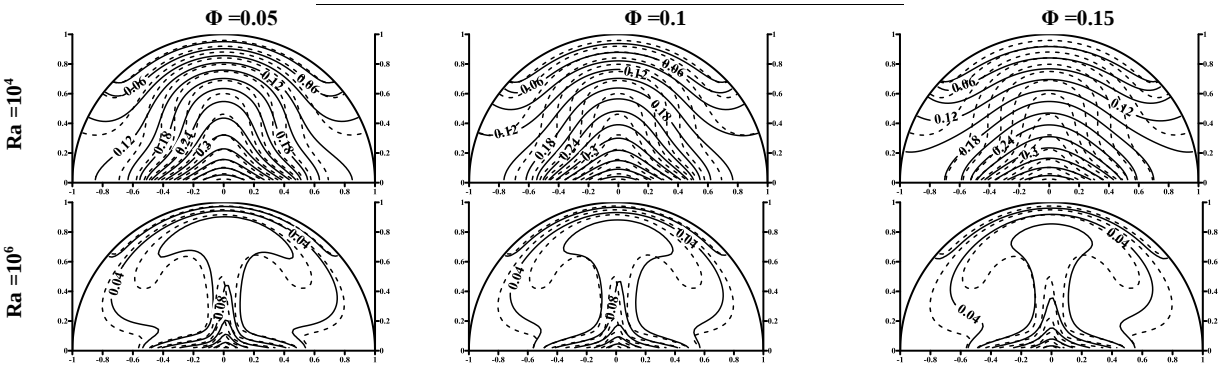

Fig. 3. Isotherms.

5.3. Average Nusselt number

The average Nusselt number illustrates in Fig. 5 to examine the effect of the nanoparticles volume fraction on heat transfer for various Rayleigh number. As observed in this figure, the average Nusselt number increases as the Rayleigh and nanoparticles volume fraction increase. The effect of nanoparticles volume fraction increases as Rayleigh increase. This is due to increase the conduction for high value of Rayleigh number.

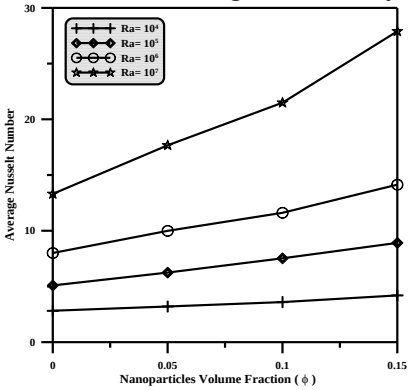

Fig. 5. Average Nusselt number.

5.4. Entropy generation and Bejan number

The entropy distribution above one half of the cavity plots in Fig.4 due to symmetry. In this figure, the intensive concentration of the total entropy generation locate near the heat flux and the cold wall. The addition of the nanoparticles is reduced the entropy generation due to reduce the fluid movement and increase the heat transfer by conduction. The effect of nanoparticles volume fraction on total entropy contour decreases as Rayleigh increases. The total entropy generation near the corners is very small due to the fluid movement in these corners is very small.

In order to check the irreversibility of the system, the percentage increasing in Bejan number due to added particles plots in Fig.5. The percentage increasing of Bejan number increases as nanoparticles volume fraction increases. The effect of nanoparticles volume fraction on percentage increasing in Bejan decreases as Rayleigh increases.

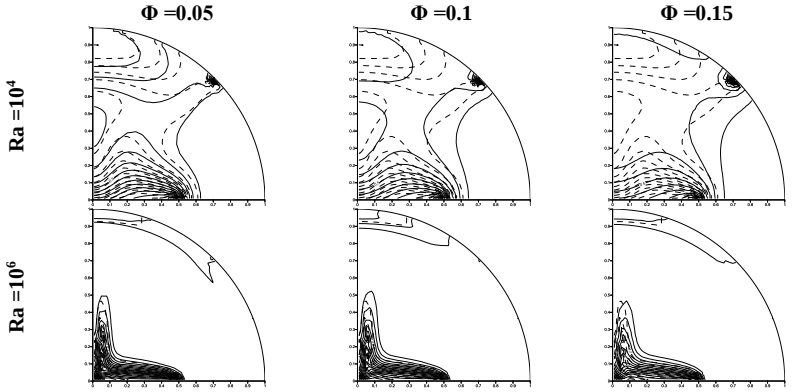

Fig. 4. Entropy generation.

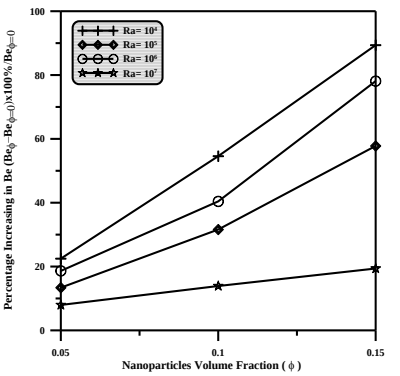

Fig. 5. Bejan Number.

6. Conclusion

The effect of nanoparticles on natural convection and the entropy generation a semi-circular cavity heated by heat source at base wall has been investigated numerically using finite element method. The influence of Rayleigh number ($10^4 \leq Ra \leq 10^7$) and nanoparticles volume fraction ($0 \leq \Phi \leq 0.15$) on the streamfunction, isotherms, Nusselt number, total entropy generation and Bejan number are performed. The main conclusions of the present analysis are:

i. The maximum streamfunction value increases as Rayleigh number increase and decreases as Φ increase.
ii. The percentage increasing in Bejan number increases as the nanoparticles volume fraction increases.
iii. The effect of nanoparticles volume fraction on average Nusselt number increases as Rayleigh increases.

7. References

[1] A. Al-Zamily, Effect of magnetic field on natural convection in a nanofluid-filled semi-circular enclosure with heat flux, Computers & Fluids 103 (2014) 71-85.
[2] T. Grosana, C. Revnic, I. Popa, D. Inghamc, Magnetic field and internal heat generation effects on the free convection in a rectangular cavity filled with a porous medium, Int. J. Heat Mass Transfer 52 (2009) 1525−1533.
[3] S.C. Saha, Scaling of free convection heat transfer in a triangular cavity for Pr>1, Energy and Buildings 43 (2011) 2908−2917.
[4] H. Saleha, R. Roslanb, I. Hashima, Natural convection heat transfer in a nanofluid-filled trapezoidal enclosure, Int. J. Heat Mass Transfer 54 (2011) 194−201.
[5] G. Saha, Finite element simulation of magnetoconvection inside a sinusoidal corrugated enclosure with discrete isoflux heating from below, Int. Commu. Heat Mass Transfer 37 (2010) 393–400.
[6] G. Saha, S. Saha, M. Hasan, M. Islam, Natural convection heat transfer within octagonal enclosure, IJE Trans. 23(2010) 1-10.
[7] W. Aich, I. Hajri, A. Omri, Numerical analysis of natural convection in a prismatic enclosure, Thermal Sci. 15 (2011) 437-446.
[8] M. Matin, I. Pop, Natural convection flow and heat transfer in an eccentric annulus filled by Copper nanofluid, Int. J. Heat Mass Transfer 61 (2013) 353–364.
[9] S. Aminossadati , B. Ghasemi, Natural convection cooling of a localised heat source at the bottom of a nanofluid-filled enclosure, European Journal of Mechanics B/Fluids 28 (2009) 630–640.
[10] A. Mahmoudi, I. Pop, M. Shahi, F. Talebi, MHD natural convection and entropy generation in a trapezoidal enclosure using Cu–water nanofluid, Computers & Fluids 72 (2013) 46–62.

Available online at www.sciencedirect.com

ScienceDirect

Procedia Engineering 00 (2015) 000–000

Procedia Engineering

www.elsevier.com/locate/procedia

6th BSME International Conference on Thermal Engineering (ICTE 2014)

Viscosity measurement of methanol based SiO_2 nanofluids

R.M. Mostafizur[a*], R. Saidur[a], A.R. Abdul Aziz[b], M.H.U. Bhuiyan[a]

[a]*Department of Mechanical Engineering, Faculty of Engineering, University of Malaya, 50603 Kuala Lumpur, Malaysia.*
[b]*Department of Chemical Engineering, Faculty of Engineering, University of Malaya, 50603 Kuala Lumpur, Malaysia.*

Abstract

This work studied about the viscosity of methanol based nanofluids with SiO_2 nanoparticles at various volume fractions and temperatures in order to investigate the enhancement in heat transfer. SiO_2 nanoparticles of 5~15nm sizes are suspended into methanol base fluid at four different concentrations which are 0.01, 0.05, 0.10 and 0.15 vol% and the nanofluids preparation were completed through sonication using ultrasonic homogenizer. The viscosity of prepared nanofluids was measured by LVDV III ultra-programmable viscometer at four different temperatures (5, 10, 15, 20 °C). The measurement uncertainty is about 2.98% for pure methanol. The results show that, the viscosity increased with increasing volume concentration while the viscosity decreased with increasing temperature and increases is observed to be 11.3% over the basefluid at 0.15 vol% and 20 °C. Therefore, this study reveals that the viscosity enhancement depends on both volume fraction and temperature.

Peer-review under responsibility of organizing committee of the 6th BSME International Conference on Thermal Engineering (ICTE 2014).

Keywords: Nanofluid; Volume concentration; Viscosity; Temperature

1. Introduction

Nanofluid is an advanced fluid, a suspension of metallic or non-metallic nanoparticles with a typical size of (1-100 nm) dispersed into the base fluid. The concept of nanofluids was first introduced by Choi, in 1995 [1] .It is a new class of heat transfer fluids due to its attractive enhancements on thermophysical properties and heat transfer. Therefore,

* Corresponding author: Tel: +60-3-79677611, Fax: +60-3-79675317
E-mail address: mostafiz.rahman@live.com (R.M. Mostafizur)

Peer-review under responsibility of organizing committee of the 6th BSME International Conference on Thermal Engineering (ICTE 2014).

researchers are trying to improve the performance of nanofluids in many industrial applications such as power generation, heating or cooling processes, chemical processes, and microelectronics [2-5].

Nomenclature

MBNF	methanol baased nanofluids	Superscript	
Greek Symbol		*bf*	base fluid
φ	volume concentration	*nf*	nanofluid
μ	viscosity		

Viscosity of nanofluid is one of the important parameters in all thermal applications involving fluid flow. Besides, it is important to calculate the pressure drop, accurate pumping power, Prandtl and Reynolds numbers and the convective heat-transfer coefficient in forced convection. It measures the interface friction, which is the internal resistance of fluid layers. According to literature, the nanofluid viscosity depends on many parameters such as; particle volume concentration, particle size, temperature, extent of clustering, surfactants and properties of base fluids [6, 7]. Several researchers have studied about viscosity for different nanoparticles suspended in different nanofluids (i.e. water, engine oil, ethylene glycol, ionic liquid, etc.) and found that the viscosity increases with increased volume concentration of nanoparticles [8, 9]. Their results showed nanofluid viscosity as a function of nanoparticle volume concentrations. They also reported that that the heat transfer might increase while the pressure drop and volume concentration increases.

Tavman et al. [10] measured the effective viscosity of SiO_2–water using vibro–viscometer at different particle concentrations and temperatures. They found effective viscosity of nanofluids increased with the increasing particle concentration and decrease with the increase in temperature and their results cannot be predicted by Einstein model. Namburu et al. [11] experimentally investigated the viscosity of different sizes of SiO_2 nanoparticles with 60:40 mixture of ethylene glycol and water at a particle volume concentration ranges 0 to 10% and temperature ranges from –35 to 50 ^{o}C. According to their results, nanofluid shows non–Newtonian behavior at lower temperatures and Newtonian behavior at higher temperatures. The results also showed that viscosity increases with increase in volume concentrations and viscosity found 1.8 times higher over the base fluids at 10 vol%.

Firouzfar et al. [12] used methanol–silver nanofluids in a thermosyphon heat exchanger at HVAC (Heating, Ventilation and Air conditioning) system to compare the energy savings with that of pure methanol. The main objective of this study is to measure the viscosity of SiO_2–methanol nanofluids at different volume concentrations and temperatures and compared with values predicted by classical models. This findings helped to use methanol nanofluids in different type of heat pipes (i.e; conventional, vapor–dynamic thermosyphons, sorption, micro/miniature) at a temperature range of 200–500 K [13]. Lee et al. [14, 15] and Pineda et al. [16] experimentally investigated the rate of carbon dioxide (CO_2) applying various method. Their experimental results showed methanol based nanofluids enhanced the absorption of CO_2. Some literature focuses on thermal conductivity measurement and rheology behavior of methanol based nanofluids [17-19].To the best of authors' knowledge no literature available on viscosity of MBNF. Therefore, the present work will help to fill the research gap about the effect of nanoparticle concentration and temperature on viscosity of MBNF.

2. Materials and method

2.1. Preparation and dispersion characteristics of nanofluids

In this study, SiO_2 (purity 99.5%) nanoparticles and methanol (purity 99.9%) were selected for investigation. The nanoparticles are procured from Sigma Aldrich, USA and methanol collected from R&M Chemical. The nanoparticles structure and composition were characterized with Field Emission Scanning Electron Microscopy (FESEM). AURIGA (made by Zeiss, Germany) FESEM was used in this study. Fig. 1 (a) shows the FESEM image of SiO_2 nanoparticle. The size of SiO_2 nanoparticles is about 5~10 nm.

The nanoparticles are then suspended into the base fluid (methanol) and shaking by an incubator for 30 min at 150 rpm. The suspension was mixed by using an ultra-sonication homogenizer for 1 h so that, the nanoparticles are uniformly and evenly distributed. The sonication process was maintained at frequency of 20 KHz and power equals to 500W. The methanol based nanofluids microstructure was analyzed using Transmission Electron Microscopy (TEM) with 120 kV and 20,000 magnification scale by TEM LIBRA 120 (Zeiss, Germany). Fig. 1 (b) show the TEM image of SiO_2–methanol nanofluids and assumed the shape of nanoparticles are almost spherical. It also shows that, the nanoparticles are dispersed well and less agglomerations in solutions.

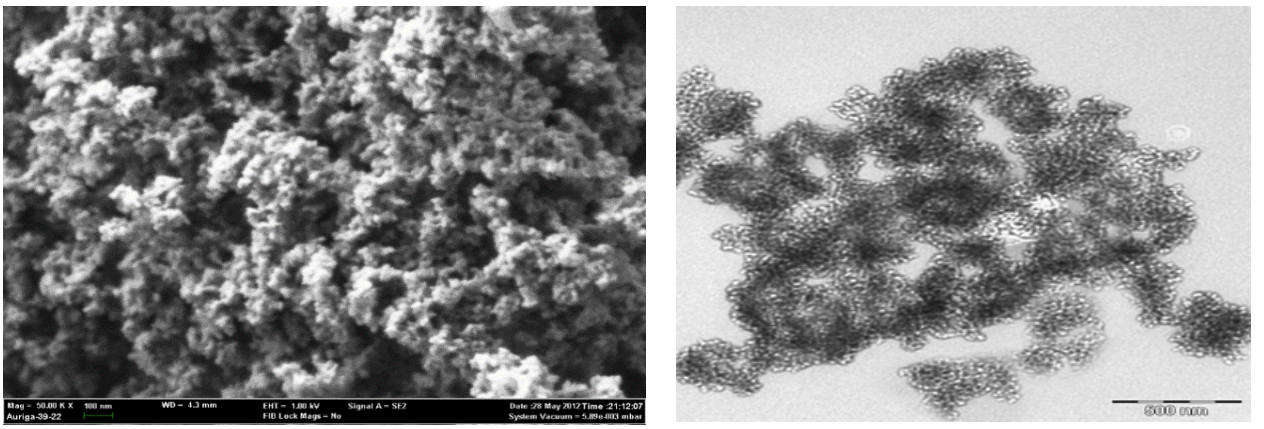

(a) **(b)**

Fig. 1. (a) FESEM image of SiO_2 nanoparticles (b) TEM image of SiO_2–methanol nanofluids

2.2. Measurement of effective viscosity

The mostly used devices to measure viscosity are LVDV series viscometers. These devices are suitable to measure low viscosity. A viscometer named LVDV III ultra-programmable was used to measure the viscosity of methanol based nanofluids. The measurement range of this equipment is 1–6,000,000 mPas. The rotating spindle was submersed into the nanofluids and the viscous effect was developed against the spindle due to deflection of low adapter. The device was connected with a computer to store and collect data with the help of rheocal 32 software. In this experiment, the viscosity of 0.01, 0.05, 0.1 and 0.15 vol% of SiO_2–methanol is measured at temperature range between 5 ºC –20 ºC. For temperature control, a refrigerated circulating bath was used. The schematic diagram of the viscosity measurement setup is shown in fig. 2.

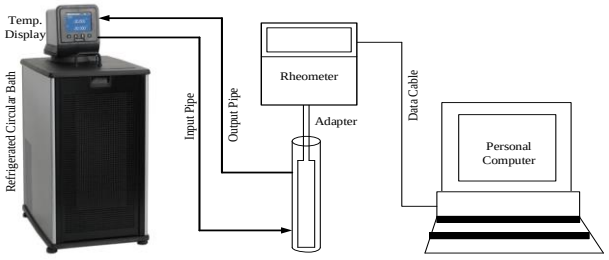

Fig. 2. Schematic setup for the viscosity measurement

All data were recorded three times and the corresponding averages are plotted. Then the measured value of viscosities for 0.01–0.15 vol.% of methanol based nanofluids at 20 °C were compared with the existing familiar models as well as some previous studies experimental results. These models are as follows:

In 1906 Einstein [20] suggest the pioneer one which infinitely dilute suspension for spherical particle and low volume concentration as follows:

$$\mu_{nf} = (1 + 2.5\varphi)\mu_{bf} \quad (1)$$

In 1977 Batchelor [21] proposed a formula for viscosity of rigid and spherical shape particles nanofluids as follows:

$$\mu_{nf} = (1 + 2.5\varphi + 6.2\varphi^2)\mu_{bf} \quad (2)$$

Furthermore, Song et al. [22] proposed a model for measured the viscosity of SiO_2–water nanofluds which is defined as:

$$\mu_{nf} = (1 + 56.5\varphi)\mu_{bf} \quad (3)$$

3. Result and discussion

The viscosity of methanol was first measured to calibrate the experimental apparatus. The viscosity was measured at temperature 5, 10, 15 and 20 °C and then compared with reference data [23]. Fig. 2 shows the comparison between measured data obtained from experiment in this study with existing literature data. The results show relatively acceptable consensus with the existing data. The uncertainty in the measurement of viscosity is approximately 2.98%.

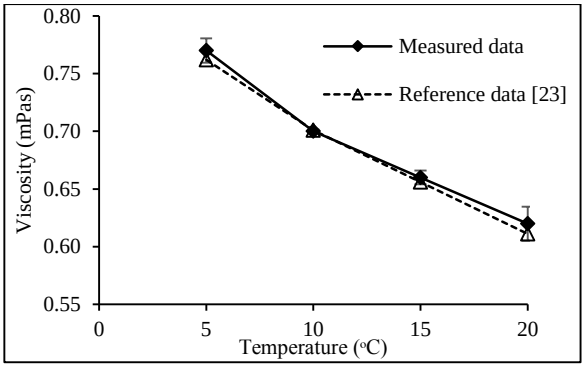

Fig. 2. Viscosity comparison with measured and reference data

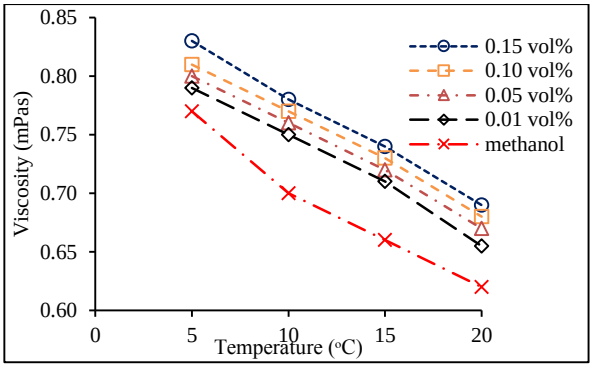

Fig. 3. Viscosity of SiO_2–methanol as a function of temperature and volume concentration

Viscosity of SiO_2–methanol nanofluids as a function of temperature and volume concentration is shown in fig. 3. The results indicate that viscosity of SiO_2–methanol nanofluids in every volume concentration is higher than of pure methanol. Fig. 3 indicates that viscosity increases with increase in volume concentrations. For example, the viscosity value is 0.79 mPas and 0.83 mPas for 0.01vol% and 0.15 vol% respectively at 5 °C temperature. Similar results found in all volume concentration. Furthermore, fig. 3 also illustrated that viscosity decreases with increase in temperatures. The 0.01 vol% nanofluids at 20 °C is 20.6% lower than at 5 °C. Viscosity values of 0.65 mPas and 0.79 mPas at 20 °C and 5 °C respectively at 0.01 vol%. Similar results were found for 0.05, 0.10 and 0.15 vol% respectively. This occurred due to the weakening adhesion force of the particles. By increasing temperature, the velocity of individual molecules increases and the interaction time between neighboring molecules of a fluid decreases. Brownian motion of nanoparticles at high temperature also influences and hence decreases the viscosity of nanofluids.

Fig. 4 shows the comparison of measured viscosity with the values obtained from existing correlations at 20 °C. It was observed that the measured viscosity in this experiment was significantly higher than that of the value obtained from the equations. Thus, the equations are not appropriate to evaluate the viscosity of methanol based nanofluids

[24]. It might happen because of these equations are generalized models developed to estimate the viscosity of a suspension. Therefore, agglomeration cluster of nanoparticles can be considered as a one of the reasons for higher viscosity.

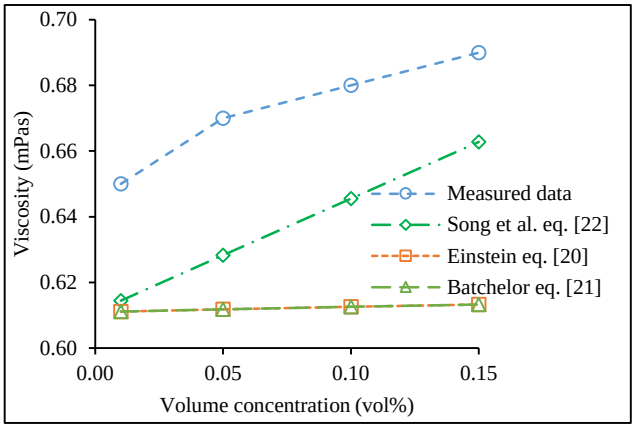

Fig. 4. Comparison of measured viscosity with the values obtained from existing correlations

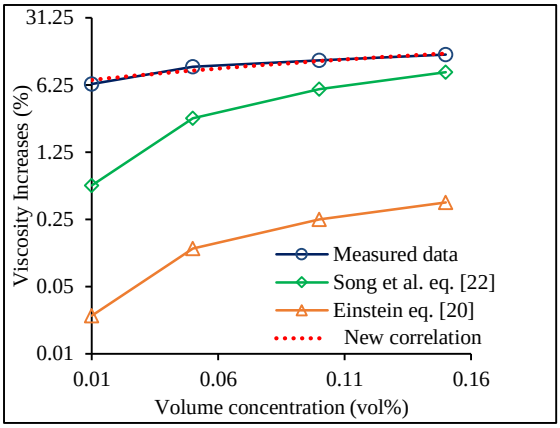

Fig.5. Viscosity increase of SiO_2–methanol nanofluids as a function of volume concentration

Viscosity increase of SiO_2–methanol nanofluids as a function of volume concentration at temperature 20 °C is observed in fig. 5. It is found that the viscosity of nanofluid increases with increasing particle volume concentrations. The measured viscosity of 0.01, 0.05, 0.10 and 0.15 vol% nanofluid at 20 °C are 5.6, 8.1, 9.7 and 11.3% respectively higher than methanol at the same temperature. The maximum viscosity increase is 11.3% at 0.15 vol% nanofluid. The viscosity increment is slightly higher than the existing correlations. This is because the Einstein equation is a generalized model developed for suspension foe viscosity and Song et al. equation developed for SiO_2–water nanofluids. The difference may happen due to agglomeration, particle size, different interaction between nanoparticles and molecules of base fluids. Thus, a new linear correlation has been proposed hereby based on the experimental results for measuring viscosity of methanol based nanofluids:

$$\frac{\mu_{nf}}{\mu_{bf}} = 44.703\varphi + 6.601 \tag{4}$$

The correlation is valid for a particle volume fraction of 0.01–0.15% and temperature of 20 °C. Fig. 5 shows comparison between the measured value and value obtained from proposed new correlation. The results show that the correlation coefficient (R^2) value of this present correlation is about 0.95 which is close to 1.

4. Conclusion

In this study viscosity of SiO_2–methanol nanofluids are investigated at different volume concentrations and temperatures. The experimental results are then compared with existing correlations. The findings of this study are summarized as follows:

(a) Viscosity increases with increase in volume concentrations. Moreover, it decreases with the increase in temperatures.

(b) Viscosity increases about 11.3% with nanoparticle volume concentration 0.15 vol% and at temperature 20 °C.

(c) The existing correlations for predicting the viscosity of methanol nanofluids gave lower values than the experimental values.

Therefore, find an optimal concentration for better heat transfer performance.

Acknowledgement

"This research is supported by High Impact Research MoE Grant UM.C/625/1/HIR/MoE/ENG/40 from the Ministry of Education Malaysia".

References

1. Choi, S.U. and J. Eastman, Enhancing thermal conductivity of fluids with nanoparticles, 1995, Argonne National Lab., IL (United States).
2. Sohel, M.R., S.S. Khaleduzzaman, R. Saidur, A. Hepbasli, M.F.M. Sabri and I.M. Mahbubul, An experimental investigation of heat transfer enhancement of a minichannel heat sink using Al_2O_3–H_2O nanofluid, International Journal of Heat and Mass Transfer. 74 (2014) 164-172.
3. Nuntaphan, A., S. Vithayasai, N. Vorayos, N. Vorayos and T. Kiatsiriroat, Use of oscillating heat pipe technique as extended surface in wire-on-tube heat exchanger for heat transfer enhancement, International Communications in Heat and Mass Transfer. 37 (2010) 287-292.
4. Ashrafmansouri, S.-S. and M. Nasr Esfahany, Mass transfer in nanofluids: A review, International Journal of Thermal Sciences. 82 (2014) 84-99.
5. He, Y., S. Vasiraju, and L. Que, Hybrid nanomaterial-based nanofluids for micropower generation, RSC Advances. 4 (2014) 2433-2439.
6. Wang, X., X. Xu and S.U. S. Choi, Thermal conductivity of nanoparticle-fluid mixture, Journal of thermophysics and heat transfer. 13 (1999) 474-480.
7. Timofeeva, E.V., J.L. Routbort and D. Singh, Particle shape effects on thermophysical properties of alumina nanofluids, Journal of Applied Physics. 106 (2009) 014304.
8. Chandrasekar, M., S. Suresh and A. Chandra Bose, Experimental investigations and theoretical determination of thermal conductivity and viscosity of Al_2O_3/water nanofluid, Experimental Thermal and Fluid Science. 34 (2010) 210-216.
9. Murshed, S.M.S., K.C. Leong and C. Yang, Investigations of thermal conductivity and viscosity of nanofluids, International Journal of Thermal Sciences. 47 (2008) 560-568.
10. Tavman, I., A. Turgut, M. Chirtoc, H. Schuchmann and S. Tavman, Experimental investigation of viscosity and thermal conductivity of suspensions containing nanosized ceramic particles, Archives of Materials Science. 34 (2008) 99-104.
11. Namburu, P., D. Kulkarni, A. Dandekar and D. Das, Experimental investigation of viscosity and specific heat of silicon dioxide nanofluids. Micro & Nano Letters, IET. 2 (2007) 67-71.
12. Firouzfar, E., M. Soltanieh, S.H. Noie and S.H. Saidi, Energy saving in HVAC systems using nanofluid, Applied Thermal Engineering. 31 (2011) 1543-1545.
13. Yang, X., Y. Yan and D. Mullen, Recent developments of lightweight, high performance heat pipes, Applied Thermal Engineering. 33 (2012) 1-14.
14. Lee, J.W. and Y.T. Kang, CO_2 absorption enhancement by Al_2O_3 nanoparticles in NaCl aqueous solution, Energy. 53 (2013) 206-211.
15. Lee, J.W., J.-Y. Jung, S.-G. Lee and Y.T. Kang, CO_2 bubble absorption enhancement in methanol-based nanofluids, International Journal of Refrigeration. 34 (2011) 1727-1733.
16. Torres Pineda, I., J.W. Lee, I. Jung and Y.T. Kang, CO_2 absorption enhancement by methanol-based Al_2O_3 and SiO_2 nanofluids in a tray column absorber, International Journal of Refrigeration. 35 (2012) 1402-1409.
17. Pang, C., J.-Y. Jung, J.W. Lee and Y.T. Kang, Thermal conductivity measurement of methanol-based nanofluids with Al_2O_3 and SiO_2 nanoparticles, International Journal of Heat and Mass Transfer. 55 (2012) 5597-5602.
18. Mostafizur, R.M., A.R. Abdul Aziz, R. Saidur, M.H.U. Bhuiyan and I.M. Mahbubul, Effect of temperature and volume fraction on rheology of methanol based nanofluids, International Journal of Heat and Mass Transfer. 77 (2014) 765-769.
19. Mostafizur, R.M., M.H.U. Bhuiyan, R. Saidur and A.R. Abdul Aziz, Thermal conductivity variation for methanol based nanofluids, International Journal of Heat and Mass Transfer. 76 (2014) 350-356.
20. Einstein, A., Eine neue bestimmung der moleküldimensionen, Annalen der Physik. 324 (1906) 289-306.
21. Batchelor, G., The effect of Brownian motion on the bulk stress in a suspension of spherical particles, Journal of Fluid Mechanics. 83 (1977) 97-117.
22. Song, S., C. Peng, M.A. Gonzalez-Olivares, A. Lopez-Valdivieso and T. Fort, Study on hydration layers near nanoscale silica dispersed in aqueous solutions through viscosity measurement, Journal of Colloid and Interface Science. 287 (2005) 114-120.
23. Thermophysical Properties - Methanol 11.09.2013]; Available from: http://www.engineeringtoolbox.com.
24. Mahbubul, I.M., R. Saidur and M.A. Amalina, Latest developments on the viscosity of nanofluids, International Journal of Heat and Mass Transfer. 55 (2012) 874-885.

Experimental investigation on the thermal conductivity of ZnO-Water nanofluid with SDS (surfactant

I.M. Shahrul (Malaysia), R. Saidur (Malaysia), N.D. Azema (Malaysia), I.M. Mahbubul (Malaysia)

Abstract

Nowadays, improving the efficiency of thermal equipment and system with reducing emission of heat is one of the scientific challenges in this modern globe. Nanofluid is a new engineering medium in which nanoparticles (with diameter of less than 100nm) dispersed in a base fluid. Thermal conductivity is the key thermophysical properties of the fluids for which fluids are used as a medium of thermal transport. In this paper, original investigation has done on the stability and thermal conductivity of ZnO-DW (ZnO nanoparticles dispersed in distilled water) nanofluid with SDS (Sodium Dodecyl Sulfate) as surfactant. The nanofluids were prepared by the two step method using an ultrasonic homogenizer machine. Stability of the nanofluids has been checked by photo capturing method and zeta sizer machine. Thermal conductivity have been measured at different volume concentrations (i.e. 0.02 to 0.1 vol.%) of ZnO in DW and various temperature ranges (i.e. from 10 °C to 50 °C). It is found that, stability and thermal conductivity of the nanofluids were increased for adding SDS compared to without surfactants. Beside this, the thermal conductivity of the nanofluids increases with the increase of volume concentration of ZnO nanoparticles and temperature. Compared to DW, the highest improvement in thermal conductivity of the nanofluids with SDS has found approximately from 7 to 35% for volume concentration changed from 0.02 to 0.1% at 50 °C. In addition, the lowest increment was found approximately 5% for 0.02 vol% of nanoparticles at the temperature of 10 °C. Therefore, the improvement in stability and thermal conductivity of the nanofluids will have great opportunity to improve the performance of the thermal equipment and systems.

Keywords: Nanofluid, Thermal Conductivity, Sodium Dodecyl Sulfate, ZnO-water

Available online at www.sciencedirect.com

ScienceDirect

Procedia Engineering00 (2015) 000–000

Procedia Engineering

www.elsevier.com/locate/procedia

6th BSME International Conference on Thermal Engineering (ICTE 2014)

Effects of Circular Riblets Rough Microchannel on Friction and Fluid Flow using LBM

M.A.Taher[a], L.K.Saha[b], Y.W Lee[a]*

[a]*Deparment of Mechanical and Automotive Engineering, Pukyong National University, Busan, Korea.*
[b]*Deparment of Applied Mathematics, University of Dhaka, Bangladesh.*

Abstract

Simulation of fluid flow and friction in a circular shaped ribbed microchannel using the Lattice Boltzmann Method (LBM) has been studied in the present paper. In micro-flows, the local density variation is still relatively small, but the total density changes, therefore, in order to account this density variation and its effect on the kinematic viscosity ν, a new relaxation time is used. The roughness geometry is modeled as a series of circular riblets with a relative roughness (ε) height up to a maximum 10% of the channel height. To analyze the roughness effects, the friction coefficients in terms of Poiseuille number, Pn, has been discussed. Actually, the friction factor properties of riblets, depending on the particular geometry, are analyzed in the slip flow regime at Knudsen number, Kn, ranging from 0.01 to 0.10 with other controlling parameters. The velocity profiles in terms streamlines near the riblets are demonstrated to be responsible for the roughness effect. Finally the results have been compared with previous published works and it is found to be in good agreement.

Peer-review under responsibility of organizing committee of the 6th BSMEInternational Conference on Thermal Engineering (ICTE 2014).

Keywords: Lattice-Boltzmann, Friction factor, Knudsen number, Reynolds number, Surface Roughness;

1. Introduction

Flow physics on the microscale has attracted considerable attention by many researchers due to the rapid advancement of micromachining technology in the recent years. In microscale flow system, as the relative roughness becomes very large, the friction factor effect on surface roughness cannot be ignored, especially for gas

* Corresponding author. Tel.: 82-51-6297730
E-mail address: ywlee@pknu.ac.kr

Peer-review under responsibility of organizing committee of the 6th BSME International Conference on Thermal Engineering (ICTE 2014).

flow in micro channels [1]. Actually, in microchannels, the main effects are rarefaction effects, essentially quantified by the Knudsen number Kn. According to the Rarefied Gas Dynamics (RGD), Knudsen number is defined as Kn=λ/L, where λ is the gas mean free path and L is the characteristic length of the flow system. It is investigated by many researchers that surface roughness may have a significant impact on microchannel performances, both in terms of pressure drop and heat transfer [2]. Recently, some investigations have been found via Lattice Boltzmann Method (LBM), neglecting compressibility effects. Actually, the LBM based on Boltzmann equation (BE), has attracted much attention as a novel alternative to traditional methods for numerically solving the Navier-Stokes (N-S) equation. Lattice gas models with an appropriate choice of the lattice symmetry in fact represent numerical solutions of the Navier-Stokes equations and therefore able to describe the hydrodynamic problems have been discussed by [3-5]. It is commonly recognized that the Lattice Boltzmann method (LBM) can faithfully be used to simulate the incompressible Navier-Stokes (N-S) equations with high accuracy and this lattice BGK(LBGK) model, the local equilibrium distribution has been chosen to recover the N–S macroscopic equations[6]. The rarefaction effect is considered to be the most important factor that leads to different flow behaviors of rarefied gas dynamics in micro or nanoscale flows. Recently, some other authors [7-9] developed the method and studied micro flows in smooth microchannels by LBM. Up to now, few researchers have found in mirco gas flow to investigate the friction factor with surface roughness in MEMS devices. The roughness effect is one of the most important factors, especially in microchannels, for the friction factor in microfluidic systems. The roughness effect on friction factor in terms of Poiseuille number using LBM have been discussed by [10-11]. In their investigation, they considered the rectangular type of surface roughness elements that are distributed uniformly and symmetrically on the top and bottom walls. In the present study, the authors would like to investigate the rarefaction effect with circular shaped riblets rough microchannel. A few investigations of this type of fluid flow problem using LBM are found in the literature, but to the author's knowledge, the above mentioned problem has not been studied yet by this method. To analyze the friction factor in the slip flow regime, Knudsen number(Kn) ranging from 0.001-0.10, the Poiseuille number, Pn, for different cases have numerically been discussed with varying the relative roughness height from ε=0% to 10% and the results are compared with smooth channel.

Nomenclature

d	Diameter or height of the riblet (m)
D	Hydraulic diameter (m)
e_i	Discrete particle velocity vector (m/s)
F_i^{eq}	Particle equilibrium distribution function
F_i	Discrete particle distribution function
G	Gap between pick position of two roughnesses at the top and bottom walls
H	Height of the microchannel (m)
Kn	Knudsen number
L	Length of the microchannel (m)
P	Pressure (Pa)
Pn	Poiseuille number
S	Distance between centres of two riblets (m)
Greek letters	
ε	relative roughness height (%)
τ	Relaxation parameter for momentum
ρ	Density of the fluid (kg/m^3)
v	kinematic viscosity(m^2/s)

2. Formulation of the Problem

2.1. Mathematical Analysis

To ensure the model satisfies the N-S equations for a fluid under the influence of body force, the Lattice-Boltzmann equation (LBE) can be written as [4]

$$F_i(\vec{x}+\Delta t\,\vec{e}_i, t+\Delta t) - F_i(\vec{x},t) = -\frac{1}{\tau}(F_i(\vec{x},t) - F_i^{eq}(\vec{x},t)) \tag{1}$$

The function $F_i(\vec{x},t)$ is the particle distribution function and F_i^{eq} is the discrete equilibrium distribution function with lattice velocity vectors $\vec{e}_i$ [4]. The relaxation parameter, $\omega = 1/\tau$, depends on the local macroscopic variables, ρ and $\rho\vec{u}$. These variables should satisfy the following laws of conservation

$$\rho = \sum_i F_i^{eq} \quad \text{and} \quad \rho\vec{u} = \sum_i \vec{e}_i\, F_i^{eq} \tag{2}$$

For two dimensional D2Q9 model, the equilibrium distribution function can be defined as [3,4]

$$F_i^{eq} = \rho w_i[1 + \frac{3}{c^2}\,\vec{e}_i.\vec{u}^{eq} + \frac{9}{2c^4}(\vec{e}_i.\vec{u}^{eq})^2 - \frac{3}{2c^2}\,u^{eq^2}] \tag{3}$$

Where w_i is the lattice weighting factors. To apply the LBM in micro flow, a problem is arisen how to relate τ with Kn. The microscopic flows are usually characterized by the Knudsen number Kn defined as the ratio λ/H, where λ is the mean free path and H is the characteristics length.

$$\mathrm{Kn} = \frac{\lambda}{\mathrm{H}} = \sqrt{\frac{\pi\gamma}{2}}\,\frac{\mathrm{Ma}}{\mathrm{Re}} \tag{4}$$

Where γ is the specific heat ratio, Ma is the Mach number and Re is the Reynolds number. Because of its micro-scale and high Knudsen number (Kn) flow, corresponding to the slip flow regime, a special treatment should be considered for the relaxation time (τ). In previous lattice-BGK models, the relaxation time τ was chosen to be a constant during the computational procedure. This is applicable only for nearly-incompressible fluids. In micro-flows, the local density variation is still relatively small, but the total density changes, for instance the density difference between the inlet and outlet of a very long channel could be quite large. In order to account for this density variation and its effect on the kinematic viscosity v, Niu et al.[8] proposed a new relaxation time τ' in place of τ in equation (1) in the following way:

$$\tau' = \frac{1}{2} + \frac{1}{\rho}\left(\tau - \frac{1}{2}\right) \tag{5}$$

2.2. Numerical Analysis and Boundary Conditions

Consider the two dimensional microchannels with designed different roughness and boundary conditions are shown in Fig.1.

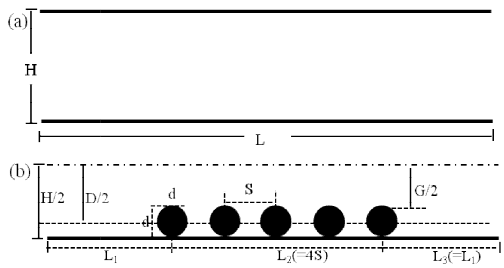

Fig.1. Physical model and coordinate systems for (a) smooth and (b) rough microchannels.

The surface roughness is modeled by a series of circular riblets both on the top and bottom walls at a distance H=100μm from each other and the length L=240 μm. The relative roughness, ε=d/H, varies from 0% -10%, where d is the diameter of the circular riblet. So, the hydraulic diameter D is changed with ε. The hydraulic diameter of the channel is calculated by D = (H+G)/2, where G is the gap between pick position of two roughness elements at the top and bottom walls. S is the distance between two consequent centres of riblets. It is noted that, with increasing the

roughness height, i.e. the diameter of circular riblet, the absolute gap between two consequent riblets reduces, though the centre to centre distance, S, is always constant. To investigate the roughness effect on flow characteristics, the friction coefficient *f* is defined as an average value either over a portion of rough section of the channel or over a single geometrically periodic roughness element [2]. In both cases *f* is defined as

$$f = \frac{\Delta p}{\Delta L} \frac{D}{\frac{1}{2}\langle\rho\rangle\langle u\rangle^2} \tag{6}$$

The variations of ΔP and ΔL are computed between the inlet and outlet section, either the whole rough portion of the channel or of the single roughness element, $\langle\rho\rangle$ and $\langle u\rangle$ are the cross sectional average value. The product of the friction factor *f* and the Reynolds number Re is often referred to as the friction constant, called Poiseuille number, Pn= *f* Re. The Poiseuille number Pn is then written in terms of local Re as

$$Pn = fRe = \frac{2\,\Delta p}{\Delta L} \frac{D}{\langle\mu\rangle\langle u\rangle} \tag{7}$$

In order to simulate a fully developed laminar channel flow upstream of the main channel, a parabolic velocity profile can be used at the inlet and outlet with a maximum velocity *U* at the midpoint of the channel. At the top and bottom wall, slip velocity boundary conditions are imposed by the standard bounce back treatment in order to eliminate the effect of compressibility. A series of computations carried out at a pressure ratio P_i/P_e =1.4, 1.3 and 1.2 for Kn= 0.02, 0.05 and 0.10 respectively, where P_i and P_e are the inlet and exit pressure respectively. Actually, the interaction between the gas molecules and the wall boundary are integrated into a single parameter, namely the tangential momentum accommodation coefficient (TMAC), σ. For D2Q9 lattice model, the particle distribution functions (F_i) on the wall, using the combined bounce rule, are introduced [9, 10]. The tangential momentum accommodation coefficient, σ is used to measured the integral characteristics on the wall boundary. So it has a great influence on numerical results.

3. Result and Discussions

In order to verify with the conventional benchmark, the friction factor *f*Re in terms of Poiseuille number (Pn) at Knudsen numbers, Kn=0.05 is shown in Fig.2. The rectangular shaped roughness geometry with various relative roughness height, $0\% \leq \varepsilon \leq 10\%$, and Knudsen number, Kn = 0.05 is considered. It is seen that he present results are in excellent agreement with Liu et al. [10]. Therefore, we would like to extend our work in circular shaped of roughness geometry.

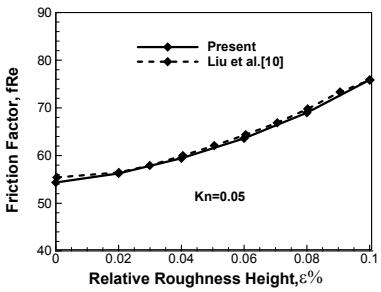

Fig.2. Friction factor in terms of Poiseuille number (Pn = *f* Re) in a rectangular shaped rough microchannel.

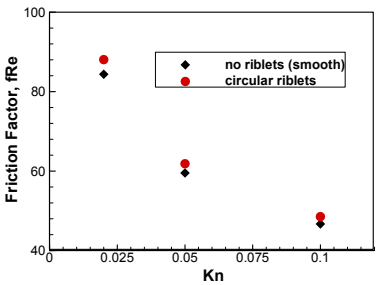

Fig.3. Friction factor as a function of Knudsen number for smooth (♦) and circular riblets (●) rough microchannels.

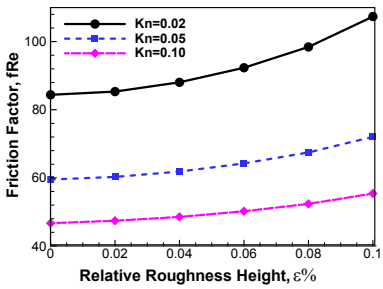

Fig.4. Effects of the surface roughness and Knudsen number on the friction factor.

Fig.3 illustrates the friction factor with relative roughness height for smooth channel and circular riblets rough channels for constant relative roughness height, ε =4%. It is seen that the friction significantly decreases with increasing the rarefaction effects namely the Knudsen number within the slip flow region ranging from 0.01 to 0.10. This is obvious because of higher Knudsen number caused the higher velocity slip on the wall. However, the opposite phenomenon is observed with increasing the relative roughness height ε up to 10% as shown in Fig.4. The friction factor with various roughness heights for different rarefaction effect (Kn=0.02, 0.05 and 0.10) with constant gap between roughness elements are illustrated in Fig4. It is seen that the friction factor increased with relative roughness height and significantly decreased with increasing the Knudsen number.

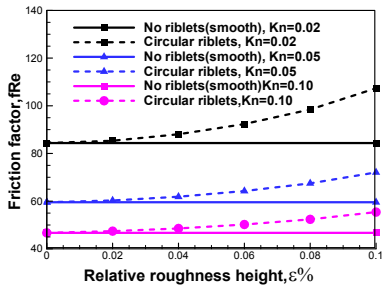

Fig.5. Friction factor with relative roughness for Kn=0.02, 0.05 and 0.10 on smooth (solid lines) and circular riblets(dashed lines) channels.

Fig.5 reveals the friction factor with relative roughness height for smooth channel (solid lines) and circular (dashed lines) riblets rough channels for different Knudsen number, Kn=0.02, 0.05 and 0.10. For smooth channel, roughness height, ε=0.0, so the friction is constant. This is obvious because of no pressure drop between inlet and outlet section. However, in the cases of roughness geometry, the pressure drop increased with roughness height and consequently the friction factor increases with increasing the relative roughness height. Comparing the friction for smooth and rough channels, it is clearly seen that the more friction occurred in the rough circular riblets microchannel.

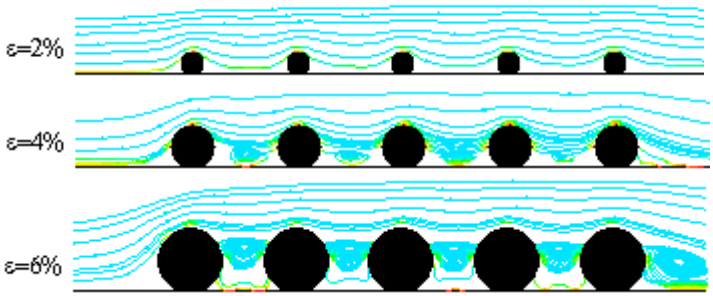

Fig.6 Streamlines near the rough surface of square rough channel for Kn=0.02 with various relative roughness height.

The near wall stream wise vortices with different roughness height, ε=2%, 4% and 6% are depicted in Fig. 6 for Kn=0.02. With increasing the roughness height, the absolute gap between two consequent circular riblets decreases

and the flow recirculation zones are observed between the riblets. It is noted that the vortices are generated and driven by the relative riblets height and gap between the riblets. From the above figures, it has shown that the roughness elements caused the expansion and compressions of the streamlines near rough surface, which increased the pressure drop and consequently the friction increases. These phenomena are observed in rarefied gas micro flow in rough microchannels because of rarefaction effect adjacent to surfaces. Similar flow behaviors are observed for different Knudesn number, Kn=0.05 and 0.10, not shown in figure. The size and shape of vortices not only depend on the riblets height and gap but also on Knudsen number. Therefore, it may conclude that the microchannel rough surfaces may cause the statistical change in the fluid flow behavior as well as friction factor for laminar flow

4. Conclusions

In the present study, the Lattice Boltzmann Method (LBM) has successfully been applied to investigate the friction factor of rarefied gas flow in both smooth and rough microchannels. The surface roughness elements are taken to be considered in circular shaped with relative roughness height varies from ε =0% to 10%. From this study, it may conclude that the friction factor and the flow behaviors in a rough microchannel strongly depend on the Knudsen number and relative roughness height. The friction factor in a microchannel with surface roughness is higher than that in smooth channel. It is seen that the friction factor increased with relative roughness height but significantly decreased with increasing the Kundsen number, Kn, ranging from 0.01 to 0.10. Moreover, it is observed that the fluid flow behaviours in terms of streamlines near the rough surface are affected by the roughness geometry as well as roughness height. It is obvious, because the roughness elements caused the expansion and compressions of the streamlines near rough surface, which increased the pressure drop and consequently the friction is increased. These phenomena are observed in rarefied gas micro flow in rough microchannels.

References

[1] B-Y. Cao, M. Chen, Z-Y. Guo, Effect of surface roughness on gas flow in microchannels by molecular dynamics, Int. J. Engineering Science 44 (2006)927-937.

[2] O. Rovenskaya, G. Croce, Numerical investigation of microflow over rough surfaces: coupling approach, Journal of Heat Transfer 135(2013)101005-1-101005-8.

[3] G. R. McNamara, G. Zanetti, Use of the Boltzmann equation to simulate lattice-gas automata, Physical Review Letters 61(1998)2332-2335.

[4] X. Wei, K. Mueller, A. F. Kaufman, The lattice Boltzmann method for simulating gaseous Phenomena, IEEE Transactions on Visualization and computers Graphics 10(02)(2004)164-176.

[5] M .A. Taher, Y.W. Lee, H. D. Kim, Numerical study of the effect of wedge angle of a wedge-shaped body in a channel using Lattice Boltzmann method, Procedia Engineering 56(2013) 232-238.

[6] H. Chen, S. Chen, W. H. Matthaeus, Recovery of the Navier-Stokes equations using a lattice-gas Boltzmann method, Physical Review A 45(8)(1992)5339-5342.

[7] S. Chen, Z. Tian, Simulation of microchannel flow using the lattice Boltzmann method, Physica A 388(2009) 4803-4810.

[8] X. D. Niu, C. Shu, Y. T. Chew, A thermal lattice Boltzmann model with diffuse scattereing boundary condition for micro thermal flows, Computers and Fluid 36(2007)273-281.

[9] S. H. Kim, H. Pitsch, Slip velocity and Knudsen layer in the lattice Boltzmann method for microscale flows, Physical review E 77(2008)026704-1-026704-12.

[10] C. Liu, J. Yang, Y. Ni, A multiplicative decomposition of Poiseuille number on rarefaction and roughness by lattice Boltzmann simulation, Computers and Mathematics with Applications 61(2011)3528-3536.

[11] Z. Chai, Z. Guo, L. Zheng, B. Shi, Lattice Boltzmann simulation of surface roughness effect on gaseous flow in a microchannel, J. Applied Physics104(2008)014902-1-014902-8.

Available online at www.sciencedirect.com

ScienceDirect

Procedia Engineering 00 (2015) 000–000

Procedia Engineering

www.elsevier.com/locate/procedia

6th BSME International Conference on Thermal Engineering (ICTE 2014)

Analysis of Heat Transfer and Entropy Generation of TiO_2-Water Nanofluid Flow in a Pipe under Transition

Goutam Saha and Manosh C. Paul*

Systems, Power and Energy Research Division, School of Engineering,
University of Glasgow, Glasgow G12 8QQ, UK

Abstract

Single and multi-phase numerical simulations are carried out to investigate the heat transfer and entropy generation behaviour of transitional flow of TiO_2−H_2O nanofluid in a circular pipe. Results reveal that the small diameter of nanoparticles has the highest heat transfer rate for χ = 6% and the TiO_2-water nanofluid shows higher heat transfer rate using multi-phase model compared to that of the single phase model. Also no optimal Reynolds has been observed which could minimise the total entropy generation. New correlations are proposed to calculate the average Nusselt number using a nonlinear regression analysis with a standard deviation of error of less than 0.5%.

Peer-review under responsibility of organizing committee of the 6th BSMEInternational Conference on Thermal Engineering (ICTE 2014).

Keywords: Nanofluid; heat transfer; entropy generation; single phase model; multi-phase model;

1. Introduction

Industries developing technology related to heat transfer are more concern on the design of new thermal systems, thus research is in progress to investigate the hydrodynamic and heat transfer behaviour of new forms of heat transfer fluid such as one called nanofluid. Choi [1] first used nanofluid and verified that the addition of nanoparticles into a base fluid helps to increase the thermal conductivity and hence enhances the heat transfer rate of nanofluid. Several experimental and numerical investigations have also been carried out by researchers to investigate the effect of nanoparticle size diameters, volume concentrations and different nanofluids on the heat transfer behaviour in a circular pipe in laminar flow regime using single and multi-phase models, as reported in [2-15]. However, a very few experimental works of nanofluid have been found in transition flow regime [16, 17].

*Corresponding author. Tel.: +44(0)141 330 8466; fax: +44(0)141 330 4343.
Email address: Manosh.Paul@glasgow.ac.uk (M.C. Paul)

Peer-review under responsibility of organizing committee of the 6th BSME International Conference on Thermal Engineering (ICTE 2014).

To the best of our knowledge, no research has been carried out to-date to understand the transitional behaviour of heat transfer and total entropy generation of the TiO_2–water nanofluid in a circular pipe. Hence, the objective of our study is to analyse this using both single and multi-phase models.

2. Governing Equations

Two-dimensional axi-symmetric model of a horizontal circular pipe with a length (L) of 1.0 m and a circular section with diameter, D_h, of 0.019 m is considered as shown in Fig. 1. The dimensional steady state governing equations for the fluid flow and heat transfer for the single- and multi-phase models can be expressed as (Fluent [18]):

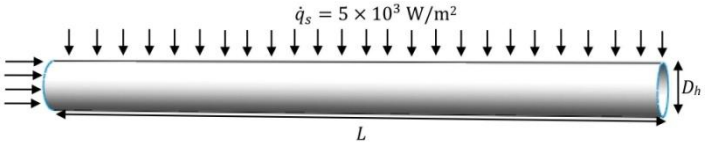

Figure 1: Schematic diagram of the geometry under consideration

Single Phase Model (SPM)

$$\nabla.\left(\rho_m \vec{V}_m\right) = 0 \tag{1}$$

$$\nabla.\left(\rho_m \vec{V}_m \vec{V}_m\right) = -\nabla P_m + \nabla.\left[\mu_m \nabla \vec{V}_m - \sum_{s=1}^{n} \chi_s \rho_s \overline{v_s}\ \overline{v_s}\right] \tag{2}$$

$$\nabla.\left(\rho_m \vec{V}_m C_p T\right) = \nabla.\left(\lambda_m \nabla T - C_p\ \rho_m \overline{vt}\right) \tag{3}$$

Multi-phase Mixture Model (MPM)

$$\nabla.\left(\rho_m \vec{V}_m\right) = 0 \tag{4}$$

$$\nabla.\left(\rho_m \vec{V}_m \vec{V}_m\right) = -\nabla P_m + \nabla.\left[\mu_m \nabla \vec{V}_m - \sum_{s=1}^{n} \chi_s \rho_s \overline{v_s}\ \overline{v_s}\right] + \nabla.\left(\sum_{s=1}^{n} \chi_s \rho_s \vec{V}_{dr,s}\ \vec{V}_{dr,s}\right) \tag{5}$$

$$\nabla.\left[\sum_{s=1}^{n} \chi_s \vec{V}_s (\rho_s H_s + P_m)\right] = \nabla.\left(\lambda_m \nabla T - C_p \rho_m \overline{vt}\right) \tag{6}$$

$$\nabla.\left(\chi_p\ \rho_p \vec{V}_m\right) = -\nabla.\left(\chi_p\ \rho_p \vec{V}_{dr,p}\right) \tag{7}$$

The equations for the kinetic energy (κ) and specific dissipation rate of kinetic energy (ω) used in the SST $\kappa - \omega$ model are given by [19]

$$div\left(\rho_m \kappa \vec{V}_m\right) = div\left\{\left(\mu_m + \frac{\mu_{t,m}}{\sigma_k}\right) grad\ \kappa\right\} + G_\kappa - \rho_m \kappa \omega\ \beta_1 \tag{8}$$

$$div\left(\rho_m \omega \vec{V}_m\right) = div\left\{\left(\mu_m + \frac{\mu_{t,m}}{\sigma_\omega}\right) grad\ \omega\right\} + G_\omega - \rho_m \omega^2 \beta_2 + 2(1 - F_1)\rho_m\ \sigma_{\omega,2}\ \frac{grad\ \omega\ grad\ \kappa}{\omega} \tag{9}$$

The total entropy generation equation for a circular pipe of length L is proposed by Ratts and Raut [20] and defined as

$$E_{gen} = \frac{\pi D_h^2\ L\ \dot{q}_s^2}{\lambda_{nf}\ \overline{Nu}\ T_{avg}} + \frac{32 \dot{m}^3 f L}{\rho_{nf}^2 \pi^2 D_h^5\ T_{avg}} \tag{10}$$

At the pipe inlet, a uniform velocity and a uniform temperature $T_{in} = 293\ K$, with a constant intensity $I = 3\%$ based on the hydraulic diameter, $D_h = 0.019\ m$ have been stated. At the pipe outlet, a pressure outlet boundary condition has been specified. On the pipe wall, a no-slip boundary condition is introduced and uniform heat flux

boundary condition has been implemented. Also, further details about the thermophysical properties of nanofluid, base fluid (water) and nanoparticles could be found in our recent publication, Saha and Paul [21].

3. Results and Discussion

Numerical simulations are carried out with $Re = 2300$ to 10×10^3, $Pr = 7.04$ to 20.29, $\chi = 0$ to 6%, and $d_p = 10$ to $40\ nm$. The governing non-linear partial differential equations for the continuity, momentum, energy and other scalars together with the suitable boundary conditions are discretised and hence solved by using the Finite volume solver Fluent 6.3. For all the simulations carried out in the present analysis, convergence criteria for the solutions are considered when the residuals become less than 10^{-8}.

The grid sensitivity test is carried out by varying the total number of grid distributions in both the axial *(Nx)* and radial *(Nr)* directions. It is found that the grid $Nx = 500 \times Nr = 100$ generate most reasonable result. In order to validate the accurateness of the present numerical findings, validation has been done for the base fluid (water) against the existing experimental data values as well as correlations for different $Re = 2300$ to 10^4 and $Pr = 7.04$. Figure $2(a)$ shows the variation of the Darcy friction factor between the present result and the correlation of Blasius [22] and other experimental results of Chandrasekar *et al.* [14] and Naik *et al.* [15]. Maximum deviation of 10.35% for $Re = 2300$ and minimum deviation of 0.17% are observed for $Re = 10 \times 10^3$. Also from Fig. 2(b), it is observed that the maximum deviation between the present average Nusselt number result and the Gnielinski equation [23] is 28.75% for $Re = 3100$. Also, the maximum deviation between our average Nusselt number result and the experimental result of Naik *et al.* [15] is 2.01% for $Re = 2291$ which shows very good agreement with the experimental result. The reason behind such small variation may be due to the near wall mesh distribution and temperature gradient at the wall. At the end, it is to be assumed that the present predictions are realistic for $Re = 2300$ to 10^4 under transition flow regime.

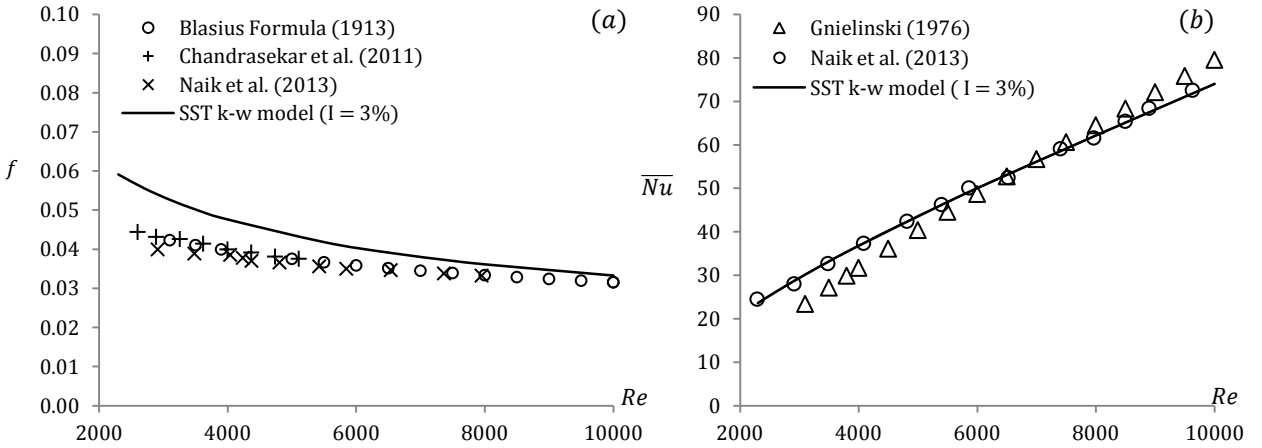

Figure 2: Comparison of the (a) Darcy friction factor, *f* and (b) average Nusselt number, $\overline{Nu}$ of the base fluid (water) with different correlations and experimental results for different *Re*

3.1 Local and average heat transfer analysis

Figure 3a shows the axial variation of local Nusselt number for TiO_2-water nanofluid with $d_p = 10\ nm$ and $\chi = 2\%$. From this figure, it is easy to locate the critical distance measured from the upstream where the transition actually begins. It is also observed that the enhancement of local Nusselt number increases in the entrance region and then rapidly decreases with the axial distance until a minimum value can be predicted from the breakdown of laminar flow. When this minimum value is achieved, Nusselt number started to rise again and then reaches a constant value as the flow tends to be fully developed. It is also found that critical distance is strongly dependent on the Reynolds number. As the Reynolds number increases, such critical distance decreases monotonically. Moreover,

the critical distance moves to a distance close to the upstream of the pipe when the Reynolds number increases from 2300 to 10×10^3 and then it tends to vanish for the Reynolds number greater than 10×10^3. It means that there is a laminar state between the upstream and the breakdown point. This outcomes also strongly support the observations made by Abraham *et al.* [24].

Figures 3b shows the variation of average Nusselt number with the Reynolds number for different nanoparticles volume concentrations of TiO_2-water nanofluids using both single phase model (SPM) and multi-phase model (MPM). The results indicate that the average Nusselt number monotonically increases with the increase of nanoparticle volume concentration. It is also observed that higher average Nusselt number is achieved using the multi-phase model than the single-phase model. This is due to the slip velocity which may not be zero when the interaction between the fluid and particle phase is considered. This variation becomes more significant for higher nanoparticle volume concentrations as well as small nanoparticle size diameters. This is noteworthy because of rapid movement of smaller nanoparticles within the fluid. Particularly for the single phase model, TiO_2–water nanofluid and $\chi = 2\%$, 4% and 6% with $d_p = 10\ nm$, the maximum percentage enhancement is approximately 3.29, 11.34 and 29.34 respectively, while for multi-phase model, it is approximately 3.50, 12.37 and 31.24 respectively.

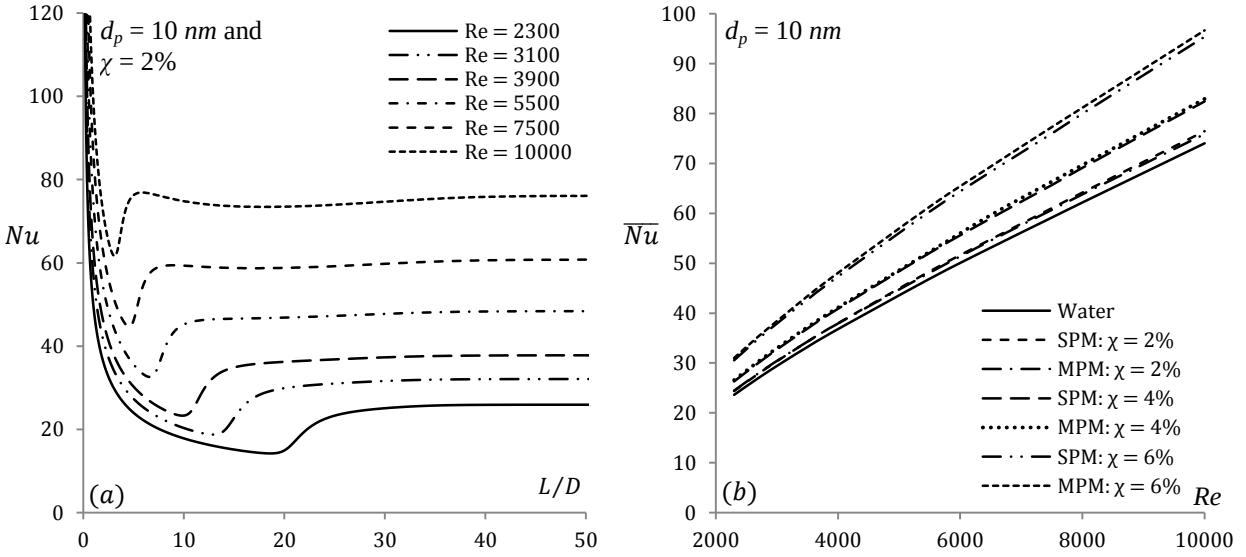

Figure 3: Variation of local and average Nusselt number of TiO_2-H_2O nanofluid for different *Re*

3.2 Entropy generation analysis

Figure 4 show the variation of the total entropy generation for TiO_2-water nanofluids using both single phase and multi-phase model. It is seen that the total entropy generation decreases as the Reynolds number increases with the decrease of the nanoparticles size diameter. Also, insignificant effect of frictional entropy generation on total entropy generation is observed for different nanoparticles size diameter and volume concentration. Particularly for $\chi = 2\%$ and TiO_2-water nanofluid, total entropy generation rapidly decreases as the Reynolds number increases. This occurs due to the enhancement of average Nusselt number and increase of thermal conductivity of nanofluid. Also, the rapid reduction of total entropy generation means that effect of friction entropy generation is negligible and the effect of thermal entropy generation becomes more significant. It shows, the behaviour of thermal entropy generation is similar to total entropy generation. On the other hand, it is observed that increases in nanoparticles volume concentration make an impact on total entropy generation being reduced. Moreover, total entropy generation decreases as the nanoparticles size diameter decrease. This happens due to the significant increase of heat transfer rate as well as the increase of thermal conductivity of nanofluids too. However, no optimal Reynolds has been observed which could minimize the total entropy generation.

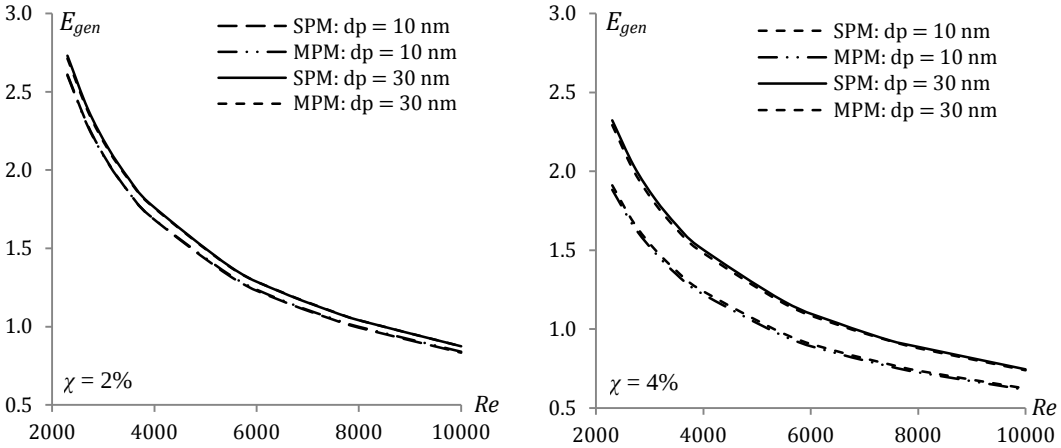

Figure 4: Variation of total entropy generation with different Reynolds number for TiO_2-water nanofluid

3.3 Correlations

By using the non-linear regression analysis, following correlations have been proposed with maximum standard deviation of error of 5% for the numerical computation of the average Nusselt number. Besides, validation between the present numerical results of the average Nusselt number and suggested correlations are presented in Fig. 5. A good agreement between the numerical results and the proposed correlations is observed.

Single Phase Model (SPM):

$$\overline{Nu} = 0.03930\, Re^{0.76745} Pr^{0.24165} \left(\frac{d_f}{d_p}\right)^{-0.0007074}$$

Multi-phase Model (MPM):

$$\overline{Nu} = 0.037768\, Re^{0.76536} Pr^{0.26123} \left(\frac{d_f}{d_p}\right)^{-0.0062903}$$

where

$2300 \le Re \le 10 \times 10^3,\ 8.45 \le Pr \le 20.29,\ 10 \le d_p(nm) \le 40,\ 0 < \chi(\%) \le 6.$

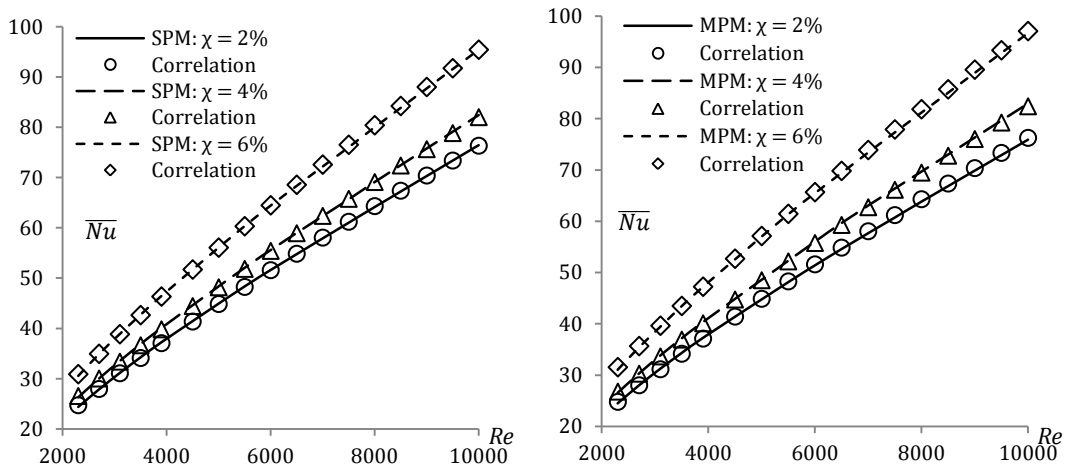

Figure 5: Validation of the proposed correlations with the numerical results for TiO_2-water nanofluid and d_p = 10 *nm* using single phase and multi-phase model

4. Conclusion

In the present analysis, heat transfer and entropy generation behaviour of transition nanofluid flow inside a circular pipe is investigated using both single and multi-phase models. It is observed that addition of smaller nanoparticles in the base fluid (water) helps to enhanced heat transfer rate. Such enhancement is always found higher for multi-phase model than the single phase model. It is also found that there exists no Re such that total entropy generation can be optimized. At the end, two new correlations are proposed for the calculation of average heat transfer rate.

Nomenclature

β_1, β_2	Model constants
C_p	Specific heat capacity (J/kg K)
D_h	Diameter of a pipe (m)
d_f	Fluid molecular diameter (m)
d_p	Diameter of nanoparticle (nm)
E_{gen}	Entropy generation (W/K)
F_1, F_2	Blending functions
f	Darcy friction factor
G_κ	Generation of turbulent kinetic energy
G_ω	Production of ω
H	Enthalpy (J/kg)
I	Turbulent intensity
L	Length (m)
$\dot{m}$	Mass flow rate (kg/s)
N_x, N_r	Number of grid distribution in axial and radial directions
Nu	Nusselt number
P	Pressure (N/m^2)
Pr	Prandtl number
$\dot{q}_s$	Heat flux of the pipe (W/m^2)
Re	Reynolds number
T, t	Time average and fluctuating temperature (K)
V, v	Time average and fluctuating velocity components (m/s)
Greek symbols	
ρ	Density (kg/m^3)
μ	Dynamic viscosity (kg/ ms)
λ	Thermal conductivity (W/m K)
κ	Turbulent kinetic energy (m^2/s^2)
ω	Specific rate of turbulent dissipation (m^2/s^3)
μ_t	Turbulent molecular viscosity
σ_κ	Effective Prandtl number for turbulent kinetic energy
σ_ω	Effective Prandtl number for specific rate of dissipation
χ	Nanoparticle volume concentration
Subscripts	
avg	Average
m	Mixture
s	Secondary phase

References

[1] S. Choi, Enhancing thermal conductivity of fluids with nanoparticles, In Developments and Applications of Non-Newtonian Flows, ASME, FED. 231/MD 66 (1995) 99–105.

[2] S.Z. Heris, M.N. Esfahany, S.G. Etemad, Experimental investigation of convective heat transfer of Al_2O_3/water nanofluid in circular tube, Int. J. Heat Fluid Flow. 28 (2007) 203–210.

[3] K.S. Hwang, S.P. Jang, S.U.S. Choi, Flow and convective heat transfer characteristics of water-based Al_2O_3 nanofluids in fully developed laminar flow regime, Int. J. Heat Mass Transf. 52 (2009) 193–199.

[4] K.B. Anoop, T. Sundararajan, S.K. Das, Effect of particle size on the convective heat transfer in nanofluid in the developing region, Int. J. Heat Mass Transf. 52 (2009) 2189–2195.

[5] E. Esmaeilzadeh, H. Almohammadi, S.N. Vatan, A.N. Omrani, Experimental investigation of hydrodynamics and heat transfer characteristics of Al_2O_3/water under laminar flow inside a horizontal tube, Int. J. Therm. Sci. 63 (2013) 31-37.

[6] S.E.B. Maıga, S.J. Palm, C.T. Nguyen, G. Roy, N. Galanis, Heat transfer enhancement by using nanofluids in forced convection flows, Int. J. Heat Fluid Flow. 26 (2005) 530–546.

[7] E.E. Bajestan, H. Niazmand, W. Duangthongsuk, S. Wongwises, Numerical investigation of effective parameters in convective heat transfer of nanofluids flowing under a laminar flow regime, Int. J. Heat Mass Transf. 54 (2011) 4376–4388.

[8] J. Bayat and A.H. Nikseresht, Investigation of the different base fluid effects on the nanofluids heat transfer and pressure drop, Heat Mass Transf. 47 (2011) 1089–1099.

[9] M.K. Moraveji, M.Darabi, S.M.H. Haddad, R. Davarnejad, Modeling of convective heat transfer of a nanofluid in the developing region of tube flow with computational fluid dynamics, Int. Commun. Heat Mass Transf. 38 (2011) 1291–1295.

[10] S. Mirmasoumi and A. Behzadmehr, Effect of nanoparticles mean diameter on mixed convection heat transfer of a nanofluid in a horizontal tube, Int. J. Heat Fluid Flow. 29 (2008) 557–566.

[11] Y. He, Y. Mena, Y. Zhao, H. Lu, Y. Ding, Numerical investigation into the convective heat transfer of TiO_2 nanofluids flowing through a straight tube under the laminar flow conditions, Appl. Therm. Eng. 29 (2009) 1965–1972.

[12] M.H. Fard, M.N. Esfahany, M.R. Talaie, Numerical study of convective heat transfer of nanofluids in a circular tube two-phase model versus single-phase model, Int. Commun. Heat Mass Transf., 37 (2010) 91–97.

[13] K.V. Sharma, L.S. Sundar, P.K. Sarma, Estimation of heat transfer coefficient and friction factor in the transition flow with low volume concentration of Al_2O_3 nanofluid flowing in a circular tube and with twisted tape insert, Int. Commun. Heat Mass Transf. 36 (2009) 503-507.

[14] M. Chandrasekar, S. Suresh, A.C. Bose, Experimental studies on heat transfer and friction factor characteristics of Al_2O_3/water nanofluid in a circular pipe under transition flow with wire coil inserts, Heat Transf. Eng. 32 (2011) 485-496.

[15] M.T. Naik, G.R. Janardana, L.S. Sundar, Experimental investigation of heat transfer and friction factor with water–propylene glycol based CuO nanofluid in a tube with twisted tape inserts, Int. Commun. Heat Mass Transf. 46 (2013) 13-21.

[16] J.P. Meyer, T.J. McKrell, K. Grote, The influence of multi-walled carbon nanotubes on single-phase heat transfer and pressure drop characteristics in the transitional flow regime of smooth tubes, Int. J. Heat Mass Transf. 58 (2013) 597–609.

[17] C.C. Tang, S. Tiwari, M.W. Cox, Viscosity and Friction Factor of Aluminum Oxide–Water Nanofluid Flow in Circular Tubes, J. Nanotechnol. Eng. Med. 4 (2013) 1-6.

[18] Fluent 6.3 user guide, Fluent Inc., Lebanon, 2006.

[19] F.R. Menter, Two-equation eddy-viscosity turbulence models for engineering applications, J. AIAA 32 (1994) 1598-1605.

[20] E.B. Ratts and A.G. Raut, Entropy generation minimization of fully developed internal flow with constant heat flux, J. Heat Transf. 126 (2004) 656-659.

[21] G. Saha and M.C. Paul, Numerical analysis of heat transfer behaviour of water based Al_2O_3 and TiO_2 nanofluids in a circular pipe under the turbulent flow condition, Int. Commun. Heat Mass Transf., 56 (2014) 96-108.

[22] H. Blasius, Grenzschichten in Flussigkeiten mit kleiner reibung (German), Z. Math. Physics. 56 (1908) 1-37.

[23] V. Gnielinski, New equations for heat and mass transfer in turbulent pipe and channel flow, Int. Chem. Eng. 16 (1976) 359-368.

[24] J.P. Abraham, E.M. Sparrow, J.C.K. Tong, Heat transfer in all pipe flow regimes: laminar, transitional/intermittent, and turbulent, Int. J. Heat Mass Transf. 52 (2009) 557-563.

Cooling performance investigation of electronic's cooling system using Al2O3-H2O nanofluid

M.R. Sohel (Malaysia), R. Saidur (Malaysia), S.S. Khaleduzzaman (Malaysia)

Abstract

The nanofluid as a coolant is an innovative idea applied to the electronic device cooling system. In this study, the thermal performances of a minichannel heat sink are experimentally investigated for cooling of electronics using nanofluid coolant instead of conventional coolant. The Al2O3-H2O nanofluid including the volume fraction ranging from 0.05 vol.% to 0.2 vol.% was used as a coolant. The effects of different flow rates of the coolant on the overall thermal performances are also investigated. The flow rate was ranged from 0.50 L/min to 1.25 L/min. The coolant was passed through a custom made copper minichannel heat sink consisting of the channel height of 0.8 mm and the channel width of 0.5 mm. The experimental results showed the higher improvement of the cooling performances using nanofluid instead of pure distilled water. The heat transfer coefficient was successfully amended. Also the nanofluid significantly lowered the heat sink base temperature compared to the distilled water.

Keywords:heat transfer, nanofluid, entropy, minichannel, heat sink.

Available online at www.sciencedirect.com

ScienceDirect

Procedia Engineering 00 (2015) 000–000

Procedia Engineering

www.elsevier.com/locate/procedia

6th BSME International Conference on Thermal Engineering (ICTE 2014)

Effect of nanoparticles concentration and their sizes on surface tension of nanofluids

M.H.U. Bhuiyan[a]*, R. Saidur[a,b], M.A. Amalina[a], R.M. Mostafizur[a], AKMS Islam[c]

[a] *Department of Mechanical Engineering, Faculty of Engineering, University of Malaya, 50603 Kuala Lumpur, Malaysia.*

[b] *Nanocombicat, NANOCAT, University of Malaya, 50603 Kuala Lumpur, Malaysia.*

[c] *Department of Mechanical and Chemical Engineering, Islamic University of Technology, Gazipur 1704, Bangladesh.*

Abstract

"Nanofluids", a colloidal mixture consisting of nano-sized particles dispersed in a fluid medium with amended thermo-physical properties play a critical role in the heat transfer performance of a thermal system. Surface tension is the surface energy per unit area or the force per unit length dominates the transportation of the liquid and shows a significant role in heat transfer. However, a few numbers of studies demonstrated about the effect of surface tension of nanofluids. Thus, the present experimental study investigates the effect of nanoparticles concentration as well as the influence of variation of nanoparticles along with their sizes. The nanofluids are prepared by dispersing Al_2O_3(13nm and 50 nm),TiO_2 (21nm) and SiO_2 (5~15nm and 10~20nm) nanoparticles in Distilled Water (DW).The traditional Du-Noüy ring method was used to measure the value of the surface tension of nanofluids by an automatic surface tensiometer (DCAT 11EC). The results show that the surface tension of the nanofluids increases with increase in concentration and nanoparticle sizes. Besides,TiO_2-DW nanofluids exhibit higher surface tension than Al_2O_3-DW and SiO_2-DW nanofluids respectively. All in all, the results indicate surface tension of the nanofluids enhances from 2.62 % to 4.82% in comparison with the base fluids for concentration variation of 0.05 Vol % to 0.25 Vol % at 25 °C.

Peer-review under responsibility of organizing committee of the 6th BSME International Conference on Thermal Engineering (ICTE 2014).

Keywords: Nanofluid; Volume concentration; Viscosity; Temperature.

* Corresponding author. Tel.: +6-0142171354; fax: +603-7967-5310.
E-mail address: mhub2k2@yahoo.com

Peer-review under responsibility of organizing committee of the 6th BSME International Conference on Thermal Engineering (ICTE 2014).

1. Introduction

"Nanofluids" denoting a suspension of nanoparticles (nominally 1–100 nm in size) in conventional base fluids introduced by Choi et al.[1] in 1995.It has shown promising potentiality with advancement of it's thermo-physical properties in the heat transfer performance[2].Surface tension is one of the major property which influences the heat transfer performance of a thermal system. It is the amount of surface free energy per unit area of the liquid droplet[3]. It has play an important role to find the shape of a liquid droplet which strongly influences the heat and mass transfer of a thermal system.Moreover, It has proved the critical impact on the boiling heat transfer[4], thermal performance of heat pipes[5],increasing critical heat flux (CHF)[6] and also influencing bubble or droplet formation[7]. Further, the addition of nanoparticles creates surface roughness which effect on transportation behaviour of the liquid surface by the alteration of surface tension as well as surface wettability[8]. Besides, the capillary actions of the working fluids in heat pipes also causes by surface tension[9]. Additionally, the merit number, maximum heat transport capability of the heat pipe is defined by the ratio of the product of the surface tension, the density and the latent heat of vaporization to the viscosity of the working fluids[10]. Therefore, surface tension of the nanofluids is one of the key parameter to optimize the utility of nanofluids in the heat transfer applications.

Nomenclature

DW	Distilled Water	RPM	Revolution per minute
nm	Nanometer	KHz	Kilohertz
h	Hour	°C	Degree Celsius

At present, a comprehensive studies have been observed about thermo-physical properties of nanofluids which are mostly emphasis on thermal conductivity, viscosity, density and specific heat[11-13]. Nonetheless,an insufficient studies have been performed to measure the surface tension of the nanofluids[14]. Besides,there were no remarkable deviations observed in the surface tension of Al_2O_3–H_2O nanofluids[15, 16]. However, Zhu et al.[17] found the surface tension of the nanofluids decreases with increase in volume concentrations and temperatures. They also noticed that surface tension of the Al_2O_3–H_2O nanofluid increases with increase in nanoparticle sizes. Similarly, Radiom et al.[18]observed that the surface tension of TiO_2–DIW(de ionized water) nanofluids depends on the particle concentration and also exhibits a decreasing trend at higher concentrations. On the other hand, Kim et al.[19] pointed out that the surface tension of Al_2O_3, ZrO_2 and SiO_2 nanofluids increases at lower concentration. Correspondingly, Tanvir et al.[20] demonstrated surface tension of nanofluids increases linearly with increase in both the concentration and particle size. Besides,Saeid et al.[21] revealed that at first the surface tension of Bi_2Te_3 nanofluids decreases and then again increases with increase in concentration.

In a nutshell, the aforementioned studies demonstrated indefinite results on the surface tension of nanofluids about concentration and particle sizes. Because of the reults of surface tension influences by many factors such as: measurement methods, measuring instruments, nanoparticle sizes, base fluids and concentrations.Thus, the present experimental study investigates the surface tension of Al_2O_3–DW, TiO_2–DW and SiO_2–DW nanofluids in terms of 0.05 Vol % to 0.25 Vol% concentrations along with the variation of nanoparticles and their sizes at constant 25 °C temperatures.

2. Methodology

2.1. Materials, Sample preparation and distribution of nanofluids

In the present study, the two step method was applied to prepare the different volume fractions (0.05 Vol % to 0.25 Vol %). First, Al_2O_3 (13nm and 50 nm), TiO_2 (21nm) and SiO_2 (5~15nm and 10~20nm) nanoparticles were

purchased and then dispersed in distilled water (DW). Afterwards, the samples were sonicated and obtain the desired nanofluids. All the nanoparticles were bought from Sigma Aldrich, Malaysia and DW prepared at own laboratory.

To find the required volume fraction, the mass of the nanoparticles was first calculated by a digital weight gauge then dispersed in the required amount of distilled water. Next, the mixture was vigorously vibrated by a mechanical shaker (an orbital incubator type) for 1 h at 150 RPM to homogenize the nanoparticles in distilled water. Subsequently, an ultrasonic homogenizer was used to produce high amplitudes and breaking down the particle clusters. As a result, the nanoparticles were uniformly and evenly distributed in the solution. The sonication process was maintained in a series of 2–second long pulses in 2 seconds apart for 2 h at the frequency of 10 kHz (50% amplitude of total capacity 20 kHz). Moreover, the process was performed in a refrigerated circulator bath (C–DRC 8, CPT Inc., South Korea) to maintain a constant temperature (20°C) within the mixture. The microstructure of the nanofluids was analyzed after 24 h of preparation using the Transmission Electron Microscopy (TEM) with 120 kV and 20,000 magnification scale by using TEM LIBRA 120, made by Zeiss, Germany. Figure 1 shows that the nanoparticles are dispersed well and any strong agglomerations were not detected among the particles.

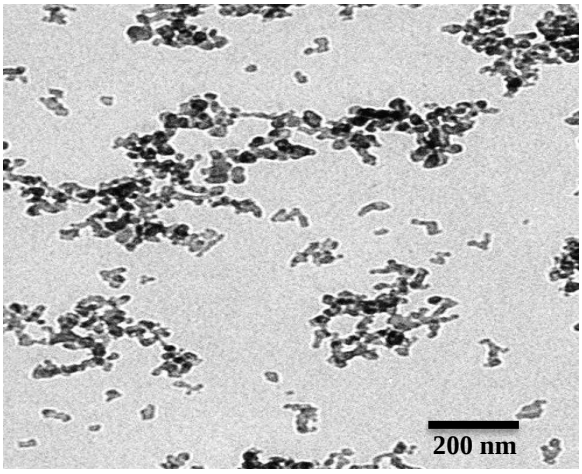

(a)

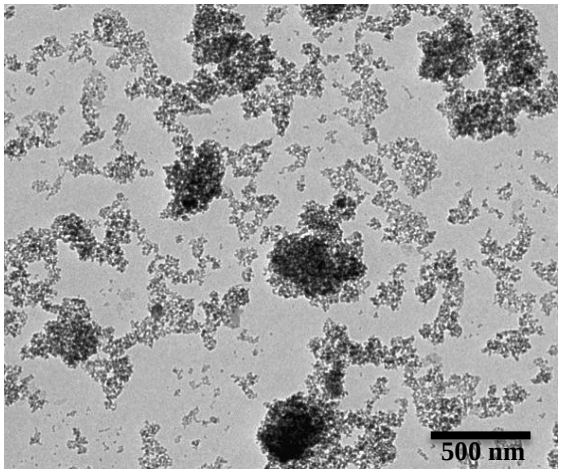

(b)

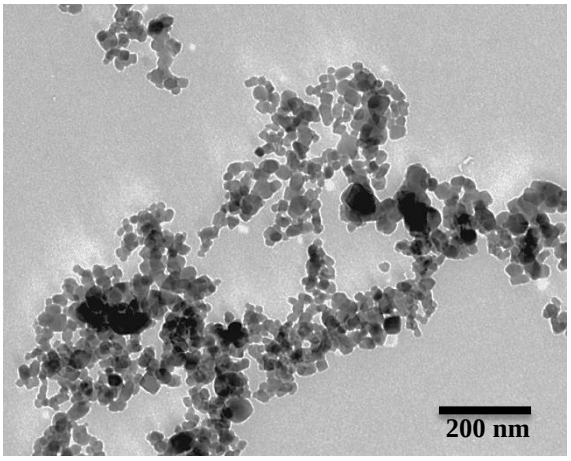

(c)

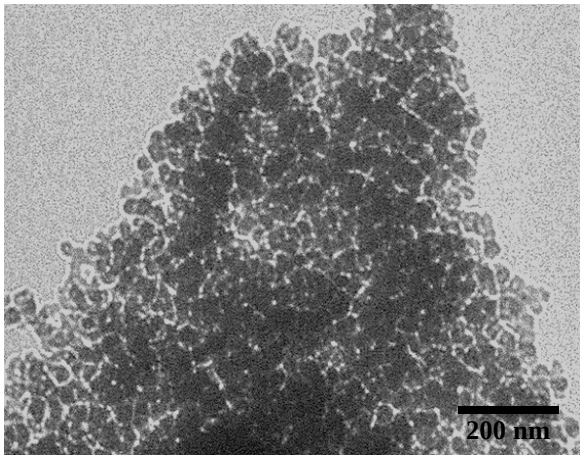

(d)

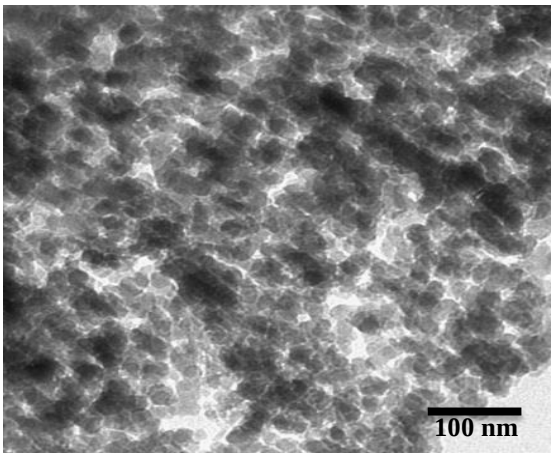

(e)

Fig. 1. image of a) Al_2O_3 (13 nm) b) Al_2O_3 (50 nm) c) TiO_2 (21 nm) d) SiO_2 (5~15 nm) and e) SiO_2 (10~20 nm) nanoparticles dispersed in DW.

2.2. Measurement of Surface tension of nanofluids

In the present study, the surface tension of the nanofluids measured by using Du–Noüy ring method (DIN 53915 and ASTM- 971) by an automatic surface tensiometer (DCAT 11EC, Data Physics Instruments GmbH, and Germany). The tensiometer contains a high performance electro-dynamic compensation balance (0.1 mg to 210 g ± 0.01 mg) with an auto calibration function. The measuring range of the instrument is 1 to 1000 mNm^{-1}; ± 0.001 mNm^{-1}. A Du–Noüy ring RG11, (Platinum-Iridium, and Part no.2000321), 70 mm diameter sample vessels, as well as SCAT 31 software were used to collect the values of surface tension. Fig.2 shows that the value of surface tension measured by pulling and pushing on the ring at an interval of time. Three readings were taken to a particular concentration and the average value was taken for the final calculation. All the measurements were performed at atmospheric pressure.

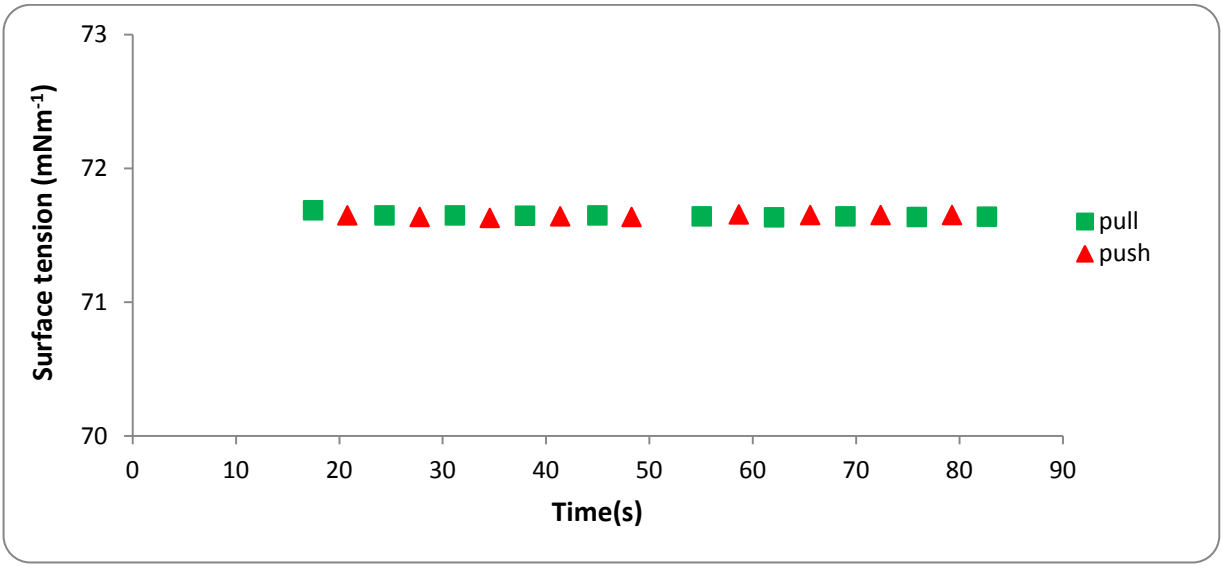

Fig.2. Surface tension of nanofluids as a function of time

3. Result and discussion

3.1. Effect of concentration

The effect of variation of volume concentrations (from 0.05 to 0.25 Vol %) on the surface tension of the nanofluids have been plotted in Fig. 3. The results clearly show that the value of the surface tension of the nanofluids increases with the increase in nanoparticle volume fractions. For example, surface tension of TiO_2–DW nanofluids varies from 71.67 mNm^{-1} to 72.44 mNm^{-1} for the concentrations of 0.05 to 0.25 Vol % at 25 °C. The similar trends are also observed for surface tension of Al_2O_3 (50 nm, 13 nm)–DW and SiO_2 (5~15nm and10~20 nm)–DW nanofluids. The results agree with the experimental studies of Godson et al.[22] and Tanvir et al.[20]. As the volume fractions increases, the addition of nanoparticles increases concurrently and, then the surface tension of the nanofluids increases consequently. As the amount of nanoparticles increases in the base fluid, more nanoparticles are driven to the liquid surface and try to get closer to each other. As a result, a strong, cohesive force exerted between the molecules and resulting higher surface tension of nanofluids[20].Besides, when the concentration increases, the mean spacing between the molecules and the nanoparticles reduces.Hence, an attractive Van der Waals force is employed over the electrostatic repulsion force between the molecules which increases the surface tension of the nanofluids.

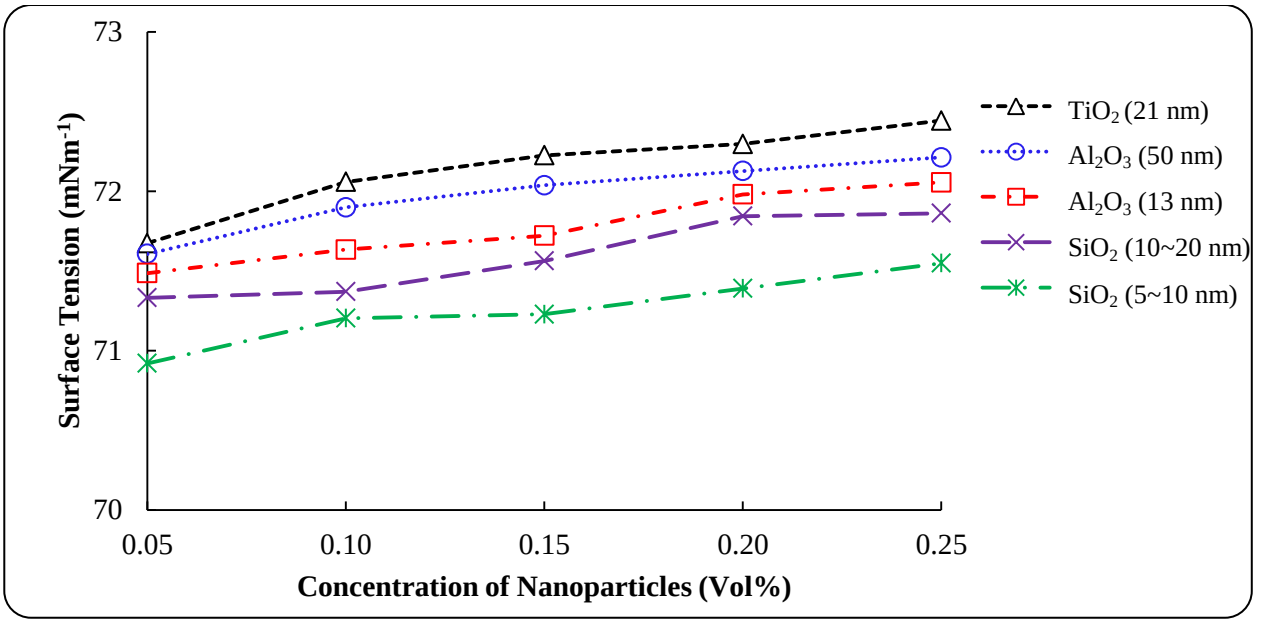

Fig. 3. Surface tension of nanofluids as a function of volume concentration at 25°C

3.2 Effect of variant nanoparticles and their sizes

Apart from volume concentration, variety of nanoparticles and their sizes are also influencing the result of surface tension of the nanofluids which are clearly expresses in the Fig. 4.The results indicate that the surface tension of TiO_2–DW nanofluid is higher than that of Al_2O_3(50 nm and 13 nm)–DW and SiO_2(10~20 nm and 5~15 nm)–DW nanofluids respectively due to the difference of their bulk densities.When the density changes, the attraction between the nanoparticles and water molecules changes, thus the Van der Waals forces of the liquid surface has also changes and resultant a variation of surface tension for different nanofluids.

The Fig.4 also reveals that surface tension of nanofluids increases with the increase in nanoparticle sizes. The results are consistent with the findings of Tanvir et al.[20].This is due to the fact that the smaller nanoparticles exhibit

higher surface charge density compare to the larger nanoparticles[23]. As a result, the electrostatic repulsion force between the nanoparticles and the liquid molecules increases which enhances the adsorption to the surface and therefore, reduces the surface tension of smaller size nanoparticls[24]. Moreover,when the particle size increases,the surface area as well as the surface free energy decreases and consequently increases the surface tension of the nanofluids.

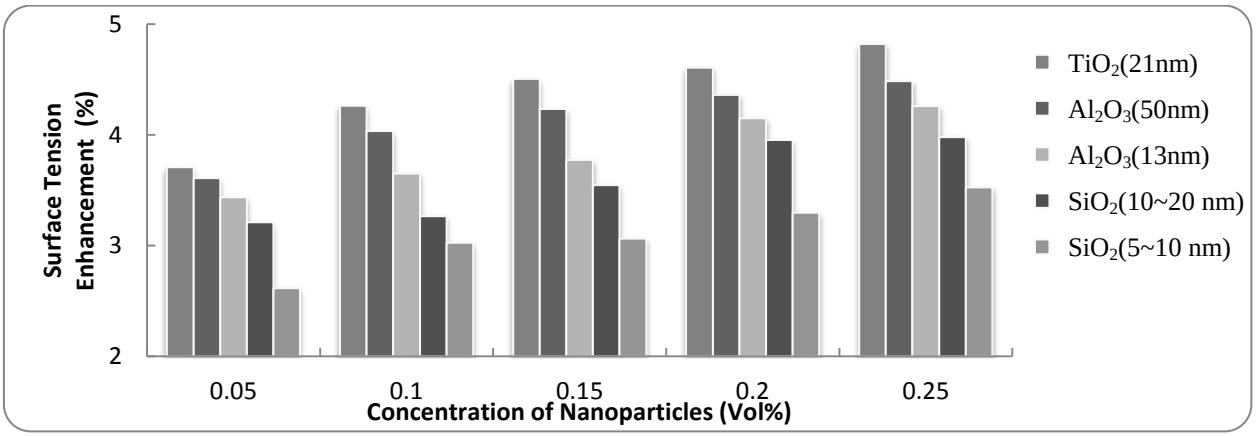

Fig. 4. Enhancement of Surface tension of nanofluids as a function of volume concentration at 25°C

3.3 The surface tension enhancement of the nanofluids

Besides the surface tension of the nanofluids increases with increase in concentration and particle sizes, it is also enhanced compared to the pure base fluids. The surface tension of distilled water found 69.11 mNm^{-1} at 25 °C. However, the measured value of the surface tension of the nanofluids indicates an increasing trend in comparison to the base fluids. The Fig.4 also exhibits the enhancement of surface tension of nanofluids with respect to concentration and particle size. It is shown that the surface tension of nanofluids enhances consecutively in TiO_2-DW, Al_2O_3-DW and SiO_2-DW nanofluids.The improvements are observed about 2.62% to 4.82% from 0.05 to 0.25 Vol% at 25 °C. When the nanoparticles added in the liquid, the molecules of nanoparticles and water interact with each other. As a result, the forces of nanoparticles and the adjacent nanoparticles along with the forces of liquid molecules intervened in the liquid surfaces. And hence, an attractive Van der Waals forces are exerted which increases the surface free energy and resulting the enhancement of surface tension.The findings are also analogous with the outcomes of Moosavi et al.[25].

4. Conclusion

The experimental study inferred that the surface tension of nanofluids alters with base fluid with the influence of concentration, nanoparticle types and their sizes. And, the study point out the surface tension of the nanofluids increases compared to that of the base fluid in all cases. The following statements are addressed as the outcome of this study.

a) The surface tension of the nanofluids increases with increase in concentration.
b) The Surface tension value of Al_2O_3, TiO_2 and SiO_2 nanofluids differs with each other due to the variation of nanoparticles bulk density. And larger nanoparticles exhibits a higher surface tension than that of smaller nanoparticles.

More studies are essential to find the suitable models or correlations for the prediction of the enhancement of surface tension with respect to all of the effective parameters.

Acknowledgement

"This research is supported by High Impact Research MoE Grant UM.C/625/1/HIR/MoE/ENG/40 from the Ministry of Education Malaysia".

Reference

1. Choi, S.U.S. and J.A. Eastman, *Enhancing thermal conductivity of fluids with nanoparticles*. 1995. Medium: ED; Size: 8 p.
2. Taylor, R., et al., *Small particles, big impacts: A review of the diverse applications of nanofluids.* Journal of Applied Physics, 2013. **113**(1): p. 011301-19.
3. Gräfe, W., *A simple quantum mechanical model for the contribution of electronic surface states to surface stress, strength and electrocapillarity of solids.* Journal of Materials Science, 2013. **48**(5): p. 2092-2103.
4. Raveshi, M.R., et al., *Experimental investigation of pool boiling heat transfer enhancement of alumina–water–ethylene glycol nanofluids.* Experimental Thermal and Fluid Science, 2013. **44**(0): p. 805-814.
5. Arab, M. and A. Abbas, *Optimization-Based Design and Selection of Working Fluids for Heat Transfer: Case Study in Heat Pipes.* Industrial & Engineering Chemistry Research, 2013. **53**(2): p. 920-929.
6. You, S.M., J.H. Kim, and K.H. Kim, *Effect of nanoparticles on critical heat flux of water in pool boiling heat transfer.* Applied Physics Letters, 2003. **83**(16): p. 3374-3376.
7. Vafaei, S. and D. Wen, *Effect of Gold Nanoparticles on the Dynamics of Gas Bubbles.* Langmuir, 2010. **26**(10): p. 6902-6907.
8. Vafaei, S., D. Wen, and T. Borca-Tasciuc, *Nanofluid Surface Wettability Through Asymptotic Contact Angle.* Langmuir, 2011. **27**(6): p. 2211-2218.
9. Jiang, L., et al., *Thermal performance of a novel porous crack composite wick heat pipe.* Energy Conversion and Management, 2014. **81**(0): p. 10-18.
10. Reay, D., R. McGlen, and P. Kew, *Heat pipes: Theory, design and applications*. 2013: Butterworth-Heinemann.
11. Mostafizur, R.M., et al., *Thermal conductivity variation for methanol based nanofluids.* International Journal of Heat and Mass Transfer, 2014. **76**(0): p. 350-356.
12. Barbés, B., et al., *Thermal conductivity and specific heat capacity measurements of Al2O3 nanofluids.* Journal of Thermal Analysis and Calorimetry, 2013. **111**(2): p. 1615-1625.
13. Yiamsawas, T., et al., *Experimental studies on the viscosity of TiO2 and Al2O3 nanoparticles suspended in a mixture of ethylene glycol and water for high temperature applications.* Applied Energy, 2013. **111**(0): p. 40-45.
14. Khaleduzzaman, S.S., et al., *Effect of particle concentration, temperature and surfactant on surface tension of nanofluids.* International Communications in Heat and Mass Transfer, 2013. **49**(0): p. 110-114.
15. Golubovic, M.N., et al., *Nanofluids and critical heat flux, experimental and analytical study.* Applied Thermal Engineering, 2009. **29**(7): p. 1281-1288.
16. Das, S.K., N. Putra, and W. Roetzel, *Pool boiling characteristics of nano-fluids.* International Journal of Heat and Mass Transfer, 2003. **46**(5): p. 851-862.
17. Zhu, B.J., et al. *Thermophysical Properties of Al2O3-Water Nanofluids*. in *Materials Science Forum*. 2011. Trans Tech Publ.
18. Radiom, M., C. Yang, and W.K. Chan. *Characterization of surface tension and contact angle of nanofluids*. in *Fourth International Conference on Experimental Mechanics*. 2009. International Society for Optics and Photonics.
19. Kim, S.J., et al., *Surface wettability change during pool boiling of nanofluids and its effect on critical heat flux.* International Journal of Heat and Mass Transfer, 2007. **50**(19–20): p. 4105-4116.
20. Tanvir, S. and L. Qiao, *Surface tension of Nanofluid-type fuels containing suspended nanomaterials.* Nanoscale research letters, 2012. **7**(1): p. 1-10.
21. Saeid, V., et al., *The effect of nanoparticles on the liquid–gas surface tension of Bi 2 Te 3 nanofluids.* Nanotechnology, 2009. **20**(18): p. 185702.
22. Godson, L., et al. *Measurement of viscosity and surface tension of silver deionized water nanofluid*. in *37th National & 4th International Conference on Fluid Mechanics and Fluid Power, December*.
23. Abbas, Z., et al., *Size-Dependent Surface Charging of Nanoparticles.* The Journal of Physical Chemistry C, 2008. **112**(15): p. 5715-5723.
24. Brown, M.A., et al., *Effect of Surface Charge Density on the Affinity of Oxide Nanoparticles for the Vapor–Water Interface.* Langmuir, 2013. **29**(16): p. 5023-5029.
25. Moosavi, M., E.K. Goharshadi, and A. Youssefi, *Fabrication, characterization, and measurement of some physicochemical properties of ZnO nanofluids.* International Journal of Heat and Fluid Flow, 2010. **31**(4): p. 599-605.

Available online at www.sciencedirect.com

ScienceDirect

Procedia Engineering 00 (2015) 000–000

Procedia Engineering

www.elsevier.com/locate/procedia

6th BSME International Conference on Thermal Engineering (ICTE 2014)

MHD Convective Stagnation Flow of Nanofluid over a Shrinking Surface with Thermal Radiation, Heat Generation and Chemical Reaction

Mohammad Wahiduzzaman[a,*], Md. Shakhaoath Khan[b] and Ifsana Karim[b]

[a]*Mathematics Discipline, Science Engineering and Technology School,Khulna University, Khulna-9208, BANGLADESH*
[b]*Department of Chemical Engineering, School of Engineering, University of Newcastle, Callaghan, NSW 2308, AUSTRALIA.*

Abstract

The present study numerically investigates the phenomena of the steady two-dimensional magnetohydrodynamic(MHD) stagnation-point and heat-mass transfer flow of a nanofluid past a shrinking sheet with the influence of thermal radiation, heat generation and chemical reaction. The effect of Brownian motion and thermophoresis are well-thought-out instantaneously. A similarity solution is presented which depends on the magnetic parameter (M), Grashof number (G_r), modified Grashof number (G_m), heat generation parameter (Q), radiation parameter (R), Brownian motion number (N_b), thermophoresis number (N_t), Prandtl number (P_r), Lewis number (L_e), Chemical reaction parameter (γ) and the ratio of the rate constants of the shrinking velocity to the free stream velocity (α). A shooting technique is employed to solve this similarity model numerically. The results of the present analysis is going to observe the velocity, temperature, concentration, the wall shear stress, the Nusselt number and the Sherwood number at the different situation and dependency of different parameters. A comparative study is also being shown between the previously published results and the present results for the accuracy and interesting findings of the present research.

Peer-review under responsibility of organizing committee of the 6th BSME International Conference on Thermal Engineering (ICTE 2014).

Keywords: Magnetohydrodynamic stagnation-point flow, Heat transfer, Nanofluid, Shrinking sheet.

* Corresponding author. Mob.: + 880 1913 262715
E-mail address: wahidmathku@gmail.com

Peer-review under responsibility of organizing committee of the 6th BSME International Conference on Thermal Engineering (ICTE 2014).

1. Introduction

Boundary layer flow behavior over a stretching surface is vital in engineering processes, such as, materials manufactured by extrusion, annealing and tinning of copper wires, glass blowing, continuous cooling and fibre spinning. At the time of manufacture of these sheets, the melt issues from a slit and is subsequently stretched to achieve the desired thickness and the final product of desired characteristic depends on the rate of cooling and the process of stretching. For the flow over a shrinking sheet, the fluid is attracted towards a slot and as a result it shows quite different characteristics from the stretching case. From a physical point of view, vorticity generated at the shrinking sheet is not confined within a boundary layer and a steady flow is not possible unless either a stagnation flow is applied or adequate suction is applied at the sheet. As discussed by Goldstein [1], this new type of shrinking flow is essentially a backward flow. Miklavcic and Wang [2] were the first who have investigated the flow over a shrinking sheet with suction effect. Steady two-dimensional and axisymmetric boundary layer stagnation point flow and heat transfer towards a shrinking sheet was analyzed by Wang [3]. The existence and uniqueness results for MHD stagnation point flow over a stretching/shrinking sheet were considered by Van Gorder et al.[4].. All studies mentioned above refer to the stagnation point flow towards a stretching/shrinking sheet in a viscous and Newtonian fluid. Bachok et al. [5] investigated the effects of solid volume fraction and the type of the nanoparticles on the fluid flow and heat transfer characteristics of a nanofluid over a shrinking sheet. Effects of magnetic field and thermal radiation on stagnation flow and heat transfer of nanofluid over a shrinking surface were investigated by Samir Kumar Nandy and Ioan Pop [6]. To the author's knowledge no studies have thus far been communicated with regard to MHD boundary layer stagnation flow and heat transfer of a nanofluid past a shrinking sheet with thermal radiation, heat generation and chemical reaction. The objective of the present work is therefore to extend the work of Samir Kumar Nandy and Ioan Pop [6] by taking Heat Generation and Chemical Reaction. The effects of magnetic field parameter (M), Brownian motion parameter (N_b), thermophoresis number (N_t), Prandtl number (P_r), Lewis number (L_e), radiation parameter (R), Grashof number (G_r), Modified Grashof umber (G_m), Chemical Reaction parameter (γ) and the velocity ratio parameter (α) on the relevant flow variables are described in detail. The present study is of immediate interest to all those processes which are highly affected with heat enhancement concept e.g. cooling of metallic sheets or electronic chips etc.

2. Flow analysis

Consider the steady two-dimensional MHD stagnation-point flow of an incompressible viscous electrically conducting nanofluid impinging normally on a shrinking sheet. The fluid is subjected to a uniform transverse magnetic field of strength B_0. Fig. 1 describes the physical model and the coordinate system, where the x and y axes are measured along the surface of the sheet and normal to it, respectively. It is assumed that the velocity of the stretching/shrinking sheet is $u_w(x) = cx$ and the velocity outside the boundary layer is $U(x) = ax$, where a and c are constants with $a > 0$. We note that $c > 0$ and $c < 0$ correspond to stretching and shrinking sheets respectively. Instantaneously at time $t > 0$, temperature of the plate and species concentration are raised to $T_w (> T_\infty)$ and $C_w (> C_\infty)$ respectively, which are thereafter maintained constant, where T_w, C_w are temperature and species concentration at the wall and T_∞, C_∞ are temperature

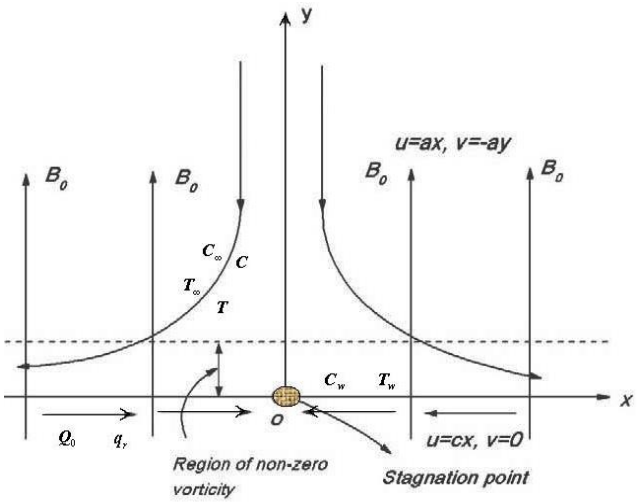

Fig. 1. Physical model and the coordinate system.

and species concentration far away from the plate respectively.The basic steady conservation of mass, momentum, thermal energy and nanoparticles equations for nanofluids can be written in Cartesian coordinates x and y as,

$$\frac{\partial u}{\partial x}+\frac{\partial v}{\partial y}=0 \tag{1}$$

$$u\frac{\partial u}{\partial x}+v\frac{\partial u}{\partial y}=U\frac{du}{dx}+\upsilon\frac{\partial^2 u}{\partial y^2}+\frac{\sigma {B_0}^2}{\rho}(U-u)+g\beta(T-T_\infty)+g\beta^*(C-C_\infty) \tag{2}$$

$$u\frac{\partial T}{\partial x}+v\frac{\partial T}{\partial y}=\alpha_m\frac{\partial^2 T}{\partial y^2}-\frac{1}{\rho C_p}\frac{\partial q_r}{\partial y}+\tau\left[D_B\frac{\partial C}{\partial y}\frac{\partial T}{\partial y}+\frac{D_T}{T_\infty}\left(\frac{\partial T}{\partial y}\right)^2\right]+\frac{\overline{Q}}{\rho C_P}(T-T_w) \tag{3}$$

$$u\frac{\partial C}{\partial x}+v\frac{\partial C}{\partial y}=D_B\frac{\partial^2 C}{\partial y^2}+\frac{D_T}{T_\infty}\frac{\partial^2 T}{\partial y^2}-K_r(C-C_\infty) \tag{4}$$

In writing Eq. (2), we have neglected the induced magnetic field since the magnetic Reynolds number for the flow is assumed to be very small. This assumption is justified for flow of electrically conducting fluids such as liquid metals e.g., mercury, liquid sodium etc. Here u and v are the velocity components along the x and y directions, respectively, $U(x)$ is the free stream velocity, T is the fluid temperature and C is the nanoparticle volume fraction, σ is the electrical conductivity of the fluid, υ is the kinematic viscosity, α_m is the thermal diffusivity, ρ is the density of the base fluid, D_B is the Brownian diffusion coefficient, D_T is the thermophoresis diffusion coefficient, C_p is the specific heat at constant pressure, q_r is the radiative heat flux and τ is the ratio of the effective heat capacity of the nanoparticle material to the heat capacity of the ordinary fluid and K_r is the chemical reaction parameter. It is assumed that the wall temperature T_w and the nanoparticle volume fraction C_w are constant at the surface. Also when y tends to infinity, the ambient values of the temperature and the nanoparticle volume fraction attain to constant values of T_∞ and C_∞, respectively. The boundary conditions for the problem are;

$$\begin{aligned} &u=u_w=cx,\ v=0,\ T=T_w,\ C=C_w \quad \text{at} \quad y=0\\ &u\to U(x)=ax,\ \ T=T_\infty,\ C=C_\infty \qquad \text{as} \quad y\to\infty \end{aligned} \tag{5}$$

The radiative heat flux q_r is described by Rosseland approximation (see [35]) such that

$$q_r=-\frac{4\delta}{3k_1}\frac{\partial T^4}{\partial y} \tag{6}$$

where, δ is the Stefan-Boltzmann constant and K_1 is the mean absorption coefficient. Assuming the temperature difference with in the flow is such that T^4 can be expanded in a Taylor series about T_∞ and neglecting higher order terms, we get $T^4\approx 4{T_\infty}^3T-3{T_3}^4$. Hence from Eq. (6), using the above result, we have

$$\frac{\partial q_r}{\partial y}=-\frac{16\delta {T_\infty}^3}{3k_1}\frac{\partial^2 T}{\partial y^2} \tag{7}$$

2. Mathematical Formulation

To attain the similarity solution of Equations. (1)–(4) with the boundary conditions (Eq. (5)), the stream function and the dimensionless variables can be defined as follows:

$$\psi=x\sqrt{a\upsilon}\ f(\eta),\ \theta(\eta)=\frac{T-T_\infty}{T_w-T_\infty},\ \varphi(\eta)=\frac{C-C_\infty}{C_w-C_\infty},\ \eta=y\sqrt{\frac{a}{\upsilon}} \tag{8}$$

where the stream function ψ is defined in the usual way as $u = \frac{\partial \psi}{\partial y}$ and $v = -\frac{\partial \psi}{\partial x}$.

$\therefore u = axf'(\eta)$

$\therefore v = -\sqrt{a\upsilon}\, f(\eta)$

Using the above mentioned non-dimensional variable, the non-linear, non-dimensional, coupled ordinary differential equations have been obtained as;

$$f''' + ff'' - (f')^2 + M(1 - f') + \lambda_T \theta + \lambda_M \varphi = 0 \tag{9}$$

$$\frac{(1+4R)}{P_r}\theta'' + f\theta' + N_b \theta'\varphi' + N_t (\theta')^2 + Q\theta = 0 \tag{10}$$

$$\varphi'' + L_e\, f\, \varphi' + \frac{Nt}{Nb}\theta'' - \gamma R_e\, L_e\, \varphi = 0 \tag{11}$$

where the notation primes denote differentiation with respect to η and M is the dimensionless magnetic parameter, R is the thermal radiation parameter, G_r is the Grashof number, G_m is the Modified Grashof number, λ_T is the Thermal convective parameter, λ_M is the Mass convective parameter, P_r is the Prandtl number, and N_b is the Brownian motion parameter, N_t is the thermophoresis parameter, Q is the heat source parameter and L_e is the Lewis number, γ is the Chemical reaction parameter, R_e is the Local Reynolds number which are defined as

$$M = \frac{\sigma {B_0}^2}{\rho a}, G_r = \frac{g\beta x^3 (T_w - T_\infty)}{\upsilon^2}, G_m = \frac{g\beta^* x^3 (C_w - C_\infty)}{\upsilon^2},\ \lambda_T = \frac{G_r}{{R_e}^2},\ \lambda_M = \frac{G_m}{{R_e}^2}\ P_r = \frac{\upsilon}{\alpha_m}, R = \frac{4\delta {T_\infty}^3}{3k_1 \alpha_m \rho C_p},$$

$$Q = \frac{\overline{Q}}{\rho C_p a}\ N_b = \frac{\tau D_B (C_w - C_\infty)}{\upsilon},\ N_t = \frac{\tau D_T (T_w - T_\infty)}{\upsilon T_\infty},\ L_e = \frac{\upsilon}{D_B},\ \gamma = \frac{K_r \upsilon}{U^2} \text{ and } R_e = \frac{U x}{\upsilon} \tag{12}$$

Eq. (10) shows that the temperature actually does not depend on Prandtl number (P_r) and the thermal radiation parameter (R) independently, but depends only on a combination of them which is the effective Prandtl number (P_{reff}). Introducing the effective Prandtl number $P_{reff} = \frac{P_r}{1+4R}$, Eq.(10) can be written as

$$\frac{1}{P_{reff}}\theta'' + f\theta' + N_b \theta'\varphi' + N_t (\theta')^2 + Q\theta = 0 \tag{13}$$

The effect of the thermal radiation in the linearized Rosseland approximation on the heat transfer characteristics of various boundary layer flows is discussed in some details in the reference [36].

The corresponding boundary conditions are

$$\begin{aligned} &f(0) = 0,\ f'(0) = \alpha = \frac{c}{a},\ \theta(0) = 1,\ \varphi(0) = 1 && \text{at} \quad \eta = 0 \\ &f'(\eta) \to 1,\ \ \theta(\eta) \to 0,\ \varphi(\eta) \to 0 && \text{as} \quad \eta \to \infty \end{aligned} \tag{14}$$

where α is the ratio of the rates of the stretching/shrinking velocity and the free stream velocity.

It is to be noted that this boundary value problem reduces the classical problem of flow and heat transfer due to a stretching/shrinking surface in a viscous fluid when $N_b = N_t = 0$. In this case, the boundary value problem for φ becomes ill-posed without physical significance. The physical quantities of interest are the skin friction coefficient C_f, the local Nusselt number Nu_x and the local Sherwood number Sh_x which are defined as

$$C_f = \frac{\tau_w}{\rho U^2(x)},\ Nu_x = \frac{x q_w}{k(T_w - T_\infty)},\ Sh_x = \frac{x q_m}{D_B (C_w - C_\infty)} \tag{15}$$

where τ_w is the shear stress along the stretching surface, q_w and q_m are the wall heat and mass fluxes, respectively. Hence, using Eqs. (8) and (15), we get

$$R_{e_x}^{\frac{1}{2}} C_f = f''(0),\ Nu_x R_{e_x}^{-\frac{1}{2}} = -\theta'(0),\ Sh_x R_{e_x}^{-\frac{1}{2}} = -\varphi'(0) \tag{16}$$

where, $R_{e_x} = \dfrac{U(x)x}{\upsilon}$ is the local Reynolds number based on the free stream velocity $U(x)$.

3. Results and discussion

Equations. (9), (11) and (13) subject to the boundary conditions (Eq. (14)) have been solved numerically using sixth order Rung–Kutta method with shooting technique for some values of the physical parameters involved in the present problem. In order to investigate the physical representation of the problem, the numerical values of velocity (f') temperature (θ) and concentration (φ) have been computed for resultant principal parameters. Fig. 2 shows the trajectories of skin friction coefficient $f''(0)$ with $\alpha < 0$ (shrinking sheet) and $\alpha > 0$ (stretching sheet) for

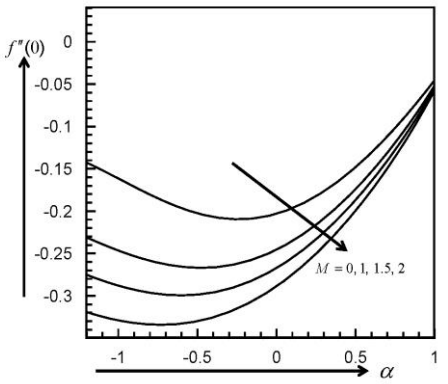

Fig. 2. Variation of the skin friction coefficient $f''(0)$ with α for different values of the magnetic parameter M with $N_b = N_t = 0.1$, $L_e = 2$, $P_r = 5$, $\lambda_1 = 2$, $\lambda_m = 2$, $\gamma = 1$, $R_c = 1$ and $R = 0.5$.

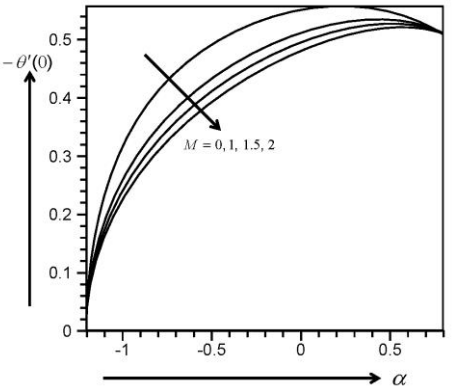

Fig. 3. Variation of the Nusselt number $-\theta'(0)$ with α for different values of the magnetic parameter M with $N_b = N_t = 0.1$, $L_e = 2$, $P_r = 5$, $\lambda_1 = 2$, $\lambda_m = 2$, $\gamma = 1$, $R_c = 1$ and $R = 0.5$.

different values of the magnetic parameter (M). The figure reveals that the values of $f''(0)$ decreases as $|\alpha|$ decreases In Fig. 3, the temperature gradient at the sheet (the Nusselt number) $-\theta'(0)$, which is proportional to the rate of heat transfer from the sheet, is plotted for different values of the magnetic parameter M. It is observed that $|-\theta'(0)|$ decreases with an increase in M. On the other hand, influence of the magnetic parameter M on the Sherwood number $-\varphi'(0)$ is shown in Fig. 4. The figure reveals that $|-\varphi'(0)|$ decreases when M increases.

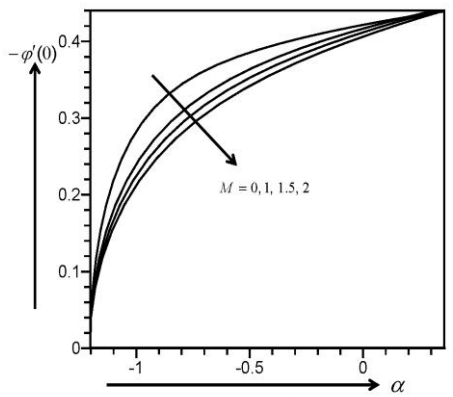

Fig. 4. Variation of the Sherwood number $-\varphi'(0)$ with α for different values of the magnetic parameter M with $N_b = N_t = 0.1$, $L_e = 2$, $P_r = 5$, $\lambda_1 = 2$, $\lambda_m = 2$, $\gamma = 1$, $R_c = 1$ and $R = 0.5$.

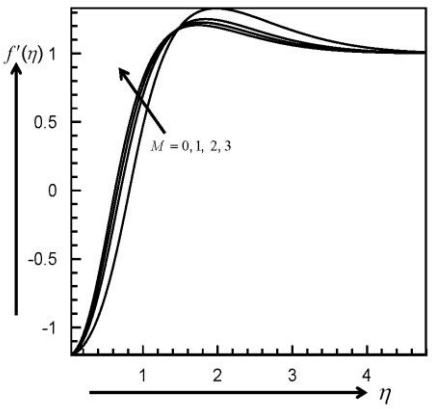

Fig.5. Variation of the velocity profiles $f'(\eta)$ for several values of M with $\alpha = -1.20$ $N_b = N_t = 0.1$, $L_e = 1$, $P_r = 1$, $\lambda_1 = 2$, $\lambda_m = 2$, $\gamma = 1$, $R_c = 1$ and $R = 0.2$.

The effect of the magnetic parameter (M) on the horizontal velocity component $f'(\eta)$ is shown in Fig. 5. The figure indicates that the velocity increases with the increasing values of the magnetic parameter (M). From a physical point of view, this follows from the fact that as in this case, Lorentz force is positive and consequently as M increases, this Lorentz force is also increases and hence accelerates the flow. Fig. 6 represents the variation of the temperature distribution $\theta(\eta)$ for several values of M. The figure exhibits the temperature decreases with increase in M. Physically this is explained as follows. The extent of reverse cellular flow above the sheet decreases with increase in M and as a result, the temperature field is influenced by the advection of the fluid velocity above the sheet. The effects of the Brownian motion parameter (N_b) and thermophoresis parameter (N_t) on temperature profiles $\theta(\eta)$ are shown in Figs. 7 and 8. It is observed that with the increasing values of N_b and N_t, the fluid temperature decreases and increases respectively. For small particles, Brownian motion is strong and the parameter N_b will have high values and for large particles, N_b will have small values. Hence Brownian motion can exert a significant enhancing influence on temperature profiles and the temperature in the boundary layer increases with the increase in N_b. Again thermophoresis parameter (N_t) also serves to warm the boundary layer for low values of Prandtl number (P_r) and Lewis number (L_e). Fig. 9 shows the influence of effective Prandtl number (P_{reff}) on the temperature profile $\theta(\eta)$ for fixed values of other parameters. It is to be noted that P_{reff} is nothing but a simple rescaling of the Prandtl number (P_r) by a factor

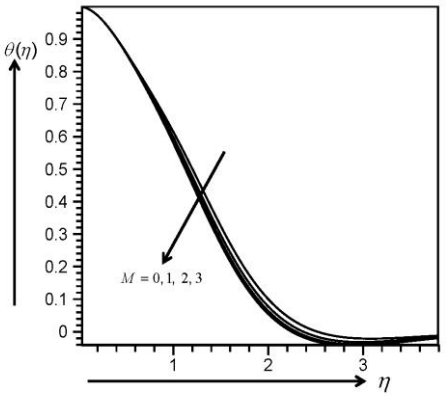

Fig.6. Variation of the temperature profiles $\theta(\eta)$ for several values of M with $\alpha = -1.20$ $N_b = N_t = 0.1$, $L_e = 1$, $P_r = 1$, $\lambda_t = 2$, $\lambda_m = 2$, $\gamma = 1$, $R_e = 1$ and $R = 0.2$.

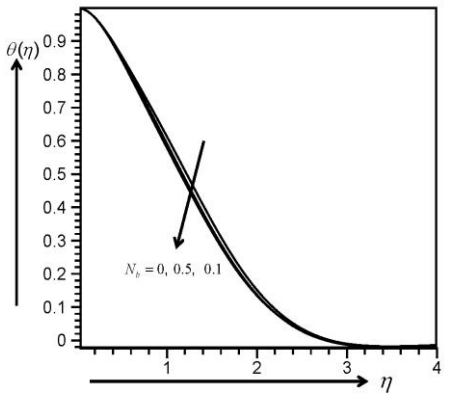

Fig.7. Variation of the temperature profiles $\theta(\eta)$ for several values of N_b with $\alpha = -1.20$ $N_t = 0.1$, $L_e = 1$, $M = 0.1$, $P_r = 0.71$, $\lambda_t = 2$, $\lambda_m = 2$, $\gamma = 1$, $R_e = 1$ and $R = 0.2$.

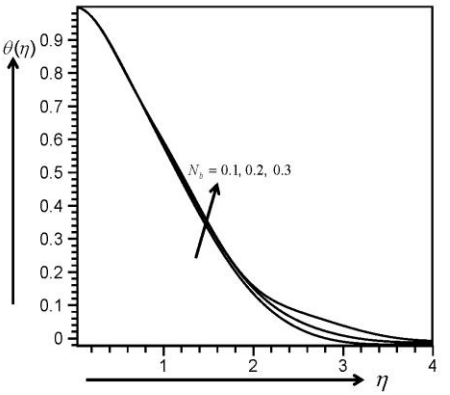

Fig.8. Variation of the temperature profiles $\theta(\eta)$ for several values of N_b with $\alpha = -1.20$ $N_t = 0.1$, $L_e = 1$, $M = 0.1$, $P_r = 0.71$, $\lambda_t = 2$, $\lambda_m = 2$, $\gamma = 1$, $R_e = 1$ and $R = 0.2$.

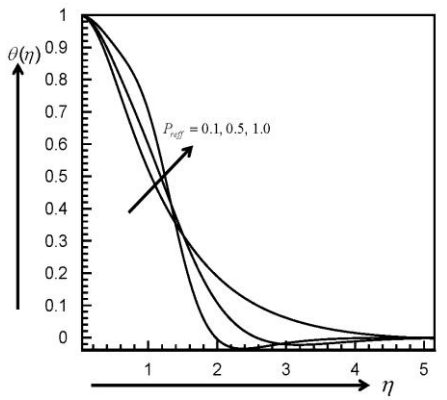

Fig.9. Variation of the temperature profiles $\theta(\eta)$ for several values of P_{reff} with $\alpha = -1.20$ $N_b = N_t = 0.1$, $L_e = 1$, $M = 0.1$, $\lambda_t = 2$, $\lambda_m = 2$, $\gamma = 1$, $R_e = 1$ and $R = 0.2$.

involving the radiation parameter (R). It is observed from the figure that the temperature at a point decreases with an increase in the effective Prandtl number except a small region near the sheet for the first solution branch. From a physical point of view, if P_{reff} increases, the thermal diffusivity decreases and this phenomenon leads to decrease the thermal boundary layer thickness. But, interestingly, for the second solution, up to a certain region, $\theta(\eta)$ increases as P_{reff} increases and beyond this region, $\theta(\eta)$ decreases as P_{reff} increases. The variation of the concentration profiles $\varphi(\eta)$ for different values of the Lewis number (L_e) and Brownian motion parameter (N_b) are shown in Figs. 10 and 11, respectively. Generally Lewis number, the ratio of thermal diffusivity to mass diffusivity, is used to characterize fluid flows where there is simultaneous heat and mass transfer by convection. Fig. 10 shows that the solution branches of $\varphi(\eta)$ decreases with an increase in L_e. The same feature as in the case of L_e is also observed for the Brownian motion parameter N_b and is depicted in Fig. 11. Presentation of full stability

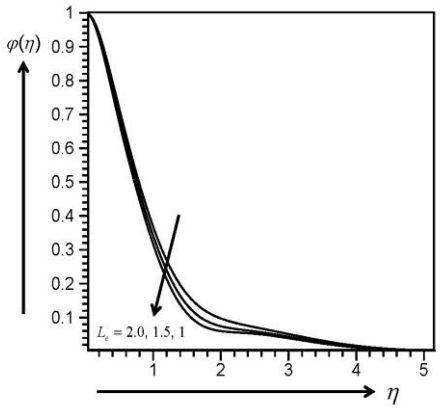

Fig.10. Variation of the concentration profiles $\varphi(\eta)$ for several values of L_e with $\alpha = -1.20$ $N_b = N_t = 0.1$, $M = 0.1$, $P_r = 0.71$, $\lambda_1 = 2$, $\lambda_m = 2$, $\gamma = 1$, $R_e = 1$ and $R = 0.2$.

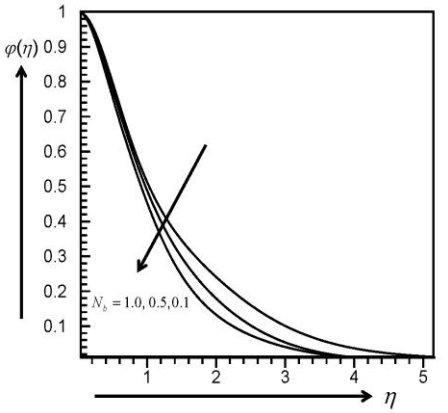

Fig.11. Variation of the concentration profiles $\varphi(\eta)$ for several values of N_b with $\alpha = -1.20$ $N_t = 0.1$, $L_e = 1.0$ $M = 0.1$, $P_r = 0.71$, $\lambda_1 = 2$, $\lambda_m = 2$, $\gamma = 1$, $R_e = 1$ and $R = 0.2$

analysis is beyond the scope of the present work since a stability analysis requires an unsteady flow, whereas our problem is a steady one.

3. Conclusion

The present paper deals with the analysis of MHD Convective Stagnation Flow of Nanofluid over a Shrinking Surface in the presence of thermal radiation, heat generation and chemical reaction. Numerical solutions of the resulting system of nonlinear ordinary differential equations are obtained by using the shootingmethod coupled with Runge-Kutta scheme. The effects of various parameters such as magnetic field parameter (M), Brownian motion parameter (N_b), thermophoresis number (N_t), Prandtl number (P_r), Lewis number (L_e), radiation parameter (R), Grashof number (G_r), Modified Grashof umber (G_m), Chemical Reaction parameter (γ) and the velocity ratio parameter (α) on the dimensionless velocity, temperature, and concentration profiles have been studied graphically. The influence of different parameters of on the skin friction, Nusselt number, and Sherwood number are shown graphically as well. From the present numerical investigation, the following inferences can be drawn:

- **i.** Velocity increases but temperature profile decreases with the increasing values of M.
- **ii.** With the increasing values of N_b and N_t, the fluid temperature decreases and increases respectively.
- **iii.** It is observed that the temperature at a point decreases with an increase in the effective Prandtl number.
- **iv.** The solution branches of $\varphi(\eta)$ decreases with an increase in L_e. The same feature as in the case of L_e is also observed for the Brownian motion parameter N_b.

Acknowledgment

We thank the reviewer for his useful comments and suggestions that led to definite improvement in the paper.

References

[1] S. Goldstein, On backward boundary layers and flow in converging passages, J. Fluid Mech. 21 (1965) 33–45.
[2] M. Miklavcic, C.Y. Wang, Viscous flow due to a shrinking sheet, Q. Appl. Math. 64(2006) 283–290.
[3] C.Y. Wang, Stagnation flow towards a shrinking sheet, Int. J. Nonlinear Mech. 43(2008) 377–382.
[4] R.A. Van Gorder, K. Vajravelu, I. Pop, Hydromagnetic stagnation-point flow of a viscous fluid over a stretching/shrinking sheet, Meccanica 47 (1) (2012) 31–50.
[5] N. Bachok, A. Ishak, I. Pop, Stagnation-point flow over a stretching/shrinking sheet in a nanofluid, Nanoscale Res. Lett. 6 (2011) 623–632.
[6] Samir Kumar Nandy, Ioan Pop, Effects of magnetic field and thermal radiation on stagnation flow and heat transfer of nanofluid over a shrinking surface, . International Communications in Heat and Mass Transfer 53 (2014) 50–55.

Thermophysical properties of Aluminium oxide-water nanofluid: A review

Shafi Noor (Bangladesh), M. Monjurul Ehsan (Bangladesh), A.K.M. Sadrul Islam (Bangladesh)

Abstract

Heat transfer enhancement using nanofluid has been an active area of research over the past few years and these studies were carried out numerically and experimentally in both laminar and turbulent flow. However this enhancement is due to change in the thermophysical properties of nanofluid. Despite of presence of numerous studies on the properties of nanofluid in the literature, it has been observed that there are disproportionateness among the experimental results and the empirical correlation proposed by different researchers. A small change in the properties can affect greatly the results of heat transfer rate in case of numerical study considering a single phase flow. Therefore the present study summarizes recent researches carried out for thermophysical properties such as density, specific heat, thermal conductivity and viscosity of Al2O3-water nanofluid which involve the corresponding effect of temperature, volume fraction and diameter on the properties as well.

Keywords: nanofluid, aluminium oxide, thermophysical propertiy, viscosity, thermal conductivity, volume fraction

Available online at www.sciencedirect.com

ScienceDirect

Procedia Engineering00 (2015) 000–000

Procedia Engineering

www.elsevier.com/locate/procedia

6th BSME International Conference on Thermal Engineering (ICTE 2014)

Analysis of MHD Jeffery-Hamel Flow with Nanoparticle by Hermite- Padé Approximation

Md. S. Alam [a]* **, *M.A.H. Khan*** [b]

[a]*Department of Mathematics, Jagannath University, Dhaka-1100, Bangladesh*

[b]Department of Mathematics, Bangladesh University of Engineering and Technology, Dhaka-1000, Bangladesh

Abstract

The combined effects of nanoparticle and magnetic field on the nonlinear Jeffery-Hamel flow are analyzed in the present study. The basic governing equations are solved into series solution using a semi-numerical analytical technique called Hermite- Padé approximation. The velocity profiles are presented in divergent channel for various values of nanoparticle solid volume fraction, Hartmann number, Reynolds number and channel angle. The dominating singularity behavior of the problem is analysed numerically and graphically. The critical relationship between the parameters is studied to observe the instability of the problems for nanofluid.The relationship between the velocity profiles and the parameters of the flow with the effect of nanoparticle solid volume fraction and Hartmann number are also performed qualitatively.

Peer-review under responsibility of organizing committee of the 6th BSMEInternational Conference on Thermal Engineering (ICTE 2014).

Keywords: Jeffery-Hamel flow; magnetohydrodynamic; nanofluid; dominating singularity; Hermite- Padé approximation.

* Corresponding author. Tel.: +88-02-9582775; fax: +88-02-7113752.
*E-mail address:*sarwar@math.jnu.ac.bd

Peer-review under responsibility of organizing committee of the 6th BSME International Conference on Thermal Engineering (ICTE 2014).

1. Introduction

The study of flows in convergent-divergent channel is very important due to its industrial, aerospace, chemical, civil, environmental, mechanical and bio- mechanical engineering applications. Various applications of this type of mathematical model are to understand the flow of rivers and canals and the blood flow in the human body.

Nomenclature

α	channel angle	ϕ	nanoparticle volume fraction
η	dimensionless angle	μ	dynamic viscosity
θ	any angle	ν	kinematic viscosity
ρ	density	B_0	electromagnetic induction
σ	conductivity of the fluid	$u(r,\theta)$	velocity along radial direction
P	fluid pressure		

Subscripts

nf	nanofluid	f	base fluid
s	nano-solid particle		

Jeffery [1] and Hamel [2] first studied the two-dimensional steady motion of a viscous fluid through convergent-divergent channels which is called classical Jeffery-Hamel flow in fluid dynamics. Later, this problem is extensively studied by various researchers. A survey of information on this problem can be found in [3]. The theory of MHD is inducing current in a moving conductive fluid in the presence of magnetic field; such induced current results force on ions of the conductive fluid. The theoretical study of MHD channel has been a subject of great interest due to its extensive applications in designing cooling systems with liquid metals, MHD generators, accelerators, pumps, and flow meters [4-5]. The small disturbance stability of MHD plane-Poiseuille flow was investigated by Makinde and Motsa [6] and Makinde [7]. Their results showed that magnetic field had stabilizing effects on the flow. Damping and controlling of electrically conducting fluid can be achieved by means of an electromagnetic body force (Lorentz force), which produced by interaction of an applied magnetic field and an electric current that usually is externally supplied. Anwari et al. [8] studied the fundamental characteristics of linear Faraday MHD theoretically and numerically, for various loading configurations. Homsy et al. [9] emphasized on the idea that in such problems, the moving ions drag the bulk fluid with themselves, and such MHD system induces continued pumping of conductive fluid without any moving part.

Apart from using numerical methods, the Jeffery-Hamel flow problem was solved by other techniques including the Homotopy analytical method (HAM),the Homotopy perturbation method (HPM), the Adomain decomposition method (ADM) and the spectral-Homotopy analysis method. Recently, the three analytical methods such as Homotopy analysis method, Homotopy perturbation method and Differential transformation method (DTM) were used

by Joneidi et al. [10] to find the analytical solution of Jeffery-Hamel flow. Moreover, the models on classical semi-analytical methods have experienced a revival, in connection with the scheme of new hybrid numerical-analytical techniques for nonlinear differential equations, such as Hermite–Padé approximation method, which demonstrated itself as a powerful benchmarking tool and a prospective substitute to traditional numerical techniques in various applications in science and engineering. The classical Jeffery-Hamel problem was extended in Axford [11] to include the effects of external magnetic field on conducting fluid. Motsa et al. [12] found the solution of the nonlinear equation for the MHD Jeffery-Hamel problem by using novel hybrid spectral-homotopy analysis method. Moghimi et al. [13] also solved the Jeffery-Hamel flow problem by using the homotopy perturbation method. Taking into account the rising demands of modern technology, including chemical production, power station, and microelectronics, there is a need to develop new types of fluids that will be more effective in terms of heat exchange performance. The term ‘nanofluid’ was envisioned to describe a fluid in which nanometer-sized particles were suspended in conventional heat transfer basic fluids [14]. More recently, the effects of magnetic field and

nanoparticle on the Jeffery-Hamel flow using a powerful analytical method called the Adomian decomposition method were studied by Sheikholeslami et al. [15]. Many studies on nanofluids are being conducted by scientists and engineers due to their diverse technical and biomedical applications. Examples include nanofluid coolant: electronics cooling, vehicle cooling, transformer cooling, super powerful and small computers cooling and electronic devices cooling; medical applications: cancer therapy and safer surgery by cooling and process industries; materials and chemicals: detergency, food and drink, oil and gas.

The aim of this work is to apply the perturbation method with MAPLE to find the approximate solutions into series of nonlinear differential equations governing the MHD Jeffery-Hamel flow with the effect of nanoparticles volume fraction on velocity profiles, and a comparison between the Hermite–Padé approximation (HPA) and ADM results is provided. The series is analysed to show the velocity profiles with effect of ϕ and Hartmann number *Ha* and the change in singularity graph for channel angle α and flow Reynolds number *Re* by the effect of ϕ with the help of approximation method as an extension of Sheikholeslami et al. [15]. The combined effect of nanoparticle and magnetic field to the relation among velocity field, channel angle and Reynolds number in the flow using HPA is not addressed yet.

2. Mathematical formulation

Consider a steady two-dimensional laminar incompressible flow of conducting viscous nanofluid from a source or sink between two channel walls intersect at an angle 2α in the axis of z. A cylindrical coordinate system (r,θ,z) is used and assume that the velocity is purely radial and depends on r and θ so that there is no change in the flow parameter along the z-direction. Further it is presumed that there is a magnetic field acting in the vertical downward direction. The continuity equation, the Navier-Stokes equations and Maxwell's equations in reduced polar coordinates are [13]

$$\frac{\rho_{nf}}{r}\frac{\partial}{\partial r}(ru(r,\theta))=0, \tag{1}$$

$$u(r,\theta)\frac{\partial u(r,\theta)}{\partial r}=-\frac{1}{\rho_{nf}}\frac{\partial P}{\partial r}+\nu_{nf}\left(\frac{\partial^2 u(r,\theta)}{\partial r^2}+\frac{1}{r}\frac{\partial u(r,\theta)}{\partial r}+\frac{1}{r^2}\frac{\partial^2 u(r,\theta)}{\partial \theta^2}-\frac{u(r,\theta)}{r^2}\right) -\frac{\sigma {B_0}^2}{\rho_{nf} r^2}u(r,\theta), \tag{2}$$

$$\frac{1}{\rho_{nf} r}\frac{\partial P}{\partial \theta}-\frac{2\nu_{nf}}{r^2}\frac{\partial u(r,\theta)}{\partial \theta}=0, \tag{3}$$

$$\rho_{nf}=\rho_f(1-\phi)+\rho_s\phi,\ \ \mu_{nf}=\frac{\mu_f}{(1-\phi)^{2.5}},\ \ \nu_{nf}=\frac{\mu_f}{\rho_{nf}}, \tag{4}$$

Here, ϕ is the solid volume fraction. The boundary conditions are as follows:

At the centerline of the channel: $\dfrac{\partial u(r,\theta)}{\partial \theta}=0.$

At the boundary of the channel: $u(r,\theta)=0.$

Considering purely radial flow, the continuity Eq. (1) implies that

$$f(\theta)=ru(r,\theta) \tag{5}$$

The dimensionless form of the velocity parameter can be obtained according to [2]

$$f(\eta)=\frac{f(\theta)}{f_{\max}},\ \text{where}\ \eta=\frac{\theta}{\alpha} \tag{6}$$

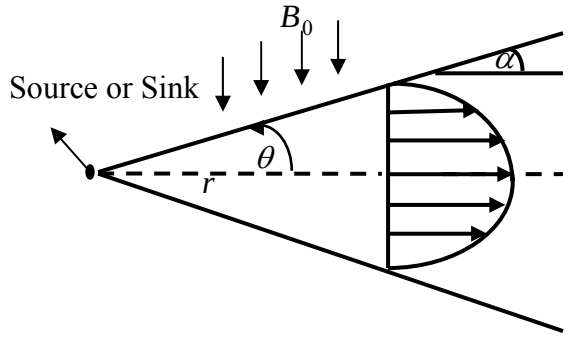

Fig.1 Geometry of the problem

Substituting (5) into (2) and (3) and eliminating the pressure term P, the nonlinear ordinary differential equation can be written as [15]

$$f'''(\eta) + 2\alpha \,\mathrm{Re}\, A^*(1-\phi)^{2.5} f(\eta) f'(\eta) + (4-(1-\phi)^{1.25} Ha)\alpha^2 f'(\eta) = 0, \tag{7}$$

$$A^* = (1-\phi) + \frac{\rho_s}{\rho_f}\phi, \quad Ha = \sqrt{\frac{\sigma {B_0}^2}{\rho_f \nu_f}}, \tag{8}$$

$$\mathrm{Re} = \frac{f_{\max}\alpha}{\nu_f} = \frac{U_{\max} r\alpha}{\nu_f} \quad \begin{pmatrix} divergent\ channel : \alpha > 0,\ f_{\max} > 0 \\ convergent\ channel : \alpha < 0,\ f_{\max} < 0 \end{pmatrix} \tag{9}$$

Where A^* is a parameter, Hartmann number *Ha* and Reynolds number *Re*, channel angle α .
The boundary conditions are reduced to following form:

$$f(0) = 1,\ f'(0) = 0,\ f(1) = 0. \tag{10}$$

Physically, these boundary conditions mean that maximum values of velocity are observed at centerline $\eta = 0$ as shown in Fig. 1. Also, the rate of velocity is zero at $\eta = 0$ and at the solid boundary, the no-slip condition is considered.

3. Series analysis

The following power series expansion is considered in terms of the parameter α as equations (7) and (10) are non-linear for velocity field

$$f(\eta) = \sum_{i=0}^{\infty} f_i(\eta)\alpha^i, \tag{11}$$

We then find that $f(\eta)$ has a singularity at $\alpha = \alpha_c$ of the form

$f(\eta) \sim C(\alpha_c - \alpha)^{\delta_c}$ with the critical exponent δ_c .

The non-dimensional governing equations are then solved into series solution by substituting the Eq. (11) into Eqs. (7) and (10) and equating the coefficients of powers of α .

Order zero (α^0) :

$$\frac{d^3 f_0(\eta)}{d\eta^3} = 0, \tag{12}$$

$$f_0(0) = 1,\ f_0'(0) = 0,\ \ f_0(1) = 0 \tag{13}$$

Order one (α^1) : $$\frac{d^3 f_1(\eta)}{d\eta^3} + 2\,\mathrm{Re}\,A^*(1-\phi)^{2.5}\, f_0(\eta)\frac{df_0(\eta)}{d\eta} = 0, \tag{14}$$

$$f_1(0) = 0,\ f_1'(0) = 0,\ \ f_1(1) = 0 \tag{15}$$

With the help of algebraic programming language MAPLE, we have computed the first 42 coefficients for the series of the velocity $f(\eta)$ in terms of α , Ha , Re, ϕ , A^* . The first few coefficients of the series for $f(\eta)$ are as follows:

$$f(\eta,\alpha,Ha,\mathrm{Re},\phi,A^*) = 1-\eta^2 - \frac{1}{30}\eta^2(\eta-1)(\eta+1)(\eta-2)(\eta+2)\,\mathrm{Re}\,A^*(1-\phi)^{2.5}\alpha + \frac{1}{12}\eta^2(\eta-1)(\eta+1)$$
$$(4-(1-\phi)^{1.25}Ha)\alpha^2 + \frac{1}{5040}\eta^2(\eta-1)(\eta+1)(5\eta^4-9\eta^2-9)\,\mathrm{Re}(1-\phi)^{2.5}A^*(4-(1-\phi)^{1.25}Ha)\alpha^3 \tag{16}$$
$$+ O(\alpha^4)$$

Applying differential and algebraic approximate methods to the series we determine the comparison between HPA and ADM solution and the convergence of critical values and the change in singularity graph for the channel angle and flow Reynolds number by the positive effect of nanoparticle volume fraction. The effect of magnetic field and nanoparticle on velocity field are also shown graphically using differential approximate method. The utility of the solution series has widened using Hermite-Pade' approximants method described below.

4. Computational procedure: Hermite-Padé approximants.

In the present analysis, we shall employ a very efficient solution method, known as Hermite-Padé approximants, which was first introduced by Padé [17] and Hermite [18]. Drazin –Tourigney[19] Approximants is a particular kind of algebraic approximants and Khan [20] introduced High-order differential approximant as a special type of differential approximants. More information about the above mentioned approximants can be found in the respective references.

5. Results and Discussions

The main objective of the current work is to analyze the effect of nanoparticle and high magnetic field on Jeffery-Hamel flow of viscous incompressible conducting fluid by using Hermite-Padé approximants. Although there are four parameters of interest in the present problem the effects of nanoparticle volume fraction ϕ , channel angle α , Reynolds number *Re* and Hartman number *Ha*. At first, viscous fluid ($\phi = 0$) with magnetic field effect is considered, and finally nanofluid flow without magnetic field ($Ha = 0$) is investigated. The series (16) is analyzed by differential approximation method to show the variation in the critical value α_c and Re_c with critical exponent β_c for various values of ϕ significantly. The results of the numerical computations of velocity profiles for different values of the aforementioned parameters are displayed graphically in Figures. (2)- (5) and the comparison between ADM and HPA solutions is shown in table by analyzing the series in (16) using Hermite- Padé approximation (HPA) method. The values by HPA and ADM method are compared in Table 1 when $\phi = 0$, $\mathrm{Re} = 25$, and $\alpha = 5^\circ$. It is noticed that there is a good agreement between the HPA and ADM results. Hence, such results confirm the accuracy of Hermite- Padé approximation method. In this table, difference is defined as follows: $\text{difference} = \left| f(\eta)_{\mathrm{ADM}} - f(\eta)_{\mathrm{HPA}} \right|$ .Table 2 displays the convergence of $\alpha_c \approx 0.08730158 \approx 5^\circ$ up to 15 decimal places at $d = 7$ using $N = 42$ terms with $\mathrm{Re} = 286$, $Ha = 0$ and $\phi = 0.2$ and the values of β_c confirm that α_c is a simple pole using HODA. Moreover, it is seen from Table 3 that the critical channel semi-angle α_c decreases uniformly for the nanoparticle volume fraction $\phi = 0,\ 0.05,\ 0.1,\ 0.15,\ 0.2$ with $Ha = 0$ at $d = 7$ taking $N = 42$. It is observed from Table 4 that the critical Reynolds number Re_c converges to 12 decimal places and Re_c is a pole verified by the values of β_c . Table 5 represents that Re_c almost identical for $\phi = 0,\ 0.05,\ 0.1,\ 0.15,\ 0.2$ with $Ha = 0$ at $d = 7$ taking $N = 42$.

Table. 1 Comparison between ADM solution and HPA solution for velocity when $\phi = 0$, Re = 25, and $\alpha = 5^{\circ}$

	$Ha = 0$			$Ha = 250$			$Ha = 500$		
η	ADM	HPA	Difference	ADM	HPA	Differen	ADM	HPA	Difference
0.0	1.000000	1.000000	0.000000	1.000000	1.000000	0.000000	1.000000	1.000000	0.000000
0.1	0.986637	0.987221	0.000584	0.990196	0.988723	0.001473	0.992695	0.990224	0.002471
0.2	0.947127	0.949319	0.002192	0.960841	0.955136	0.005705	0.970544	0.960953	0.009591
0.3	0.883146	0.887563	0.004417	0.912079	0.899943	0.012136	0.912273	0.912323	0.00005
0.4	0.797259	0.803959	0.0067	0.811225	0.824219	0.012994	0.832683	0.844478	0.011795
0.5	0.692638	0.701095	0.008457	0.713799	0.729267	0.015468	0.743421	0.757440	0.014019
0.6	0.572716	0.581931	0.009215	0.604866	0.616433	0.011567	0.643816	0.650935	0.007119
0.7	0.440850	0.449556	0.008706	0.476625	0.486859	0.010234	0.515303	0.524163	0.00886
0.8	0.300013	0.306907	0.006894	0.325834	0.341211	0.015377	0.361234	0.375515	0.014281
0.9	0.152552	0.156476	0.003924	0.171160	0.179355	0.008195	0.194730	0.202234	0.007504
1.0	0.000000	0.000000	0.000000	0.000000	0.000000	0.000000	0.000000	0.000000	0.000000

Table 2 Estimates of critical angles α_c and corresponding exponent δ_c at Re = 286, $Ha = 0$, $\phi = 0.2$

d	N	α_c	δ_c
2	7	0.087791814807783	-0.81857308585
3	12	0.087301495423310	-1.00000278437
4	18	0.087301579020751	-1.00000000000
5	25	0.087301587301587	-1.00000000000
6	33	0.087301587301587	-1.00000000000
7	42	0.087301587301587	-1.00000000000

Table 3 Numerical values of critical angles α_c and corresponding exponent δ_c at Re = 286, $Ha = 0$.

ϕ	α_c	δ_c
0	0.129532298313616	-1.000000000000
0.05	0.105332830881605	-0.999999999999
0.1	0.093857368991825	-1.000000000000
0.15	0.088633460885129	-0.999999999999
0.2	0.087301587301587	-1.00000000000

Table 4 Numerical values of critical Reynolds number Re_c and corresponding exponent δ_c at $\alpha = 0.0873$, $Ha = 0, \phi = 0.2$.

d	N	Re_c	δ_c
2	7	288.957669152957	-0.63794257823868
3	12	286.941934247595	-0.99957972630227
4	18	286.939323918124	-0.9999999999996
5	25	286.939323918119	-1.0000000000000
6	33	286.939323918121	-1.0000000000000
7	42	286.939323918121	-1.0000000000000

Figures 2 and 3 show the effect of magnetic field on the velocity profiles for divergent channels. A resemblance is observed between the ADM and HPA solutions. The velocity curves show that the rate of alteration is significantly reduced with increase of Hartmann number. The transverse magnetic field opposes the alteration phenomena clearly. Because the variation of Ha leads to the variation of the Lorentz force due to magnetic field and the Lorentz force produces more resistance to the alternation phenomena.

Table 5 Numerical values of critical Reynolds number Re_c and corresponding exponent δ_c at $\alpha = 0.0873$, $Ha = 0$.

ϕ	Re_c	δ_c
0	286.939323918122	-1.00000000000
0.05	286.939323918121	-1.00000000000
0.1	286.939323918120	-0.99999999999
0.15	286.939323918120	-0.99999999999
0.2	286.939323918121	-1.0000000000000

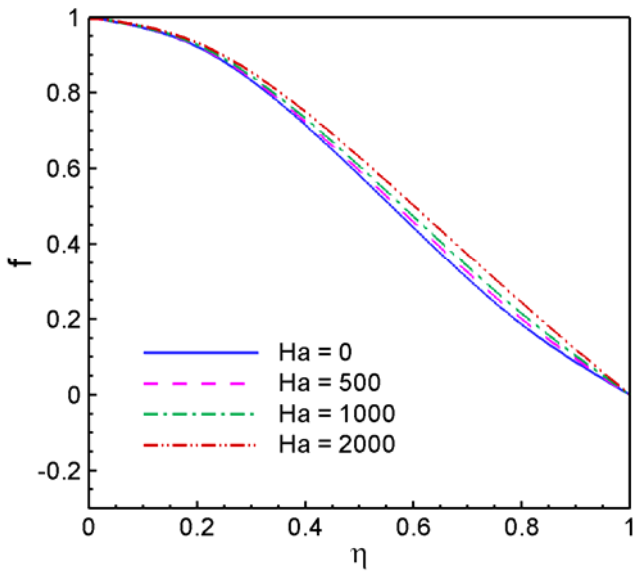

(a) $\alpha = 2.5^\circ, \mathrm{Re} = 200, \text{and } \phi = 0$

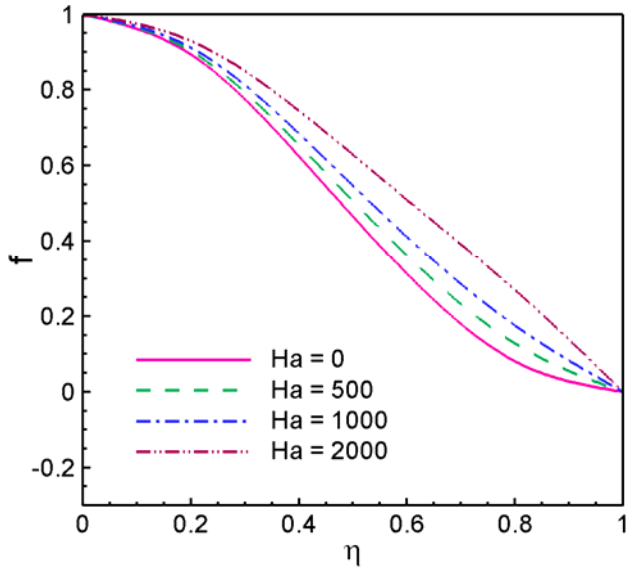

(b) $\alpha = 5^\circ, \mathrm{Re} = 200, \text{and } \phi = 0$

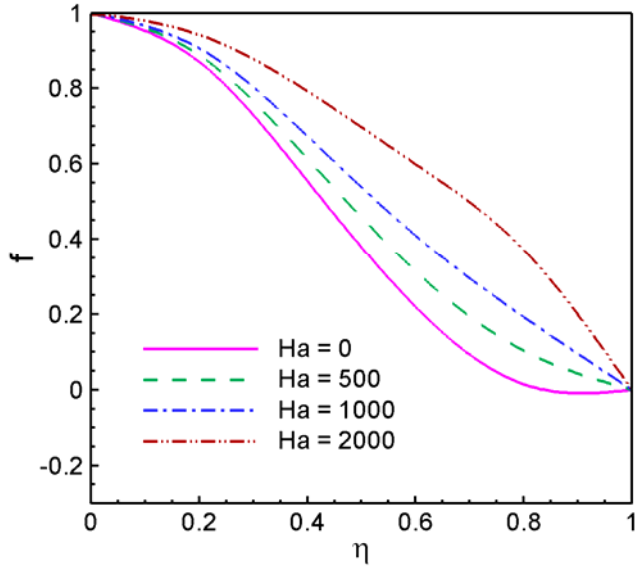

(c) $\alpha = 7.5^\circ, \mathrm{Re} = 200, \text{and } \phi = 0$

Fig .2 Velocity profile in divergent channel with different values of α and *Ha*.

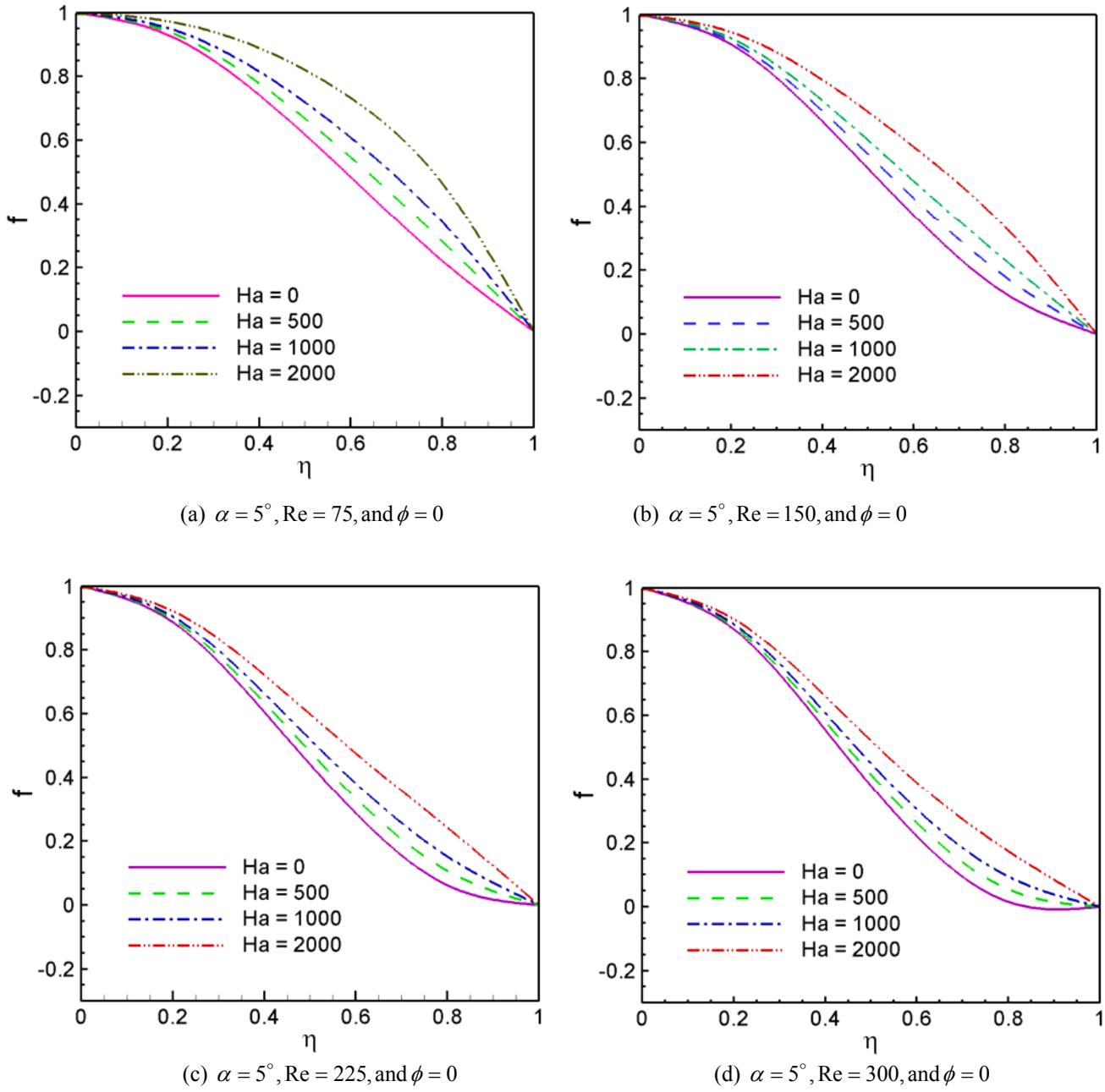

(a) $\alpha = 5^{\circ}, \mathrm{Re} = 75, \text{and } \phi = 0$ (b) $\alpha = 5^{\circ}, \mathrm{Re} = 150, \text{and } \phi = 0$

(c) $\alpha = 5^{\circ}, \mathrm{Re} = 225, \text{and } \phi = 0$ (d) $\alpha = 5^{\circ}, \mathrm{Re} = 300, \text{and } \phi = 0$

Fig. 3 Velocity profile in divergent channel with different values of *Re* and *Ha*.

It is seen from Figure 2 that the velocity increases moderately with rising *Ha* at a small angle $\alpha = 2.5^{\circ}$, but the differences between velocity profiles are more noticeable at larger angles. However, the backflow does not occur in converging channel but it is detected in diverging channel for higher values of α at a critical Reynolds number when $Ha = 0$. Whereas to diminish the backflow an increased *Ha* is essential. Figure 3 represents the consequences of magnetic field at $\alpha = 5^{\circ}$ with different Reynolds numbers. In Fig. 3(a) at $\alpha = 5^{\circ}, \mathrm{Re} = 75$ as Hartmann number increases the velocity increases and no backflow is observed. It can be seen from Fig. 3(b) that at $\alpha = 5^{\circ}, \mathrm{Re} = 150$ backflow starts when magnetic field is absent, this properties is abolished with rising Hartmann

number. The backflow enlarges at high Reynolds number, hence larger magnetic field is required to abolish it. Moreover, it is detected from Fig. 3(c) at $\alpha = 5^{\circ}, \mathrm{Re} = 225$ that backflow is abolished at $Ha = 2000$ whereas there occurs backflow for each values of Hartmann number in Fig. 3(d) at $\alpha = 5^{\circ}, \mathrm{Re} = 300$.

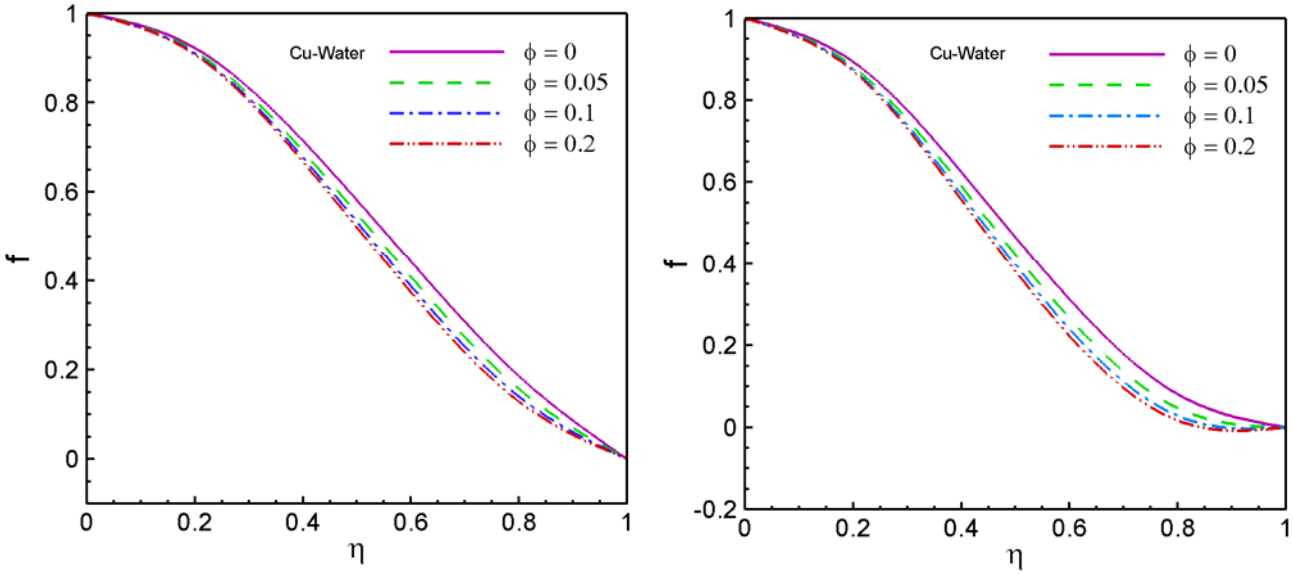

(a) $\alpha = 5^{\circ}, \mathrm{Re} = 100, \text{and } Ha = 0$ (b) $\alpha = 5^{\circ}, \mathrm{Re} = 200, \text{and } Ha = 0$

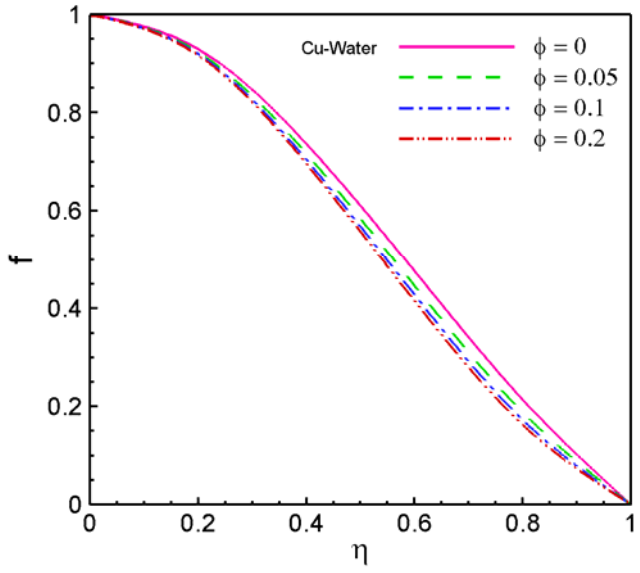

(c) $\alpha = 2^{\circ}, \mathrm{Re} = 200, \text{and } Ha = 0$

Fig.4 Effects of nanoparticle volume fraction on velocity profiles.

Moreover, a Cu-Water nanofluid flow is considered and the effect of nanoparticle volume fraction is analysed. It is

assumed that the base fluid and the nanoparticles are in thermal equilibrium and no slip occurs between them. The densities of water and Cu are $\rho_f = 998.1$ and $\rho_s = 8933$ respectively.

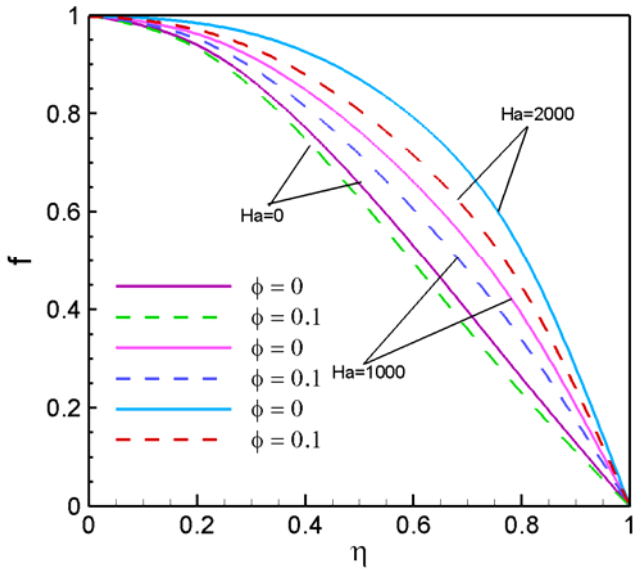

Fig.5 Velocity profiles for several values of Hartmann number and solid volume fraction $\alpha = 5^{\circ}, \mathrm{Re} = 50$.

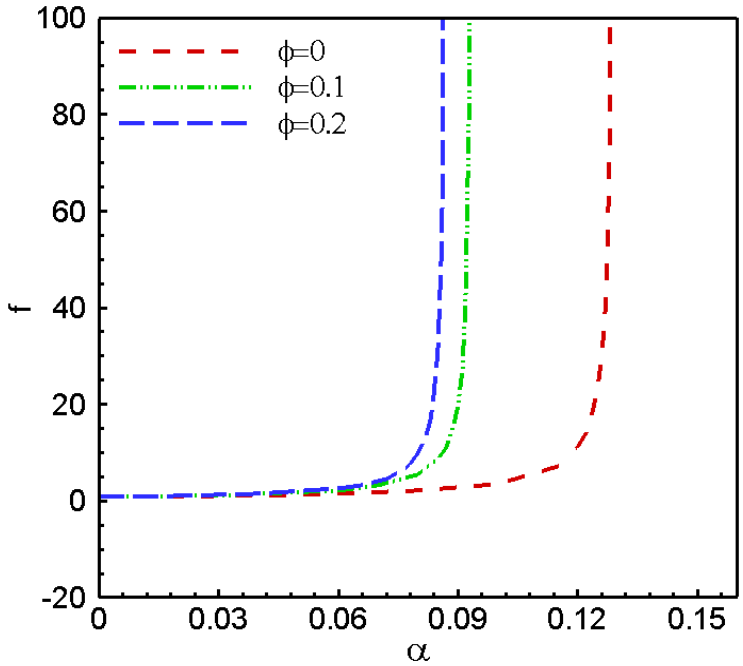

Fig 6: Approximate singularity diagram of α in the $(\alpha - f(\eta = 0.5))$ plane at $Ha = 0,\ \mathrm{Re} = 286.93$ with different ϕ obtained by Drazin-Tourigny method for $d = 7$.

Fig. 4 implies that as nanoparticle volume fraction increases the boundary layer thickness increases. It is also

observed that at high values of Reynolds number and channel angle, backflow starts with rising nanoparticle volume fraction. Fig. 5 predicts the combined effects of magnetic field and nanoparticle volume fraction on the velocity for divergent channel with fixed Reynolds number. The figure represents sensible increases in the velocity with rising Hartmann number for both viscous and nanofluid that coincide with those results of [21]. It is also observed that for all Hartmann numbers there is no backflow in the viscous fluid $\phi = 0$, nevertheless backflow starts for nanofluid with $Ha = 0$ at $\alpha = 5^{\circ}, \mathrm{Re} = 50$ and this phenomenon is abolished with the rising values of Hartmann number. Employing the algebraic approximation method to the series (16) we have obtained the singularity graph of α and Re . Figure 6 shows the effect of nanoparticles on the singularity diagram of α. It is interesting to note that the curve turns at α_c, and as the values of ϕ increase, the singular points as simple poles change from $\alpha \approx 0.12953229 \approx 7.5^{\circ}$ to $\alpha \approx 0.09385736 \approx 5.5^{\circ}$ and then to $\alpha \approx 0.08730158 \approx 5^{\circ}$ respectively. Moreover, from Figure 7 it is observed that the solution diagram of *Re* also turns at Re_c .The singular points remain almost similar and the three curves coincides for different values of ϕ. The conjecture of Figures 6 and 7 is consistent with the results shown in Tables 3 and 5 using differential approximation.

Fig. 8 illustrates the relation between velocity profile and Reynolds number for different values of solid volume fraction and Hartmann number. In Fig. 8(a) the effect of Reynolds number *Re* on the fluid velocity is noticed at fixed Hartmann number $Ha = 1000$ for both viscous fluid and nanofluid. The velocity decreases when *Re* increases for both types of fluid, because the increment of *Re* increases $f_{\max}$, results reduction in fluid velocity. Moreover, there is a significant diminution in velocity for rising values of ϕ. Fig. 8(b) demonstrates the relation between velocity and Reynolds number with the effect of Hartmann number. The effect of magnetic field enhances the velocity curves positively for nanofluid noticed in the figure From Figure 9 the relation between velocity field and channel angle for different values of solid volume fraction and Hartmann number is observed. In Figure 9(a) for viscous and nanofluid the velocity curves decrease for rising values of α. Again ϕ acts to reduce the fluid velocity for every values of α. There occurs a significant variation in the velocity curve as α increases for various values of Hartmann number in Figure 9(b).

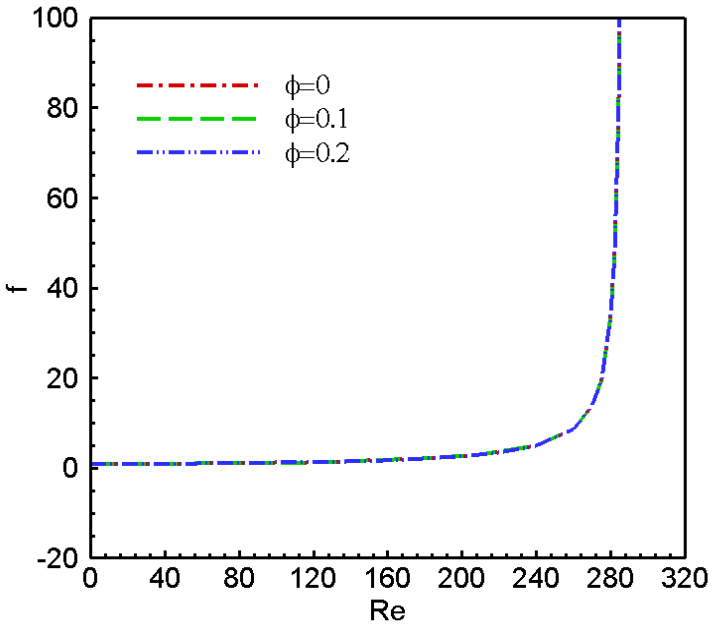

Fig 7: Approximate singularity diagram of *Re* in the $(\mathrm{Re}- f(\eta = 0.5))$ plane at $Ha = 0,\ \alpha = 0.0873$ with different ϕ obtained by Drazin-Tourigny method for $d = 7$.

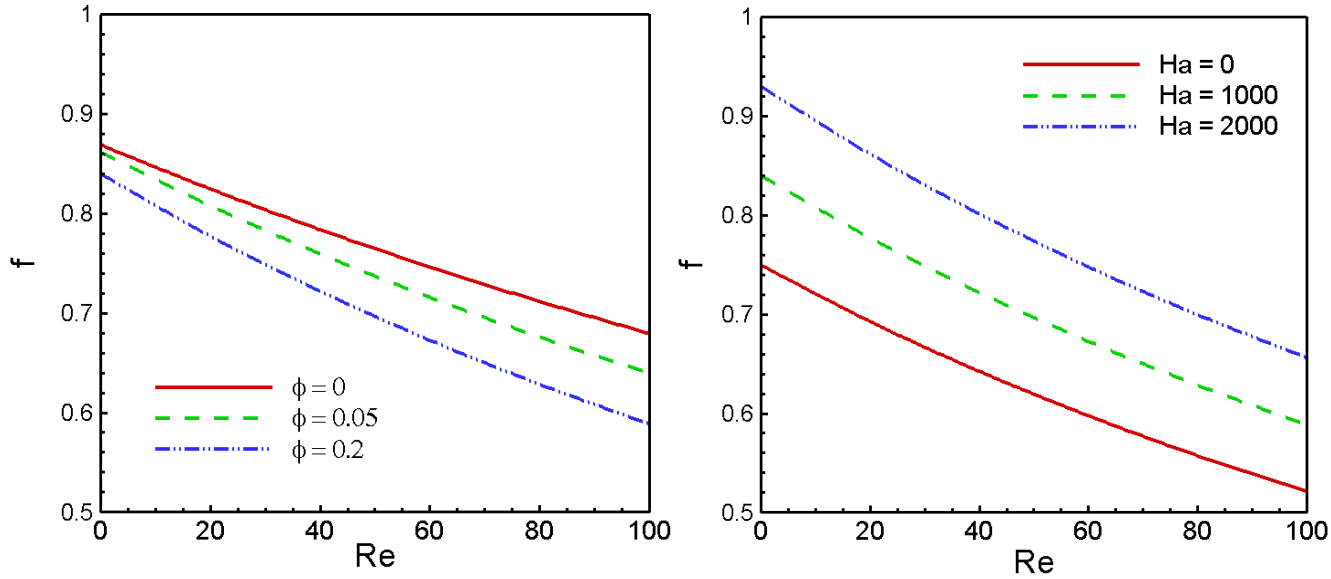

(a) (b)

Fig.8 Relation between velocity profiles and Reynolds number (a) for several values of solid volume fraction at $Ha = 1000$ and (b) for several values of Hartmann number at $\phi = 0.2$ with $\alpha = 5^{\circ}$.

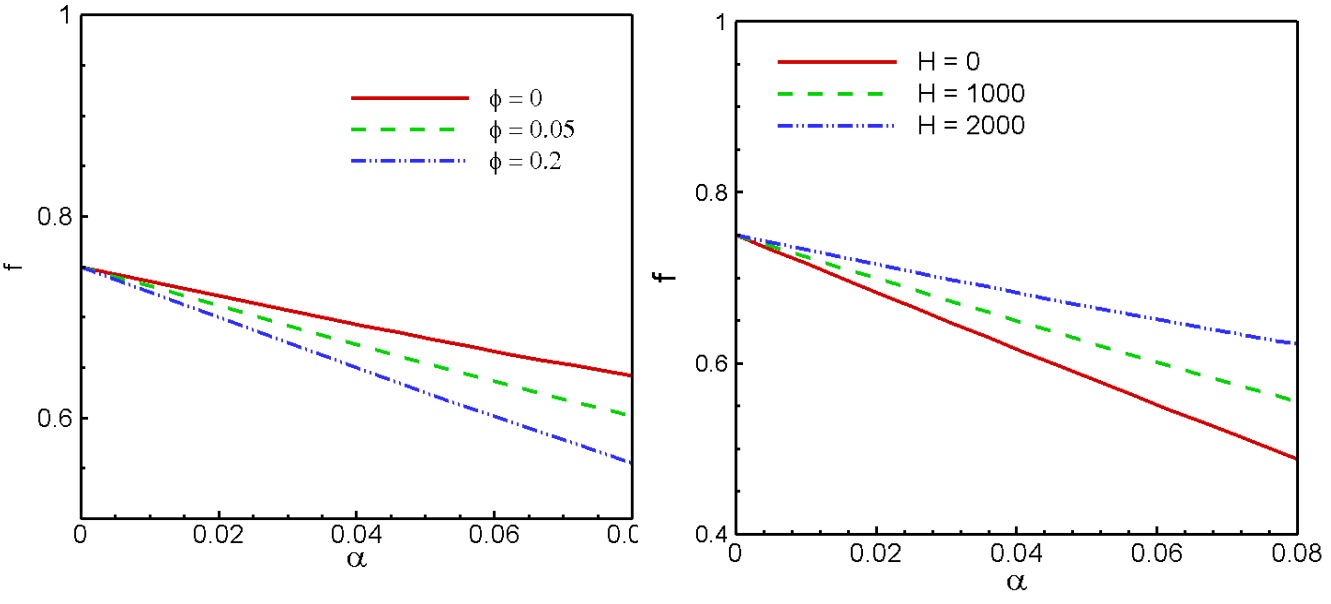

(a) (b)

Fig.9 Relation between velocity profiles and α (a) for several values of solid volume fraction at $Ha = 1000$ and (b) for several values of Hartmann number at $\phi = 0.2$, with $\mathrm{Re} = 200$.

6. Conclusion

The magnetohydrodynamic Jeffry-Hamel flow problem in the nanofluid is investigated using a special type of

Hermite-Padé approximation technique. A comparison is made between the available results obtained by different methods such as Adomian decomposition method, Differential Transform method and the present approximate solutions. The accurate numerical approximation of the critical parameters of the flow is obtained. The numerical study indicates that HPA is a powerful approach for solving this problem. The influence of various physical parameters on the velocity field is discussed in detail. The basic conclusions are as follows:

- Increasing Reynolds number leads to reduction of fluid velocity in the channel.
- Increasing Hartmann number produces to backflow reduction. High Hartmann number is required to decline of backflow in larger angles or Reynolds number.
- The velocity decreases as nanoparticle volume fraction increases.
- The dominating singularity behaviour of the wall divergence semi-angle and flow Reynolds number is analysed with the effect of nanoparticle volume fraction.
- The relationship among velocity field, Reynolds number and channel angle due to the variation of solid volume fraction and Hartmann number is also analysed.

Moreover, we provide a basis for guidance about new approximants idea for summing power series that should be chosen for many problems in fluid mechanics and similar subjects.

Acknowledgements

This work is done within the framework the PhD program of the corresponding author under Department of Mathematics, Bangladesh University of Engineering and Technology, Dhaka. Financial support from the Bangabandhu Fellowship on Science and ICT project is acknowledged.

References

[1] G. B. Jeffery, The two-dimensional steady motion of a viscous fluid, Philosophical Magazine 6(1915) 455-465.
[2] G. Hamel, Spiralförmige Bewgungen Zäher Flüssigkeiten, Jahresbericht Der Deutschen Math. Vereinigung 25 (1916) 34-60.
[3] Q. Esmaili, A. Ramiar, E. Alizadeh, D.D. Ganji, An approximation of the analytical solution of the Jeffery–Hamel flow by decomposition method, Physics Letters A 372 (2008) 3434–3439.
[4] J.E. Cha, Y.C. Ahn, M.H. Kim, Flow measurement with an electromagnetic flow meter in two-phase bubbly and slug flow regimes, Flow Measurement and Instrumentation 12(5-6) (2002) 329–339.
[5] M. Tendler, Confinement and related transport in extrap geometry, Nuclear Instruments and Methods in Physics Research, 207(1-2) (1983) 233–240.
[6] O.D. Makinde, S.S. Motsa, Hydromagnetic stability of plane Poiseuille flow using Chebyshev spectral collocation method, J. Ins. Math. Comput. Sci. 12(2) (2001) 175–183.
[7] O.D. Makinde, Magneto-hydrodynamic stability of plane-Poiseuille flow using multi-deck asymptotic technique, Math. Comput. Model. 37(3-4) (2003) 251–259.
[8] M. Anwari, N. Harada, S. Takahashi, Performance of a magnetohydrodynamic accelerator using air-plasma as working gas, Energy Conversion Management 4(2005) 2605–2613.
[9] A. Homsy, S. Koster, J.C.T. Eijkel, A. Ven der Berg, F. Lucklum, E. Verpoorte, N.F. De Rooij, A high current density DC magnetohydrodynamic (MHD) micropump, Royal Society of Chemistry's Lab on a Chip 5 (2005) 466–471.
[10] A.A. Joneidi, G. Domairry, M. Babaelahi, Three analytical methods applied to Jeffery–Hamel flow, Commun. Nonlinear Sci. Numer. Simulat. 15 (2010) 3423–3434.
[11] W.I. Axford, The Magnetohydrodynamic Jeffrey–Hamel problem for a weakly conducting fluid, Q. J. Mech. Appl. Math. 14 (1961) 335–351.
[12] S.S. Motsa, P. Sibanda, F.G. Awad, S. Shateyi, A new spectral-homotopy analysis method for the MHD Jeffery–Hamel problem, Computers & Fluids 39 (2010) 1219–1225.
[13] S.M. Moghimia, D.D. Ganji, H. Bararnia, M. Hosseini, M. Jalaal, Homotopy perturbation method for nonlinear MHD Jeffery–Hamel Problem, Computers and Mathematics with Applications 61 (2011) 2213–2216.
[14] C.S. Kaka, A. Pramuanjaroenkij, Review of convective heat transfer enhancement with nanofluids. International Communications in Heat and Mass Transfer, 52(13-14) (2009) 3187–3196.
[15] M. Sheikholeslami, D.D. Ganji, H.R. Ashorynejad, H.B. Rokni, Analytical investigation of Jeffery-Hamel flow with high magnetic field and nanoparticle by Adomian decomposition method, Appl. Math. Mech. Engl. Ed. 33 (2012) 25–36.
[16] S.M. Aminossadati, B. Ghasemi, Natural convection cooling of a localized heat source at the bottom of a nanofluid-filled enclosure. Eur. J. Mech. B/Fluids 28(2009) 630–640.
[17] H. Padé, Sur la représentation approchée d'une fonction pour des fractions rationnelles, Ann. Sci. École Norm. Sup. Suppl. 9(1892) 1-93.
[18] C. Hermite, Sur la généralisation des fractions continues algébriques, Annali di Mathematica Pura e Applicata 21(2) (1893) 289-308.
[19] P.G. Drazin, Y. Tourigny, Numerically study of bifurcation by analytic continuation of a function defined by a power series, SIAM Journal of Applied Mathematics. 56(1996) 1-18.
[20] M.A.H. Khan, High-Order Differential Approximants, Journal of Computational and Applied Mathematics 149(2002) 457-468.
[21] J.C. Umavathi, M. Shekar, Effect of MHD on Jeffery-Hamel flow in Nanofluids by DTM, Int. J. of Eng. Res. And Appl. 3(5)(2013) 953-962.

Available online at www.sciencedirect.com

ScienceDirect

Procedia Engineering 00 (2015) 000–000

Procedia Engineering

www.elsevier.com/locate/procedia

6th BSME International Conference on Thermal Engineering (ICTE 2014)

Natural Convection Flow of Cu-H_2O Nanofluid along a Vertical Wavy Surface with Uniform Heat Flux

Farjana Habiba[a,]*, Md.Mamun Molla[b], M.A. Hakim Khan[c]

[a]*Department of Natural Science, Stamford University Bangladesh, Siddeswari Road, Dhaka-1217, Bangladesh*
[b]*Department of Electrical Engineering & Computer Science, North South University, Dhaka, Bangladesh*
[c]*Department of Mathematics, Bangladesh University of Engineering & Technology(BUET), Dhaka-1000, Bangladesh*

Abstract

A numerical study on natural convection flow of Cu-Water nanofluid along a vertical wavy surface with uniform heat flux has been carried out. The governing boundary layer equations are transformed into parabolic partial differential equations by applying a suitable set of variables. The resulting nonlinear system of equations are then mapped into a regular rectangular computational domain and solved numerically by using an implicit finite difference method. Numerical results are thoroughly discussed in terms of velocity and temperature distributions, surface temperature distribution, skin friction coefficient and Nusselt number coefficient for selected key parameters such as solid volume fraction of nanofluid (ϕ) and amplitude (a) of surface waviness. In addition, velocity vectors, streamlines and isotherms are plotted to visualize momentum and thermal flow pattern within the boundary layer region.

Peer-review under responsibility of organizing committee of the 6th BSME International Conference on Thermal Engineering (ICTE 2014).

Keywords: Natural convection; Nanofluid; Uniform heat flux; Vertical wavy Surface; Finite difference method

* Corresponding author. Tel.: 01552323503; fax: +0-000-000-0000 .
*E-mail address:*farjanahabiba4@gmail.com

Peer-review under responsibility of organizing committee of the 6th BSME International Conference on Thermal Engineering (ICTE 2014).

1. Introduction

Natural convection heat transfer plays an important role in various branches of engineering, for instance industrial cooling systems, nuclear reactors, solar collectors, transportation industries, biochemical applications, heat exchangers, electronic cooling devices and so forth. Therefore, numerous theoretical and computational investigations have been performed on natural convection heat transfer effect in regular surfaces for saving energy as well as getting better performance and minimizing operating costs. However, flow over roughened surface is very common in industries and in several heat transfer devices since irregular surfaces transfer more heat energy compared to flat surfaces. Thus effects of irregular surfaces on convective heat transfer enhancement have been carried out by several investigators. Natural convection and mixed convection heat transfer along a vertical wavy surface have been investigated first time by Yao [1, 3] and Moulic and Yao [2] respectively. Later on, Molla et al. [4] studied natural convection flow along a vertical wavy surface with uniform surface temperature in presence of heat generation/ absorption. Again, Molla and Hossain [5] studied the effect of radiation on mixed convection flow along a vertical wavy surface. Molla et al. [6] also studied natural convection flow along a vertical complex wavy surface with uniform heat flux. All these results showed that the surface geometry plays a vital role in heat transfer effect. In all research works illustrated above, air has been considered as working fluid which has a low thermal conductivity and thus the heat transfer effect is inherently limited. In order to improve the heat transfer performance of conventional fluids (such as water, oil, ethylene glycol), a large number of numerical and experimental research works were conducted by dispersing highly conductive micro-sized solid particles in base fluid since Maxwell's

Nomenclature

a	Amplitude of wavy surface
C_f	Skin friction coefficient
Gr	Grashof number
k	Thermal conductivity
$\hat{n}$	Unit vector normal to the wavy surface
Nu	Nusselt number
$\Pr$	Prandtl number
q_w	Uniform heat flux at the surface
T	Fluid temperature

Greek symbols

β	Thermal expansion coefficient
θ, Θ	Dimensionless temperature function
μ	Viscosity
ρ	Density
ϕ	Solid volume fraction of nanofluid
α	Thermal diffusivity
ν	Kinematic viscosity
$\sigma(x)$	Non-dimensional surface profile
τ	Shear stress
ψ	Stream function

Subscript

m	Average condition
w	Surface condition
∞	Ambient condition
f	Fluid
s	Nanoparticles
nf	Nanofluid

theoretical work was published more than 100 years ago. However, due to the large size and high density of particles, there is no perfect way to prevent the particles in clogging or settling out of suspension sedimentation. To overcome those, efforts have been made to develop a new innovative type of heat transfer fluid termed as nanofluid by dispersing ultrafine solid particles (small enough not to clog or settle down) in base fluid. Choi [7] is the first who coined the term nanofluid in 1995 and Choi et al. [8] showed that the thermal conductivity of the fluid could be increased up to approximately two times with the addition of small amount (less than 1% by volume) of nanoparticles to conventional fluid. In almost two decades, a number of investigations related to heat transfer enhancement using nanofluids have been conducted. Xuan and Li [9] introduced a procedure for preparing a nanofluid consisting of water and 5 volume% Cu nanoparticles and revealed a great potential of nanofluid in enhancing thermal conductivity. Khanafer and Vafai [10] analysed thermophysical characteristics of nanofluids. They introduced several relative correlations for the thermophysical properties of nanofluids based on available experimental data. Khanafer et al. [11] investigated a problem of buoyancy-driven heat transfer enhancement of nanofluids in a two-dimensional enclosure. They analysed four different models based on physical properties of nanofluid for a range of Grashof numbers and volume fractions. It was found that the suspended nanoparticles substantially increase heat transfer rate for any given Grashof number. Santra et al. [12] conducted a study of heat transfer augmentation in a differently heated square cavity using copper-water nanofluid. Oztop and Abu-Nada [13] studied natural convection flow in nanofluid-filled partially heated rectangular enclosures with different types of nanoparticles. They found an increase in mean Nusselt number with the volume fraction of nanoparticles and an enhancement in heat transfer at low aspect ratio. Abu-Nada and Oztop [14] studied the influence of inclination angle and volume fraction of nanoparticle on natural convection heat transfer and fluid flow in a two-dimensional square enclosure filled with Cu-nanofluid and noticed a remarkable enhancement in heat transfer for copper nanoparticles. Basak and Chamkha [15] investigated natural convection of various nanofluids (Cu-water, Al_2O_3-water, TiO_2-water) confined with square cavities with various thermal boundary layer based on visualization of heat flow via heat functions or heat lines. They found that Cu-water and Al_2O_3-water exhibit larger enhancement of heat transfer rates.
The above review of literature clearly indicates that natural convection flow is mainly related to heated enclosures of regular surfaces filled with nanofluids. So attention has been given to analyze the effect of nanofluid on natural convection flow along a vertical wavy surface. Here Cu-water nanofluid is considered as working fluid due to the excellent thermo-physical properties of Cu-nanoparticles and low cost preparations as well. The thermal characteristics of nanofluid are extracted from Khanafer's model [10]. The Navier-Stokes and energy equations are coupled with volume fraction of nanoparticles, Prandtl number and amplitude of surface waviness to describe the phenomenon systematically. These boundary layer equations are solved numerically by using a very efficient implicit finite difference method designated by Yao [1, 3]. Finally, solutions are obtained graphically having Prandtl number *Pr=6.2* for various values of solid volume fraction of nanofluid (ϕ) and amplitude of wavy surface (a) in terms of velocity and temperature profiles, skin friction coefficient, surface temperature, average and total Nusselt number coefficients. In addition, streamlines, isotherms and velocity vectors are plotted to observe the flow pattern within the boundary layer.

2. Mathematical formulation

A semi-infinite vertical wavy surface immersed in a nanofluid at the ambient temperature T_∞ is shown schematically in Fig. 1 allowing for the surface which is subjected to a uniform heat flux q_w normal to the surface. The boundary layer analysis outlined below allows the shape of the wavy surface, $\hat{\sigma}(\hat{x})$ to be arbitrary. But the detailed numerical work assumes that the surface exhibits a particular sinusoidal-based deformation from the flat surface. Therefore the wavy surface can be described by

$$\hat{y}_w = \hat{\sigma}(\hat{x}) = \hat{a}\sin(2\pi\,\hat{x}/L) \tag{1}$$

where *L* is the fundamental wavelength associated with wavy surface and $\hat{a}$ is the amplitude of surface waviness. The fluid oncoming to the surface is a water based nanofluid containing uniform copper nanoparticles. The nanofluid is sufficiently dilute with volume fraction ≤ 0.2 such that fluid is considered incompressible and the flow is also assumed to be laminar and steady. The base fluid (water) and the nanoparticles are assumed to be in thermal

equilibrium and no slip occurs between them. The thermo-physical properties are assumed to be constant.

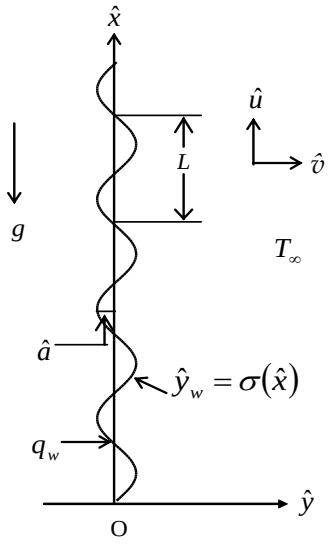

Fig.1. Physical model and coordinate system

2.1. Governing equations

The mass, momentum and energy equations in dimensional form are as follows:

$$\frac{\partial \hat{u}}{\partial \hat{x}} + \frac{\partial \hat{v}}{\partial \hat{y}} = 0 \tag{2}$$

$$\hat{u}\frac{\partial \hat{u}}{\partial \hat{x}} + \hat{v}\frac{\partial \hat{u}}{\partial \hat{y}} = -\frac{1}{\rho_{nf}}\frac{\partial \hat{p}}{\partial \hat{x}} + \frac{\mu_{nf}}{\rho_{nf}}\left(\frac{\partial^2 \hat{u}}{\partial \hat{x}^2} + \frac{\partial^2 \hat{u}}{\partial \hat{y}^2}\right) + \frac{(\rho\beta)_{nf}}{\rho_{nf}} g(T - T_\infty) \tag{3}$$

$$\hat{u}\frac{\partial \hat{v}}{\partial \hat{x}} + \hat{v}\frac{\partial \hat{v}}{\partial \hat{y}} = -\frac{1}{\rho_{nf}}\frac{\partial \hat{p}}{\partial \hat{y}} + \frac{\mu_{nf}}{\rho_{nf}}\left(\frac{\partial^2 \hat{v}}{\partial \hat{x}^2} + \frac{\partial^2 \hat{v}}{\partial \hat{y}^2}\right). \tag{4}$$

$$\hat{u}\frac{\partial T}{\partial \hat{x}} + \hat{v}\frac{\partial T}{\partial \hat{y}} = \alpha_{nf}\left(\frac{\partial^2 T}{\partial \hat{x}^2} + \frac{\partial^2 T}{\partial \hat{y}^2}\right) \tag{5}$$

The boundary conditions are followed by Molla et al. [6]

2.2. Effective thermo-physical properties of nanofluid

- Viscosity : $\mu_{nf} = \mu_f / (1-\phi)^{2..5}$ (6)
- Density : $\rho_{nf} = (1-\phi)\rho_f + \phi\rho_s$ (7)
- Heat capacitance : $(\rho c_p)_{nf} = (1-\phi)(\rho c_p)_f + \phi(\rho c_p)_s$ (8)
- Thermal diffusivity : $\alpha_{nf} = k_{nf} / (\rho c_p)_{nf}$ (9)
- Thermal conductivity : $\frac{k_{nf}}{k_f} = \frac{k_s + 2k_f - 2\phi(k_f - k_s)}{k_s + 2k_f + \phi(k_f - k_s)}$ (10)

Table1. Thermo-physical properties of nanofluid

Properties	Pure water	Cu	Al_2O_3	TiO_2
C_p (J/kg K)	4179	385	765	686.2
ρ (kg/m^3)	997.1	8933	3970	4250
k (W/m K)	0.613	401	40	8.9538
β (1/K)	21×10^{-5}	1.67×10^{-5}	0.85×10^{-5}	0.9×10^{-5}

2.3. Transformation of governing equations

Following Molla et al. [6], a set of non-dimensional parameters is introduced to reduce governing equations into dimesionless form. Thus for both thermo-physical properties of nanofluid and $Gr \to \infty$ the reduced forms of non-dimensional equations are:

$$\frac{\partial u}{\partial x}+\frac{\partial v}{\partial y}=0 \tag{11}$$

$$u\frac{\partial u}{\partial x}+v\frac{\partial u}{\partial y}=\psi_1\left(1+\sigma_x{}^2\right)\frac{\partial^2 u}{\partial y^2}-\frac{\sigma_x\sigma_{xx}}{1+\sigma_x{}^2}u^2+\psi_2\frac{\sigma_x}{1+\sigma_x{}^2}\theta \tag{12}$$

$$u\frac{\partial \theta}{\partial x}+v\frac{\partial \theta}{\partial y}=\frac{1}{\mathrm{Pr}}\lambda\left(1+\sigma_x{}^2\right)\frac{\partial^2 \theta}{\partial y^2} \tag{13}$$

Here $\psi_1=\dfrac{1}{(1-\phi)^{2.5}\left[(1-\phi)+\phi\left(\rho_s/\rho_f\right)\right]}$, $\psi_2=\dfrac{(1-\phi)+\phi\left(\rho_s/\rho_f\right)\left(\beta_s/\beta_f\right)}{(1-\phi)+\phi\left(\rho_s/\rho_f\right)}$,

$$\lambda=\frac{k_{nf}/k_f}{(1-\phi)+\phi\left(\rho c_p\right)_s/\left(\rho c_p\right)_f} \tag{14}$$

The corresponding boundary conditions for the present problem take the form:

$$u=0,\ \ v=0,\qquad \frac{\partial \theta}{\partial y}=-\frac{1}{\sqrt{1+\sigma_x^2}}\ \text{ at }\ y=0 \tag{15}$$

$$u=0,\qquad \theta=0\ \text{ as }\ y\to\infty \tag{16}$$

3. Numerical methods

We introduce a set of transformations followed by Molla et al. [6] to obtain parabolic form of dimensionless equations. Solutions of this non-linear system of parabolic equations (11) — (14) with corresponding boundary conditions (Eqns. (15)—(16)) are obtained by using an efficient finite difference method developed by L.S.Yao [1, 3]. The diffusion terms in continuity, momentum and energy equations are discretized by central difference scheme while a backward difference scheme is adopted for the convection terms. The resulting system of tri-diagonal

algebraic equations is solved by Gaussian elimination method. In computation, we start with the energy equation to determine θ and then use momentum equation to calculate tangential velocity *u*. Finally the continuity equation is solved directly for normal velocity *v*. The computation is started at *X = 0.0*, and then marches upstream. The size of the computational domain is *X=4.0* and *Y=80.0*. Here the grid size in the *y* direction is fixed at *0.01* while the step size in *x* direction is fixed at *0.005*. After solving θ , *u*, *v* and their derivatives, computations of local skin friction coefficient and Nusselt number are of practical interest.

The skin friction coefficients obtained by using a set of transformations are defined as

$$C_{f_x}(Gr)^{1/5} \Big/ \left\{2(5X)^{2/5}\right\} = \sqrt{1+\sigma_x^2}\,\frac{\partial U}{\partial Y}\Big]_{Y=0} \tag{17}$$

And the average Nusselt number is defined as

$$Nu_m\left(\frac{5X}{Gr}\right)^{1/5} = \frac{X^{1/5}\int_0^X \sqrt{1+\sigma_x{}^2}\,dX}{\int_0^X \sqrt{1+\sigma_x{}^2}\,X^{1/5}\Theta(X,0)dX} \tag{18}$$

4. Results and discussion

In the present study, numerical analysis of natural convection flow of nanofluid along a vertical wavy surface with uniform heat flux has been studied by developing a very efficient numerical code to carry out a number of simulations for a wide range of controlling parameters such as solid volume fraction of nanofluid (ϕ) and amplitude of surface waviness (*a*). It is to be mentioned here that $\phi=0.0$ corresponds to the pure fluid and pure water has been considered as the base fluid having *Pr=6.2* following Khanafer et al. [11]. Uniform copper nanoparticles are used extensively during investigation to analyze the effect of nanofluid on the momentum and thermal features. Moreover, three different nanoparticles such as Copper (Cu), Alumina (Al_20_3) and Titania (TiO_2) are used to compare their effects on the rate of heat transfer enhancement. Numerical results are presented and interpreted for two controlling parameters ϕ and *a* to know their effects on velocity and temperature profiles, surface temperature, skin friction coefficients and Nusselt number coefficients. Moreover, streamlines, isotherms and velocity vectors are also drawn to analyze the flow pattern. All numerical results are obtained for selected values of volume fraction of nanoparticles ($0.0 \le \phi \le 0.2$) and various values of amplitude ($a=0.1, 0.3, 0.5$) of wavy surface. For variation due to ϕ, amplitude is taken as $a=0.3$ while volume fraction is considered as $\phi=0.10$ for the variation of *a*.

The tangential and normal velocity distributions for different values of volume fractions of Cu-water nanofluid have been presented in Fig.2. It is seen that the tangential velocity decreases slightly inside the boundary layer while boundary layer thickness remains almost same with increasing values of solid volume fraction of nanofluid. This is due to the fact that the density and viscosity of nanofluid increases with increasing volume fraction and reduces the fluid flow. Fig.2. also shows that the normal velocity increases significantly away from the surface but no remarkable change is seen near the surface with increasing values of ϕ since ϕ increases energy transport through the fluid within the boundary layer.

The corresponding fluid temperature distribution and surface temperature distribution for different values of ϕ are shown in Fig.3. It is evident that the temperature distribution decreases with increasing ϕ near the surface. But at the position of *Y=0.75*, temperature profiles take a constant value and then increase with increasing values of ϕ. This is because heat transfer features of a nanofluid increase significantly with ϕ and consequently the movements of particles increase energy exchange rates in the fluid. Hence thermal dispersion is enhanced in the flow of nanofluid.

It is also found that the development of surface temperature profiles are oscillatory and these oscillations become weaker as it moves away from the leading edge and decrease gradually along the surface with increasing volume

fraction of nanoparticles.

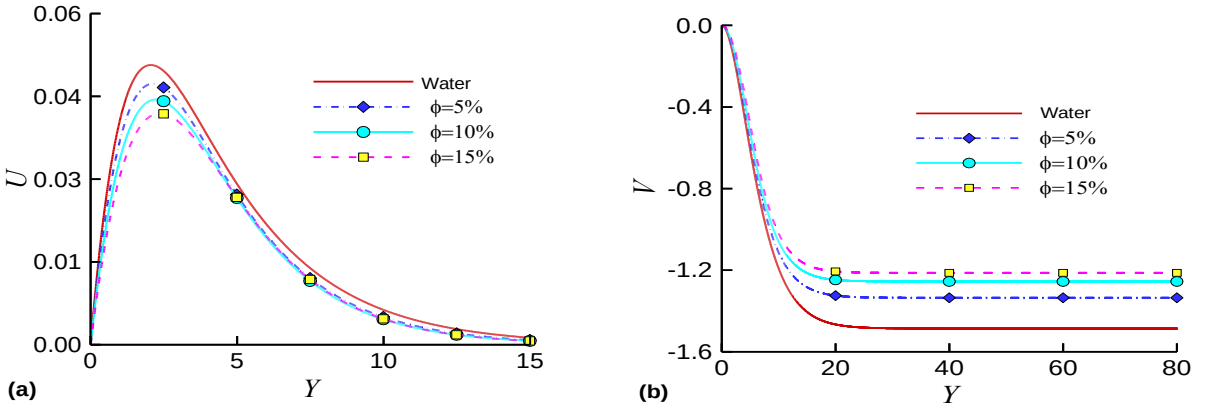

Fig. 2. Tangential and normal velocity profiles for Cu-Water nanofluid with a=0.3, Pr=6.2

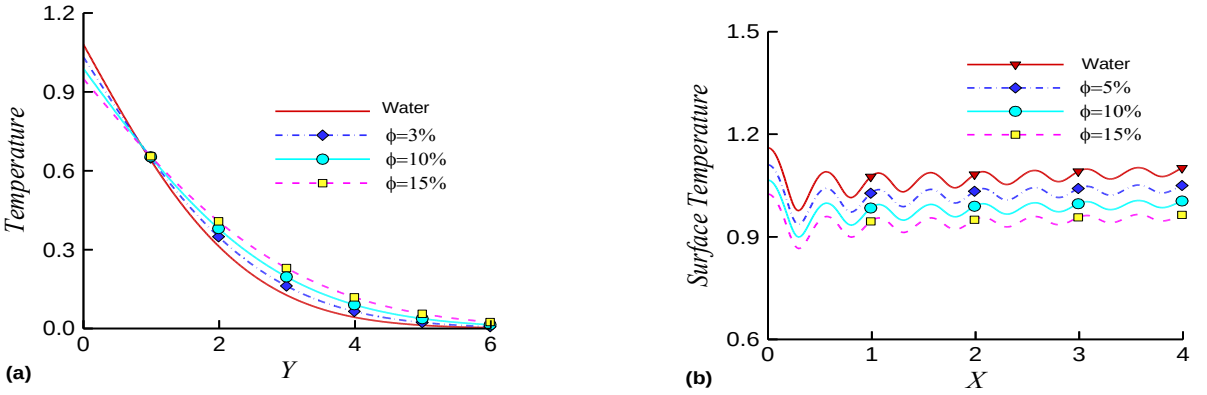

Fig. 3. (a) Fluid temperature distribution; (b) Surface temperature distribution for various values of ∅ with *a=0.3, Pr=6.2*

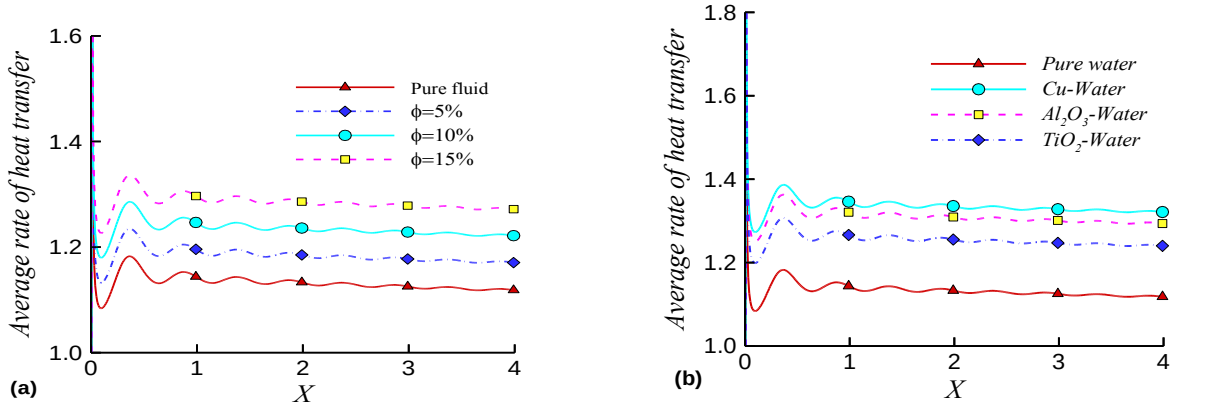

Fig.4. Average Nusselt number for (a) various volume fractions of nanofluid (*a=0.3)*; (b) different nanofluids (*a=0.3, ∅=0.2*)

The effects of volume fraction of nanoparticles and several nanofluids on average rate of heat transfer in terms of average Nusselt number are shown in Fig.4. It is observed that the average rate of heat transfer increases with

increasing $\emptyset$ since thermal conductivity of nanofluid increases with $\emptyset$. Though viscosity of nanofluid increases with increasing $\emptyset$ and it has reverse effect on heat transfer enhancement rate. But it is clear from Table1. that thermal conductivity of Cu-nanoparticle is higher as compared to its viscosity for any percentage of nanoparticles. Also heat transfer rate is proportional to the temperature gradient which increases with increasing $\emptyset$. Again, three types of nanoparticles such as Cu, Al_20_3 and TiO_2 are used to develop an assessment of their effects on average rate of heat transfer in terms of average Nusselt number for $\emptyset=0.2$. It is found that nanofluid can enhance Nusselt number significantly. The lowest rate of heat transfer is obtained for TiO_2 due to the domination of conduction mode of heat transfer since TiO_2 has the lowest value of thermal conductivity as compared to Cu and Al_20_3 as given in Table1. However, the difference between two impacts of Al_20_3 and Cu nanoparticles on heat transfer enhancement is negligible. The thermal conductivity of Al_20_3 is approximately one tenth of Cu as given in Table1. But Al_20_3 has a unique property that is its low thermal diffusivity. The reduced value of thermal diffusivity leads to high temperature gradients and therefore huge enhancement in heat transfers. The Cu nanoparticles have heavy thermal diffusivity and thus it reduces temperature gradient which affects heat transfer performance of Cu nanoparticles.

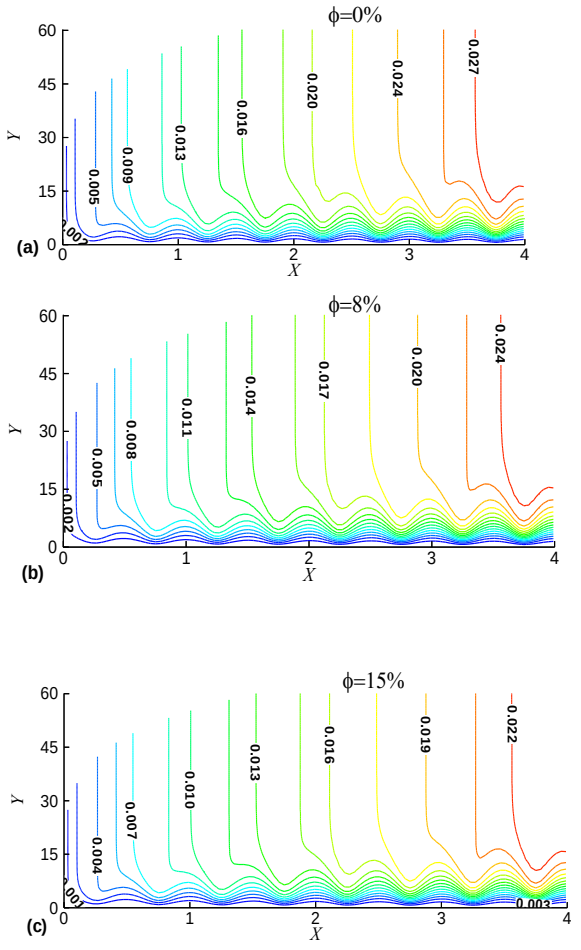

Fig.5. Streamline contours for various volume fractions (a=0.3)

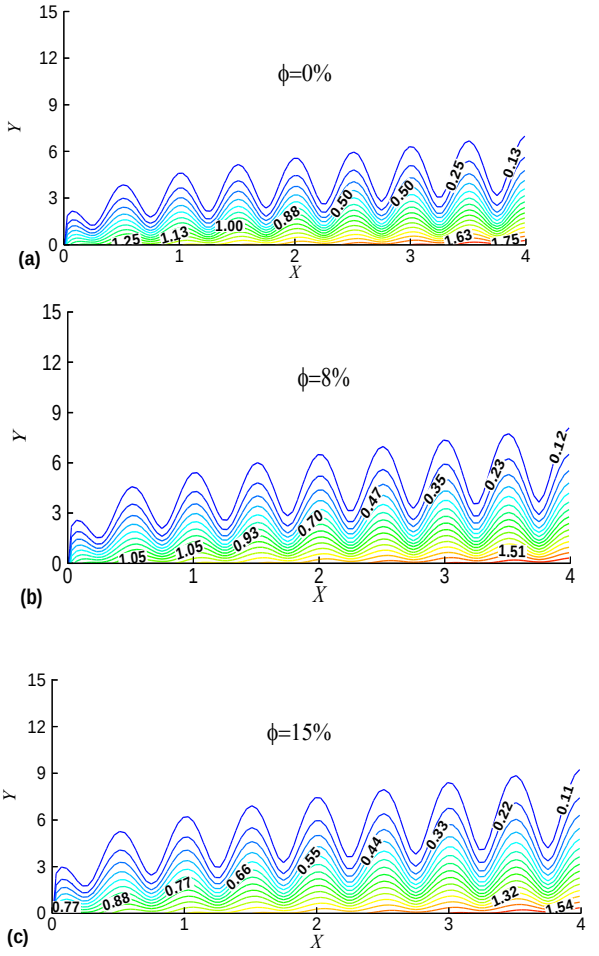

Fig.6. Isotherms for various volume fractions (a=0.3)

Streamlines and isotherms for various volume fractions of Cu-nanoparticles are illustrated in Fig.5. and Fig.6 respectively. It is observed that the strength of flow decreases as $\emptyset$ increases. Here $\psi_{max}=0.027$, 0.024 and 0.022 for $\emptyset=0.0$, 0.08 and 0.15 respectively. It is also noticed that the thermal boundary layer reduces for large values of $\emptyset$. This is due to the fact that $\emptyset$ amplifies heat transfer enhancement rate. Moreover, huge viscous effect for large $\emptyset$ reduces flow rate. It is marked here that isotherm contours exhibit an oscillatory pattern because of amplitude of

surface waviness.

Velocity vectors of wavy surface for various ∅ are shown in Fig.7. where *∅=0%* corresponds pure water. It is observed that the flow pattern is sinusoidal because of wavy surface but no significant change is marked in the intensity of fluid flow with increasing *∅*.

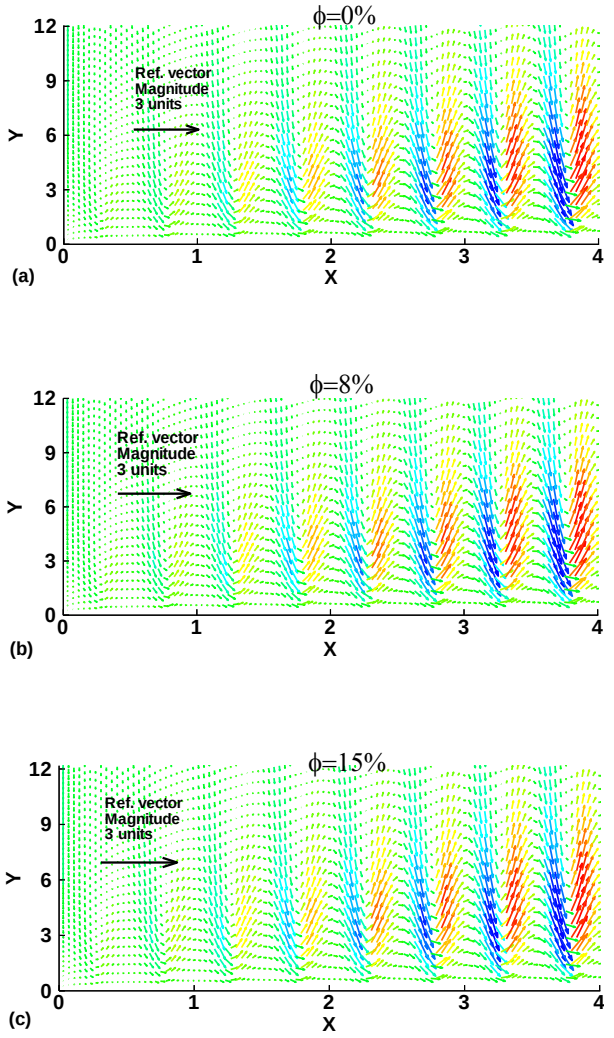

Fig.7. Velocity vectors for various volume fractions.

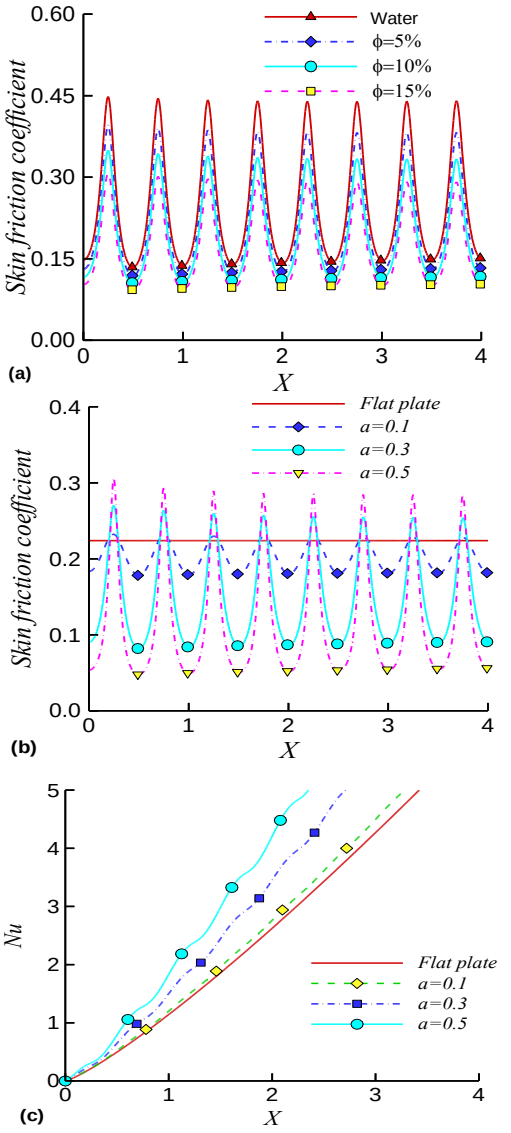

Fig. 8. Skin friction coefficient for (a) various volume fractions (b) various amplitudes; (c) Total Nusselt number

The effects of solid volume fraction of nanofluid (*∅*) and amplitude of wavy surface (*a*) on surface shear stress in terms skin friction coefficients are displayed in Fig.8. It is clear that the skin friction coefficients exhibit a sinusoidal behaviour along the wavy surface. Skin friction coefficient decreases slightly with increasing ∅ as it increases fluid density and consequently reduces fluid motion. It is also seen that skin friction coefficient increases with increasing values of amplitude. Moreover, to study the geometric effect on heat transfer rate, the influence of amplitude of wavy surface on total rate of heat transfer in terms of total Nusselt number is depicted in

Fig. 8. It is observed that total Nusselt number increases with increasing values of *a* as it accelerates fluid motion which augments temperature gradient.

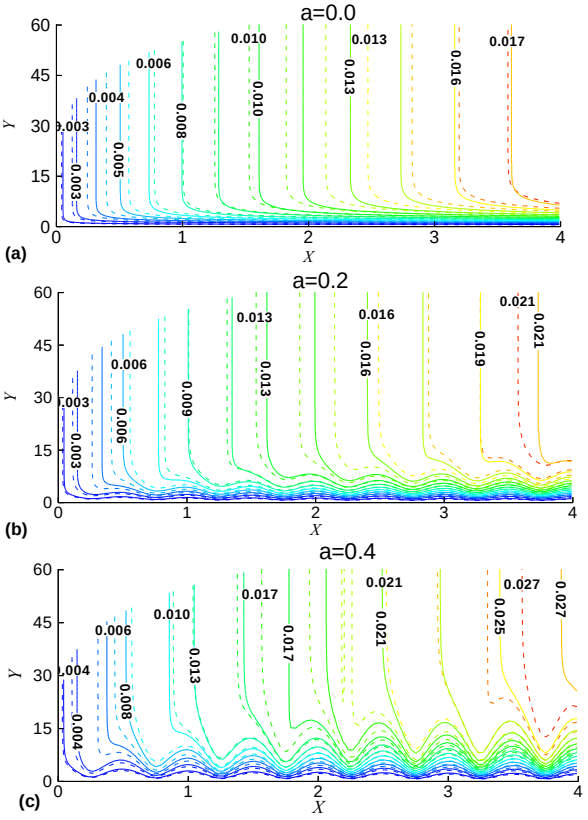

Fig.9. Comparison of streamlines contours between nanofluid (——) and pure fluid (- - - -) for $\emptyset$=10%.

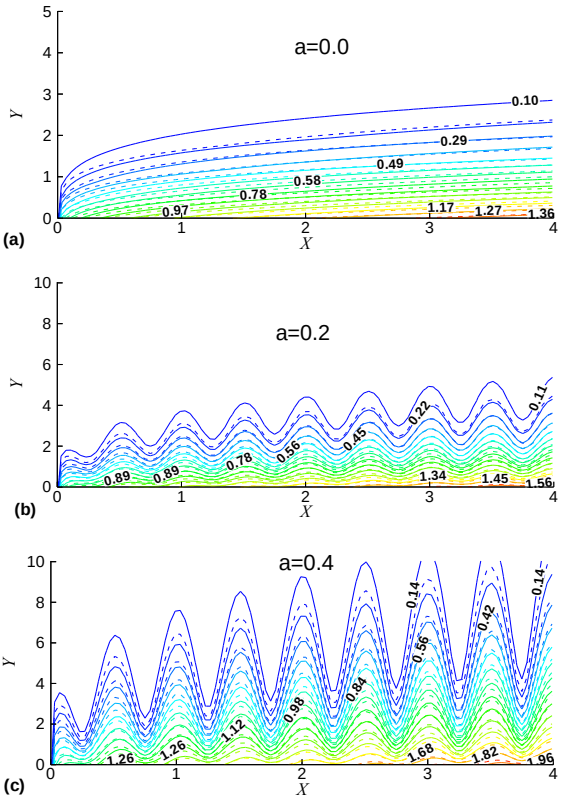

Fig. 10. Comparison of isotherm contours between nanofluid (——) and pure fluid (- - - -) for $\emptyset$=10%.

A comparison between pure water (plotted by dashed lines) and Cu-water nanofluid (plotted by solid lines) as well as the effect of amplitudes of surface waviness on streamlines and isotherms are illustrated in Fig.9. and Fig.10. respectively. It is clearly seen from Fig.9. that the shapes of flow patterns are affected by amplitude. The maximum values of ψ for *a=0.0, 0.2* and *0.4* are *0.017, 0.021* and *0.027* respectively which specify that the flow flux of the boundary layer increases significantly with the increasing wave amplitude. It is also seen that for constant value of stream function, the intensity of pure water is larger than that of Cu-water nanofluid. Unlike flat surface, isotherms for wavy surface show a sinusoidal behaviour in Fig.10. Both velocity and temperature gradients increase while amplitude increases. Therefore thermal boundary layer becomes thicker with the increasing values of amplitude of wavy surface.

5. Conclusion

A numerical study has been performed to investigate the effect of solid volume fraction of Cu-nanoparticles as well as amplitude of surface waviness on natural convection boundary layer flow along a vertical wavy surface with uniform heat flux. Various volume fractions of nanoparticles and different values of amplitude of wavy surface have been considered for momentum and temperature fields as well as skin frictions and heat transfer rates. In addition, contours of streamlines, isotherms and velocity vectors are also drawn to analyze flow pattern. From the present study some findings are summarized as follows:

- The average rate of heat transfer increases with increasing values of solid volume fraction of nanoparticles and the total rate of heat transfer also increases for increasing values of amplitude. However, the Nusselt number for Cu-nanoparticles was found larger among others.
- The skin friction coefficient decreases with rising values of ϕ and increases with increasing values of a.
- Tangential velocity decreases for increasing values of both ϕ and a. Normal velocity increases slightly with increasing values of a near the surface when it decreases sinificantly away from the surface. It also increases with increasing values of ϕ throughout the boundary layer.
- Both surface temperature and fluid temperature distribution within the boundary layer increase with increasing values of a. But the surface temperature decreases with increasing ϕ . When ϕ increases, the fluid temperature decreases near the surface but increases slightly away from the surface.
- Flow pattern is remarkably affected by amplitude of surface waviness whereas ϕ causes minor influence on fluid flow which is observed from streamlines and velocity vectors. The maximum value of stream function decreases when both ϕ and a increase.
- The thickness of thermal boundary layer increases significantly with increasing values of a while it reduces slightly with rising values of ϕ.

References

[1] Yao, L.S., Natural convection along a vertical wavy surface, ASME J. Heat Transfer vol. 105, pp. 465–468 (1983).

[2] Moulic, S.G. and Yao, L.S., Natural convection along a vertical wavy surface with uniform heat flux, ASME J. Heat Transfer vol. 111, pp. 1106–1108 (1989).

[3] Yao, L.S., Natural convection along a vertical complex wavy surface, International Journal of Heat and Mass Transfer vol. 49, pp. 281-286 (2006).

[4] Molla, M.M., Hossain, M.A. and Yao, L.S., Natural convection flow along a vertical wavy surface with uniform surface temperature in presence of heat generation/ absorption, International Journal of Thermal Sciences vol. 43, pp. 157-163 (2004).

[5] Molla, M.M. and Hossain, M.A., Radiation effect on mixed convection laminar flow along a vertical wavy surface, International Journal of Thermal Sciences vol. 46, no. 9, pp. 926-935 (2007).

[6] Molla, M.M., Hossain, M.A. and Yao, L.-S., Natural convection flow along a vertical complex wavy surface with uniform heat flux, Journal of Heat Transfer vol. 129, no. 10, pp. 1403-1407 (2007).

[7] Choi, S.U.S., Enhancing thermal conductivity of fluids with nanoparticles, in: The proceeding of the 1995 ASME International Mechanical Engineering Congress and Exposition, San Francisco, USA, ASME, FED 231/MD 66, pp. 99-105 (1995).

[8] Choi, S.U.S., Zhang Z.G., Yu W., Lockwood F.E., Grulke E.A., Anomalously thermal conductivity enhancement in nanotube suspensions, Appl. Phys. Lett. 79, pp 2252-2254 (2001).

[9] Xuan, Y. and Li, Q., Heat Transfer enhancement of nanofluids, Int. J. of Heat and Fluid Flow vol. 21, pp. 58-64 (2000).

[10] Khanafer, K. and Vafai, K., A critical synthesis of thermophysical characteristics of nanofluids, International Journal of Heat and Mass Transfer vol. 54, pp. 4410-4428 (2011).

[11] Khanafer, K., Vafai, K. and Lightstone, M., Buoyancy-driven heat transfer enhancement in a two-dimensional enclosure utilizing nanofluids, International Journal of Heat and Mass Transfer vol. 46, pp. 3639-3653 (2003).

[12] Santra, A.K., Sen, S. and Chakraborty, N., Study of heat transfer augmentation in a differently heated square cavity using copper-water nanofluid, International Journal of Thermal Sciences vol. 47, pp. 1113-1122 (2008).

[13] Oztop, H.F. and Abu-Nada, E., Numerical study of natural convection in partially heated rectangular enclosures filled with nanofluids, Int. J. of Heat and Fluid Flow vol. 29, pp. 1326-1336 (2008).

[14] Abu-Nada, E. and Oztop, H.F., Effect of inclination angle on natural convection in enclosures filled with Cu-water nanofluid, International Journal of Heat and Fluid Flow vol. 30, pp. 669-678 (2009).

[15] Basak, T. and Chamkha, A.J., Heatline analysis on nanural convection for nanofluids confined within square cavities with various thermal boundary conditions, International Journal of Heat and Mass Transfer vol. 55, pp. 5526-5543 (2012).

Available online at www.sciencedirect.com

ScienceDirect

Procedia Engineering 00 (2015) 000–000

Procedia Engineering

www.elsevier.com/locate/procedia

6th BSME International Conference on Thermal Engineering (ICTE 2014)

Mixed Convection Heat Transfer inside a Square Cavity Filled with Cu-water Nanofluid

Mohammad Nasim Hasan*, Khondokar Samiuzzaman, S. Hayatul Haque, Sumon Saha, Md. Quamrul Islam

Department of Mechanocal Engineering, Bangladeah University of Engineering and Technology, Dhaka-1000, Bangladeah

Abstract

In the present study, mixed convection heat transfer inside a square cavity filled with Cu-water nanofluid has been investigated numerically. The bottom wall of the cavity is maintained at a constant high temperature while the vertical sidewalls are assumed to be at a constant low temperature. The top wall of the cavity is insulated and moving at a constant velocity. Galerkin finite element method has been employed to solve the continuity, momentum and energy balance equations for the present problem. Analysis of thermal and flow fields inside the cavity has been analysed in terms of isotherms, streamlines and heatlines for a wide range of the Richardson number and solid volume fraction of the nanoparticle. Particular attention was paid to the case of pure mixed convection case with the Richardson No being equal to 1 for various combinations of natural convection and forced convection effects. The heat transfer performance of the system has been analysed in terms of average Nusselt number over the heated wall for various parameters. The present study shows that the distribution of streamline, isothermal lines and heatlines are very sensitive to Richardson number. The present study also shows that larger heat transfer rates can be achieved with nanofluid than the base fluid for all conditions.

Peer-review under responsibility of organizing committee of the 6th BSME International Conference on Thermal Engineering (ICTE 2014).

Keywords: Heat transfer; Nanofluid; Mixed Convection; Heatlines

* Corresponding author. Tel.: +88-02-9665636; fax: +88-02-9665636
E-mail address: nasim@me.buet.ac.bd

Peer-review under responsibility of organizing committee of the 6th BSME International Conference on Thermal Engineering (ICTE 2014).

1. Introduction

Nanofluid is a base fluid having metallic nano sized particles [1]. Thermal conductivity of nanofluid is higher than conventional fluids used for heat transfer applications and therefore gains much attention recently.

Nomenclature

C_p	specific heat, $Jkg^{-1}k^{-1}$	**Greek symbols**	
g	acceleration due to gravity, ms^{-2}	α	thermal diffusivity, m^2s^{-1}
k	thermal conductivity, $Wm^{-1}k^{-1}$	β	thermal expansion co-efficient, K^{-1}
L	side of the square cavity, m	μ	dynamic viscosity, Pa.s
T	temperature, K	π	Heatfunction
u, v	dimensional velocity components, ms^{-1}	ψ	Streamfunction
U, V	non-dimensional velocity components	ρ	density, kgm^{-3}
x, y	dimensional Cartesian coordinate	φ	volume fraction
X, Y	non dimensional coordinates	**Subscript**	
U_0	dimensional lid velocity, ms^{-1}	avg	average value
Pr	Prandtl number	nf	Nanofluid
Gr	Grashof number	f	Basefluid
Re	Reynolds number	h	Hot
Ri	Richardson number	c	Cold

As the demand for using nanofluid is increasing, several studies on convective heat transfer using nanofluids have been reported in recent years. Jou and Tzeng [2] reported a numerical study on natural convection heat transfer phenomena inside a two-dimensional rectangular cavity filled with nanofluids. Their results indicate that increasing the volume fraction of nanoparticles causes heat transfer to increase. Alleborn et al. [3] investigated mixed convection in a shallow cavity with a moving hot bottom wall and a moving top cold wall. Aydm [4] considered both assisting and opposing mechanisms of mixed convection in a lid driven cavity. Khanafer and Chamkha [5] numerically studied mixed convection flow in a lid-driven cavity and reported the effects of the Darcy number and Richardson number on the flow and heat transfer characteristics. Heatline concept was developed by earlier researchers [6] to have a better insight of the conductive as well as convective heat transfer. Although, mixed convection heat transfer with nanofluid have been studied for various geometric configuration as well as various thermal and flow boundary conditions in the past, no attention has been paid to the case of mixed convection inside a square cavity filled with nanofluid with an insulated top wall moving at constant speed with the sidewalls being cold and the bottom wall being maintained at a constant high temperature. Therefore, the present study aims to explore the mixed convection characteristics of the aforementioned case.

2. Physical Model and Governing Equations

The two-dimensional square cavity considered in the present study is shown in Figure 1. The fluid within the cavity is water based nanofluid containing Copper (Cu) nanoparticle. The fluid is sufficiently dilute with volume fraction (φ) $\leq$ 0.2, such that it is considered incompressible and Newtonian. The Boussinesq approximation is adopted to account for the variations of temperature as a function of density and to couple in this way the temperature field to the flow field. The dissipation effect due to the viscous term is neglected and no heat generation is considered. Therefore, the governing equations (i.e. continuity, momentum and energy) for the present problem can be obtained in non-dimensional form as follows:

$$\frac{\partial U}{\partial X}+\frac{\partial U}{\partial Y}=0 \tag{1}$$

$$U\frac{\partial U}{\partial X}+V\frac{\partial U}{\partial Y}=-\frac{\partial P}{\partial X}+\frac{\mu_{nf}}{\rho_{nf}\nu_f}\frac{1}{Re}\left(\frac{\partial^2 U}{\partial X^2}+\frac{\partial^2 U}{\partial Y^2}\right) \tag{2}$$

$$U\frac{\partial V}{\partial X}+V\frac{\partial V}{\partial Y}=-\frac{\partial P}{\partial Y}+\frac{\mu_{nf}}{\rho_{nf}\nu_f}\frac{1}{Re}\left(\frac{\partial^2 V}{\partial X^2}+\frac{\partial^2 V}{\partial Y^2}\right)+\frac{(\rho\beta)_{nf}}{\rho_{nf}\beta_f}(Ri)\theta \tag{3}$$

$$U\frac{\partial \theta}{\partial X}+V\frac{\partial \theta}{\partial Y}=\frac{\alpha_{nf}}{\alpha_f}\frac{1}{RePr}\left(\frac{\partial^2 \theta}{\partial X^2}+\frac{\partial^2 \theta}{\partial Y^2}\right) \tag{4}$$

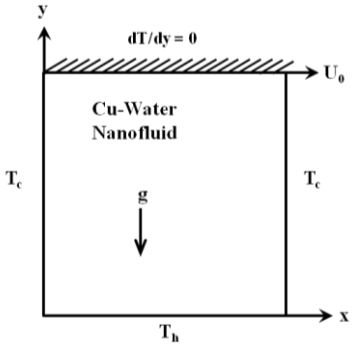

Fig. 1: Physical model of the present study

Various non-dimensional parameters and numbers that appear in the above equations are defined as follows:

$$X=\frac{x}{L},Y=\frac{y}{L},U=\frac{u}{U_0},V=\frac{v}{U_0},\theta=\frac{T-T_c}{T_h-T_c},P=\frac{p}{\rho_{nf}U_0^2},\ Ri=\frac{Gr}{Re^2},Re=\frac{U_0 L}{\nu_f},Gr=\frac{g\beta_f(T_H-T_c)\mathrm{L}^3}{\nu_f^2},Pr=\frac{\nu_f}{\alpha_f} \tag{5}$$

Various thermo-physical properties of Cu-water nanofluid are determined on the basis of the base fluid properties, nano particle properties as well as the volume fraction of the nano particle (φ) as described in [7] listed below:

$$\rho_{nf}=(1-\varphi)\rho_f+\varphi\rho_s \tag{6}$$

$$(\rho C_p)_{nf}=(1-\varphi)(\rho C_p)_f+\varphi(\rho C_p)_s \tag{7}$$

$$(\rho\beta)_{nf}=(1-\varphi)(\rho\beta)_f+\varphi(\rho\beta)_s \tag{8}$$

Moreover, for dynamic viscosity (μ_{nf}) and effective thermal conductivity (k_{nf}) of the nanofluid, Brickman model [8] and Maxwell-Garnetts model [9] are followed respectively as:

$$\mu_{nf}=\frac{\mu_f}{(1-\phi)^{2.5}} \tag{9}$$

$$k_{nf}=k_f\left(\frac{k_s+2k_f-2\phi(k_f-k_s)}{k_s+2k_f+\phi(k_f-k_s)}\right) \tag{10}$$

Table 1: Thermo physical properties of base fluid and nano particles

Properties	Base fluid (Water)	Nanoparticle (Cu)
C_p (Jkg $^{-1}$ K $^{-1}$)	4179	385
k (Wm $^{-1}$K $^{-1}$)	0.613	401
ρ (kgm $^{-3}$)	997.1	8933
β (K^{-1})	21×10 ^{5}	1.67×10 ^{5}
μ (Pa.s)	9.09×10^{-4}	--

The boundary conditions for the present problem are specified as follows:

Topwall	Bottom wall	Vertical sidewalls
$\frac{\partial\theta}{\partial Y}=0, U=1, V=0$	$\theta=1, U=V=0$	$\theta=0, U=V=0$

The average Nusselt number over the top moving wall can be expressed as

$$Nu_{avg}=\frac{1}{L}\int_0^L\left(-\frac{k_{nf}}{k_f}\right)\frac{\partial T}{\partial y}dx=\int_0^1\left(-\frac{k_{nf}}{k_f}\right)\frac{\partial\theta}{\partial Y}dX \tag{11}$$

The velocity field within the cavity can be displayed by using the stream function (ψ) obtained from velocity components U and V while the heat flow can be visualized better in terms of the heat function (Π) obtained from conductive heat fluxes $\left(-\frac{\partial\theta}{\partial X},-\frac{\partial\theta}{\partial Y}\right)$ as well from convective fluxes $(\mathrm{U}\theta,\mathrm{V}\theta)$ as defined below:

$$U=\frac{\partial\psi}{\partial Y},\mathrm{V}=-\frac{\partial\psi}{\partial X} \tag{12}$$

$$\frac{\partial\Pi}{\partial Y}=U\theta-\frac{\alpha_{nf}}{\alpha_f}\frac{\partial\theta}{\partial X},\ -\frac{\partial\Pi}{\partial X}=V\theta-\frac{\alpha_{nf}}{\alpha_f}\frac{\partial\theta}{\partial Y} \tag{13}$$

The no slip boundary condition at the walls corresponds to $\psi = 0$ at all boundaries. For heat function (Π), a reference value $\Pi = 0$ is assumed at (X = 0, Y = 1) which leads to a Dirichlet boundary condition ($\Pi = 0$) at the top insulated wall and a Neumann boundary condition ($n.\nabla \Pi = 0$) for isothermal bottom and sidewalls.

3. Numerical Procedure

The numerical procedure used to solve the governing equations for the present work is the finite element method. It provides the smooth solutions at the interior domain including the corner regions. The non-linear parametric solution method has been chosen to solve the governing equations. This approach will result in substantially fast convergence assurance. A non-uniform triangular mesh arrangement is implemented in the present investigation especially near the heated wall to capture the rapid changes in the dependent variables. A grid sensitivity test was made and it was confirmed that a total 7528 elements were sufficient enough to produce accurate results in the present study. Results obtained from the present model have been compared against the numerical results reported by Nada and Chamkha [10] for the case of mixed convection with nanofluid inside a square cavity as shown in Table 2. To assess the accuracy of the heat function formulations, a comparison has been made against the results reported by Basak and Chamkha [11] as shown in Fig. 2. A very close agreement has been obtained as per Table 2 and Fig. 2, which confirms that the present model is accurate and valid.

Table 2. Validation of the present work by Nada and Chamkha's work ($\varphi = 0.1$, water-Alumina nanofluid)

Ri	Nu_{avg} [11]	Nu_{avg} [Present code]
0.2	3.098952	3.036907
0.5	2.554669	2.536389
2	1.884410	1.896643
5	1.594969	1.605914

4. Result and Discussion

The numerical code developed in the present study has been used to carry out a number of simulations for various values of the Richadrson number, ($0.001 \leq Ri \leq 10$) and volume fraction of the nanoparticle ($0 \leq \varphi \leq 0.2$). Note that the Richardson No, *Ri*, by definition resembles the dominance of inertia effect (characterized by *Re*) over the natural convection effect (characterized by *Gr*).

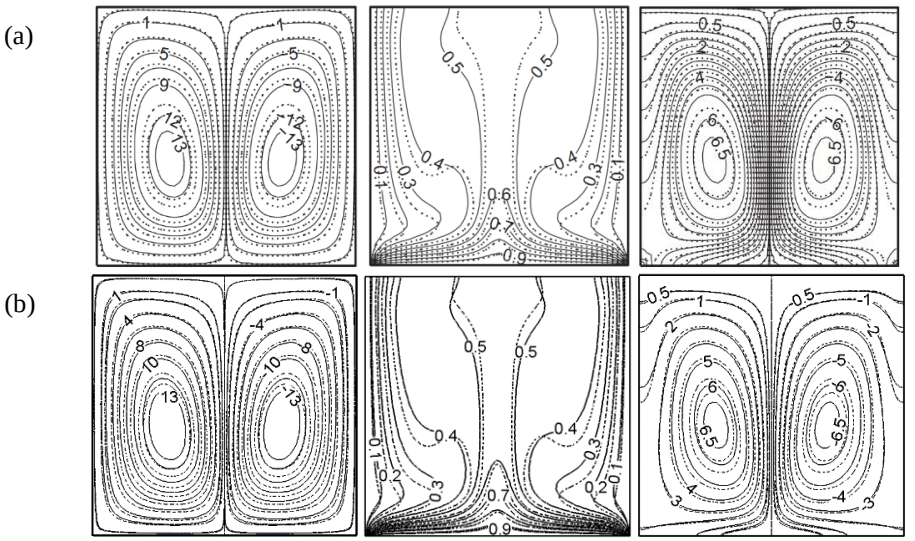

Fig. 2: Streamlines (ψ), isotherms (θ) and Heatlines (Φ) with φ = 0.1 (solid line) and $\varphi = 0$ (dotted line) for Ra = 10^5 (a) reported by Basak and Chamkha [11] (b) Present work

4.1. Effect of Richardson Number

Richardson number represents the relative comparison of natural convection and forced convection. Typically, the natural convection is negligible when $Ri < 0.1$, forced convection is negligible when $Ri > 10$, and neither is negligible when $0.1 < Ri < 10$. Figure 3 depicts the distributions of streamlines, isotherms and heat lines for base fluid ($\varphi = 0.0$) and nanofluid ($\varphi = 0.1$) for three different values of Richardson number (*Ri* = 0.001, 1, 10). The Reynolds number (*Re*), in these cases is kept constant at 100. Therefore, as *Ri* varies in the range of 0.001-10, the Grashof No. (*Gr*) assumes values in the range of 10-10^5. As shown in Fig. 3, for all three values of *Ri*, the velocity field is characterized mainly by a single clockwise circulating cell. For lower value of Ri, the centre of the circulating cell reside at the upper part of the cavity due to the shearing effect of the top moving lid. However, the centre of the circulation gradually moves towards the centre of the cavity as *Ri* increases. This is due to the fact that for a fixed mechanical effect of the moving lid, increase in *Ri*, results in more buoyancy effect to affect the flow field inside the cavity. As a result, the strength of the circulation increase with *Ri*. As an example: for the nanofluid case with $\varphi = 0.1$, maximum absolute value of the stream function, $|\Psi_{max}|$ varies as 0.105, 0.1099 and 0.1404 for the values of *Ri* number 0.001, 1 and 10 respectively. Similar to the flow field, the isotherms as well as the heatlines are also found to undergo significant changes with *Ri* as depicted in Fig. 3. As the flow field is characterized by mechanical shear near the top wall at lower values of *Ri*, a relatively thick thermal boundary layer exists near the hot bottom wall in this case. As *Ri* increases, the thermal boundary layer becomes thinner near the bottom wall as well as sidewalls which indicates greater heat transfer in these regions. The distribution of heatlines shows the path of heat flow inside the cavity. The distribution of heatlines clearly shows that a conduction dominated region exists near the bottom wall at lower values of Ri that gradually suppressed at higher values of *Ri* when the majority of the cavity undergoes convection dominated heat transfer. Similar type of variations in the distribution of streamline, isotherms and heat lines with Richardson No. are also found in case of nanofluid with $\varphi = 0.2$.

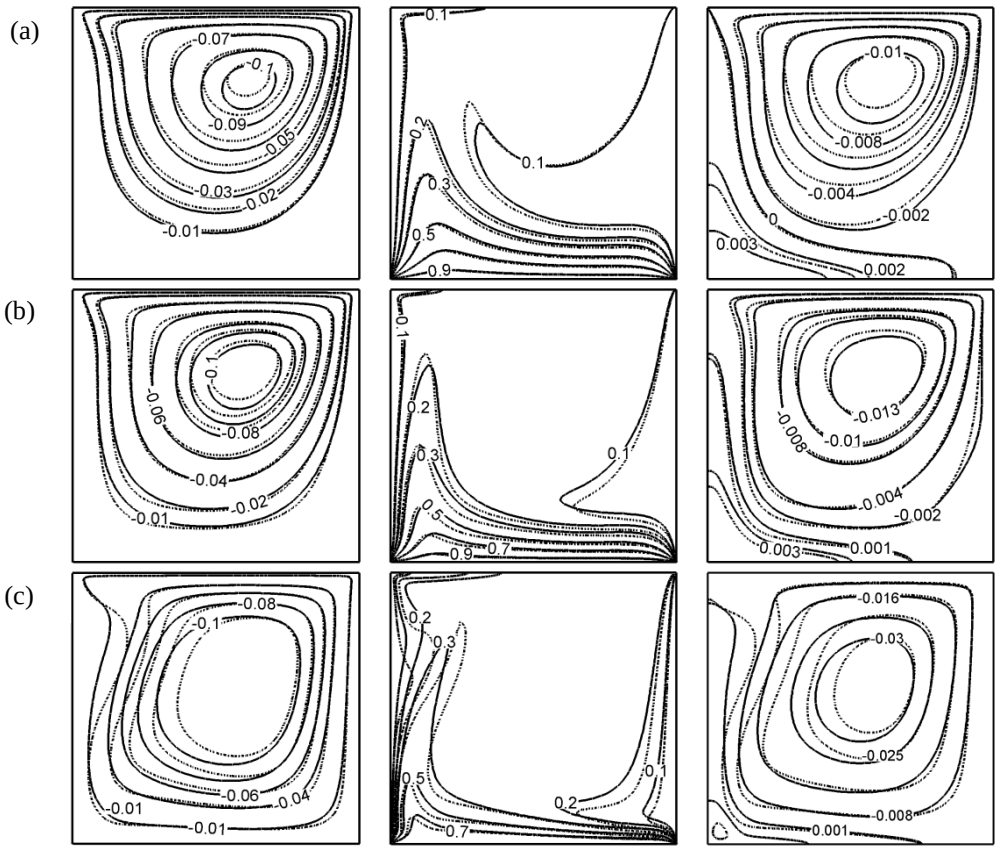

Fig. 3: Streamlines (Ψ), Isotherms (θ) and heatlines (π) for isothermally heated bottom wall with $\varphi = 0.1$ (solid line) and $\varphi = 0$ (dotted line) for $Re = 100$ and (a) $Ri = 0\ 001$, (b) $Ri = 1$ and (c) $Ri = 10$.

4.2. Effect of Grashoff Number in case of pure mixed convection (Ri = 1.0)

Fig. 4 shows streamlines, isotherms and heatlines for pure mixed convection (*Ri = 1.0).* For this case, different values of *Gr* number (100, 1000, 100000) have been considered. The streamlines in Fig. 4 show that for pure mixed convection with low *Gr* and *Re* numbers, the flow field is very weak. As the *Gr* number is increased from 100 to 100000, the flow field gets stronger. It results in clustered isothermlines adjacent to the bottom surface. It is evident from the figure that as *Gr* number is increased, the thermal boundary layer thickness near the hot bottom wall decreases due to strong fluid motion. The figure also shows that the degree of asymmetry for isotherms and heatlines increases as *Gr* number is increased. The heatlines represent conduction dominated heat transfer for *Gr=100*. As the value of *Gr* number increases, buoyancy effect and inertia effect both increase which results in convection heat transfer to dominate conduction heat transfer.

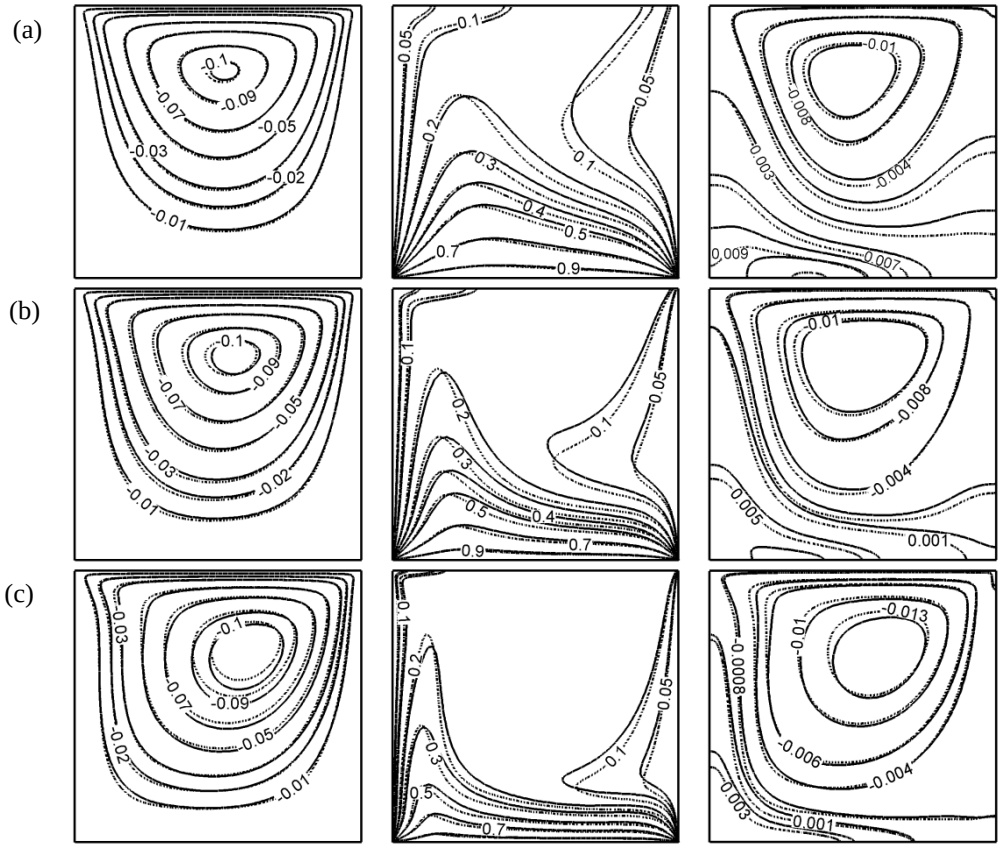

Fig. 4: Streamlines (Ψ), Isotherms (θ) and heatlines (п) for isothermally heated bottom wall with $\varphi = 0.1$ (solid line) and $\varphi = 0$ (dotted line) for $Ri=1$ and (a) $Gr = 100$, (b) $Gr = 1000$ and (c) $Gr = 10000$.

4.3. Average Nusselt Number (Nu_{avg})

Figure 5 shows the variation of the average Nusselt number over the heated bottom wall (Nu_{avg}) against Richardson number for various volume fractions for a constant mechanical effect of the moving lid (Re = 100) the heated bottom wall. As shown in Fig. 5, when Ri is increased the average value of the Nusselt number also increases for any volume fraction of the nanoparticle. But the change in the average Nusselt number is more prominent for greater values of Ri. This is due to the increased natural convection effect at higher values of Ri. Again, for a fixed value of Ri, the average Nusselt number is also higher for higher volume fraction of nanoparticle which manifests that addition of nanoparticle results in enhanced heat transfer. The average Nusselt number changes linearly with volume fraction of nanoparticle for all cases.

Figure 6 depicts the variations of the average Nusselt number (Nu_{avg}) in case of pure mixed convection for various values of Gr number. It shows that the average Nusselt number does not change much for $Gr \leq 10^3$. This is due to the fact that the fluid flow field is very weak for these cases. But for the case with $Gr \geq 10^3$, the average Nusselt number increases rapidly with Gr number.

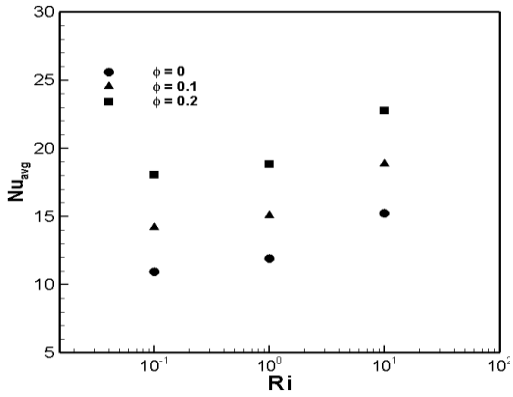

Fig.5: Average Nusselt number of the heated bottom wall against Richardson number for *Re = 100*

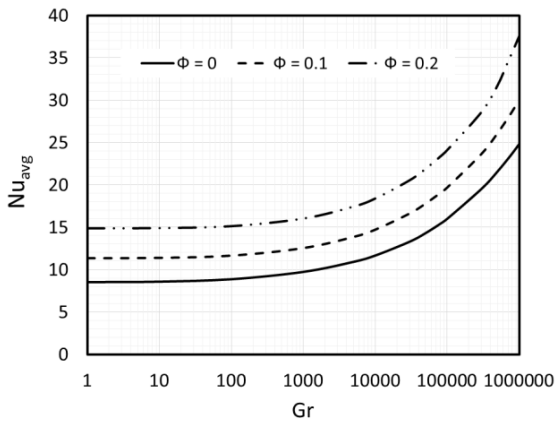

Fig.6: Average Nusselt number of the heated bottom wall against Richardson number for *Re = 100*

5. Conclusion

Finite element based simulations have been performed to study the heat transfer enhancement with Cu-water nanofluid during mixed convection inside a square cavity. The bottom wall of the cavity is maintained at a constant high temperature while the vertical sidewalls are assumed to be at a constant low temperature. The top wall of the cavity is insulated and moving at a constant velocity. Enhancement of heat transfer rates has been illustrated via isotherms associated with trajectory of heat flow via heatline method. For a constant mechanical effect of the moving lid, as the Richardson number increases greater effect of natural convection is manifested through the isotherms, streamlines and heatlines which in turn enhance the heat transfer. Addition of nanoparticle has been found to result in increased heat transfers for any values of the Richardson numbers; however its effect becomes prominent at higher values. For the pure mixed convection case with the Richardson number being equal to unity, higher heat transfer rate is obtained when natural convection effect corresponds to a Grashof No greater than 10^3. This trend has been found for all cases; with and without nanoparticles.

References

[1] Stephen US Choi and JA Eastman. Enhancing thermal conductivity of fluids with nanoparticles. Technical report, Argonne National Lab., IL U.S.A, 1995.

[2] Rong-Yuan Jou and Sheng-Chung Tzeng. Numerical research of natural convective heat transfer enhancement filled with nanofluids in rectangular cavitys. International Communications in Heat andMass Transfer, vol 33, pp. 727–736, 2006

[3] N Alleborn, H Raszillier, and F Durst. Lid-driven cavity with heat and mass transport. International Journal of Heat and Mass Transfer, vol 42, pp. 833–853, 1999.

[4] Orhan Aydm. Aiding and opposing mechanisms of mixed convection in a shear-and buoyancy-driven cavity. International communications in heat and mass transfer, vol 26, pp. 1019–1028, 1999.

[5] Khalil M Khanafer and Ali J Chamkha. Mixed convection flow in a lid-driven cavity filled with a fluid-saturated porous medium. International Journal of Heat and Mass Transfer, vol 42, pp. 2465–2481, 1999.

[6] S Kimura and A Bejan. The heatline visualization of convective heat transfer. Journal of heat transfer, vol 105, pp. 916–919, 1983.

[7] Y. xuan, W. Roetzel, Conceptions for heat transfer correlations of nano-fluids International Journal of Heat and Mass Transfer, vol 43, pp. 3701–3707, 2000.

[8] H.C. Brickman, The viscosity of concentrated suspensions and solution, Journal of Chemical Physics, vol 20, pp. 571-581, 1952

[9] J. C. Maxwell-Garnett, Colours in metal glasses and in metallic films, Philos., Transactions of Royal Society, Series, A 203, pp. 385-420, 1904

[10] Eiyad Abu-Nada and Ali J Chamkha. Mixed convection flow in a lid-driven inclined square cavity filled with a nanofluid. European Journal of Mechanics-B/Fluids, vol 29, pp. 472–482, 2010.

[11] Tanmay Basak and Ali J Chamkha. Heatline analysis on natural convection for nanofluids confined within square cavities with various thermal boundary conditions. International Journal of Heat and Mass Transfer, vol 55, pp. 5526–5543, 2012.

Available online at www.sciencedirect.com

ScienceDirect

Procedia Engineering00 (2015) 000–000

Procedia Engineering

www.elsevier.com/locate/procedia

6th BSME International Conference on Thermal Engineering (ICTE 2014)

Effect of tilt angle on pure mixed convection flow in trapezoidal cavities filled with water-Al_2O_3 nanofluid

Mahmudul Hasan Hasib*, Md. Saddam Hossen, Sumon Saha

Department of Mechanical Engineering, Bangladesh University of Engineering and Technology, Dhaka 1000, Bangladesh

Abstract

A numerical study is carried out to investigate the effect of tilt angle of the cavity on mixed convection heat transfer inside two different lid-driven trapezoidal cavities; one having heated wall on short base and another having heated wall on long base. In this investigation, the top wall is maintained at isothermal cold temperature, which is moving in its own plane at a constant speed while a constant high temperature is provided at the bottom surface of the cavity. The cavity is assumed to be filled with water-Al_2O_3 nanofluid. The governing Navier–Stokes and thermal energy equations and boundary conditions are non-dimensionalised and are solved using Galerkin finite element method. Attention is paid in the present study on the pure mixed convection regime at Richardson number, Ri = 1 where the natural and the forced convection are equally dominated. Parametric investigations are carried out by taking base wall tilt angle from 0^o to 45^o with a step of 15^o and also varying Reynolds numbers from 0.1 to a maximum order of 10^4 with the corresponding Grashof numbers varying from 0.01 to a maximum order of 10^8 for Ri = 1. Simulations are carried out by considering both plain fluid (water) and nanofluid with 10% solid-volume fraction of nanoparticles. Flow and heat transfer characteristics are explained using streamline and isotherm contours, and the variation of average Nusselt number of the heated wall and average fluid temperature of the cavity are analysed for different tilt angles.

Peer-review under responsibility of organizing committee of the 6th BSMEInternational Conference on Thermal Engineering (ICTE 2014).

*Keywords:*mixed convection; nanofluid; Richardson number; trapezoidal cavity; Nusselt number.

* Corresponding author. Tel.: +88 - 019 -1479 - 6443;
E-mail address: hasib_67@yahoo.com

Peer-review under responsibility of organizing committee of the 6th BSME International Conference on Thermal Engineering (ICTE 2014).

1. Introduction

Mixed convection is the process of heat transfer including both natural and forced convection, which bears a great importance due to its wide applications such as cooling of electronic devices, lubrication technologies, heating and drying technologies, food processing, float glass production, flow and heat transfer in solar ponds, thermal hydraulics of nuclear reactors, dynamics of lakes, crystal growing, metal coating, reservoirs and cooling ponds, materials processing and so on.

There have been numerous studies in the past on mixed convective flow in lid-driven cavities. However, majority of these investigations considered the cases of simple geometry like square, rectangular or triangular cavities. Only a few studies considered the configuration of lid-driven trapezoidal cavities for mixed convection problems [1-5]. These cavities can be divided into two categories based on the length of the top and the bottom walls. Hossain *et al.* [1], Chowdhury *et al.* [2], Hasan *et al.* [3] and Mamun *et al.* [4] considered mixed convection inside a lid-driven trapezoidal cavity having heated wall on the short base. On the other hand, Bhattacharya *et al.* [5] performed investigation on lid-driven trapezoidal cavity with heated long base. Among these works, only Mamun *et al.* [4] showed the effect of cavity tilt angle on mixed convection heat transfer. Recently, Cheng [6] only pointed out the combined effect of Reynolds and Grashof numbers on pure mixed convection flow in a lid-driven square cavity. However, to the best of the authors' knowledge, no attention has been paid to investigate the effect of tilt angle on pure mixed convection flow inside the lid-driven trapezoidal cavity filled with nanofluid.

Nanofluid, after gaining popularity in various industrial applications, has become one of the effective means for the enhancement of convective heat transfer. This is because metallic nanoparticles such as copper, aluminum, silver, silicon, etc., with higher thermal conductivity improve the thermo-physical properties of the mixture of conventional base fluids like water, ethylene glycol, etc. Although many researchers such as Tiwari and Das [7], Talebi *et al.* [8], Abu-Nada and Chamkha [9] and Salari *et al.* [10] carried out investigations on mixed convection inside a lid-driven square cavity filled with nanofluid, a similar analysis inside a trapezoidal cavity is still missing. Therefore, the main objective of the present study is to present the influence of the cavity tilt angle of two different trapezoidal cavities filled with water-Al_2O_3 nanofluid on pure mixed convective flow condition. The combined effects of Reynolds and Grashof numbers on the characteristics of mixed convection heat transfer are also revealed via streamline and isotherm plots, and the variation of average Nusselt number and average fluid temperature of the cavity.

2. Problem formulation

Two lid-driven trapezoidal cavities with different base and top walls but equal domain area are considered in the present study. The schematic diagrams of these cavities along with their co-ordinate system are shown in Figs. 1 (a)

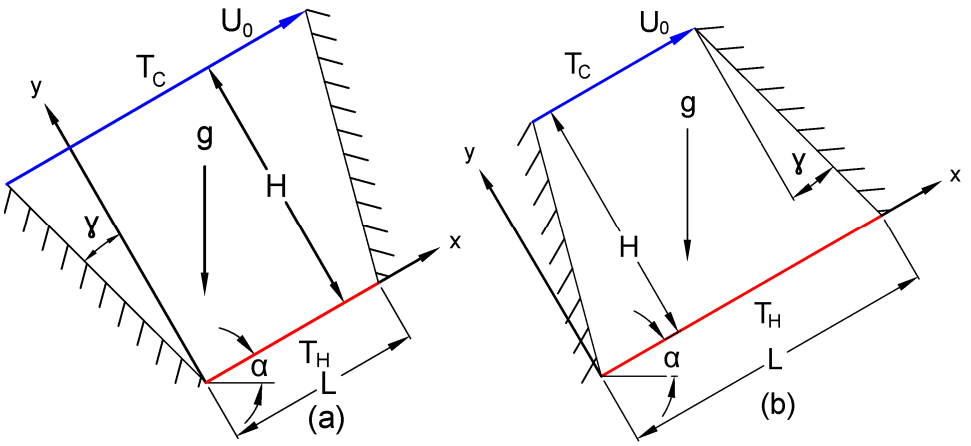

Fig. 1. Schematic representation of trapezoids having heated wall on (a) short base and (b) long base.

and (b). The first trapezoidal cavity has short base wall and long top wall with aspect ratio of L/H = 0.732, whereas the second cavity has long base wall and short top wall with aspect ratio of L/H = 1.268. Both cavities are filled with water-Al_2O_3 nanofluid and have the adiabatic sidewalls inclined at an angle γ = 15° with the y-axis. Constant isothermal high (T_h) and low (T_c) temperatures are maintained at bottom and top walls respectively. In addition, the top wall of the cavities is allowed to move in its own plane along positive x-direction at a constant speed U_o, which justifies the name "lid-driven trapezoid". Both cavities are inclined at an angle a with the horizontal reference x-axis and thus arising opposing flow condition where the shear flow caused by the moving top wall opposes the buoyancy driven flow caused by the thermal non-homogeneity of the cavity boundaries.

The working fluid is assumed to be incompressible and Newtonian. The Boussinesq approximation is adopted to account for the variations of temperature as a function of density and to couple in this way the temperature field to the flow field. The dissipation effect due to the viscous term is neglected and no heat generation is considered. Then the governing equations for steady laminar mixed convection can be expressed by using conservation of mass, momentum and energy equations in the dimensionless form as follows:

$$\frac{\partial U}{\partial X}+\frac{\partial V}{\partial Y}=0, \tag{1}$$

$$U\frac{\partial U}{\partial X}+V\frac{\partial U}{\partial Y}=-\frac{\partial P}{\partial X}+\frac{\mu_{nf}}{\rho_{nf}\nu_f}\frac{1}{Re}\left(\frac{\partial^2 U}{\partial X^2}+\frac{\partial^2 U}{\partial Y^2}\right)+\frac{(\rho\beta)_{nf}}{\rho_{nf}\beta_f}(Ri\sin\alpha)\Theta, \tag{2}$$

$$U\frac{\partial V}{\partial X}+V\frac{\partial V}{\partial Y}=-\frac{\partial P}{\partial Y}+\frac{\mu_{nf}}{\rho_{nf}\nu_f}\frac{1}{Re}\left(\frac{\partial^2 V}{\partial X^2}+\frac{\partial^2 V}{\partial Y^2}\right)+\frac{(\rho\beta)_{nf}}{\rho_{nf}\beta_f}(Ri\cos\alpha)\Theta, \tag{3}$$

$$U\frac{\partial \Theta}{\partial X}+V\frac{\partial \Theta}{\partial Y}=\frac{\alpha_{nf}}{\alpha_f}\frac{1}{RePr}\left(\frac{\partial^2 \Theta}{\partial X^2}+\frac{\partial^2 \Theta}{\partial Y^2}\right). \tag{4}$$

The dimensionless parameters in the above equations are defined as follows:

$$X=\frac{x}{H},\ Y=\frac{y}{H},\ U=\frac{u}{U_0},\ V=\frac{v}{U_0},\ P=\frac{p}{\rho_{nf}U_0^2},\ \Theta=\frac{T-T_c}{T_H-T_c}, \tag{5}$$

where X and Y are the non-dimensional coordinates varying along horizontal and vertical directions respectively, U and V are the non-dimensional velocity components in the X and Y-directions respectively, Θ is the non-dimensional temperature and P is the non-dimensional pressure. The non-dimensional governing parameters appeared in the above equations are Reynolds number (Re), Grashof number (Gr), Prandtl number (Pr) and Richardson number (Ri) respectively and those are defined as follows:

$$Re=\frac{U_0 H}{\nu_f},\ Gr=\frac{g\beta_f(T_H-T_c)H^3}{\nu_f^2},\ Pr=\frac{\nu_f}{\alpha_f},\ Ri=\frac{Gr}{Re^2}. \tag{6}$$

The thermo-physical properties of the nanofluid (water-Al_2O_3) are obtained from the relations listed in table 1 whereas the individual thermo-physical properties of water and Al_2O_3 are presented in table 2.

Table 1. Thermo-physical relationship for the nanofluid.

Property	Equation
Effective density, ρ_{nf}	$\rho_{nf}=(1-\phi)\rho_f+\phi\rho_s$
Effective viscosity, μ_{nf}	$\mu_{nf}=\mu_f(1-\phi)^{-2.5}$
Thermal expansion coefficient, β_{nf}	$\beta_{nf}=\left\lfloor(1-\phi)(\rho\beta)_f+\phi(\rho\beta)_s\right\rfloor/\rho_{nf}$
Effective thermal diffusivity, α_{nf}	$\alpha_{nf}=k_{nf}/(\rho C_p)_{nf}$
Effective thermal conductivity, k_{nf}	$k_{nf}=k_f\left[k_s+2k_f-2\phi(k_f-k_s)\right]/\left[k_s+2k_f+\phi(k_f-k_s)\right]$
Heat capacitance, $(\rho C_p)_{nf}$	$(\rho C_p)_{nf}=(1-\phi)(\rho C_p)_f+\phi(\rho C_p)_s$

Table 2. Thermo-physical properties of water and Al_2O_3 nanoparticles [9].

Fluid / Solid	ρ (kg/m^3)	C_p (J/kgK)	k (W/mK)	β (1/K)	μ (Pa.s)
Water	997.1	4179	0.613	2.1×10^{-4}	0.001003
Al_2O_3	3970	765	25	8.5×10^{-6}	–

Table 3. Non-dimensional boundary conditions of the present problem.

Dependent variables	Top wall	Bottom wall	Inclined side walls
Velocity	$U = 1$, $V = 0$	$U = V = 0$	$U = V = 0$
Temperature	$\Theta = 0$	$\Theta = 1$	$\partial\Theta/\partial N = 0$

Here, ϕ is the solid-volume fraction of the nanoparticles and the subscript '*s*', '*f*' and '*nf*' represent the properties of nanoparticles, base fluid and nanofluid, respectively. The non-dimensional boundary conditions for the present problem are specified in table 3.

Two important non-dimensional parameters such as average temperature (Θ_{av}) of the fluid inside the cavity and average Nusselt number (Nu) of the heated wall are evaluated in the present investigation in order to describe the characteristics of mixed convection heat transfer. Those parameters are defined as follows:

$$\Theta_{av} = \frac{1}{A}\int \Theta dA, \tag{7}$$

$$Nu = -\frac{k_{nf}}{k_f}\frac{H}{L}\int_0^{L/H} \frac{\partial \Theta}{\partial Y} dX. \tag{8}$$

3. Numerical procedure

The non-dimensional governing equations (1-4) for the present problem are solved using Galerkin finite element method. The detailed procedures to apply this technique in order to transform a set of partial differential equations into a set of nonlinear algebraic equations can be found in [11]. The computational domain is discretized using non-uniform eight noded quadrilateral mesh elements and finer mesh is chosen especially near the solid walls to capture the rapid changes in the dependent variables. All eight nodes are associated with velocities as well as temperature, whereas only the corner nodes are associated with pressure. The nonlinear equations are solved iteratively using Broyden's method with an *LU*-decomposition preconditioner. The relative tolerance for the convergence criteria is set to be 10^{-6}.

3.1. Grid independence check

Seven sets of mesh elements are selected to perform the check for grid size independency. The numbers of mesh elements chosen for this test are 50 × 50, 60 × 60, 65 × 65, 70 × 70, 75 × 75, 80 × 80 and 85 × 85. Table 4 shows the comparison of using different mesh elements and from these comparisons, it is confirmed that 75 × 75 non-uniform mesh elements are sufficient to produce results within reasonable accuracy and independent of any further mesh refinement. Hence, we have selected 75 × 75 mesh elements to carry out all simulations.

Table 4. Grid independence check using the variation of Nu of two different trapezoids for $Ri = 1$, $Re = 100$, $Gr = 10^4$, $\alpha = 45^o$ and $\phi = 0.1$.

Mesh elements	50 × 50	60 × 60	65 × 65	70 × 70	**75 × 75**	80 × 80	85 × 85
Nu for trapezoid with short base	5.532206	5.533684	5.534144	5.534718	**5.535055**	5.535490	5.535749
Nu for trapezoid with long base	3.341667	3.379983	3.391738	3.406716	**3.415262**	3.415640	3.415928

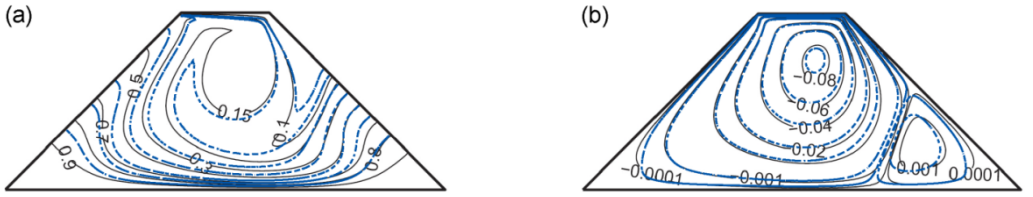

Fig. 2. Comparison of (a) isotherm and (b) streamline contours of the present computation (dashed blue lines) with those of Bhattacharya *et al.* [5] (solid black lines) for Re = 100, Pr =10, Ri = 0.1 and $\alpha = 30^o$.

3.2. Code Validation

Both qualitative and quantitative validations of the present numerical code are performed before starting the simulation of the present problem. The qualitative comparison is made with the results obtained for mixed convection flows in a trapezoidal enclosure as mentioned by Bhattacharya *et al.*[5]. Fig. 2 shows the comparison of isotherm and streamline contours obtained by the present code for the trapezoid having hot wall on long base and cavity tilt angle of 0^o with the aforementioned paper [5]. It is found that the present numerical results are almost in close agreement with the mentioned one [5], in terms of isotherm and streamline plots. Further quantitative validation is carried out in terms of average Nusselt number of the heated wall of a lid-driven square cavity filled with water-Al_2O_3 nanofluid and inclined at an angle 30^o with the horizontal axis as obtained by Abu-Nada and Chamkha [9]. The comparison is shown in table 5 and the agreement is found to be satisfactory. Therefore, both qualitative and quantitative comparisons validate the present computations and lend us confidence for the use of the present code.

Table 5. Comparison of Nu from the present code with the results of Abu-Nada and Chamkha [9] for Gr = 100, $\alpha = 30^o$ and $\phi = 0.1$.

Ri	0.2	0.5	2	5
Nu from present code	3.093933	2.607961	1.9717	1.670371
Nu from Abu-Nada and Chamkha [9]	3.186897	2.651015	1.9755	1.671118

4. Results and discussions

The present study has carried out investigation of pure mixed convection for different tilt angles of two lid-driven trapezoidal cavities. The simulations are performed by considering both plain fluid (water) and nanofluid (water-Al_2O_3) with 10% solid-volume fraction of nanoparticles. Reynolds number is varied from 0.1 to a maximum order of 10^4 with a view to understand the combined effect of Re and Gr at Ri = 1 on the flow and the thermal fields. The cavity tilt angle is considered to vary from 0^o to 45^o with a step-angle of 15^o.

4.1. Effect of cavity tilt angle on flow and thermal fields

Figs. 3 and 4 are dedicated for the investigation of the effect of cavity tilt angle (α) on the streamline and the isotherm profiles inside the trapezoidal cavities with short and long bases, respectively, for constant Reynolds (Re = 200) and Richardson (Ri = 1) numbers. Careful observations yield that, for all values of α, two circulating cells appear inside the cavity. Upper clockwise rotating cell corresponds to the mechanical effect of lid inducing forced convection, and lower counter-clockwise circulating cell represents natural convection due to buoyancy effect.

For horizontal trapezoids ($\alpha = 0^o$), primary lid-driven circulation occupies major portion of the cavity, whereas the comparatively smaller secondary eddy due to buoyancy appears at lower right portion (see Figs. 3(a) and 4 (a)). Presence of only vertical component of the buoyancy force results in aiding core flow at $\alpha = 0^o$, whereas due to the effect of inclination angle of the cavity, the opposing buoyancy driven flow against the flow of the moving lid gives rise to the secondary eddy. With increasing tilt angle, this circulating cell almost dominantly capture the flow region especially at $\alpha = 45^0$ (see Figs. 3 (g) and 4 (g)) indicating the adverse effect on convection heat transfer.

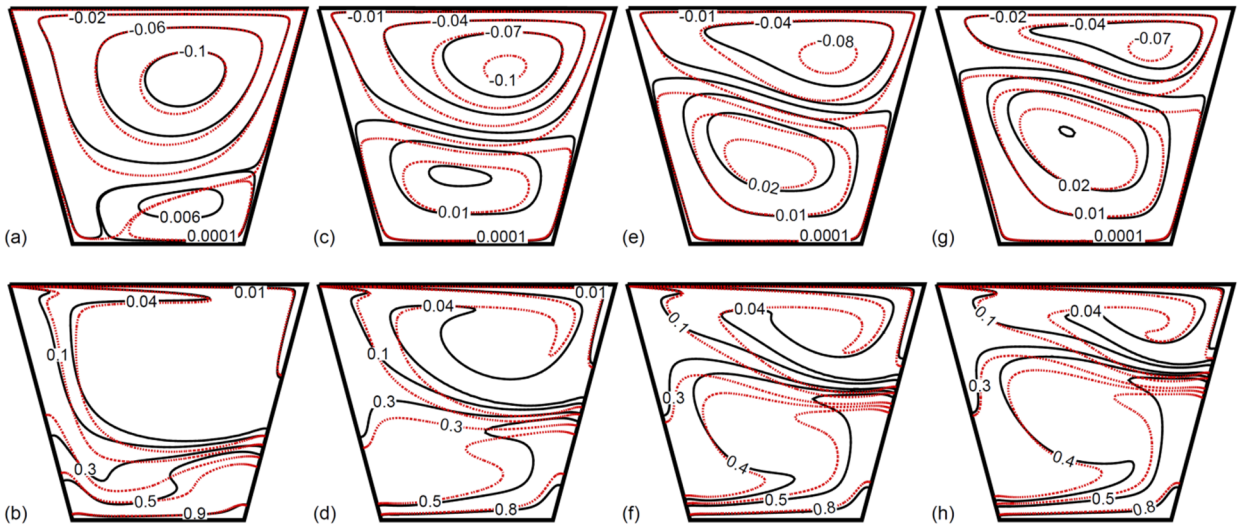

Fig. 3. Comparison of streamlines (top row) and isotherm (bottom row) contours inside trapezoidal cavity with short base at Re = 200, Ri = 1, Gr = 4×10^4 for (a), (b) $\alpha = 0^o$; (c), (d) $\alpha = 15^o$; (e), (f) $\alpha = 30^o$ and (g), (h) $\alpha = 45^o$. The solid black line represents data for plain fluid ($\phi = 0$) whereas the red dashed line represents data for nanofluid with $\varphi = 0.1$.

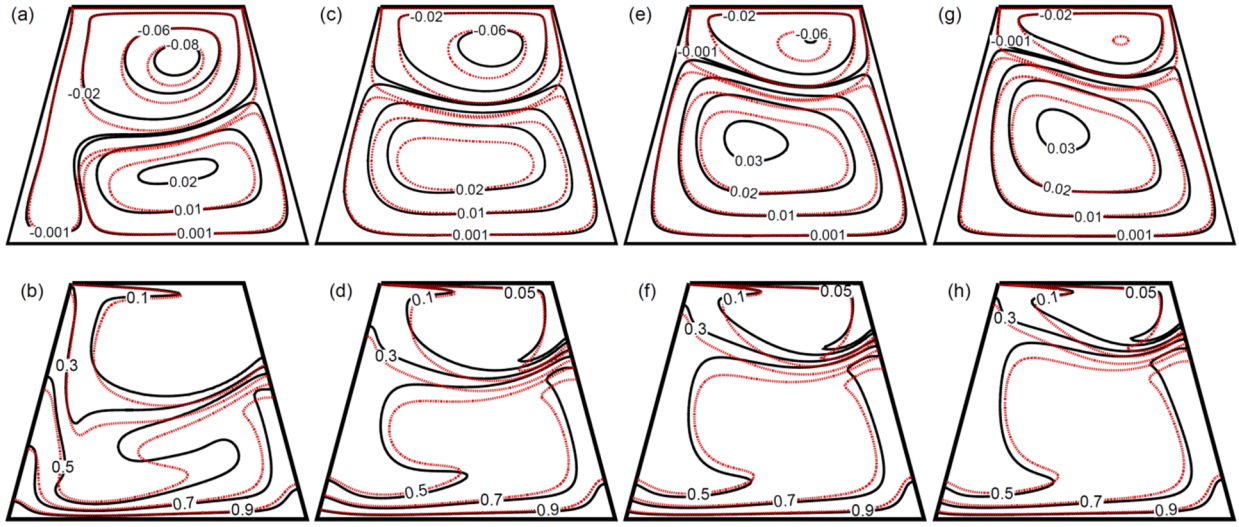

Fig. 4. Comparison of streamlines (top row) and isotherm (bottom row) contours inside trapezoidal cavity with long base at Re = 200, Ri = 1, Gr = 4×10^4 for (a), (b) $\alpha = 0^o$; (c), (d) $\alpha = 15^o$; (e), (f) $\alpha = 30^o$ and (g), (h) $\alpha = 45^o$. The solid black line represents data for plain fluid ($\phi = 0$) whereas the red dashed line represents data for nanofluid with $\varphi = 0.1$.

Lid-driven trapezoids with short and long base show almost similar behaviours in terms of streamline contours, except that the buoyancy induced counter clockwise vortex is relatively larger for the trapezoid with long base (see Figs. 4 (c), (e) and (g)). This is because this type of trapezoids possess longer heated wall and shorter mechanical lid which results in reduced lid effect and increased buoyancy effect.

While observing the isotherm contours, it reveals that the contours have comparatively uniform distribution at inclination angle, $\alpha = 0^0$ (see Figs. 3 (b) and 4 (b)). Core flow due to the mechanical effect of moving lid dominates in the upper zone providing low temperature region, whereas the contours are clustered near the bottom wall

providing higher temperature gradient. For $\alpha = 15^0$, we can see from Figs. 3 (d) and 4 (d) that the isotherm contour lines are more distorted than those for $\alpha = 0^0$. Both driving mechanisms give individual isothermal zone, with a high temperature gradient at their interaction region at $\alpha = 15^0$. With increasing α, the nonlinearity of the contour lines increases and the isothermal zone is mainly influenced by the buoyancy effect, which shifts high temperature gradient interaction region towards upper wall (see Figs. 3 (f), (h) and 4 (f), (h)).

There is also remarkable variation of streamlines and isotherms between nanofluid and plain fluid for all tilt angles of the cavities. However, at moderate inclination angles $\alpha = 15^0$ and 30^0, influence of the buoyancy force and moving lid on nanofluid and base fluid is remarkable. Mostly moving lid affects the nanofluid and base fluid profiles in these figures. At higher inclination angle ($\alpha = 45^0$), both nanofluid and plain fluid is mostly influenced by the buoyancy force, and follow completely different profiles for these two types of trapezoids.

4.2. Combined effect of Reynolds and Grashof numbers on flow and thermal fields

Apart from the change of tilt angle, both Reynolds and Grashof numbers also play a great role to influence the temperature and the flow fields. Figs. 5 and 6 show the variation of streamline and isotherm contours with the change of Reynolds and Grashof numbers simultaneously, where Richardson number and tilt angle are kept constant at $Ri = 1$ and $\alpha = 45^o$, respectively. Three different Reynolds numbers (Re = 10, 100 and 10^3) are considered here for comparison of flow and thermal fields where the corresponding Grashof numbers become 100, 10^4 and 10^6 for fixed $Ri = 1$.

It is easily understood from these figures that at $Re = 10$, with corresponding $Gr = 100$, buoyancy flow converges with core flow to form a single clockwise rotating cell of semicircular structure and thus indicates dominating flow field (see Figs. 5 (a) and 6 (a)). With the further increase of Reynolds and Grashof numbers, a gradually expanding counter-clockwise rotating vortex appears at the bottom of the enclosure and thus opposes the circulating flow. At $Re = 10^3$ and $Gr = 10^6$, this secondary circulating cell almost dominantly capture the flow region (see Figs. 5 (e) and 6 (e)) indicating the dominating effect of buoyancy induced convection heat transfer.

Like streamlines, the isotherm contours show significant change with increasing Re and Gr. At $Re = 10$ and $Gr = 100$, isothermal contours possess nearly uniform distribution (see Figs. 5 (b) and 6 (b)) with steep temperature gradient along the Y-direction. Single circulation exists in the cavity with high temperature gradient and thus having stratified thermal boundary layer. With increasing Reynolds and Grashof numbers, the buoyancy effect becomes dominant, which ultimately induce reduced temperature gradient. As a result, relatively significant nonlinear contours with huge isothermal zone occupy most of the cavity region (see Figs. 5 (d), (f) and 6 (d), (f)).

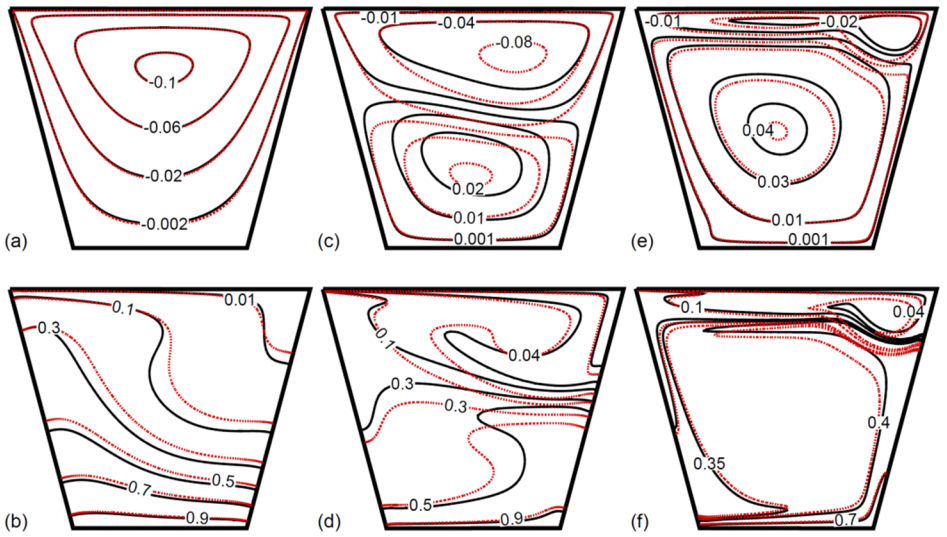

Fig. 5. Comparison of streamlines (top row) and isotherm (bottom row) contours inside trapezoidal cavity with short base at $Ri = 1$ and $\alpha = 45^o$ for (a), (b) $Re = 10$, $Gr = 100$; (c), (d) $Re = 100$, $Gr = 10^4$ and (e), (f) $Re = 10^3$, $Gr = 10^6$. The solid black line represents data for plain fluid ($\phi = 0$) whereas the red dashed line represents data for nanofluid with $\varphi = 0.1$.

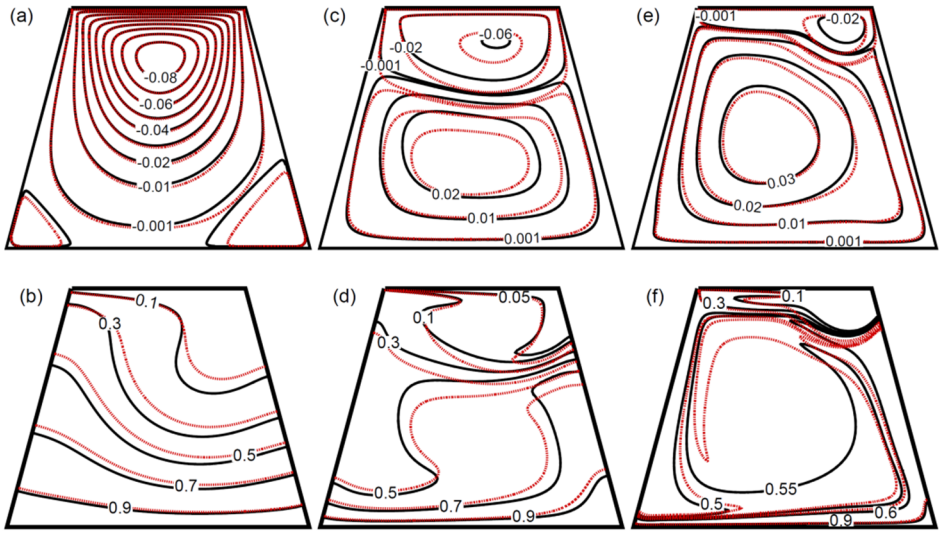

Fig. 6. Comparison of streamlines (top row) and isotherm (bottom row) contours inside trapezoidal cavity with long base at $Ri = 1$ and $\alpha = 45^{o}$ for (a), (b) $Re = 10$, $Gr = 100$; (c), (d) $Re = 100$, $Gr = 10^4$ and (e), (f) $Re = 10^3$, $Gr = 10^6$. The solid black line represents data for plain fluid ($\phi = 0$) whereas the red dashed line represents data for nanofluid with $\varphi = 0.1$.

Figs. 5 and 6 are also dedicated for comparing the presence of nanofluid on flow and temperature profiles between two different types of trapezoids. At low *Re* and *Gr*, the profiles of streamline for both nanofluid and plain fluid coincide, whereas the isotherm patterns clearly show the influence of nanofluid due to improved thermo-physical properties. Similar observations are also found for higher values of *Re* and *Gr*. However, at moderate values of *Re* and *Gr*, streamline and isotherm contours follow completely different profiles. The nanofluid seems to alter the flow and the thermal region for both types of trapezoids (see Figs. 5 (c), (d) and 6 (c), (d)).

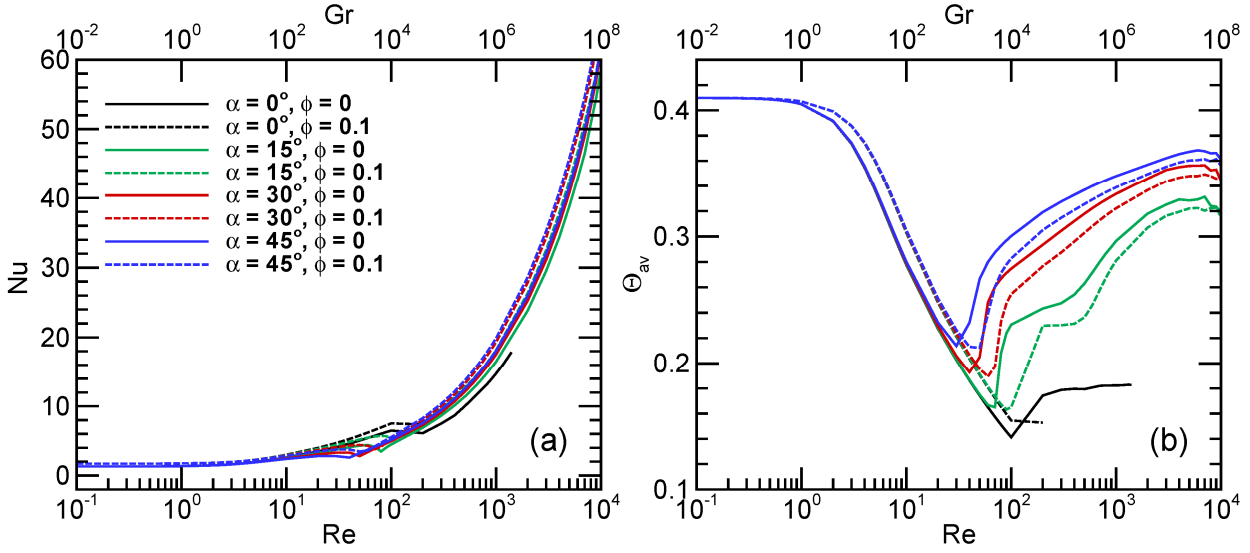

Fig. 7. Variation of (a) average Nusselt number of the heated wall and (b) average temperature of the fluid inside cavity with both Reynolds and Grashof numbers for different tilt angle of the trapezoidal cavity with hot wall on short base. The results are shown for both plain fluid (solid lines) and nanofluid (dashed lines) with $\phi = 0.10$.

4.3. Evaluation of the performance of heat transfer

Figs.7 and 8 show the effect of increasing both Reynolds and Grashof numbers on the average Nusselt number for the cases of $\phi = 0$ and 0.1 at $Ri = 1$for various inclination angles. It can be observed that the average Nusselt number along the bottom wall of the trapezoidal cavity increases continuously with increasing *Re* and *Gr* simultaneously. However, three important distinct points can be observed from this figure. First, the transition from conduction to convection regime is noticed within the laminar zone, where *Nu* remains constant for both plain fluid and nanofluid. The second and third observations are the beginning and the end of transition from laminar to chaos within very narrow region. A sudden but gradual drop of average Nusselt number is observed for both plain fluid and nanofluid, where the influence of increasing both Reynolds and Grashof numbers is overwhelmed in the pure mixed convective flows.

While observing the effect of inclination angle on heat transfer, Figs. 7 and 8 clearly indicate that there is completely opposite behaviour for the variation of *Nu* with respect to α between these two trapezoidal cavities. Apart from the conduction dominated region, *Nu* increases with increasing α for short based trapezoid (see Fig. 7 (a)) while for long based trapezoid, *Nu* decreases with increasing α (see Fig. 8 (a)). This is mainly due to the length of the heated base wall, which influence the buoyancy effect with the change of the tilt angle. Since the side-corners of the short based trapezoid have obtuse angle and those for the long based trapezoid have acute angle, better convective flow over the bottom wall appears in short based cavity, whereas convective flow deteriorates for the long based one.

For both types of trapezoids, average temperature of the cavity increases with increasing tilt angle after the transition from laminar to chaos (see Figs. 7(b) and 8 (b)). It is evident that all inclined trapezoids reach to the transition point at lower *Re* than the horizontal one. Moreover, Figs. 7 (a) and 8 (a) also reveal that *Nu* for nanofluid is greater than base fluid for all inclination angles, and all Reynolds and Grashof numbers, which clearly indicates heat transfer augmentation by using nanofluid. Observing Figs. 7 (b) and 8 (b), it can be concluded that after a certain value of *Re*, average temperature for cavities filled with nanofluid becomes less than those of the base fluidfor all α implying better heat transfer due to the presence of nanofluid.

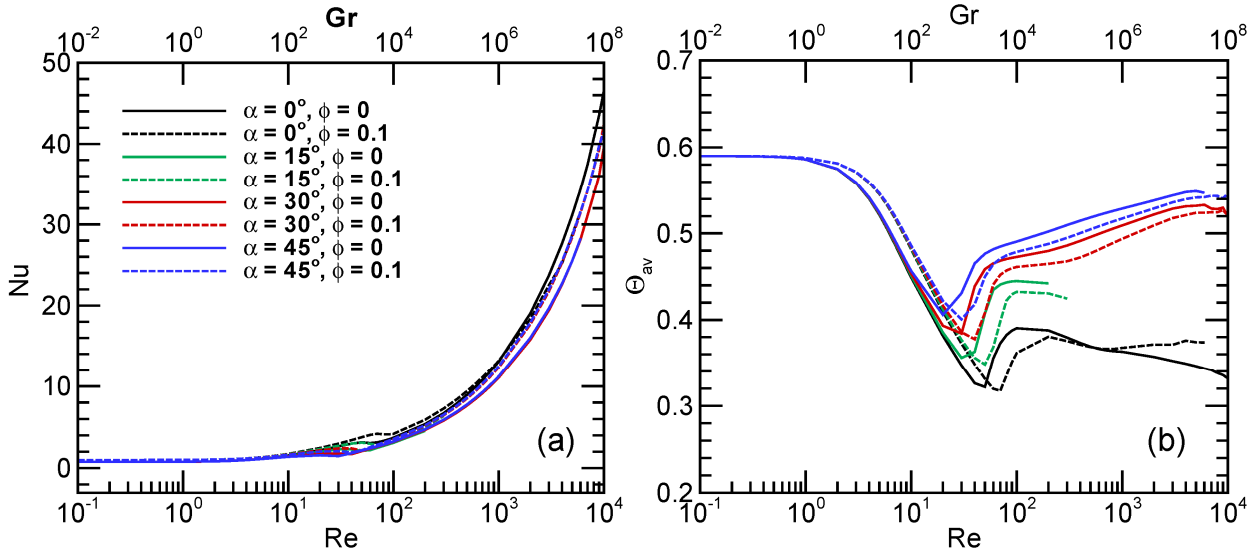

Fig. 8. Variation of (a) average Nusselt number of the heated wall and (b) average temperature of the fluid inside cavity with both Reynolds and Grashof numbers for different tilt angle of the trapezoidal cavity with hot wall on long base. The results are shown for both plain fluid (solid lines) and nanofluid (dashed lines) with $\phi = 0.10$.

5. Conclusion

The problems of steady mixed convection heat transfer of an incompressible, Newtonian and Boussinesq fluid inside two different 2D lid-driven trapezoidal cavities, one having heated wall on short base and another with heated wall on long base have been investigated numerically. The top wall of the cavity is maintained at the surrounding low temperature and is moving with a constant velocity. Simulations are performed for different tilt angle of these cavities with the variation of both Reynolds and Grashof numbers at fixed Richardson number. One of the important findings is that both the heat transfer and flow characteristics inside the cavities strongly depend on the choice of Reynolds and Grashof numbers at $Ri = 1$. Presence of the nanofluid in comparison to the plain fluid also significantly affects the thermal scenario inside the cavity. Overall mixed convection heat transfer characteristics from the hot bottom wall of the trapezoidal cavities are found to be influenced by the mechanical effect of the moving lid and the buoyancy-driven flow. Extensive investigation for various tilt angles suggests an interesting feature on the characteristics of mixed convection in these two lid-driven trapezoidal cavities. For short based trapezoids, tilting the enclosure increases heat transfer from heated wall, whereas for long based trapezoid, it decreases.

Acknowledgements

The authors gratefully acknowledge the support provided by the Department of Mechanical Engineering, Bangladesh University of Engineering and Technology (BUET) during this research work.

References

[1] M.N. Hossain, M.A.H. Mamun, S. Saha, Mixed convection in a trapezoidal cavity with moving lid at top wall and heating from below, International Conference on Chemical Engineering, Dhaka, Bangladesh, 2008.

[2] M.N.H.K. Chowdhury, S. Saha, M.A.H. Mamun, Mixed convection analysis in a lid driven trapezoidal cavity with isothermal heating at bottom for various aspect angles, 8th International Conference on Mechanical Engineering, Dhaka, Bangladesh, 2009.

[3] M.N. Hasan, S. Saha, G. Saha, M.Q. Islam, Effect of sidewall inclination angle of a lid-driven trapezoidal enclosure on mixed convective flow and heat transfer characteristics, 13thAsian Congress of Fluid Mechanics, Dhaka, Bangladesh, 2010.

[4] M.A.H. Mamun, T.R. Tanim, M.M. Rahman, R. Saidur, S. Nagata, Mixed convection analysis in trapezoidal cavity with a moving lid, Int. J. Mech. Mat. Eng., 5 (1) (2010) 18-28.

[5] M. Bhattacharya, T. Basak, H.F. Oztop, Y. Varol, Mixed convection and role of multiple solutions in lid-driven trapezoidal enclosures, Int. J. Heat Mass Trans., 63 (2013) 366–388.

[6] T.S. Cheng, Characteristics of mixed convection heat transfer in a lid-driven square cavity with various Richardson and Prandtl numbers, Int. J. Therm. Sci., 50 (2011) 197–205.

[7] R.K. Tiwari, M.K. Das, Heat transfer augmentation in a two-sided lid-driven differentially heated square cavity utilizing nanofluids, Int. J. Heat Mass Trans., 50 (9) (2007) 2002–2018.

[8] F. Talebi, A.H. Mahmoudi, M. Shahi, Numerical study of mixed convection flows in a square lid-driven cavity utilizing nanofluid, Int. Comm. Heat Mass Trans., 37 (1) (2010) 79–90.

[9] E. Abu-Nada, A.J. Chamkha, Mixed convection flow in a lid-driven inclined square enclosure filled with a nanofluid, Euro. J. Mech.-B/Fluids, 29 (6) (2010) 472–482.

[10] M. Salari, M.M. Tabar, A.M. Tabar, H.A. Danesh, Mixed convection of nanofluid flows in a square lid-driven cavity heated partially from both the bottom and side walls, Numer. Heat Trans., Part A: Applications, 62 (2) (2012) 158–177.

[11] O.C. Zienkiewicz, R.L. Taylor, The finite element method, 1 (1973) 128–132.

Available online at www.sciencedirect.com

ScienceDirect

Procedia Engineering 00 (2015) 000–000

Procedia Engineering

www.elsevier.com/locate/procedia

6th BSME International Conference on Thermal Engineering (ICTE 2014)

Enhancement of Heat Transfer Performance in Nuclear Fuel Rod Bundles using Nanofluids and Surface Roughness Technique

Kang Liu[1], Titan C. Paul[1], Leo A. Carrilho[1,2], Jamil A. Khan[1,*]

[1]*Department of Mechanical Engineering, University of South Carolina, Columbia, SC 29208, USA*

[2]*Currently affiliated with Westinghouse Electric Company, 5801 Bluff Road, Hopkins, SC 29061, USA*

Abstract

The experimental investigations were carried out of a pressurized water nuclear reactor (PWR) with enhanced surface using different concentration (0.5 and 2.0 vol%) of ZnO/DI-water based nanofluids as a coolant. There were two simulated nuclear fuel rods with two different types of modified outer surface roughness. The fuel rod surfaces modified were termed as two-dimensional surface roughness (square transverse ribbed surface) and three-dimensional surface roughness (diamond shaped blocks). The experimental setup consisted of a flow loop with a nuclear fuel rod section that was heated by electrical current. The variation in temperature of nuclear fuel rod was measured along the length of a specified section. Heat transfer coefficient was calculated by measuring heat flux and temperature differences between surface and bulk fluid. The experimental results were compared with the coolant as a DI-water data. The maximum heat transfer coefficient enhancement achieved compared to DI-water was 33% at $Re = 1.15 \times 10^5$ for fuel rod with three-dimensional surface roughness using 2.0 vol% nanofluids.

Peer-review under responsibility of organizing committee of the 6th BSME International Conference on Thermal Engineering (ICTE 2014).

Keywords: Nanofluids; Fuel Rod; Pressurized Water Reactor (PWR); Three Dimensional Surface Roughness; Convective Heat transfer Coefficient; Reynolds Number.

1. Introduction

One of the key challenges in all energy generation processes is the need for efficient heat removal. This need is more pronounced in nuclear rod bundles of power reactors. An efficient and high heat flux within rod bundles allows for lower temperatures in the center of the rod, resulting in more efficient power production. Though many traditional heat transfer augmentation methods are being adopted, new and more effective ways are being searched and explored by scientists.

* Corresponding author. Tel.: +1-803-777-1578; fax: +1-803-777-0106.
E-mail address: khan@cec.sc.edu

Peer-review under responsibility of organizing committee of the 6th BSME International Conference on Thermal Engineering (ICTE 2014).

In general, the techniques for single phase heat transfer enhancement are classified as: active and passive techniques. These heat transfer enhancement techniques can achieve various enhancement factors such as, boundary layer breakup, flow transition, entrance region effect, vibration, secondary flow, swirl flow, electrical fields and mixtures for increasing the heat transfer rates. Active techniques usually involve external inputs. For example, electrical power or RF signals are commonly used causing flow pulsation, vibration and synthetic-jet.

According to A. E. Bergles et al. [1], surface roughening is categorized as a passive technique. Furthermore, D. N. Ryu et al. [2] concluded that artificial surface roughness enhances heat transfer by triggering the thermal layer breakup, producing intensive turbulent mixing. This phenomenon was accompanied by undesirable increase in flow resistance.

Surface artificial roughness can be categorized respectively as one, two and three-dimensional surface roughness. The two-dimensional surface roughness are mainly used in conventional flow channels to enhance heat transfer by convection. R. J. Firth et al. [3] conducted the research on heat transfer performance and pressure drop of three different types of two and three-dimensional roughness. Results showed that that heat transfer enhancement is achieved at the expense of a higher friction factor. The thermal performance of the two-dimensional roughness was lower than the three-dimensional, while the two-dimensional transverse and helically ribbed surfaces had comparable levels of thermal performance. J. C. Han et al. [4] studied heat transfer performance of two oppositely ribbed and smooth walls in a rectangular channel. They concluded that the Stanton number and the heat transfer coefficient of the roughened wall were two to three times higher than those of the smooth wall. S. Singh et al. [5] conducted investigations on rectangular duct with one board wall roughened into discrete V-down rib under constant heat flux. The results showed that the Nusselt number and the friction factor in the roughened duct were increased by 51.4% and 26.5% respectively compared to the smooth channel. X-W Li et al. [6] conducted experiments on getting heat transfer coefficient of two-dimensional roughness tubes with various roughness heights under different Reynolds numbers. They concluded that there is a maximum Nusselt number and Reynolds number ratio for each roughness height. D. N. Ryu et al. [7] conducted the investigation to analyze the flow resistance in turbulent flow channels roughened with two-dimensional ribs (square ribs, triangular ribs, semicircular ribs, wavy wall) and three-dimensional elements. Results showed that the square ribs contributed for higher flow resistance, whereas the wavy wall had the lowest. U. Najeeb et al. [8] was focused on heat transfer enhancement and pressure drop on a simulated nuclear fuel rod with roughened surface in a closed flow loop using DI-water as the coolant. They studied a multiplicity of diamond shaped three-dimensional roughness elements distributed on the surface of the rod.

On the other hand, nanofluids are liquid in which a small amount of nanoparticles are dispersed in base liquids [9]. Eexperiments have shown significant enhancement of heat transfer, mass transfer, wetting, and spreading characteristics of nanofluids [10-13]. Different empirical models have been suggested to predict effective thermal conductivity based on experimental data. S. Z. Heris et al. [13] mixed distilled water and Al_2O_3 nanoparticles in concentrations of 0.2%, 0.5%, 1.0%, 1.5%, 2.0%, and 2.5%. A flow loop was used to investigate the convective heat transfer performance of the nanofluids. Their work showed that with the increase in both the concentration of the nanoparticles and Reynolds number the heat transfer coefficient increased. One of the important conclusions was that the increase in thermal conductivity of nanofluids was not the only reason for heat transfer enhancement. Other factors such as dispersion, chaotic movement of nanoparticles, Brownian motion and particle migration also had influence on the heat transfer of the nanofluids.

In the present paper, experiments were carried out of a pressurized water nuclear reactor (PWR) using different concentrations of ZnO/DI-water based nanofluids. Heat transfer performance experiments were performed and reported.

Nomenclature

A	Area	m^2	V	Voltage	Volt
C_p	Specific heat	kJ/kg.K	ρ	Density	kg/m^3
d	Diameter	m	φ	Volume fraction	~
I	Current	amp	μ	Dynamic viscosity	kg/s.m
l	Length	m	λ	Thermal conductivity	W/m.K
$\dot{m}$	Mass flow rate	kg/s	**Subscripts**		
Nu	Nusselt number	~	b	bulk	
P	Power	Watt	f	fluid	
Pe	Peclet number	~	i	inner	
			h	hydraulic	

Q	Volumetric flow rate	m^3/h	m	mean
$q^{"}$	Heat flux	W/m^2	o	outer
$q^{"'}$	Rate of heat generation	W/m^3	p	particle
R	Electrical resistance	ohm	s	surface
Re	Reynolds number	~	w	wall
T	Temperature	^oC	x	x-direction
v	Velocity	m/s	y	y-direction

2. Experimental Procedure

2.1. Nanofluids

2 vol% ZnO/DI-water nanofluids was purchased from Ice Dragon Cooling. The 0.5% by volume nanofluids mixture was prepared from the original nanofluids by adding DI-water in proper volume percentage.

2.2. Single Heater Element Loop Tester

A single heater element loop (Fig. 1) was built at the Department of Mechanical Engineering at University of South Carolina, Columbia. The thermal hydraulic loop can deliver up to 14.3 m^3/ h of DI-water and 13.85 m^3/ h of nanofluids. The plugged rotary pump (0.75 HP Grundfos model CRIE 10-1 unit) was used to pump the working fluid through the loop. The pump has a cool-top air-cooled shaft seal chamber that enabled it to handle the fluid up to 185°C. The loop was a closed and thermally insulated loop with one bypass that contained a shell and tube type heat exchanger and a vertical test section, which housed the simulated fuel rod. The fuel rod was connected to a 10 kW power supply.

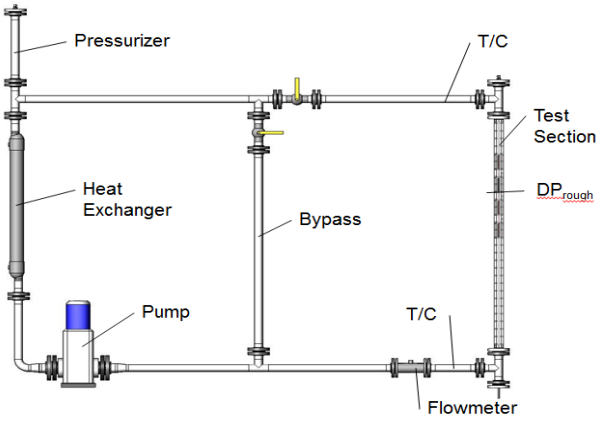

Figure 1: Single heater element loop tester

2.3. Heater/Fuel Rod

Fig. 2 shows the heater/fuel rod. The total length of the test rod was 2.1526 m. The bottom half and upper part of the rod was Nickel. The middle section was 0.5334 m long Inconel tube. All three parts were brazed together using white flux brazing paste and SA45 Brazing wire. The bottom part of the fuel rod was a solid nickel rod while middle and upper part of the rod are tubes. The outer and inner diameters of the tube are 9.5 mm and 8 mm. The rough region on the Inconel rod was 0.3 m in length. The three dimensional roughness were formed on the Inconel tube using a coarse knurling tool and a modified lathe machine.

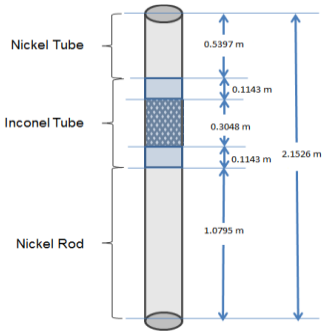

Figure 2: Heater / Fuel Rod

Eight ceramic rods of 3.2 mm diameter and 50 mm length were used to keep the alignment of the rod inside the test section. Two groups of four ceramic rods were respectively held in fittings that were machined and welded into on the test section. The alignment of the test rod was confirmed when the circumferential temperature readings from the heater rod during the thermal test did not vary more than 0.5 °C. In order to eliminate the entrance effects, the leading edge of the Inconel rod was located at a distance of more than 25 hydraulic diameters from the coolant inlet to the test section. The trailing edge of the Inconel rod was more than 15 hydraulic diameters from the top end of the tee-joint. The annular test section which contains the simulated rod was 1.524 m long with an inner diameter of 38 mm. It has flanges welded at both ends in order to securely fit into the loop. Its flow housing was made from ASTM B241 aluminum tube. The test section has a wall thickness of 6.35 mm. The cross section is as shown in Fig. 3.

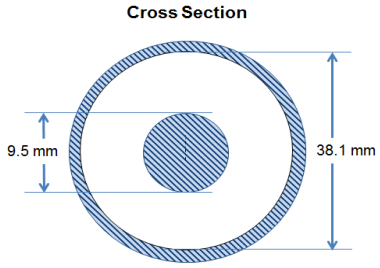

Figure 3: Cross section of the test section

As Fig. 4 shows, the total rough section on the Inconel section was 0.3 m in the middle which left the smooth section of Inconel part 45 mm on either side. The roughness had a continuous diamond shape pattern. The angle of the corrugation at each diamond was 45 degrees with a length of side 1 mm. The depth of the roughness was 0.3 mm and pitch of the pattern was 16 mm.

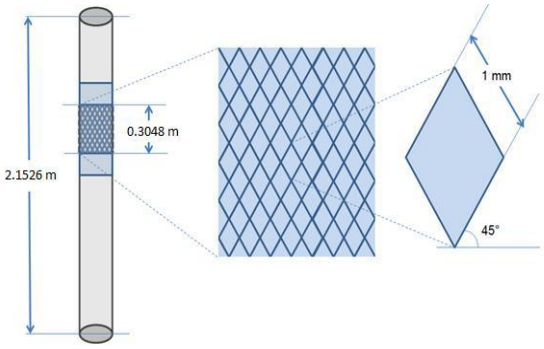

Figure 4: 3-D Surface Roughness Geometry

2.4. Thermal Test

While the flow from the pump was constant, valves were used to get the desired flow rate through the test section. Data collection began after steady-state conditions were met. The first data point recorded was defined as a smooth section point. Then, the modified section was divided into six equal-distant parts, each with its own recorded measurement. For every axial point, there are two temperature readings from the thermocouple. Each of the coolant/temperature combination examined, three different flow rates through the test section were being used to study the effect of flow rates on heat transfer. These flow rates being 4.54 m^3/h, 9.08m^3/h and 14.3 m^3/h. Also, for each temperature data point a total of 180 readings were through LabView, which record 6 readings every second for 30 seconds. A total of 8 thermal tests was performed at a range of:

- Bulk Temperature: 60 and 70 °C
- Rod temperature: 85 ~ 165 °C
- System Pressure: 0.45 ~ 0.55 MPa
- Power: 0 ~ 10 kW
- Coolant flow rate: 4.54 ~ 14.3 m^3/ h
- Differential pressure: 0.029 ~ 0.29 psi

Two different water inlet temperatures with 3D roughness at 0.5 % and 2% nanoparticle concentrations were investigated. Additionally 2D roughness were also evaluated at 0.5% nanoparticle concentration.

2.5. Data Reduction

The rate of convective heat transfer through the test section was determined by the heat balance equation:

$$q = \dot{m} * C_p(T_0 - T_i) \quad (1)$$

The fluid properties were based on the average temperature:

$$T_m = \frac{(T_0 + T_i)}{2} \quad (2)$$

The amount of total heat input to the test section from the power supply was:

$$q_{in} = P = V * I \quad (3)$$

The bulk temperature for this analysis was determined by:

$$T_b = T_{in} + \frac{Q}{\dot{m} * C_p} * \frac{x}{l} \quad (4)$$

In order to calculate the rate of heat generation for both parts of the tube, the rate of heat generation equation was applied as:

$$q''' = R\left[\frac{4I}{\pi(d_0^2 - d_i^2)}\right]^2 \quad (5)$$

The following formula was used to calculate the temperature at the outer surface of the rod:

$$T_{w,0} = T_{w,i} + \frac{q'''}{16k}\left(2d_i^2 \ln\frac{d_i}{d_o} - d_i^2 + d_o^2\right) \quad (6)$$

The total losses of heat from the system were calculated by:

$$q_{loss} = q_{in} - q_{inconel} - q_{nickel} \quad (7)$$

The hydraulic diameter d_h was calculated by subtracting the inner diameter of the test section d_i and outer diameter of the heater rodd_o:

$$d_h = d_i - d_o \quad (8)$$

Reynolds number was calculated using the following equation:

$$Re_{D_h} = \frac{\rho v d_h}{\mu} \quad (9)$$

Velocity in the test section was determined using:

$$v = \frac{Q}{A_h} \quad (10)$$

The mass flow rate in the test-section was determined by:

$$\dot{m} = \rho * v * A_h \quad (11)$$

Heat flux was calculated through the following formula:

$$q'' = \frac{q_{in}}{A_s} \quad (12)$$

Heat transfer coefficient, assuming no heat loss, was calculated using the energy balance:

$$h = \frac{q''}{(T_s - T_b)} \quad (13)$$

Lastly, Nusselt number was calculated using the following formula:

$$Nu = \frac{hd_h}{\lambda_{eff}} \quad (14)$$

For thermal conductivity of nanofluids, the empirical equation of J. R. Vazquez Penas et al. [14] was used

$$\frac{1}{\lambda_{eff}} = \frac{\phi}{\lambda_p} + \frac{1-\phi}{\lambda_f} \quad (15)$$

Heat transfer coefficients were calculated for all three of coolants. The HT_{enh} heat transfer enhancement of the different comparison group in the rough region was calculated as follows:

$$HT_{enh} = \left(\frac{h_1}{h_2} - 1\right) * 100 \quad (16)$$

The parameters h_1 and h_2 are the heat transfer coefficients of the two different types of coolant.

3. Results and Discussion

All of experimental results are presented here as different groups with the flow conditions:

Group # 1

The test conditions for the first group of thermal test are:

- Fluid inlet temperature: 70 °C
- Power: 2.88 KW
- System pressure: 0.33 ~ 0.55 MPa
- Flow rate: 4.5 m^3/ h, 9.08 m^3/h, and 14.3 m^3/h
- Roughness: three-dimensional

The surface temperature drop across the rough region of the fuel rod for all fluids used in the experiments was recorded. The heat transfer coefficient was calculated using the recorded temperatures and the above parameters.

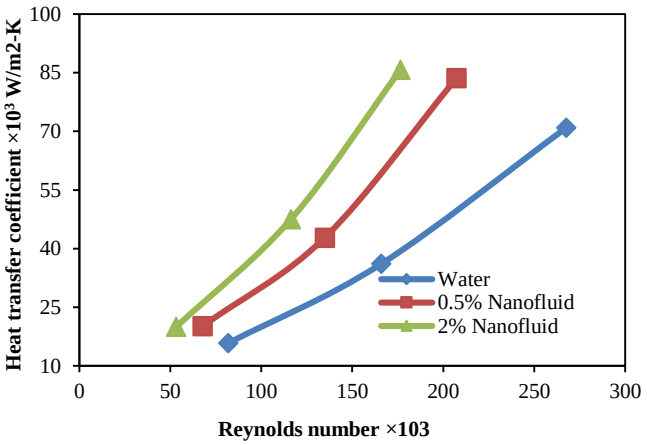

Figure 5: Heat transfer coefficient as a function of Reynolds number

Fig. 5 presents a comparison of heat transfer coefficient calculated for each fluid. It was evident from the Fig.5 that 2 vol% ZnO nanofluids provides the highest heat transfer coefficient.

Group #2

The test conditions for second group of thermal test are:

- Fluid Inlet Temperature: 80 °C
- Power: 3.98 kW
- System pressure: 0.33 ~ 0.55 MPa
- Flow rate: 4.5 m^3/hr, 9.08 m^3/hr, and 14.3 m^3/h
- Roughness: three-dimensional

For this thermal test an 8-9°C temperature drop across rough section was observed. The bulk temperature was raised by 0.5 °C across the test section.

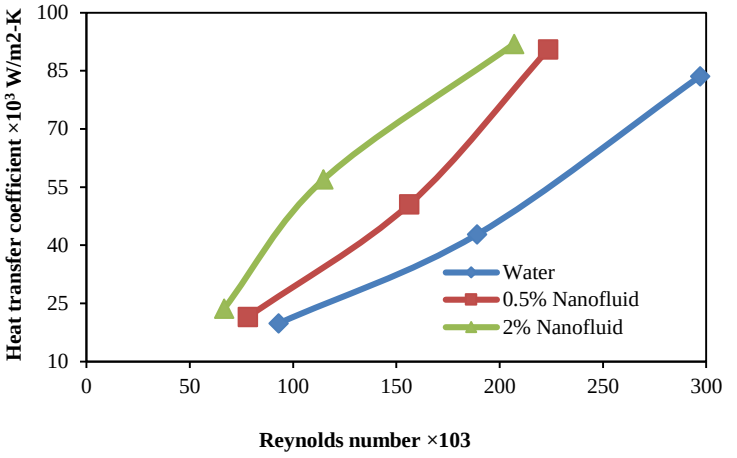

Figure 6: Heat transfer coefficient as a function of Reynolds number

Fig. 6 illustrates the heat transfer coefficient for the different fluids at various Reynolds. Since the bulk temperature for this thermal test was higher than the previous test the resulting heat transfer enhancement was also higher.

Group #3

The test conditions for the third group of thermal test are:

- Fluid Inlet Temperature: 70 °C
- Power: 2.88 KW
- System pressure: 0.33 ~ 0.55 MPa
- Flow rates: 4.5 m^3/h, 9.08 m^3/h, and 13.85 m^3/h
- Roughness: two and three-dimensional
- Fluid type: 0.5 vol% water-based ZnO nanofluid

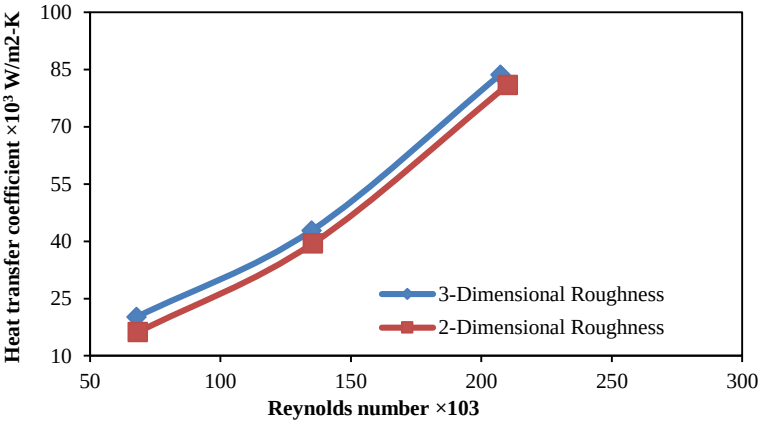

Figure 7: Heat transfer coefficient as a function of Reynolds number

Fig.7 presents a comparison between heat transfer coefficients as a function of Reynolds number for the two and the three-dimensional surface roughness. As it can be seen, the three-dimensional surface roughness provides better heat transfer than the two-dimensional.

Group #4

The test conditions for third group of thermal test are:

- Fluid Inlet Temperature: 80 °C
- Power: 2.88 kW
- System pressure: 0.33 ~ 0.55 MPa
- Flow rate: 4.5 m^3/h, 9.08 m^3/h, and 13.85 m^3/h
- Roughness: two and three-dimensional
- Fluid type : 0.5 vol% water-based ZnO nanofluids

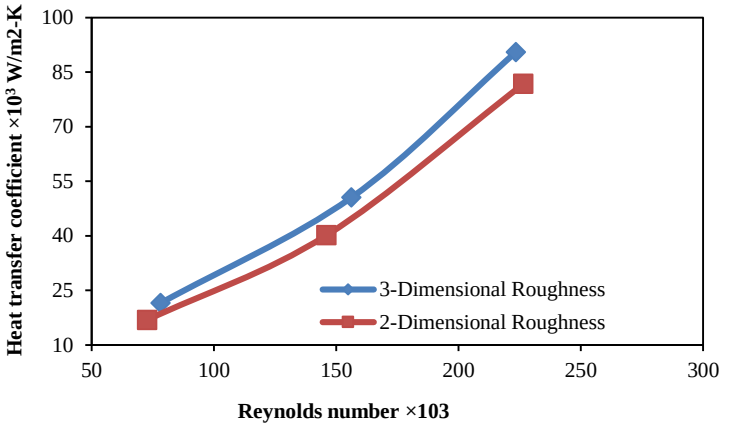

Figure 8: Heat transfer coefficient as a function of Reynolds number

Fig. 8 presents a comparison between the heat transfer coefficient as a function of Reynolds number for the two and the three-dimensional surface roughness. A similar trend of higher heat transfer coefficient for three-dimensional surface roughness was observed in this thermal test.

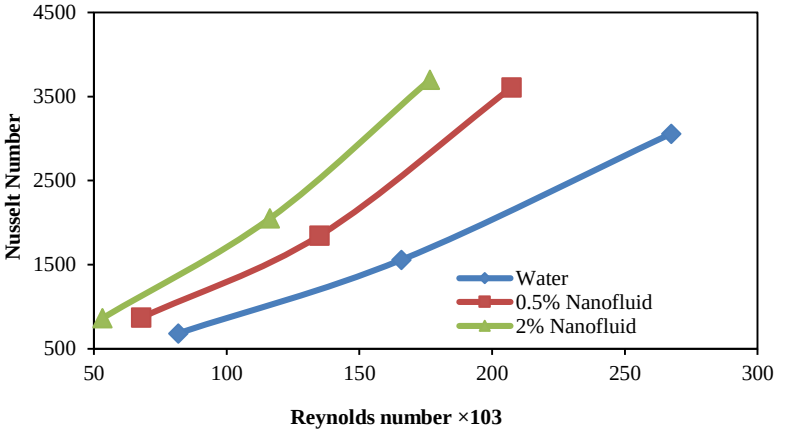

Figure 9: Nusselt number as a function of Reynolds number

Fig. 9 shows the variation of average Nusselt number as a function of Reynolds number for the first thermal test for three dimensional roughness. It was observed during the experiments that as the Reynolds number increased the bulk temperature also increased, and the rod temperature decreased. This resulted in higher heat transfer coefficients, which resulted in a higher Nusselt.

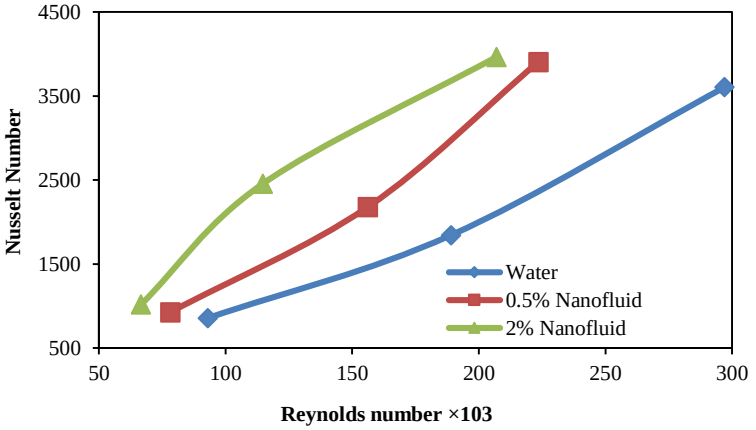

Figure 10: Nusselt number as a function of Reynolds number

Fig. 10 shows a similar variation of Nusselt as the Reynolds increases. Since the convective heat transfer coefficient was proportional to the coolant flow across the fuel rod, the higher Reynolds results in higher convective coefficient values thus higher Nusselt. For the two Nusselt-Reynolds graphs, the curve should not be continuous as the flow was turbulent. These curves show the trend of Nusselt number as Reynolds number increases. In all of the results above, enhancement of heat transfer coefficient with nanofluids is because of enhanced thermal condictivity of nanofluids compared to base fluid and particle migration behavior in the boundary layer.

4. Conclusion

The objective of this research was to experimentally investigate the enhancement in heat transfer in a simulated nuclear fuel rod bundle using different concentrations of nanofluids. The results obtained in this study were compared with the experimental results obtained by using different kinds of coolant in a simulated nuclear fuel rod bundle. A single heater element loop setup was used for experimental study. Two simulated fuel rods were used whose outer surfaces were modified to form three-dimensional and two-dimensional rough surfaces. A series of systematic thermal tests were conducted. DI-Water based Zinc oxide (ZnO) nanofluids was employed as coolant for these tests (0.5% and 2% volumetric concentration). The heat transfer rate was calculated for each fluid and surface treatment and compared to each other. The analyzed data show the following results:

1. For the same flow rate, the 2 vol% nanofluids provides the highest heat transfer coefficient compared to the DI-water.
2. Heat transfer coefficient increases as the Reynolds number increases.
3. The maximum heat transfer coefficient enhancement achieved compared to DI-water was 33% at $Re = 1.15 \times 10^5$ for fuel rod with three-dimensional surface roughness using 2 vol% ZnO nanofluid.

Acknowledgements

The authors would like to thank Westinghouse Electric Company, Columbia, SC for funding the project. Specifically they would like to thank Dr. Zeses Karoutas for providing technical and financial support and Dr. Leo Carrilho for designing the experimental facility.

References

[1] A.E. Bergles, A.R. Blumenkrantz, J. Taborek, 1974, “Performance evaluation criteria for enhanced heat ransfer surfaces”, in: Proceedings of the Fourth International Heat Transfer Conference vol. 2, pp. 239-243.
[2] D. Ryu, D. Choi, V. Patel, 2007, “Analysis of turbulent flow in channels roughened by 1321 two-dimensional ribs and three-dimensional blocks”: part II: heat transfer, Int. 1322 J. Heat Fluid Flow 28, pp. 1112–1124.
[3] Firth, R.J. and Meyer, L., 1983, “A comparison of the heat transfer and friction factor performance of four different types of artificially roughened surface”, Int. Journal of Mass and Heat Transfer, vol. 26, no. 2, pp. 175-183.

[4]Han, J.C., Park, J.S., and Lei, C.K., 1985, "Heat transfer in channels with turbulence promoters", *ASME Journal of Engineering for gas Turbine and Power,* Vol. 107, pp.628-635.
[5] Singh, S., Chander, S., Saini, J. S., 2011, "Heat transfer and friction factor correlations of solar air heater ducts artificially roughened with discrete V-down ribs", Energy, Volume 36, Issue 8 , 5053–5064.
[6] Xiao-Wei Li, Ji-an Meng, Zhi-xin Li, 2011, "Roughness enhanced mechanism for turbulent convective heat transfer, International Journal of Heat and Mass Transfer", Volume 54, Issues 9–10, April, Pages 1775-1781.
[7] Ryu, D.N., Choi, D.H., Patel, V.C., 2007, "Analysis of turbulent flow in channels roughened by two-dimensional ribs and three-dimensional blocks" Part I: Resistance. International Journal of Heat and Fluid Flow 28, 1098-1111.
[8] Umair Najeeb, Leo A .Carrilho, Jamil Khan, "Heat Transfer Characteristics of Three-Dimensional Surface Roughness in Nuclear Fuel Rod Bundles", International Mechanical Engineering Congress & Exposition, IMECE2013. Nov. 15-21, San Diego, CA.
[9] Choi, S. U. S., Eastman, J. A., 1995, "Enhancing Thermal Conductivity of Fluids with Nanoparticles" Developments Applications of Non-Newtonian Flows, ASME, New York, pp. 99-105.
[10] A. Mazumder, J. Davis, V. Rangari, and M. Curry, "Synthesis, Characterization, and Applications of Dendrimer-Encapsulated Zero-Valent Ni Nanoparticles as Antimicrobial Agents" ISRN Nanomaterials Volume 2013, Article ID 843709, 9 pages.
[11] Wang, X., Xu, X., 1999, "Thermal Conductivity of Nanoparticle–Fluid Mixture" Journal of Thermophysics and Heat Transfer, Vol. 13, No. 4, pp. 474-480.
[12] Krishnamurthy, S., Bhattacharya, P., Phelan, P. E., 2006, "Enhanced Mass Transport in Nanofluids" Nano Letter 6 (3), 419-423.
[13] S. Zeinali Heris, M. Nasr Esfahany, S.Gh. Etemad, "Experimental investigation of convective heat transfer of Al_2O_3/water nanofluid in circular tube" International Journal of Heat and Fluid Flow 28 (2007) 203–210.
[14]Jose R. Vazquez Penas, Jose M. Ortiz de Zarate and Mohamed Khayet, 2008, "Measurement of the thermal conductivity of nanofluids by the multicurrent hot-wire method", Journal of Applied Physics 104, 044314.

Available online at www.sciencedirect.com

ScienceDirect

Procedia Engineering 00 (2015) 000–000

Procedia Engineering

www.elsevier.com/locate/procedia

6th BSME International Conference on Thermal Engineering (ICTE 2014)

Molecular dynamics study of effect of different wetting conditions on evaporation and rapid boiling of ultra-thin argon layer over platinum surface

S.M. Shavik*, Mohammad Nasim Hasan, A.K.M. Monjur Morshed, M. Quamrul Islam

Department of Mechanical Engineering, Bangladesh University of Engineering and Technology, Dhaka-1000, Bangladesh

Abstract

Molecular dynamics simulations have been conducted to reveal the effect of solid-liquid interfacial wettability on the boiling phenomena of the thin liquid argon film placed over solid platinum wall. The three phase molecular system is comprised of solid platinum wall, liquid argon and argon vapor. Initially the three phase system is thermally equilibrated at 90K and after the attainment of equilibrium the temperature of solid platinum wall is suddenly increased which resembles ultrafast pulse heating. Two different degree of superheat have been considered to characterize the boiling phenomena, namely, evaporation for low degree of superheat and rapid or explosive boiling for high degree of superheat in which temperature of the wall was far above the critical temperature of argon. The solid-liquid interfacial wettability is varied to observe its effect on boiling and thus simulations are run for hydrophilic, hydrophobic and neutral surfaces. The simulation results show that surface wettability has a significant role on both cases of boiling phenomena. The nucleation of bubbles and formation of vapor films occurs more quickly for increased solid-liquid interfacial wettability. The study shows that hydrophilic surface is the most favorable surface condition for bubble nucleation.

Peer-review under responsibility of organizing committee of the 6th BSME International Conference on Thermal Engineering (ICTE 2014).

Keywords: Molecular dynamics simulation; Surface wetting; Evaporation; Explosive boiling

Nomenclature

r	Distance	Greek symbols	

* Corresponding author. Tel.: +880-1556376418; fax: +880-02-9665636.
E-mail address: shavik@me.buet.ac.bd

Peer-review under responsibility of organizing committee of the 6th BSME International Conference on Thermal Engineering (ICTE 2014).

t	Time	ε	energy scale parameter
T	Temperature	σ	length scale parameter
		ϕ	energy

1. Introduction

In the field of heat and mass transfer research, the phase change of a fluid is a fascinating and challenging topic. A large amount of heat can be transferred by phase change of a fluid. Among all the phase change phenomena, boiling of thin liquid films received more attention from the researchers for its practical applications in advanced micro or nano electromechanical systems, nano electronic cooling, laser steam cleaning of a solid surface and so on. Therefore, a good understanding of boiling phenomena of the thin liquid film is necessary at microscopic level to reveal the behavior of the phase transition from liquid to vapor. Furthermore, the study of the surface effects like change of solid-liquid surface wettability can add new dimensions to this research. Unfortunately, due to the very small scale, several difficulties occur in accurate experimentation of boiling of thin film liquid. Molecular dynamics simulation can be a very effective method to investigate such phenomena from the microscopic view point. In many molecular dynamics studies, researchers have given intensive focus on various issues of phase change process. Kimura and Maruyama [1] simulated heterogeneous nucleation of argon liquid droplet on a solid surface modeled as a constant temperature heat bath using phantom molecules. Sekine et al. [2] simulated liquid-vapor nucleation of Lennard-Jones fluid by molecular dynamics method and calculated the nucleation rate at three different temperatures by survival probability of the bubble-free state. Nagayama et al. [3] carried out MD simulations to examine the bubble behavior confined in a nanochannel with emphasis on nucleation phenomenon. Yu and Wang [4] simulated evaporation of thin argon liquid films and evaluated the net mass flux. Also they found a very thin non-evaporating layer and compared it with theoretical models. Maroo and Chung [5] performed molecular dynamics simulation of platinum heater and associated nano-scale liquid argon film evaporation and colloidal adsorption characteristics. Morshed et al. [6] studied the effect of nanostructures on evaporation and explosive boiling of thin liquid films through molecular dynamics simulation. Maruyama and Kimura [7] simulated a heterogeneous nucleation of argon vapor bubble on a solid Pt surface and measured the apparent contact angle. Most of the studies are performed to understand the behavior of the heterogeneous phase transition of thin liquid on a flat solid surface. Some studies have been performed to investigate the effect of nanostructures on phase transition. To the best of author's knowledge very few studies have been conducted to study the effect of solid-liquid interfacial wettability on phase transition of thin film liquid over a solid surface.

In the present study, both evaporation and explosive boiling of thin liquid argon film has been carried out by non-equilibrium molecular dynamics simulation (NEMD) with different solid-liquid interfacial wettability. Based on surface wettability three cases have been considered which are hydrophilic, hydrophobic and neutral surface. The simulations are performed to capture the microscopic view of the phase transition and associated other phenomena of the above mentioned three cases.

2. Simulation Method

In this study, molecular dynamics simulations are performed for a three phase system consisting liquid argon layers placed over a solid platinum wall and argon vapor which resides over the liquid layers. Fig. 1 shows the initial configuration of the simulation system, where the simulation cell is a cuboid having a dimension of 6.63 nm × 31.85 nm × 6.63 nm. The platinum wall consists of six monolayers and placed at the bottom of the simulation box. The platinum wall consists 3468 atoms arranged in a fcc (1 0 0) lattice structure corresponding to its density of 21.45×10^3 kg/m^3 and having a thickness of 1.158 nm. Ten monolayers of liquid argon having a thickness of 2.78 nm are placed over the solid wall corresponding to a density of 1.367×10^3 kg/m^3.The rest of the space is filled with 128 argon vapor atoms.

The well-known Lennard-Jones (LJ) 12-6 potential [8] was used to calculate the intermolecular forces for all atoms within the simulation domain:

$$\phi(r) = 4\varepsilon\left[\left(\frac{\sigma}{r}\right)^{12} - \left(\frac{\sigma}{r}\right)^{6}\right] \tag{1}$$

The energy parameter, ε and length parameter, σ for the interaction potential were: $\sigma_{Ar\text{-}Ar}$ = 0.34 nm, $\varepsilon_{Ar\text{-}Ar}$ = 0.0104 eV; $\sigma_{Pt\text{-}Pt}$ = 0.2475 nm, $\varepsilon_{Pt\text{-}Pt}$ = 0.52 eV; $\sigma_{Ar\text{-}Pt}$ = 0.287 nm, the energy parameter $\varepsilon_{Ar\text{-}Pt}$ of solid-liquid (Ar-Pt) interaction potential was varied for different cases. Three different types of surfaces have been considered in the present study based on the surface wettability. When $\varepsilon_{Ar\text{-}Ar} < \varepsilon_{Ar\text{-}Pt}$, the surface is considered as hydrophilic, when $\varepsilon_{Ar\text{-}Ar} > \varepsilon_{Ar\text{-}Pt}$, surface is considered as hydrophobic and when $\varepsilon_{Ar\text{-}Ar} = \varepsilon_{Ar\text{-}Pt}$, surface is considered as neutral. The relation between the surface wettability (hydrophilic, hydrophobic and neutral) and solid-liquid interaction potential, ε has been established from the work of Hens et al. [9]. So, for hydrophilic case, $\varepsilon_{Ar\text{-}Pt}$ = 0.065 eV, for hydrophobic case, $\varepsilon_{Ar\text{-}Pt}$ = 0.005 eV and for neutral case, $\varepsilon_{Ar\text{-}Pt}$ = 0.0104 eV. All the potentials were truncated at 3.5 $\sigma_{Ar\text{-}Ar}$ to increase the computational efficiency.

The equation of motion for each particle was integrated using velocity-Varlet algorithm with 5 fs time step. Periodic boundary conditions were applied in the x and z directions, whereas a simple non periodic fixed boundary condition is assumed in the y-direction. The bottom layer of the wall was kept fixed and the adiabatic imaginary boundary condition was applied to the top of the simulation domain. Langevin thermostat was applied to the certain layers of the solid wall (next two layers above the bottom layer).

Starting from the initial configuration of the simulation domain the Langevin thermostat was turned on at 90K and the simulation was run for 250 ps. Then the Langevin thermostat was switched off and the system is allowed to equilibrate for 500 ps. The thermodynamic states i.e. temperature, pressure and density of argon atom were monitored during this period to check whether it was in the equilibrium state or not. At the end of the equilibrium period, to ensure the phase transition, the Langevin thermostat was set to rise to 130K for normal boiling (evaporation) case and 250K for the explosive boiling case. The simulation in this condition was run for 1250 ps. All the simulations were performed using LAMMPS (Large scale Atomic/Molecular Massively Parallel Simulator) which is an open source code for classical MD simulation developed by Sandia National Laboratory, USA and visualization was done using VMD (Visual Molecular Dynamics).

3. Results and Discussion

3.1 Low temperature case (evaporation)

As mentioned earlier three cases are considered; hydrophilic, hydrophobic and neutral case. The snapshots of the simulation domain at different times are shown in Fig. 4 for all the three cases. When the temperature of the solid wall is suddenly increased from 90K to 130K, at initial states there is no significant movement of argon atom from liquid to vapor region but as the time progresses liquid argon atoms gradually escapes from the top layer into the vapor region as individual atom. In case of hydrophilic surface this phenomena picks up quickly. But in case of hydrophobic surface the number of atoms which reach the vapor region from liquid layer is quite few. As expected

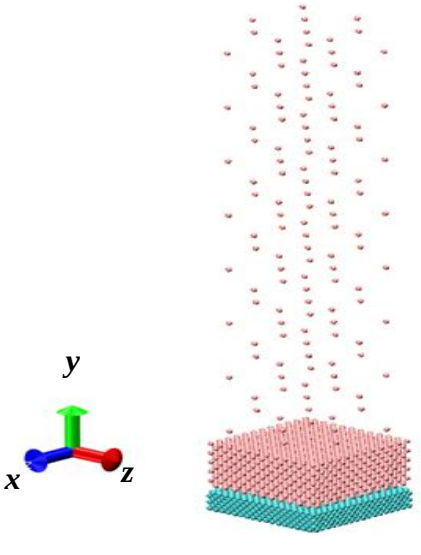

Fig.1. Initial Configuration of the simulation domain

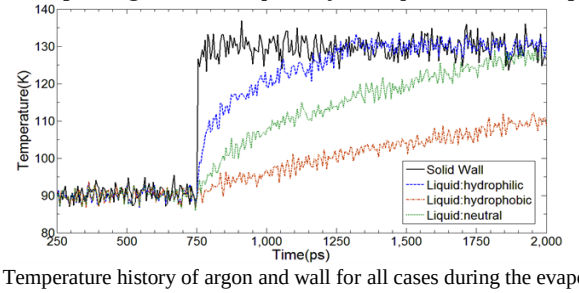

Fig.2. Temperature history of argon and wall for all cases during the evaporation

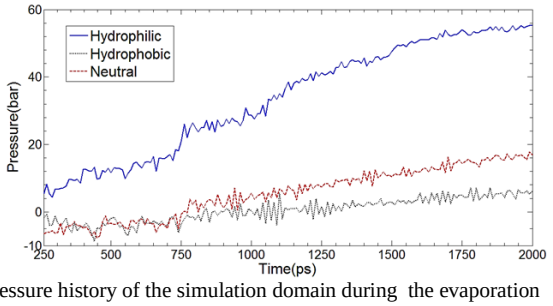

Fig.3. Pressure history of the simulation domain during the evaporation

the neutral surface shows characteristic that is in between of the former two cases. The temperature history of the solid wall and liquid argon during evaporation for all the cases is shown in Fig. 2. It can be readily observed that the temperature of liquid argon reaches to equilibrium with the solid wall much quicker in case of hydrophilic surface. Figure 3 shows the pressure history of the system for all the cases. As the volume of the system is constraint with the increase of the temperature pressure increases and follows similar trend of temperature.

For heat transfer phenomena, heat flux is an important tool for quantifying the effectiveness of heat transfer. In this study heat flux is calculated in two ways. In the first method, heat flux normal to the solid wall is calculated from the per atom potential energy, the per atom kinetic energy and per atom stress tensor [10]. Figure 6 depicts the heat flux normal to the solid wall (xz plane) for all the cases during evaporation. For all the cases the trend of the profiles are same. Just after the jump of temperature of Langevin thermostat from 90K to 130K, a high heat flux is

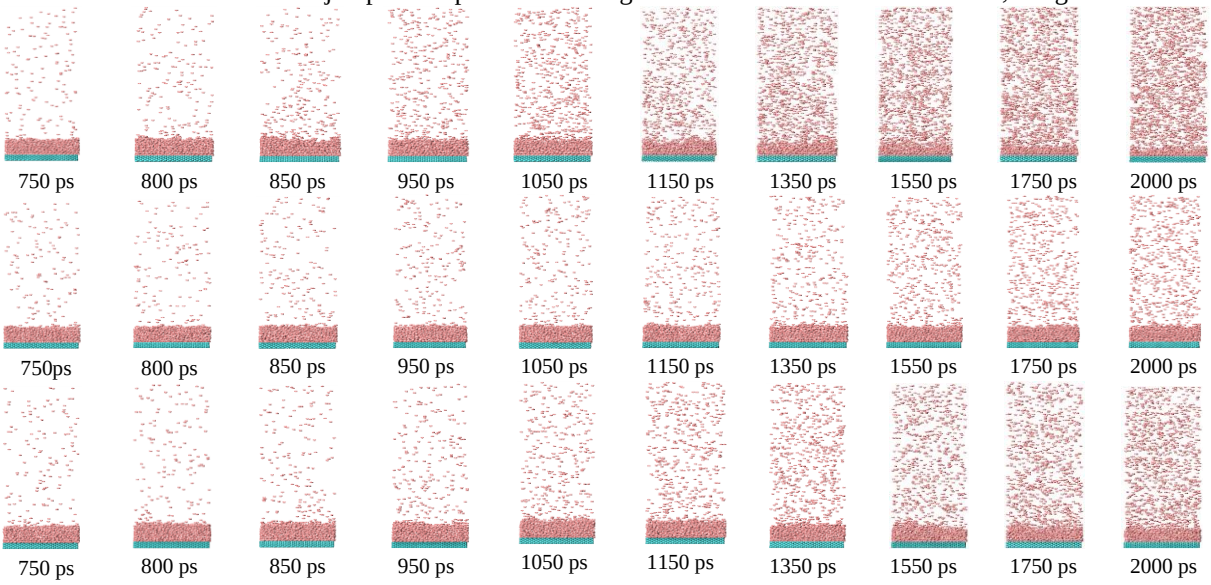

Fig.4. Snapshots from the simulation (xy plane) during evaporation on hydrophilic (first row), hydrophobic (second row) and neutral (third row) surface.

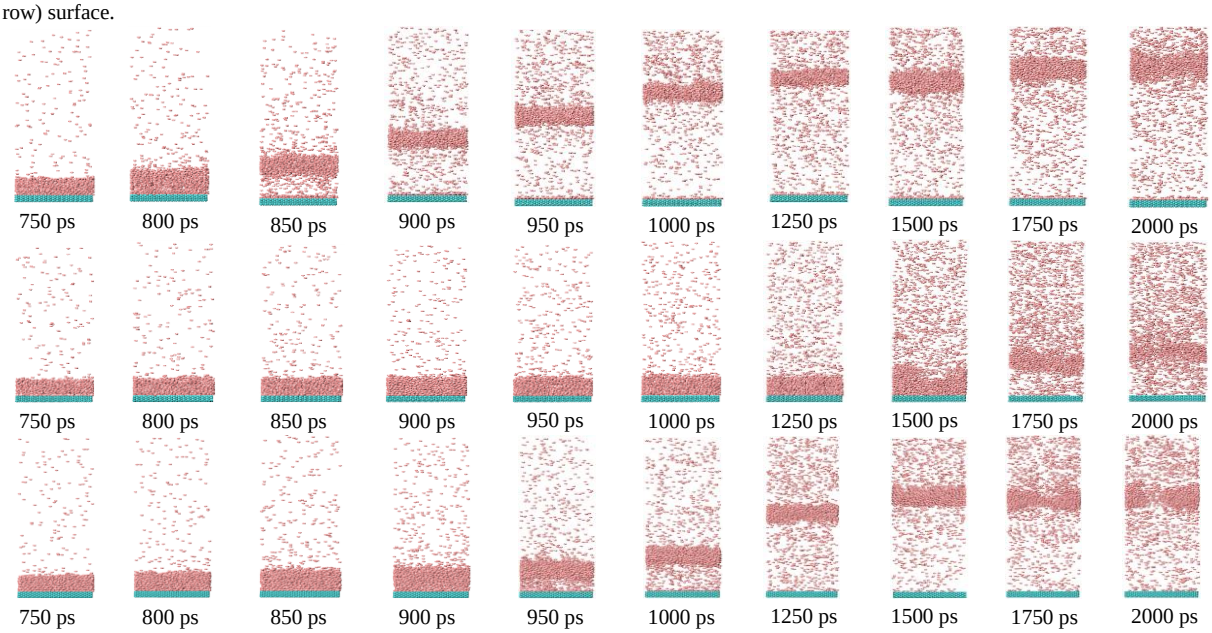

Fig.5. Snapshots from the simulation (xy plane) during explosive boiling on hydrophilic (first row), hydrophobic (second row) and neutral (third row) surface.

added within a short time. After this stage the heat flux decreases and oscillates about a mean value. The profiles of the heat flux are in good agreement with a previous study conducted by Yamamoto and Matsumoto [11]. As expected the hydrophilic case has the maximum value of heat flux which is close to 5.2×10^{-5} eV/A^{2}ps or 832 MW/m^2 which is in the order of theoretical maximum value of heat flux [9].

In the second method heat flux is calculated from the total energy added to the liquid argon atoms [5]. The heat flux calculated from the energy of the liquid during evaporation is shown in Fig. 7. The energy level of liquid suddenly jumps when the Langevin thermostat is switched to 130K to 90K, therefore, maximum heat flux occurs just at that time. Heat flux then decreases with time very sharply. The value of the heat flux is maximum for hydrophilic case and it is in the range of 750 MW/m^2 which is in the same order of magnitude of theoretical maximum value of heat flux, $q_{max,max}$, as defined by Gambill and Lienhard [12].

3.2 High temperature case (explosive boiling):

In this case, the temperature of the solid wall was set to jump from 90K to 250K, which is far greater than the critical temperature of liquid argon. Therefore, liquid argon changes phase rapidly or explosive boiling occurs. The snapshots of simulation domain during explosive boiling for all the cases are shown in Fig. 5. From the snapshots, it is very clear that among three cases under consideration, the explosive boiling phenomena occurs quickly in case of hydrophilic surface (850 ps) and occurs later in case of neutral surface (950 ps). In case of hydrophobic surface this phenomena occurs after a long time (1750 ps) as compared to hydrophilic and neutral cases. The temperature history of the system for different cases is shown in Fig. 8. Initially the temperature of the liquid increases very sharply, but after some time it starts decreasing. The temperature starts to decrease because of the separation of the liquid argon layer from the solid wall. As the temperature of the solid wall is increased very rapidly from 90K to 250K, the liquid layer adjacent to the solid wall exceed the critical temperature and instantly vaporize while other layers above are still in the liquid phase. The pressure of this vaporized layer pushes the liquid above it and therefore liquid layers separate from the solid wall. The energy flow from the solid wall to the liquid is hindered by the low density vapor region adjacent to the solid wall therefore the temperature of the liquid region falls temporarily. Figure 9 shows the pressure history of the system for all the cases. Like the temperature profile, pressure also increases initially and after some time it starts to decrease. When the vapor layer just adjacent to the solid wall pushes the liquid layers upward there is a decrease of pressure below. If the temperature and pressure history profiles are matched with explosive boiling phenomena as indicated by the snapshots in figure 5, then it is observed at the time when explosive boiling occurs and layers of liquid rises upward, both temperature and pressure decreases at that time.

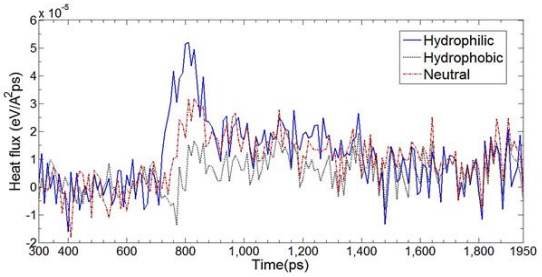

Fig.6. Heat flux normal to the surface for all cases during the evaporation

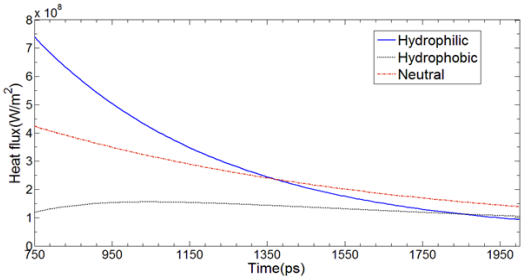

Fig.7. Temporal variation of wall heat flux calculated from energy of the liquid during the evaporation

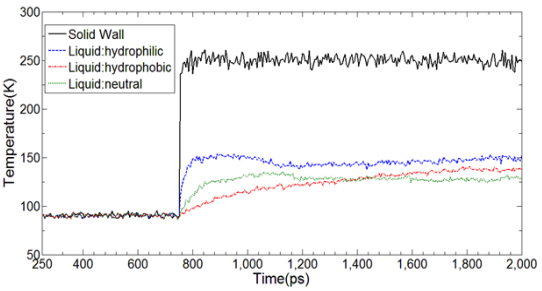

Fig.8. Temperature history of argon and wall for all cases during the explosive boiling

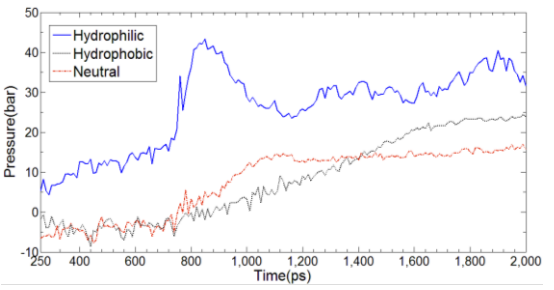

Fig.9. Pressure history of the simulation domain during the explosive boiling

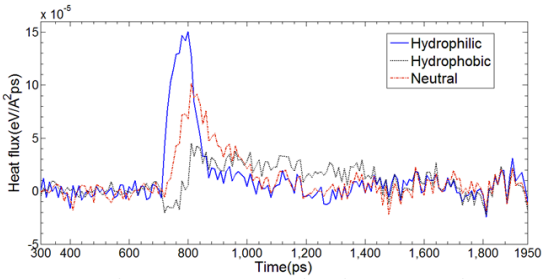

Fig.10. Heat flux normal to the surface for all cases of during the explosive boiling

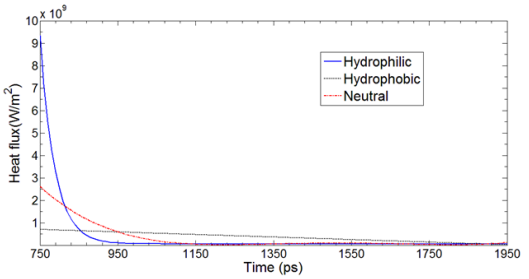

Fig.11. Wall heat flux calculated from energy of the liquid during the explosive boiling

Fig. 10 depicts the heat flux normal to the solid wall for all the cases during the explosive boiling. The trend of the heat flux profiles are similar to that of the case of evaporation but magnitude are much higher. At the moment, when the explosive boiling starts to take place, a huge amount of heat is transferred to the liquid adjacent to solid. But shortly after, the liquid layers move upward and they become detached from the solid surface and therefore energy flow is hindered. Thus there is a large drop of heat flux as indicated in Fig. 10. The value of heat flux is maximum in case of hydrophilic surface, which is around 15×10^{-5} eV/A^{2}ps or 2400 MW/m^2 which is about three times greater than the magnitude of heat flux calculated during evaporation (Fig. 6). The profiles and values of heat flux of Fig.10 shows excellent agreement with the study performed by the Yamamoto and Matsumoto [11]. Heat flux calculated from the energy added to liquid during explosive boiling shown in Fig. 11 also shows that the hydrophilic surface transfers energy most effectively however, the maximum value of heat flux for hydrophilic case is 9×10^9 MW/m^2 which is very large compared to the result of Fig. 10. This anomaly occurs because, a very high heat flux is randomly added within a very short time when explosive boiling begins and thus the energy profile consists a large energy jump in this region and when the heat flux is calculated from the slop of the energy profile it fails to capture the true nature of the phenomena.

4. Conclusion

Evaporation and explosive boiling phenomena for a thin liquid over a solid surface are closely studied by performing molecular dynamics (MD) simulation for different surface wetting conditions, namely hydrophilic, hydrophobic and neutral cases. The heat transfer rate from a solid surface to the liquid significantly increases with the increase of solid-liquid interaction potential or in other words, with the increase of the surface wettability. This is true for both evaporation and explosive boiling. The heat flux is calculated by two methods and in case of evaporation the results of both methods agrees well, but in case of explosive boiling heat flux calculated from the energy added to liquid provides an over approximation of the value of the heat flux. From heat flux point of view, the transfer of heat in case of hydrophilic surface is much greater than the neutral and hydrophobic surfaces. This has been confirmed by two different approaches adopted in this study.

References

[1] Tatsuto Kimura and Shigeo Maruyama, Molecular dynamics simulation of heterogeneous nucleation of a liquid droplet on a solid surface, Microscale Thermophysical Engineering, 6 (2002) 3–13.
[2] Marehito Sekine, Kenij Yasuokaa,, Tomoyuki Kinjob, Mitsuhiro Matsumoto, Liquid–vapor nucleation simulation of Lennard-Jones fluid by molecular dynamics method, Fluid Dynamics Research 40 (2008) 597–605.
[3] G. Nagayama, T. Tsuruta, P. Cheng, Molecular dynamics simulation on bubble formation in a nanochannel, Int. J. Heat Mass Transfer 49 (2006) 4437–4443.
[4] J. Yu, H. Wang, A molecular dynamics investigation on evaporation of thin liquid films, Int. J. Heat Mass Transfer 55 (2012) 1218-1225.
[5] S.C. Maroo, J.N. Chung, Molecular dynamic simulation of platinum heater and associated nano-scale liquid argon film evaporation and colloidal adsorption characteristics, J. Colloid Interface Sci. 328 (2008) 134–146.
[6] A.K.M.M. Morshed, Taitan C. Paul, Jamil A. Khan, Effect of nanostructures on evaporation and explosive boiling of thin liquid films: a molecular dynamics study, Applied Physics A 105 (2011) 445-451.
[7] S. Maruyama, T. Kimura, A molecular dynamics simulation of a bubble nucleation on solid surface, Int. J. Heat Technol. 18 (2000) 69–74.
[8] J.E. Lennard-Jones, A.F. Devonshire, Philos. Trans. R. Soc. Lond. Ser. A, Math. Phys. Sci. 163 (1937) 53-70.
[9] A. Hens, R. Agarwal, G. Biswas, Nanoscale study of boiling and evaporation in a liquid Ar film on a Pt heater using molecular dynamics simulation, Int. J. Heat Mass Transfer 71 (2014) 303-312
[10] LAMMPS Users Manual (http://lammps.sandia.gov – Sandia National Laboratories, USA).
[11] T. Yamamoto, M. Matsumoto, Initial stage of nucleate boiling: Molecular dynamics investigation, J. Thermal Sci. Tech. 7 (2012) 334-349
[12] W. R. Gambill, and J. H. Lienhard, An upper bound for the critical boiling heat flux, J. Heat Transfer, 111(1989) 815-818